Ph.D. Thesis

Power Law Systems and Heterogeneous Fractal Properties of Cryptocurrency Markets

Supervisor
Ken Umeno

Shinji Kakinaka

Department of Applied Mathematics and Physics
Graduate School of Informatics
Kyoto University

Contents

Abstract

It is widely acknowledged that traditional financial assets and digital coins, including cryptocurrencies, exhibit uncertainty and complexity in their price fluctuations, and a comprehensive explanation of such behavior is necessary for various financial purposes such as risk management, policy making and portfolio hedging. Although studies over the past few decades have uncovered the fluctuation characteristics of stock and commodity markets, the complex behavior of the rapidly developing cryptocurrency market has yet to be elucidated, especially in the research field of nonlinear physics as well as behavioural finance theory. Cryptocurrencies have attracted much attention from a wide range of community but they function differently compared to the conventional ones. A study focusing on their price fluctuations helps to determine what role they play in the financial society. In particular, the clarification of distribution and correlation structure is a key and important issue with significant implications for the financial community and the academic field. Therefore, an analytical framework that takes into account uncertainty and complexity is introduced, where the methods have the power to shed light on various types of anomaly phenomena reported in empirical studies. The framework provides both physical and economic interpretations for a comprehensive understanding of fluctuations and other relevant phenomena that follow.

We first focus on modelling the distribution of cryptocurrency price fluctuations. By implementing a new approach to estimating the parameters of stable distributions by flexibly designing the selection of Fourier points on the characteristic function, the validity of the stable law model is verified. At the same time, we show that a unified characterisation by both cubic and stable law is possible.

We also contribute to uncovering much of the non-linear correlation structure of the cryptocurrency market. From a fractal correlation framework, the results reveal outstanding traces of market efficiency, heterogeneous interactions among scales, and asymmetric responses of volatility to price shocks. In addition, we show that the fractal correlation can be applied to practical applications, by incorporating the fractal concept into the traditional approach of determining optimal

portfolio allocation. The academic contributions of these studies are discussed from the interdisciplinary perspectives of physics and finance.

Chapter 1

Introduction

The behavior of price fluctuation of financial assets is commonly explained by mathematical models that follow the theory based on the traditional Efficient Market Hypothesis (EMH) proposed by Fama (1970). The EMH is a hypothesis that states that share prices reflect all information, making it impossible for participants to outperform the overall market through expert stock selection. Therefore, in an "efficient" market, competition among market participants does not result in excess profits beyond what would be expected. Although the EMH is a cornerstone of modern financial theory that has contributed significantly to fields such as modern portfolio theory, financial engineering, and computational finance, the hypothesis is highly controversial and often disputed. While some researchers put effort in support of the EMH, arguing that it is pointless to try predicting market trends through fundamental and technical analysis, others point out that a large body of dissension exists. For example, the hypothesis theory lacks sufficient explanatory power for the real-world and cannot justify various empirical phenomena including crashes, price inflation, and market turbulence (Fama, 1991; Peters, 1994; Peng et al., 1994; Kristoufek, 2018). These studies pointed out that the even the weak form of the hypothesis does not hold in the real market[1]. Another issue is that the EMH-based analysis often underestimates financial market risk, making it more challenging to control risk and return of assets (Soros, 2015). Market regularities are often observed empirically, however, are called "anomalies" since they have no theoretical justification. Anomaly behaviors exist in the market with heterogeneity that cannot be explained by conventional modern portfolio theory or frameworks on market prices (Glosten and Milgrom, 1985; Easley

[1]There are three forms of market efficiency. The weak form requires that current stock prices reflect all the data of past prices. The semi-strong form suggests that prices reflect all publicly available information including new public information. The strong form states that prices reflect all private and public information, so that no information that can be used to enjoy an advantage on the market.

et al., 1996; Avramov et al., 2006; Zhang et al., 2022).

The concept of Econophysics emerged from the field of nonlinear physics plays an active role in analyzing such anomaly phenomena. In this discipline market movements are analyzed as a dynamic and complex system, thus it is possible to detect subtle but profound phenomena that cannot be captured by conventional methods without requiring the assumptions of the EMH (Jovanovic and Schinckus, 2016). Especially since the rise of cryptocurrencies, market analysis based on a nonlinear physics approach is attracting renewed attention due to the extreme volatility and heterogeneity observed in the market. The cryptocurrency market is a fast-growing emerging market based on the block-chain technology, which makes the market system completely different from the existing ones. The absence of an issuing entity or central controller means that cryptocurrencies can be traded with an unspecified number of counterparties, and speculative investment purposes are prevalent. Under such a unique system, traditional theories of price fluctuation have difficulties to be applied towards detecting the nature of price fluctuations. Another issue is that the time series of cryptocurrencies have been confirmed to have significant correlated and self-repeating structures, and their statistical laws are not yet clear (Peters, 1994; Fernández-Martínez et al., 2019). Hence, there is a need to develop an analytical model that can effectively express the characteristics of cryptocurrencies using a nonlinear physical approach. Therefore, this research aims to construct a system of analytical methods to understand the price fluctuations of the cryptocurrency market as a complex system and to elucidate its characteristics. We believe it is necessary to successfully handle its unique distributional statistical law and the correlation structure of the time series by introducing the concept of the alternative Fractal Market Hypothesis (FMH) of Peters (1994) as well as other innovations. The FMH extends the widely acknowledged EMH, and compensates for scaling factors the EMH fails to capture. Financial time series $X(t)$ are allowed to exhibit properties relevant to fractals that appear similar or self-repeating within sets of time series when viewed at different scales (Thompson and Wilson, 2016):

$$\{X(t) : t \in \mathbb{R}\} \stackrel{\mathrm{d}}{=} \left\{\eta^{-H} X(\eta t) : t \in \mathbb{R}\right\} \quad \text{for } \eta > 0.$$

This implies that market can be out of randomness, and due to the different valuations for information flows among investment horizons, market patterns exist. In effect, the FMH is known to have power to justify sudden spikes in market volatility and lack of market liquidity during crashes (Mandelbrot and Hudson, 2005; Mandelbrot, 1997). The decaying scaling exponent H is the widely known Hurst exponent, that is often used to measure the “index of dependence” or “index of long-range dependence”. However, the self-similarity structure of financial time series is usually not uniform, but rather hierarchical composed with different scaling exponents among different fluctuation levels. The scaling exponent of such an "mulitifractal" structure is expressed through the q-order fluctuation, $E[|X(t)|^q] = c(q)t^{qh(q)}$, where $h(q)$ denotes the generalized Hurst exponent (Thompson and Wilson, 2016). By utilizing the information of power-law decaying exponents, much effort has been been devoted to further understanding fractal patterns of large and small fluctuation nature.

The purpose of this study is to clarify the properties of price fluctuation phenomena in the rapidly developing cryptocurrency market through approaches from both perspectives based on behavioral finance theory and nonlinear physics. First, we will discuss the distribution statistics of cryptocurrency prices. In particular, we focus on power laws, especially the stable distribution Lévy (1937), which is a representative of power law class of distributions. Studies have found that taking into account theoretical background of the Generalized Central Limit Theorem (GCLT) (Gnedenko and Kolmogorov, 1954), the stable distribution well characterizes the distribution of the return series (Mandelbrot, 1963; Mantegna and Stanley, 1995; Xu et al., 2011; Krężolek, 2012; Yuan et al., 2014; Chronis, 2016). On the one hand, numerous research has confirmed that the tail portion generally shows an power law decay with an cubic exponent (exponent of 3), and there are solid financial theories that explain why such behavior can be observed (Clauset et al., 2009; Begušić et al., 2018). To fill in this gap, we investigate whether both arguments are not conflicting with each other and how they can be recognized as a consistent behavior. When doing this investigation, it is necessary to estimate the parameters of the stable distribution from the empirical data, but the general estimation method has many restrictions and problems regarding the parameters. The lack of a general estimation method is also an issue we should overcome Nolan (2003). We propose a more accurate and flexible parameter estimation method employing the chracteristic function. In particular, clarifying the relationship between points on the Fourier space and parameters achieves to sophisticate the estimation approach.

Then, the discussion of the correlation structure of cryptocurrency price fluctuation follows. Utilizing advanced fractal correlation analysis methods based on the concept of the FMH, we have conducted several empirical analyses. Specifically, we focus on the following phenomena and attempt to clarify their properties; the impact of the COVID-19 shock on cryptocurrency markets in terms of autocorrelations, the nature of ross-correlations between price and volatility fluctuations, and the existence of asymmetry in their cross-correlations. Such asymmetry is known as the "Leverage effect" in the field of behavioral finance (Black, 1976; Bollerslev et al., 2009; Bentes, 2018). We investigate whether the leverage effect has nonlinear properties such as multiscale and fractality. We also show that the factors behind the leverage effect can be explained not only from the economic behavior perspective but also from the dynamical framework. Finally, we will apply several types of fractal correlation analysis, which pose important keys in the above research, to portfolio theory, and work on social implementation with a view to practical use.

1.1 Properties of the Cryptocurrency Market

Bitcoin (BTC) was first released in 2009 by an anonymous person named Satoshi Nakamoto (Nakamoto, 2008), and have provided us with so many topics. Unlike other assets, cryptocurrencies are built on the block-chain technology based on the peer-to-peer network system that operates without a central bank or single administrator, while avoiding duplicated transactions and allowing cross-border electric payments open at all times. Another significant feature is that the system provides assurances of anonymity, and contributes to an incredible well-founded security (Böhme et al., 2015). Since this alternative system puts reliable transactions into practical use without an intermediary, cryptocurrencies are expected to prevail as an expedient medium of exchange.

It was not until 2013, when the BTC market underwent two price bubbles within the same year, that BTC began to be recognized by specialists and experts, increasing its awareness to a wider area. The year 2017 was a decisive year where the skyrocketing increase of market prices took notice and attracted the attention of a wide community including active online traders and academic researchers. Market capitalization temporarily marked over an astounding 200 billion dollars at its peak, however, prices turned to decline sharply at the beginning of 2018. The extreme fluctuations raised the concerns of market volatility due to strict financial regulators on cryptocurrency transactions in countries such as China and Korea. Still, they are a booming economy with market capitalization on its rising trend reaching more than 1900 billion US dollars in total by January 2022, attracting the attention of a wide community, including online traders, economic actors. During the same period, competing cryptocurrencies such as Ethereum (ETH), Ripple (XRP), Litecoin (LTC) have emerged and grown rapidly dominating more than half of the cryptocurrency market capitalization in recent years, indicating that analyzing minor coins has also become important. Given these idiosyncratic characteristics, modeling the fundamental features of BTC, along with other cryptocurrencies, plays a crucial role in various types of financial analyses. Thus, examining price fluctuations of new assets would provide us with some guidance for implementing financial management as well as keys to understand the phenomena occurring in financial systems.

Besides their rapid growth, research on cryptocurrency markets has become more active. Researchers have discussed whether cryptocurrencies should be classified as currencies, financial assets, an expedient medium of exchange, or a technological-based product (Lo and Wang, 2014; Blau, 2017; Yermack, 2015; Polasik et al., 2015; White et al., 2020), but they have not come to a complete conclusion. Moreover, BTC is less correlated with conventional assets, commodities, and the U.S. dollar, making it useful as a diversified investment for hedging purposes (Bouri et al., 2017b).

Numerous studies reveal that despite the unique system, cryptocurrency price fluctuations are incredibly complex and also exhibit stylized facts similar to what is recognized in stock and commodity markets, such as long-range dependence and long memory in volatility (Bariviera et al., 2017; Bouri et al., 2018; Cheah et al., 2018), fat-tails in price distribution, multifractality, and scaling properties (Jiang et al., 2018; Takaishi, 2018; Zhang et al., 2019). Nevertheless, cryptocurrencies tend to have more distinctive nonlinear dynamic characteristics, i.e., they tend to be more volatile (Bariviera et al., 2017; Alvarez-Ramirez et al., 2018; Drożdż et al., 2018), more inefficient, and more complex due to significant long-memory and stronger multifractality both in price and volatility (Al-Yahyaee et al., 2018; da Silva Filho et al., 2018; Telli and Chen, 2020). A in-depth study of Begušić et al. (2018) reports that the distribution of BTC returns have slowly decaying tails of power-law behavior with $2 < \alpha < 2.5$. This suggests that BTC returns, in addition to being more volatile, exhibit heavier tails than stocks, where the exponent of stock returns is known to be around 3. The BTC returns do not follow a random walk behavior and the market is significantly inefficient, but the efficiency becomes higher in recent periods (Urquhart, 2016) and the market heads to maturity (Drożdż et al., 2018). Although some studies suggest that market efficiency holds for certain periods, the returns do not generally satisfy the efficient market hypothesis (EMH) (Bariviera, 2017; Tiwari et al., 2018; Zhang et al., 2018a). Jiang et al. (2018) investigate how the Hurst exponent varies through a rolling window approach and conclude that the BTC market has a high degree of inefficiency over time. Bariviera (2017) uses a dynamical approach of detrended fluctuation analysis (DFA) proposed by Peng et al. (1994), which can be applied to non-stationary data and provides more reliable estimates of the Hurst exponent compared to the traditional rescaled range analysis (Hurst, 1957).

Other than these stylized facts, Bitcoin is uncorrelated with traditional assets and is suggested as a useful hedging tool with similar abilities to gold (Dyhrberg, 2016a,b). A "hedge" is an asset that is uncorrelated or negatively correlated with another asset or portfolio, whereas a "diversifier" is an asset that is positively but not perfectly correlated with another asset or portfolio (Diniz-Maganini et al., 2021). Bitcoin shows a property of a solid "safe-haven", defined as an asset that functions as a hedge not on average but in particular cases only, i.e., during the periods of market stress (Bouri et al., 2017b). This property indicates that the combination of financial assets with Bitcoin could help reduce the correlation levels and risks of a portfolio in times of market turmoil. Moreover, a vast application of fractal and nonlinear theory-based methods to analyzing cryptocurrency time series has shed light on the underlying physical mechanisms of their market dynamics.

1.2 Stable Distributions

In this section, we summarize the basis and properties of the stable distribution.

A fundamental theory of stochastic processes in various scientific fields is the generalized central limit theorem (GCLT), which points out that the sum of independent and identically distributed random variables converges only to the family of stable distribution (Gnedenko and Kolmogorov, 1954).

Stable distribution, also known as α-stable distribution, or Lévy's stable distribution, was first introduced by Lévy (1937), which is a family of parametric distribution with tails that are expressed as power-functions. According to Samorodnitsky and Taqqu (1994a), in the far tails the PDF can be written as,

$$f(x;\alpha,\beta,\gamma,\delta) \simeq \begin{cases} c_\alpha \gamma^\alpha \alpha (1+\beta)|x|^{-(1+\alpha)} \text{ for } (x \to +\infty) \\ c_\alpha \gamma^\alpha \alpha (1-\beta)|x|^{-(1+\alpha)} \text{ for } (x \to -\infty), \end{cases}$$

and the cumulative distribution function (CDF) written as,

$$\begin{cases} P(X > x) \simeq c_\alpha \gamma^\alpha (1+\beta)|x|^{-\alpha} \text{ for } (x \to +\infty) \\ P(X < x) \simeq c_\alpha \gamma^\alpha (1-\beta)|x|^{-\alpha} \text{ for } (x \to -\infty), \end{cases}$$

where c_α is a constant value $[\sin(\pi\alpha/2)\Gamma(\alpha)]/\pi$. Stable distribution is represented by four parameters; the scaling exponent parameter $\alpha \in (0,2]$ representing the fatness of the tail, the skewness parameter $\beta \in [-1,1]$, the scaling parameter $\gamma > 0$, and the location parameter $\delta \in \mathbb{R}$. Especially the parameters α and β determine the shape of distribution, including various forms of widely-known distributions such as the Gaussian and Cauchy distribution. Smaller value of α indicates fatter tails and hence it is well known that the variance diverges for $0 < \alpha < 2$, and also the mean cannot be defined for $0 < \alpha \leq 1$. Note that if $\beta = 0$, the distribution is symmetric, if $\beta > 0$, right-tailed, and if $\beta < 0$, left-tailed.

The definition of stable distribution is that the linear combination of independent random variables that follow a stable distribution with scaling exponent α invariably becomes again a stable distribution with the same scaling exponent. More particularly, when variables X_1, X_2 are i.i.d. copies of a random variable X and a, b are positive constant numbers, X is said to be *stable* and follows a stable distribution if there is a positive constant number c and a real number $d \in \mathbb{R}$ that satisfies

$$aX_1 + bX_2 \stackrel{\mathrm{d}}{=} cX + d,$$

also known for *stability property*. When a variable X follows a stable distribution, the notation $X \stackrel{\mathrm{d}}{=} S(\alpha, \beta, \gamma, \delta)$ is often used, where $\stackrel{\mathrm{d}}{=}$ denotes equality in distribution (Samorodnitsky and Taqqu, 1994b). Variable X can be standardized according to the following property:

$$\frac{X - \delta}{\gamma} \stackrel{\mathrm{d}}{=} S(\alpha, \beta, 0, 1). \tag{1.2.1}$$

Another important property of stable distribution is the GCLT, which implies that the only possible limit distributions for sums of i.i.d random variables is a family of stable distribution. When $\alpha = 2$, that is, when i.i.d. random variables have finite variance, the limit distribution then becomes a Gaussian according to the well-known classical Central Limit Theorem (CLT).

The PDF of stable distribution cannot be written in a closed form except for some cases; Cauchy distribution ($\alpha = 1, \beta = 0$), Lévy distribution ($\alpha = 1/2, \beta = 1$), and Gaussian distribution ($\alpha = 2$). Alternatively, the features are expressed by the characteristic function (CF), $\varphi(k)$, which is the Fourier transform of the PDF. By taking the inverse Fourier transform of the CF, the PDF can be obtained as

$$f(x) = \frac{1}{2\pi} \int_{-\infty}^{\infty} \mathrm{e}^{-ikx} \varphi(k) dk.$$

When variable X follows a stable distribution with $S(\alpha, \beta, \gamma, \delta)$, the CF is shown as

$$\begin{aligned} \varphi(k) &= \exp\left\{ i\delta k - \gamma^{\alpha} |k|^{\alpha} \left(1 - i\beta \operatorname{sgn}(k) \omega(k, \alpha)\right) \right\}, \\ \omega(k, \alpha) &= \begin{cases} \tan(\frac{\pi\alpha}{2}) & \alpha \neq 1 \\ -\frac{2}{\pi} \log|k| & \alpha = 1, \end{cases} \end{aligned} \tag{1.2.2}$$

which corresponds to the one-parameterization form of $S(\alpha, \beta, \gamma, \delta; 1)$ in Nolan (2003). This is the most popular parameterization among many other forms of the stable distribution owing to the simplicity of the form. Figure 1.1 shows the standardized stable distributions with the one-parameterization form for different parameters of α and β, as an example.

One-parameterization is preferred when one is interested in the basic properties of the distribution, but the CF takes a discontinuous form at $\alpha = 1$. Nolan

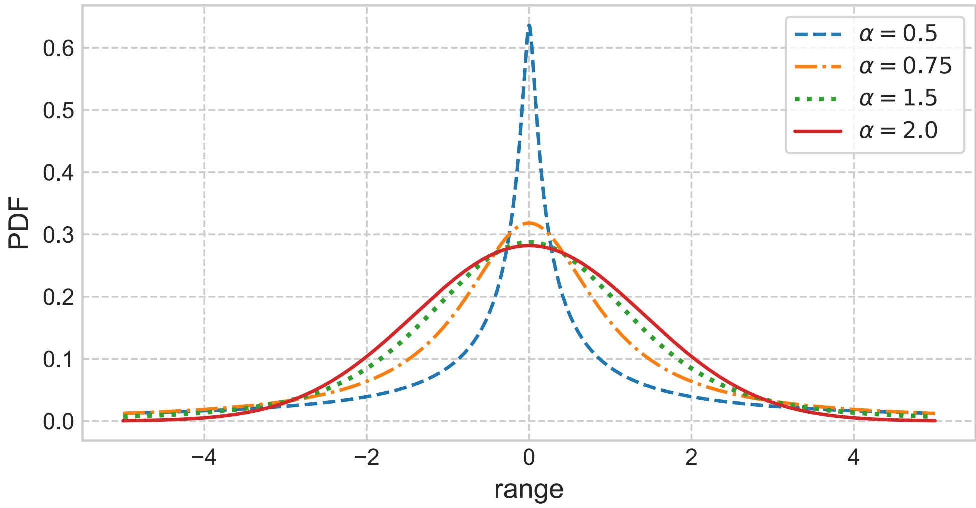

(a) stable distribution for the case of $S(\alpha,0,1,0)$

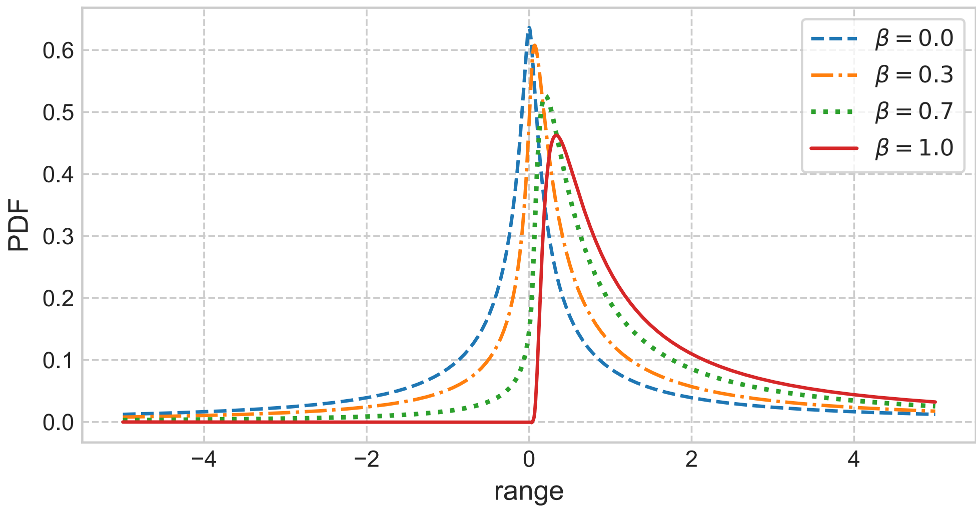

(b) stable distribution for the case of $S(0.5,\beta,1,0)$

Figure 1.1: Standardized stable distributions with the one-parameterization form for different parameters of α and β. (a) is the case of fixed $\beta = 0$, and (b) is the case of fixed $\alpha = 0.5$.

suggests the use of the zero-parameterization form $S(\alpha,\beta,\gamma,\delta_0;0)$ with different $\omega(k,\alpha)$ shown as

$$\omega(k,\alpha) = \begin{cases} -\left(|\gamma k|^{1-\alpha}-1\right)\tan(\frac{\pi\alpha}{2}) & \alpha \neq 1 \\ -\frac{2}{\pi}\log|\gamma k| & \alpha = 1, \end{cases} \tag{1.2.3}$$

giving a more complex form, but provides a continuous form. The only difference between the parameterization is the location parameter, which they are related by

$$\begin{aligned} \delta_0 &= \begin{cases} \delta + \beta\gamma\tan\frac{\pi\alpha}{2} & \alpha \neq 1 \\ \delta + \beta\frac{2}{\pi}\gamma\log\gamma & \alpha = 1 \end{cases}, \\ \delta &= \begin{cases} \delta_0 - \beta\gamma\tan\frac{\pi\alpha}{2} & \alpha \neq 1 \\ \delta_0 - \beta\frac{2}{\pi}\gamma\log\gamma & \alpha = 1 \end{cases}. \end{aligned} \tag{1.2.4}$$

In this study, we employ the simple one-parameterization, as we are interested in estimating the four parameters through the CF, and many existing estimation methods comply with that form. However, since this CF does not have a continuous form at $\alpha = 1$, arguments with different parameterizations may be more appropriate for discussing distributions when we already know that α is 1, for instance, the case of Cauchy distribution ($\alpha = 1, \beta = 0$).

1.3 Fractal Correlations

In this section, we summarize the basis of the fractal analysis method applied to investigate long-range power-law (cross) correlations within and between financial time series.

Based on the idea of FMH, the dynamical approach of detrended fluctuation analysis (DFA) of Peng et al. (1994) has become a widely utilized tool in analyzing fractal structures of a financial time series and scaling factors of its long-range correlation in a nonlinear manner. Podobnik and Stanley (2008) developed the detrended cross-correlation analysis (DCCA) to reveal power-law cross-correlation features between simultaneously recorded bivariate series. By putting DFA and DCCA techniques together, Zebende (2011) introduced the DCCA coefficient to measure the degree of cross-correlation for each specific scale quantitatively. This work promoted the development of the field into the investigation of multi-time scale dependencies of highly complex financial series.[2]

[2]See the review literature of Wątorek et al. (2021) for more information and about multi-time scale properties in cryptocurrency price fluctuations.

Multifractal detrended fluctuation analysis (MFDFA) is a generalization of the DFA algorithm, overcoming the limitations of the DFA by describing multifractal structures in terms of the generalized scaling exponents (Kantelhardt et al., 2002). The analysis of financial series using the MFDFA has lead to a breakthrough in the field of econophysics as an effective approach to detect inefficiency, multifractality, and long-memory in a nonlinear way. Studies have applied the MFDFA and found evidence that cryptocurrency markets have strong multifractality originating from correlations and fat-tails (da Silva Filho et al., 2018; Takaishi, 2018; Al-Yahyaee et al., 2018; Shrestha, 2019; Stavroyiannis et al., 2019).

The combination of DCCA and the MFDFA, the multifractal detrended cross-correlation analysis (MFDCCA, MFDXA, MF-X-DFA) (Zhou, 2008), was developed and implemented for the empirical studies of cryptocurrencies, stock prices, and crude oil markets (Zhang et al., 2018a,b; Alaoui et al., 2019; Ghazani and Khosravi, 2020). This method is a natural extension of the DCCA to multifrcatality, thus describing hierarchical fractal characteristics of cross-correlated non-stationary series. A different generalization of the DFA, the asymmetric DFA (A-DFA), was proposed by Alvarez-Ramirez et al. (2009) since financial assets may show different behavior in reaction to trends. The multifractal version was later proposed, namely, the asymmetric MFDFA (A-MFDFA) (Cao et al., 2013; Lee et al., 2017), and the further extension to cross-correlations is known as the multifractal asymmetric DCCA (MF-ADCCA) (Cao et al., 2014). The method of MF-ADCCA is a versatile tool that takes into account both the asymmetric structure and the multifractal scaling properties between the two series. An empirical study by Gajardo et al. (2018) applies the MF-ADCCA to price behaviors of BTC and leading conventional currencies, suggesting the presence and asymmetry of cross-correlations between them. Using the same approach, Kristjanpoller and Bouri (2019) find evidence of asymmetric multifractality between the main cryptocurrencies and the world currencies. These studies show that the MF-ADCCA approach is powerful for uncovering complex systems in cryptocurrency markets [3].

The algorithm of the A-MFDFA method (Cao et al., 2013) starts by calculating the profile, which is defined as $X(t) = \sum_{j=1}^{t}(x_j - \bar{x})$ for $t = 1,\ldots,N$, where $\bar{x}$ is the average over the entire return series $\{x_t : t = 1,\ldots,N\}$. Next, we divide the profile $X(t)$ and the original series x_t into $N_s = \lfloor N/s \rfloor$ non-overlapping segments of length s. If N is not a multiple of s, a short part of the profile may remain. To consider all the profile, the division is repeated starting from the other end of the data set, making $2N_s$ segments for both series.

Let $S_v = \{s_{v,i},\ i = 1,\ldots,s\}$ be the vth segment series of length s. For each seg-

[3] For more technical information and further discussion relevant to the detrending based multifractal methods, see Wątorek et al. (2021)

ment $v = 1,\dots,2N_s$, the local trend of the profile is calculated by fitting a least-square degree-2 polynomial y_v. In the same manner, the local least-square linear fit of the series $\hat{x}_{S_v}(i) = a_{S_v} + b_{S_v} i$ is estimated for each segment. The polynomial fit y_v is used to detrend the profile, and $\hat{x}_{S_v}$ is used to determine the direction of the original series. Positive (upward) or negative (downward) trends depend on the sign of the slope b_{S_v}.

The residual variance for each segment is calculated as:

$$F^2(s,v) := \frac{1}{s}\sum_{i=1}^{s}\{X[(v-1)s+i] - y_v(i)\}^2 \quad \text{for} \quad v = 1,\dots,N_s, \tag{1.3.1}$$

$$F^2(s,v) := \frac{1}{s}\sum_{i=1}^{s}\{X[N-(v-N_s)s+i] - y_v(i)\}^2 \quad \text{for} \quad v = N_s+1,\dots,2N_s. \tag{1.3.2}$$

The upward and downward q-th order fluctuation functions are calculated by taking the average over all segments as:

$$F_q^+(s) = \left\{\frac{1}{M^+}\sum_{v=1}^{2N_s}\frac{1+\operatorname{sgn}(b_{S_v})}{2}\left[F^2(s,v)\right]^{q/2}\right\}^{1/q}, \tag{1.3.3}$$

$$F_q^-(s) = \left\{\frac{1}{M^-}\sum_{v=1}^{2N_s}\frac{1-\operatorname{sgn}(b_{S_v})}{2}\left[F^2(s,v)\right]^{q/2}\right\}^{1/q}, \tag{1.3.4}$$

for any real value $q \neq 0$, and

$$F_0^+(s) = \exp\left\{\frac{1}{2M^+}\sum_{v=1}^{2N_s}\frac{1+\operatorname{sgn}(b_{S_v})}{2}\ln\left[F^2(s,v)\right]\right\}, \tag{1.3.5}$$

$$F_0^-(s) = \exp\left\{\frac{1}{2M^-}\sum_{v=1}^{2N_s}\frac{1-\operatorname{sgn}(b_{S_v})}{2}\ln\left[F^2(s,v)\right]\right\}, \tag{1.3.6}$$

for $q = 0$. $M^+ = \sum_{v=1}^{2N_s}\frac{1+\operatorname{sgn}(b_{S_v})}{2}$ and $M^- = \sum_{v=1}^{2N_s}\frac{1-\operatorname{sgn}(b_{S_v})}{2}$ respectively represent the numbers of segments with positive and negative trends under the assumption of $b_{S_v} \neq 0$ for all $v = 1,\dots,2N_s$, such that $M^+ + M^- = 2N_s$. Note that

$$F_q(s) = \left\{\frac{1}{2N_s}\sum_{v=1}^{2N_s}\left[F^2(s,v)\right]^{q/2}\right\}^{1/q} \quad \text{and} \quad F_0(s) = \exp\left\{\frac{1}{4N_s}\sum_{v=1}^{2N_s}\ln\left[F^2(s,v)\right]\right\} \tag{1.3.7}$$

correspond to the MFDFA method, which is equivalent to the case of overall trend in this study.

If the series x_k is long-range power-law correlated, then the power-law relationship $F_q^+(s) \sim s^{h^+(q)}$, $F_q^-(s) \sim s^{h^-(q)}$, and $F_q(s) \sim s^{h(q)}$ are satisfied, where the generalized Hurst exponents are calculated by performing a log-log linear regression against time scale s. There might exist crossover scales s^* separating regimes with different scaling exponents due to different regulation mechanisms on fast and slow time scales.

The order q decides which magnitude the fluctuation should be evaluated. Generalized Hurst exponents for $q > 0$, which are dominated by large fluctuations in the fluctuation function, reflect the behavior of larger fluctuations, while those for $q < 0$ reflect the behavior of smaller fluctuations. If $h(q)$ is independent of q, then the series is monofractal since the scaling behavior of the residual variance is identical for all segments. On the other hand, if the value differs depending on q, the series is multifractal where small and large fluctuations are described by different scaling exponents. It should be noticed that when $q = 2$, $h(q)$ corresponds to the Hurst exponent.

1.4 Modern Portfolio Theory

In this section, we summarize the basis of the Modern Portfolio Theory.

Modern Portfolio Theory (MPT) is a theoretical framework for portfolio construction that aims to maximize the expected return of a portfolio for a given level of risk, or equivalently minimize risk for a given level of expected return, by carefully choosing the proportions of various assets. It was first introduced by Harry Markowitz in 1952 (Markowitz, 1952), who won a Nobel Prize in Economics in 1990 for his work in this area. The MPT also suggests that investors should focus on the risk-return trade-off when making investment decisions and that they should optimize their portfolio based on their unique risk and return preferences.

Some of the essential features of the MPT are listed as follows:

- Mean-Variance Optimization (MV): A mathematical optimization technique to find the optimal portfolio that maximizes expected returns while minimizing risk, which is achieved by quantitatively modeling the portfolio's performance and calculating the mean (expected returns) and variance (risk) of each asset in the portfolio.

- Efficient Frontier: A graph that shows the optimal trade-off between risk and return for a given set of assets. The efficient frontier represents the set of portfolios that offer the highest expected return for a given level of risk, or the lowest level of risk for a given expected return.

- Capital Asset Pricing Model (CAPM): A financial model that describes the relationship between the expected return of an investment and the risk associated with that investment. The model is used to determine the expected return given the risk-free rate, the expected market return, and the security's beta. The beta measures whether its volatility in relation to the overall market is high or low.

- Correlation and Diversification: MPT emphasizes the importance of diversification in reducing portfolio risk. This is achieved by selecting assets with low correlation, which means that their returns do not move in the same direction. MPT uses the mathematical concept of correlation to measure the relationship between assets and to identify the most diversified portfolios.

- Risk Measures: MPT uses various mathematical risk measures such as standard deviation, variance, Sharpe ratio, tail risk, alpha, and beta to quantify the risk of a portfolio. These measures are used to compare the risk of different portfolios and to evaluate its performance over time.

The systematic and mathematical approach of the MPT for portfolio construction, with an emphasis on diversification, is widely acknowledged for its ability to reduce portfolio risk and increase returns through optimization techniques. However, it also has some limitations, such as assuming that the MPT lies in the EMH framework, that is, financial markets are efficient and all investors have access to the same information making rational decisions, which may not align with reality. Additionally, the MPT's reliance on historical data and disregard for other objectives such as social impact or market events can lead to misinterpretation of financial market behaviors.

To overcome the disadvantages of the MPT, the necessity of an alternative approach rises. One possible remedy may be to introduce the hypothesis framework of the FMH and allow for the existence of long-range correlations within risky assets and the fractal characteristics of their components (Kristoufek, 2018; Kristoufek and Ferreira, 2018; Tilfani et al., 2019, 2020; Chun et al., 2020; Zhang et al., 2022). The above work suggest the use of a fractal portfolio, which is a diversified investment strategy that seeks to achieve returns by investing in a variety of assets across multiple time frames. The belief that market movements are fractal and exhibit self-similar patterns over different time scales is the key to achieving the goal of reducing risk and increasing returns. The portfolio is designed to perform well in a specific market condition at different time horizons, such as short-term, medium-term, and long-term. By diversifying across different assets and time scales, the portfolio will be less affected by market fluctuations, i.e., market crashes and turbulence, and increase the likelihood of achieving positive returns over time. Therefore, the fractal portfolio is expected to be applied to quantitative investment strategies. Some work have applied this idea to traditional MPT, elevating the concepts of CAPM (Kristoufek, 2018; Kristoufek and

Ferreira, 2018; Tilfani et al., 2019, 2020) and MV (Chun et al., 2020; Zhang et al., 2022) to heterogeneous time scale dimensions.

In this research, we investigate the idea of MV optimization and enhance the model by incorporating the idea of different time scales into the risk measure to achieve a more realistic portfolio allocation strategy. At the same time, we provide supporting evidence of such a FMH framework, that is, we demonstrate that financial markets (as well as cryptocurrency markets) have a fractal pattern and investors react differently based on time, sales and market conditions. Specifically, we use information about fractality and multifractality from correlations between and within risky assets to enhance portfolio performance. The use of fractal optimization strategies illuminates the multiscale behaviors and heterogeneous properties that are not captured by the traditional MPT framework.

1.5 Outline of the thesis

We show here the outline of the thesis.

In Chapter 2, we first focus on developing the estimation procedure of stable distribution parameters so that the model can well describe fat-tail behaviors and scaling phenomena in cryptocurrency price returns. The estimation approach based upon the method of moments yields a simple procedure for estimating stable law parameters with the requirement of using momental points for the characteristic function, but the selection of points is only poorly explained and has not been elaborated. We propose a new characteristic function-based approach by introducing a technique of selecting plausible points, which could bring the method of moments available for practical use. Our method outperforms other state-of-art methods that exhibit a closed-form expression of all four parameters of stable laws. Finally, the applicability of the method is illustrated by using several data of financial assets. Numerical results reveal that our approach is advantageous when modeling empirical data with stable distributions.

In Chapter 3, we show that the behaviors of price fluctuations in emerging cryptocurrency markets can be characterized by a non-Gaussian Lévy's stable distribution with $\alpha \simeq 1.4$ under certain conditions on time intervals ranging roughly from 30 minutes to 4 hours. Our arguments are developed under quantitative valuation defined as a distance function using the Parseval's relation in addition to the theoretical background of the General Central Limit Theorem (GCLT). We also discuss the model-fitting for returns by employing the method based on likelihood ratios. Even though the cubic power-law model is a better fitting model than the Lévy's stable model in the tail part of returns, the Lévy's stable model outperforms the fit for the entire and wider range of returns. Our approach can be extended for further analysis of statistical properties and contribute to developing proper applications for financial modeling.

In Chapter 4, we investigate asymmetric multifractality and market efficiency of the major cryptocurrencies during the COVID-19 pandemic while accounting for different investment horizons. By applying the asymmetric multifractal detrended fluctuation analysis, we show that the outbreak affected the efficiency property of price behaviors differently between short- and long-term horizons. After the outbreak, the markets exhibited stronger multifractality in the short-term but weaker multifractality in the long-term. We also analyze asymmetric market patterns between upward and downward trends and between small and large price fluctuations and confirm that the outbreak has greatly changed the level of asymmetry in cryptocurrency markets.

In Chapter 5, we explore the price-volatility nexus in cryptocurrency markets and investigates the presence of asymmetric volatility effect between uptrend (bull) and downtrend (bear) regimes. The conventional GARCH-class models have shown that in cryptocurrency markets, asymmetric reactions of volatility to returns differ from those of other traditional financial assets. We address this issue from a viewpoint of fractal analysis, which can cover the nonlinear interactions and the self-similarity properties widely acknowledged in the field of econophysics. The asymmetric cross-correlations between price and volatility for Bitcoin (BTC), Ethereum (ETH), Ripple (XRP), and Litecoin (LTC) during the period from June 1, 2016 to December 28, 2020 are investigated using the MF-ADCCA method and quantified via the asymmetric DCCA coefficient. The approaches take into account the nonlinearity and asymmetric multifractal scaling properties, providing new insights in investigating the relationships in a dynamical way. We find that cross-correlations are stronger in downtrend markets than in uptrend markets for maturing BTC and ETH. In contrast, for XRP and LTC, inverted reactions are present where cross-correlations are stronger in uptrend markets.

In Chapter 6, we investigate the scale-dependent structure of asymmetric volatility effect in six representative cryptocurrencies: Bitcoin, Ethereum, Ripple, Litecoin, Monero, and Dash. By developing the dynamical approach of DFA-based fractal regression analysis, we detect whether the volatility of price changes is positively or negatively related to return shocks at different time scales. We find that the asymmetric volatility phenomenon varies by scale and cryptocurrency, and the structure is time-varying. Contrary to what is typically observed in equity markets, minor currencies show an “inverse” asymmetric volatility effect at relatively large scales, where positive shocks (good news) have a greater impact on volatility than negative shocks (bad news). The consequences are discussed in the context of who is trading in the market and heterogeneity of the investors.

In Chapter 7, we develop a portfolio strategy making use of the fractal properties and scale-dependent structure of cryptocurrency time series. The mean-

DCCA portfolio is known to consider the assets' nonlinearity and fractal characteristics by embedding the fractal correlation into the mean-variance criterion. Recent researches find that this approach often performs well with certain strategies under the assumption that scale preference of investors are constant. However, scale dependence may vary over time and reflect current market conditions. We examine whether accounting for changes in investors' scale preferences in response to market conditions improves portfolio performance. Our results support the potential effect of investor heterogeneity on portfolio risk reduction.

Chapter 2

Estimation of Stable Laws

This chapter is corresponds to paper 1 in the author's papers list.

2.1 Introduction

There are some challenges to overcome the analytic difficulties of stable distributions since the probability density function (PDF) is not always expressed in a closed form in terms of elementary functions. This is because the Fourier integral of the characteristic function (CF) defining the PDF cannot be written in a formula involving only elementary functions (Rocha et al., 2019), except for the special cases of Cauchy, Lévy, and Gaussian distributions, which have a closed formula of the PDF. Thus, the lack of closed form expression is a general issue when discussing stable distribution. Numerically approximated expressions of the PDF are known in symmetric cases based on hypergeometric functions, but those in unrestricted asymmetric cases are often too complex for estimating the parameters of the stable distribution (Crisanto-Neto et al., 2018). More practically, the estimation of all parameters is the most basic and necessary process for any application, but it remains to be one of the most controversial issues when attempting to detect stable laws. Numerous approaches have been studied for the parameter estimation. The primary approaches include the approximate maximum likelihood estimation (DuMouchel, 1973; Brorsen and Yang, 1990; Mittnik et al., 1999; Nolan, 2001), the bayesian based method (Koblents et al., 2016), the quantile method (QM) (Fama and Roll, 1971; McCulloch, 1986), the fractional lower order moment (FLOM) method (Ma and Nikias, 1995; Kuruoglu, 2001), the method of log-cumulant (MLOC) (Nicolas and Anfinsen, 2001; Pastor et al., 2016), the characteristic function-based (CF-based) method (Koutrouvelis, 1980; Press, 1972; Bibalan et al., 2017; Krutto, 2016, 2019), and their hybrid combinations. Many of them tend to have different kinds of drawbacks, such as restrictions of parameter ranges, complex estimation algorithms, high computational costs, requirements of larger datasets, and low accuracy. To the best of our knowledge, the FLOM, MOLC, and QM and some class of the CF-based methods (Press, 1972; Bibalan et al., 2017; Krutto, 2016, 2019) provide closed-form estimators of stable laws.

The CF-based method is perhaps the largest classification group, including a variety of methods and approaches developed under different techniques. In particluar, Press (1972) presents the *method of moments*, which offers a simple approach to estimate all four parameters of stable distribution using the characteristic function evaluated at four arbitrary points. The biggest advantage of this method is that it is likely to have less drawbacks compared to other primary methods, but it carries a fundamental problem. Without appropriate points given, the performance is poor, and unfortunately Press leaves unsolved the crucial idea about the choice of points at which the CF should be evaluated. The selection of the points has long been an open question, although several studies have made an effort to improve the method of moments by reducing the use of points from four to two and discussing their choice. Krutto (2016, 2019) provides some guidance on how the two positive points should be chosen through empirical searches relying on the cumulant function. Bibalan et al. (2017) focus on the absolute value of the CF and suggest an algorithmic approach where a positive point is fixed for each scaling parameter. They show accurate estimates within certain parameter ranges, but their method fails to support a wider range of parameter spaces. Thus, these approaches are not comprehensive, so that the method of detecting more appropriate points related to the CF is required for practical uses.

In this chapter, we propose an effective and practical method for estimating stable laws. We greatly improve the method of moments by introducing a new technique for the selection of two positive points at which the CF is evaluated. The technique is developed over the extension of both algorithmic and empirical search approaches. The idea of empirical search plays a role in determining the scaling related estimates, which take crucial responsibility for indicating statistical values derived in the estimation process, whereas the concept of the algorithmic approach yields various ideas of inferences based on the absolute value of the CF. Our approach realizes the possibility of choosing different values of points depending on the index parameter α, which is a new perspective. We assess and compare the performance of our method to those of other methods in terms of the Mean Squared Error (MSE) criterion and the Kolmogorov-Smirnov (KS) distance. Our proposed method generally outperforms all the other state-of-art methods that exhibit closed-form expressions for all four parameters of stable laws. It is practically straightforward and assures that there is no restriction of parameter ranges, except for $\alpha = 1$ due to the discontinuous form of the one-parameterization

CF. Finally, we apply our method to price fluctuation behaviors of several financial assets to examine the appropriateness for practical uses.

This chapter is organized as follows. Section 2 shows preliminaries on stable distribution and its basic properties. We follow in the next section to describe the existing methods for estimating the parameters of stable laws. In section 4 we propose a new technique of the CF-based parameter estimation method. The arguments for the selection of points at which the CF should be evaluated are discussed. In section 5 we report the performance with the comparison to other representative methods and present that our method provides accurate estimates of stable distribution. The last section shows application to financial data and confirms that our method is applicable for empirical studies.

2.2 Estimation Methods

This section gives an overview of the methods for the parameter estimation of the stable distribution. We review two major methods, both of which are considered as an analytical approach that provides a closed-form expression of the estimates— the quantile method and the characteristic function-based method (CF-based method). Several different approaches are explained for the CF-based method.

2.2.1 Quantile method

McCulloch (1986) proposes the use of five sample quantiles $x_{0.05}, x_{0.25}, x_{0.5}, x_{0.75}$, and $x_{0.95}$ as an informative measure for estimating the four parameters of stable laws, known as the quantile method (QM). He improves the former method of Fama and Roll (1971) by eliminating bias in estimates and relaxing estimation restrictions. The idea is to calculate the functions $\phi_i(\alpha,\beta)(i=1,2,3,4)$, where the relationships between the function values and the parameters are already studied and known beforehand. The method first sets out to estimate α and β by using the functions $\phi_1(\alpha,\beta)$ and $\phi_2(\alpha,\beta)$ independent of both γ and δ defined as

$$\phi_1(\alpha,\beta) = \frac{x_{0.95}-x_{0.05}}{x_{0.75}-x_{0.25}} \tag{2.2.1}$$

$$\phi_2(\alpha,\beta) = \frac{(x_{0.95}-x_{0.5})-(x_{0.5}-x_{0.05})}{x_{0.95}-x_{0.05}}. \tag{2.2.2}$$

Equation (2.2.1) refers to the measure of fat-tail behaviors with the focus on estimating α, and equation (2.2.2) is a measure of skewness effects with the focus on estimating β. With empirical values of sample quantiles and employing linear interpolation with tabular look-ups, the estimates $\hat{\alpha}, \hat{\beta}$ are inversely obtained. To avoid $\hat{\alpha}$ being larger than 2, outside the parameter range, $\hat{\phi}_1 = \frac{(\hat{x}_{0.95}-\hat{x}_{0.5})-(\hat{x}_{0.5}-\hat{x}_{0.05})}{\hat{x}_{0.95}-\hat{x}_{0.05}}$ can be no larger than the upper range 2.439, which corresponds to the case of $\alpha = 2$ (note that β is not identified in this case).

Next, the scale and location parameter γ and δ can be estimated using the functions defined as

$$\phi_3(\alpha,\beta) = \frac{x_{0.75} - x_{0.25}}{\gamma} \tag{2.2.3}$$

$$\phi_4(\alpha,\beta) = \frac{\mu - x_{0.5}}{\gamma} + \beta \tan\left(\frac{\pi\alpha}{2}\right). \tag{2.2.4}$$

The function $\phi_3(\alpha,\beta)$ indicates the standardized form of sample sizes for the middle part of distribution. Since it does not depend on γ nor δ, the value can be informed by tabular look-ups based on α and β, which the relations are studied and known beforehand. After calculating $\hat{\gamma} = \frac{\hat{x}_{0.75}-\hat{x}_{0.25}}{\hat{\phi}_3(\hat{\alpha},\hat{\beta})}$ in equation (2.2.3), the location parameter δ can be estimated from equation (2.2.4) using the values $\hat{\phi}_4(\hat{\alpha},\hat{\beta})$ and $\hat{\gamma}$. The relations of the parameter values and the function value $\phi_4(\alpha,\beta)$ are again, studied and known beforehand. In the case of $\alpha = 1$, $\phi_4(\alpha,\beta)$ diverges and we cannot obtain the estimates for δ. McCulloch therefore suggests a complicated approach to overcome the discontinuity of the stable CF. The method improves other issues and provides accurate estimates, however, it has parameter restrictions and can be applied only when $\alpha \geq 0.6$.

2.2.2 Characteristic function-based method

The CF-based method relies on the use of a consistent estimator of the CF $\varphi(k)$ for any fixed k. The advantage of this method essentially lies in the fact that the stable CF can be expressed explicitly, making discussions straightforward compared to methods based on other distribution forms. Under the assumption that given data $X_n\,(n = 1,2,\ldots,N)$ are *ergodic* (Arnol'd and Avez, 1968), the CF is obtained empirically by the following equation,

$$\hat{\varphi}(k) = \frac{1}{N}\sum_{n=1}^{N} \mathrm{e}^{ikX_n}. \tag{2.2.5}$$

There are several approaches for estimating parameters of stable laws that take advantage of the explicit form of CF. Koutrouvelis (1980) proposed a regression-type approach, which employs the iteration of two regression runs. Moreover, the regression of the method requires different values of initial points k depending on initial estimates of the parameters and sample sizes. The number of points necessary for the regression also varies over initial conditions. Although the accuracy of β is unsatisfactory in some cases, the method generally shows accurate estimates of α, and hence it is often suggested as a practical method for empirical analysis (Wang et al., 2015; Kateregga et al., 2017). However, some studies compare the method to McCulloch's quantile method and report that the regression-type method does not significantly improve the classical quantile method (Akgiray and Lamoureux, 1989; Garcia et al., 2011), especially for α smaller than 1. Other studies simplified the method by eliminating the iteration process and fixing the initial points to some extent, but still leaves behind the issues of estimating when α is small (Kogon and Williams, 1998; S. Borak, 2005). We do not consider the regression-type approach in this study as the method generally relies on iteration and the estimates cannot be written analytically.

Another approach is based on the method of moment (Press, 1972), which was later remodeled and simplified with the use of two given points of the CF (Krutto, 2016; Bibalan et al., 2017; Krutto, 2019). Starting off with the CF with the points k_0 and k_1, taking the absolute value cancels out the effect of parameters β and δ, and we obtain

$$\begin{cases} |\varphi(k_0;\alpha,\beta,\gamma,\delta)| = \exp(-\gamma^\alpha |k_0|^\alpha) \\ |\varphi(k_1;\alpha,\beta,\gamma,\delta)| = \exp(-\gamma^\alpha |k_1|^\alpha). \end{cases} \tag{2.2.6}$$

Taking the cumulant function, which is the natural logarithm of the CF, leads to the same discussion neutralizing the effect of parameters β and δ. The equation $\ln\varphi = \ln|\varphi| + j(\arg\varphi + 2n\pi)$ implies that the real part of the cumulant function corresponds to the natural logarithm of the absolute value of CF, shown as

$$\begin{cases} \Re\left\{\ln\varphi(k_0;\alpha,\beta,\gamma,\delta)\right\} = \ln|\varphi(k_0;\alpha,\beta,\gamma,\delta)| = -\gamma^\alpha |k_0|^\alpha \\ \Re\left\{\ln\varphi(k_0;\alpha,\beta,\gamma,\delta)\right\} = \ln|\varphi(k_1;\alpha,\beta,\gamma,\delta)| = -\gamma^\alpha |k_1|^\alpha, \end{cases} \tag{2.2.7}$$

for any value of k. We consider only the positive values for convenience, since the CF is a symmetric function. By solving the above equations simultaneously, parameters α and γ can be estimated shown as

$$\hat{\alpha} = \frac{\ln\left(-\Re\left\{\ln\hat{\varphi}(k_0)\right\}\right) - \ln\left(-\Re\left\{\ln\hat{\varphi}(k_1)\right\}\right)}{\ln k_0 - \ln k_1}, \tag{2.2.8}$$

$$\hat{\gamma} = \exp\left\{\frac{\ln k_0 \ln\left(-\Re\left\{\ln\hat{\varphi}(k_1)\right\}\right) - \ln k_1 \ln\left(-\Re\left\{\ln\hat{\varphi}(k_0)\right\}\right)}{\ln\left(-\Re\left\{\ln\hat{\varphi}(k_0)\right\}\right) - \ln\left(-\Re\left\{\ln\hat{\varphi}(k_1)\right\}\right)}\right\}. \tag{2.2.9}$$

Since the one-parameterization form in equation (1.2.2) is discontinuous at $\alpha = 1$, the estimation of the remaining parameters β and δ is divided into two cases. When $\alpha \neq 1$, the cumulant function of stable distributions with the points $k_0, k_1 > 0$ are

$$\begin{cases} \ln\varphi(k_0;\alpha,\beta,\gamma,\delta) = -\gamma^\alpha {k_0}^\alpha + i\left[\delta k_0 + \gamma^\alpha {k_0}^\alpha \beta \tan\left(\frac{\pi\alpha}{2}\right)\right] \\ \ln\varphi(k_1;\alpha,\beta,\gamma,\delta) = -\gamma^\alpha {k_1}^\alpha + i\left[\delta k_1 + \gamma^\alpha {k_1}^\alpha \beta \tan\left(\frac{\pi\alpha}{2}\right)\right]. \end{cases} \tag{2.2.10}$$

As we need the information of the parameters β and δ, we take the imaginary part. Then the parameters β and δ are estimated by solving the above equations simultaneously and using the estimates $\hat{\alpha}$ and $\hat{\gamma}$:

$$\hat{\beta} = \frac{k_1 \Im\left\{\ln\hat{\varphi}(k_0)\right\} - k_0 \Im\left\{\ln\hat{\varphi}(k_1)\right\}}{\hat{\gamma}^{\hat{\alpha}} \tan\left(\frac{\pi\hat{\alpha}}{2}\right)({k_0}^{\hat{\alpha}} k_1 - {k_1}^{\hat{\alpha}} k_0)} \tag{2.2.11}$$

$$\hat{\delta} = \frac{{k_1}^{\hat{\alpha}} \Im\left\{\ln\hat{\varphi}(k_0)\right\} - {k_0}^{\hat{\alpha}} \Im\left\{\ln\hat{\varphi}(k_1)\right\}}{k_0 {k_1}^{\hat{\alpha}} - k_1 {k_0}^{\hat{\alpha}}}. \tag{2.2.12}$$

In the case of $\alpha = 1$, the CF takes a discontinuous form and the cumulant functions are written as

$$\begin{cases} \ln\varphi(k_0; 1, \beta, \gamma, \delta) = -\gamma k_0 + i\left[\delta k_0 - \beta \frac{2}{\pi} \ln k_0\right] \\ \ln\varphi(k_1; 1, \beta, \gamma, \delta) = -\gamma k_1 + i\left[\delta k_1 - \beta \frac{2}{\pi} \ln k_1\right]. \end{cases} \tag{2.2.13}$$

Then the parameters are estimated by solving the above equations simultaneously as well:

$$\hat{\beta} = \frac{\pi}{2} \frac{k_1 \Im\left\{\ln\hat{\varphi}(k_0)\right\} - k_0 \Im\left\{\ln\hat{\varphi}(k_1)\right\}}{\hat{\gamma} k_0 k_1 (\ln k_1 - \ln k_0)} \tag{2.2.14}$$

$$\hat{\delta} = \frac{k_1 \Im\left\{\ln\hat{\varphi}(k_0)\right\} \ln k_1 - k_0 \Im\left\{\ln\hat{\varphi}(k_1)\right\} \ln k_0}{k_0 k_1 (\ln k_1 - \ln k_0)}. \tag{2.2.15}$$

For simplicity, we express the estimates as a function of given points k_0 and k_1 as follows:

$$\hat{\alpha} = F_\alpha(k_0, k_1) \tag{2.2.16}$$

$$\hat{\gamma} = F_\gamma(k_0, k_1) \tag{2.2.17}$$

$$\hat{\beta} = F_\beta(k_0, k_1, \hat{\alpha}, \hat{\gamma}) \tag{2.2.18}$$

$$\hat{\delta} = F_\delta(k_0, k_1, \hat{\alpha}), \tag{2.2.19}$$

where $\hat{\beta}$ and $\hat{\delta}$ additionally needs the information of the estimates $\hat{\alpha}$ and $\hat{\gamma}$. Sometimes, the estimates can possibly outrange the parameter spaces $\alpha \in (0, 2]$, $\beta \in [-1, 1]$, and $\gamma > 0$, especially when the true parameters are close to the borders. In such cases, the parameters are set to the closet border, except for α and γ, the estimates are set no lower than 0.01. Applications with other parameterizations use slightly different forms of CF, but the stable parameters are estimated essentially by the same procedure as explained above. For the zero-parameterization, which is another common parameterization form, the CF is replaced to its corresponding form shown in equations (1.2.3) and (1.2.4) for equations (2.2.6) and (2.2.10) (or (2.2.13)). For parameterization with a different definition of the scaling parameter written as $c\,(=\gamma^{\alpha})$ (Nikias and Shao, 1995; Bibalan et al., 2017; Liu et al., 2018), Bibalan et al. (2017) presents an alternative procedure for the estimation. They first directly obtain the scaling parameter c from taking the absolute value of the empirical CF, or the real part of the cumulant function as

$$\hat{c} = -\ln|\hat{\varphi}(1)| = -\Re\left\{\ln\hat{\varphi}(1)\right\}. \tag{2.2.20}$$

Next α is estimated as shown in equation (2.2.8). Then, the scale parameter in our criterion, $\hat{\gamma}$, is obtained as,

$$\hat{\gamma} = \exp\left(\frac{\ln\hat{c}}{\hat{\alpha}}\right). \tag{2.2.21}$$

The remaining parameters β and δ are then estimated straightforwardly as similar to the case of the one-parameterization form. By replacing $\hat{\gamma}^{\hat{\alpha}}$ to $\hat{c}$ in equations (2.2.11) and (2.2.12) (or equations (2.2.14) and (2.2.15)), and using the points k_0 and k_1 give the estimates.

2.3 Proposed Approach

In this section, we make an improvement of the CF-based method by discussing how the points related to the CF should be chosen. We propose a technique that provides a flexible selection of the points. We also clarify the difference of how the points are selected between our proposal and the procedures in other existing CF-based methods.

2.3.1 Inference of point k_1

Two positive points of the CF, k_0 and $k_1 (k_0 \neq k_1)$, are ought to be selected to identify all four parameter estimates. As mentioned before, the absolute value of the CF in equation (2.2.6) is independent of the skew and location parameters for any k, and provides information of α and γ. When $k = 1/\gamma$ is satisfied, the absolute value of the CF takes a constant value

$$\left|\varphi\left(1/\gamma\right)\right| = \mathrm{e}^{-1}. \tag{2.3.1}$$

The advantage of setting $k = 1/\gamma$ as one of the candidate points is to reduce any estimation bias influenced by certain parameter values since we expect to get a constant estimate which is independent of all four parameters. When $\gamma \gg 1$, however, empirically obtained values can cause significant estimation errors for the scale parameter in equation (2.3.1) (Krutto, 2019; Paulson et al., 1975). Therefore, we first consider a temporary estimate of the scaling parameter, $\tilde{\gamma}$, just in case the data exhibits scale far from the standardized form ($\gamma = 1$).

Take the natural logarithm of equation (2.3.1). The temporary estimate can be obtained by approximately solving the equation that numerically satisfies

$$\ln\left|\hat{\varphi}\left(1/\tilde{\gamma}\right)\right| \simeq -1, \tag{2.3.2}$$

using a simple one-dimensional search function (Brent, 2013), or any other optimization procedure. Our rough estimate $\tilde{\gamma}$ is then used for standardizing, or pre-standardizing, the candidate points. Specifically, point k_1 is set to $1/\tilde{\gamma}$, where $\ln|\varphi(k_1)|$ empirically takes -1.

As explained above, pre-standardization is preferred especially when we suspect that datasets have too large or small scales. Whenever a new set of points is required for the parameter estimation process, we conduct pre-standardization. Point k_1 is replaced to $1/\check{\gamma}$, where $\check{\gamma}$ is the latest scaling parameter estimate available at that time.

2.3.2 Inference of point k_0

For the argument of selecting point $k_0 > 0$, which is perhaps the most important proposal in our study. We focus on the absolute value of the CF. Bibalan et al. (2017) proposed to calculate the distance between two absolute values of CFs with different index parameters α, the Gaussian case ($\alpha = 2$) and the Cauchy case ($\alpha = 1$). They set $k_0 > 0$ to the point which corresponds to the maximum distance and the other point to $k_1 = 1$. Although the absolute CF changes depending on the index parameter α, their approach considers a fixed distance and essentially chooses an identical point for any value of $\alpha \in (1,2]$. In addition, the distance they consider does not account for the case of $\alpha \in (0,1]$.

Our approach is an extension of Bibalan et al. (2017), and provides a more generalized technique of selecting the points. We deal with the problem that the distance between two absolute values of CFs can vary depending on the parameters. The basic idea is to find the point where the absolute CF, $|\varphi(k;\alpha)|$, presents the *maximum sensitivity* with respect to α. In other words, we discuss the point where the distance between the absolute CF of index parameter α, $|\varphi(k;\alpha,\beta,\gamma,\delta)|$, and the absolute CF of $\alpha + \Delta\alpha$, $|\varphi(k;\alpha+\Delta\alpha,\beta,\gamma,\delta)|$, shows the largest distance. Such a point is considered as k_0 in our study.

To make our discussion more simple, we consider the absolute CF as a function of variable η:

$$|\varphi(k;\alpha,\beta,\gamma,\delta)| = \exp(-\eta^{\alpha}),$$

where $\eta = \gamma k$ ($k > 0$) is a newly introduced variable which depends on γ and k. The distance can be expressed as $\left|\exp(-\eta^{\alpha+\Delta\alpha}) - \exp(-\eta^{\alpha})\right|$. The candidate point for $\eta_0 = \gamma k_0$, where the maximum distance is achieved, can be calculated by

$$\frac{d}{d\eta}\left|\exp(-\eta^{\alpha+\Delta\alpha}) - \exp(-\eta^{\alpha})\right| = 0, \ \eta > 0. \tag{2.3.3}$$

Solving this equation for $\eta > 0$ yields two solutions, $\eta \in (0, 1/\gamma)$ and $\eta \in (1/\gamma, \infty)$. For both points, the absolute value of CF shows the largest ratio of change in a local sense. The smaller point $\eta \in (0, 1/\gamma)$ is employed, because the distance at the smaller point tends to have larger values than that at the larger point $\eta \in (1/\gamma, \infty)$, which enables us to estimate α and γ in a more desirable and informative manner. Another reason is that smaller $|k|$ is preferred rather than larger $|k|$. As $|k| \to 0$, the asymptotic variance of the empirical cumulant function decreases (Krutto, 2019). With empirical CF obtained by i.i.d. distributed datasets, the relation

$$E\left[\left|\varphi_N(k)\right|^2\right] = |\varphi(k)|^2 + \frac{1}{N}\left(1 - |\varphi(k)|^2\right), \tag{2.3.4}$$

holds (Kakinaka and Umeno, 2020a), which implies that as k becomes larger, the empirical absolute CF $|\varphi_N(k)|$ is likely to be subject to sample errors. Thus, the smaller $\eta = \gamma k$ should be considered in this study.

The above discussion implies that k should be set close to zero (but not at zero because then the CF takes a constant value and no information of the parameters will be provided). But at the same time, the employed smaller point is standapart from zero to some extent, so that the empirical CF will be more or less exposed by sample errors. Therefore, the choice of points derived from equation (2.3.3) is unsatisfactory, and hence the distance $\left|\exp(-\eta^{\alpha+\Delta\alpha}) - \exp(-\eta^{\alpha})\right|$ should be modified. To reduce the effect of sample errors, we introduce a weight function $w(\eta)$ that decreases monotonically as η becomes larger (note that the introduced variable $\eta = \gamma k$ has a linear relationship with k).

Using the weight function $w(\eta)$, we now introduce a weighted distance

$$\left|\exp(-\eta^{\alpha+\Delta\alpha}) - \exp(-\eta^{\alpha})\right| w(\eta),$$

for $\eta > 0$. For convenience, we employ $w(\eta) = \exp(-\tau|\eta|)$, where $\tau > 0$, since the CF exhibits an exponential form. This choice leads to the association of the weighted distance with a statistical measure used for goodness-of-fit tests, developed by Matsui and Takemura (2007). They propose the following test statistic based on empirical CFs,

$$\begin{aligned} D_{N,\kappa} &:= N\int_{-\infty}^{\infty}\left|\hat{\varphi}(t) - \exp\left(-|t|^{\alpha}\right)\right|^2 h(t)dt, \\ h(t) &= \exp\left(-\kappa|t|\right), \ \kappa > 0, \end{aligned} \tag{2.3.5}$$

where $h(t)$ is a monotonically decreasing weight function. $D_{N,\kappa}$ denotes the weighted L^2-distance between the empirical CF and the symmetric standardized stable CF $\varphi(t;\alpha,0,1,0)$. This weighted L^2-distance can be associated with the weighted distance we are considering now.

Taking the absolute value of a CF yields again a standardized form of a CF with $\beta = 0$ and $\delta = 0$:

$$\exp(-\eta^{\alpha}) = |\varphi(k;\alpha,\beta,\gamma,\delta)| = \varphi(\eta;\alpha,0,1,0).$$

Thus, the absolute values of CF with index parameter α and $\alpha+\Delta\alpha$ are equivalent to the symmetric standardized stable CFs, $\varphi(\eta;\alpha,0,1,0)$ and $\varphi(\eta;\alpha+\Delta\alpha,0,1,0)$, respectively. The weighted L^2-distance between these CFs essentially coincides $D_{N,\kappa}$, when the weight function satisfies

$$w(\eta) = \sqrt{h(\eta)},$$

for $\eta > 0$. In this case, the difference between the CFs can be evaluated more accurately with the background of a meaningful measurement. Following Matsui and Takemura (2007), the asymptotic distribution of $D_{N,\kappa}$ is numerically evaluated and the critical values of the test statistics are approximately obtained. Through computational simulation, they provide evidence that the test is most powerful when $\kappa = 5.0$ ($h(\eta) = \exp(-5|\eta|)$), especially for heavy tailed distributions. Thus, our choice of the weight function is $w(\eta) = \exp(-2.5|\eta|)$, since $\tau = \kappa/2$. Other weight functions such as $w(\eta) = \exp(-|\eta|)$ and $w(\eta) = \exp(-\eta^2)$ (Paulson et al., 1975; Heathcote, 1977) can be employed, but lacks a conclusive evidence for the use of these alternatives.

With the weight function, the candidate points $\eta > 0$ are calculated by solving the following equation:

$$\begin{aligned} g(\alpha,\eta) &= \frac{d}{d\eta}\left\{\left(\exp(-\eta^{\alpha+\Delta\alpha}) - \exp(-\eta^{\alpha})\right)\cdot\exp(-\tau\eta)\right\} \\ &= 0, \end{aligned} \tag{2.3.6}$$

where $\tau = 2.5$. Then we have

$$\begin{aligned} g(\alpha,\eta) &= (\alpha\eta^{\alpha-1}+\tau)\exp(-\eta^{\alpha}-\tau\eta) \\ &\quad - \left((\alpha+\Delta\alpha)\eta^{\alpha+\Delta\alpha-1}+\tau\right)\exp(-\eta^{\alpha+\Delta\alpha}-\tau\eta). \end{aligned} \tag{2.3.7}$$

For convenience, $\Delta\alpha$ is set to 0.01 for all cases in this study. Equation $g(\alpha,\eta) = 0$ indicates the relationship between the index parameter α and point η that exhibits the maximum rate of a change, or the maximum sensitivity, of the absolute CF with respect to α.

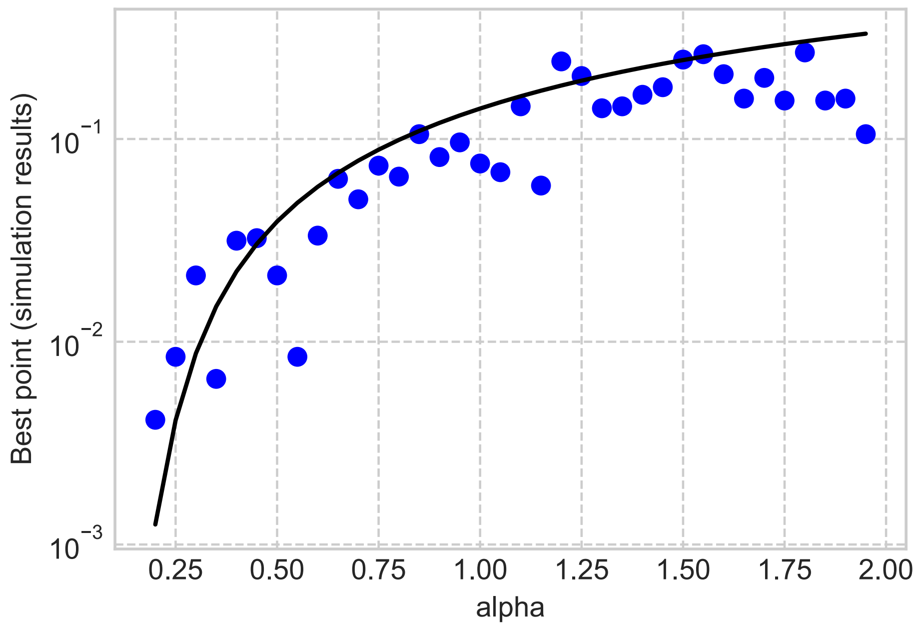

Figure 2.1: The theoretical relationship between α and η based on our proposed selection approach, $g(\alpha,\eta) = 0$ in equation (2.3.6), is shown in the solid black line. The blue plot shows the simulated results for the best point with the minimum MSE for α and β over 100 simulations. We consider the MSE of $\alpha + \frac{1}{10}\beta$ because the accuracy of β is generally worse roughly by ten times than the accuracy of α, and also that β estimates are usually susceptible to α estimates (McCulloch, 1986; Koutrouvelis, 1980; Bibalan et al., 2017). The simulation is implemented for each value of α ranging within the parameter space of 0.2 to 1.95.

There could exist some relationship between α and η since they are interrelated due to $g(\alpha,\eta) = 0$. When some estimate $\hat{\alpha}$ is given, the corresponding point is obtained by computing η that satisfies $g(\hat{\alpha},\eta) = 0$, and vice versa (the corresponding parameter α of a given point $\hat{\eta}$ can be calculated by computing the equation $g(\alpha,\hat{\eta}) = 0$). As we have discussed previously in this subsection, we focus on the point closer (smaller) to zero out of the two candidates of the calculated points from equation (2.3.6). Figure 2.1 ascertains whether our approach of equation (2.3.6) correctly estimates the parameters of stable distribution. The model clearly characterizes the distinctive relationship between α and η, which are empirically verified via simulation using synthetic data generated from random stable variables (Weron, 1996). This indicates that our selection of points is valid for identifying desired points in the estimation process.

In practice, α is unknown. Hence the selection of point $\eta_0 = \gamma k_0$ is undecidable, so that the parameters for the stable law cannot be estimated directly. To cope with this problem, we first aim to get a rough estimate of α calculated by using the temporary scale estimate $\tilde{\gamma}$. The rough estimate is considered poor as the estimation method, but it plays a role in starting off the estimation process with reasonable initial values. The accuracy of both points ($\eta_0 = \gamma k_0$ and $\eta_1 = \gamma k_1$) and the parameters $(\alpha, \beta, \gamma, \delta)$ can be improved by alternating searches of α and η from our relation model $g(\alpha, \gamma) = 0$ several times to get sophisticated estimates. With estimates η_0 and η_1, the four parameters are ultimately calculated.

2.3.3 Estimation procedures

Here we present our proposed algorithm for the estimation of all four parameters of stable laws by utilizing the relationship between α and η. Regarding the fact that empirically obtained estimates occur substantial errors induced by $\gamma \gg 1$, we conduct a pre-standardization with k replaced to $\eta = \gamma k$. Using the expressions of the estimates in equations (2.2.16) (2.2.17) (2.2.18) (2.2.19), our algorithm is written as follows:

1. Compute a temporary estimate $\tilde{\gamma}_{\text{temp}}$ from sample data X_n $(n = 1, 2, \ldots, N)$ that satisfies the equation,

$$\ln \left| \frac{1}{N} \sum_{n=1}^{N} e^{iX_n/\gamma} \right| \Bigg|_{\gamma = \tilde{\gamma}_{\text{temp}}} = -1.$$

2. Set

$$\begin{cases} \tilde{k}_0 = \xi / \tilde{\gamma}_{\text{temp}} \\ \tilde{k}_1 = 1 / \tilde{\gamma}_{\text{temp}}, \end{cases}$$

   where ξ is any initial value of $\xi \in (0, 1)$.

3. Make a rough estimate of α and γ from

$$\begin{aligned} \tilde{\alpha} &= F_\alpha(\tilde{k}_0, \tilde{k}_1) \\ \tilde{\gamma} &= F_\gamma(\tilde{k}_0, \tilde{k}_1), \end{aligned}$$

   respectively, where $F_\alpha(\cdot, \cdot)$ and $F_\gamma(\cdot, \cdot)$ are given in equations (2.2.16) and (2.2.17).

4. Compute $\tilde{\eta}$ that satisfies $g(\tilde{\alpha}, \eta)\big|_{\eta = \tilde{\eta}} = 0$, where $g(\cdot, \cdot)$ is given in equation (2.3.7).

5. Recalculate the points associated with $\tilde{\eta}$,

$$\begin{cases} \tilde{k}_0 = \tilde{\eta} / \tilde{\gamma} \\ \tilde{k}_1 = 1 / \tilde{\gamma}, \end{cases}$$

6. Estimate α and γ as

$$\hat{\alpha} = F_\alpha(\tilde{k}_0, \tilde{k}_1)$$
$$\hat{\gamma} = F_\gamma(\tilde{k}_0, \tilde{k}_1),$$

7. Compute $\tilde{\eta}$ that satisfies $g(\hat{\alpha}, \eta)\big|_{\eta=\hat{\eta}} = 0$.

8. Recalculate the points associated with $\hat{\eta}$,

$$\begin{cases} \hat{k}_0 = \hat{\eta}/\hat{\gamma} \\ \hat{k}_1 = 1/\hat{\gamma}, \end{cases}$$

9. Finally, we estimate the parameters α and γ as

$$\hat{\alpha} = F_\alpha(\hat{k}_0, \hat{k}_1)$$
$$\hat{\gamma} = F_\gamma(\hat{k}_0, \hat{k}_1),$$

10. Estimate the parameters β and δ from the functions $F_\beta(\cdot,\cdot,\cdot,\cdot)$ and $F_\delta(\cdot,\cdot,\cdot)$ given in equations (2.2.18) and (2.2.19), as

$$\hat{\beta} = F_\beta(\hat{k}_0, \hat{k}_1, \hat{\alpha}, \hat{\gamma})$$
$$\hat{\delta} = F_\delta(\hat{k}_0, \hat{k}_1, \hat{\alpha}),$$

which leads to the estimates of all four parameters of stable laws.

2.4 Numerical Assessments

In this section, we show numerical assessments for the estimation of stable laws. We compare the performances of our proposal approach to other state-of-art approaches using the MSE and the KS-distance. The comparison is studied for three approaches. We focus on the approaches of characteristic function-based methods presented by Bibalan et al. (2017) and Krutto (2019). We also compare with the traditional QM method (McCulloch, 1986; Fama and Roll, 1971) explained in subsection 3.1, to provide a benchmark with a well-known criterion. Note that all three approaches above exhibit closed-form expressions for all four estimates of stable parameters.

Bibalan et al. (2017) have shown that their approach generally outperforms other methods that yield a closed-form expression, such as the FLOM, the QM, and the MOLC. Krutto (2019) also compares the performances with several well-known methods and concludes that the method gives accurate estimates. Since both of them belong to the family of the CF-based method, the selection of the points k_0 and k_1 plays an important role. In Bibalan et al. (2017), k_1 is set to 1. Point k_0 is always set to where the point shows the maximum distance between the absolute Gaussian CF and the absolute Cauchy CF, by using the estimates of γ^α which they are calculated beforehand. It should be mentioned that the CF in this case poses a alternative definition of the scaling parameter, so we eventually obtain γ in the last procedure in equation (2.2.21). On the other hand, Krutto (2019) suggests to employ two points that satisfies

$$\begin{cases} \ln|\hat{\varphi}(k_0)| = -0.1 \\ \ln|\hat{\varphi}(k_1)| = -0.5, \end{cases}$$

under empirical searches. We examine the performance for each parameter of stable distribution in addition to the fit with the entire estimated stable distribution. We also refer to the effects of sample sizes for each estimation method. For all the simulations in this chapter, we generate $L = 500$ synthetic data of $N = 10000$ i.i.d. random stable samples. Synthetic random data sequences following a stable distribution can be generated by algorithms constructed by Chambers et al. (1976), Weron (1996), and Umeno (1998). Umeno (1998) generates random stable variables based on the superposition of chaotic processes. The classical method of Chambers et al. (1976) is widely known as the pioneer of all the methods, which the algorithm was reorganized and corrected. Weron's algorithm is our choice of method, which is simple and is the fastest in calculation.

2.4.1 Performance of parameter estimates

The performance of the estimated parameters are examined by the MSE criterion:

$$\text{MSE}(\theta) = \frac{1}{L}\sum_{l=1}^{L}\left(\theta - \hat{\theta}_l\right),$$

where θ and $L = 500$ is the parameter of stable laws and the number of times the simulation is implemented, respectively. We calculate the MSE of all four parameters and evaluate each parameter individually.

Table 2.1 shows the simulation results of the MSE associated with the estimate bias for each parameter. We consider the cases of parameters with $\alpha = 0.5, 1.5, 1.8$ and $\beta = 0, 0.5$, all with a standardized form of $\gamma = 1$ and $\delta = 0$. Note that for the QM, the method has parameter restrictions of $\alpha \geq 0.6$ and hence the cases with α smaller than 0.6 can not be implemented. Our proposed approach generally provides the most accurate estimation with the smallest MSE. Especially for the index parameter α and δ, our approach significantly improves the accuracy of the estimates. For some cases as in large values of $\alpha = 1.8$, however, the method fails to show the best performance. One possible reason may be related to the argument that the CF-based method reflects the tail part of the PDF in a more precise manner. This indicates that cases of lighter tails with α close to 2 may not benefit from the method compared to those of heavier tails with smaller α. Another possible reason may be that the accuracy of calculating the empirical CF for cases of α close to 2 is not as high as for those of smaller α. This is because the CF is given by the Fourier transformation of the PDF, and cases of larger α close to 2 have smaller sample variance but larger spectrum width.

2.4.2 Performance of the estimated distribution

Next, we examine the performance of estimating stable laws from a different perspective; evaluation of the entire distribution. We use the KS distance expressed as

$$D = \max_x |P(x) - \hat{P}(x)|,$$

which represents the maximum distance between two distributions in terms of the CDF. Here $P(x)$ and $\hat{P}(x)$ denotes the empirically obtained CDF, and the theoretical estimated CDF, respectively. The standard density and distribution functions of stable distributions are numerically derived approximately by implementing the Fourier integral formulas (Zolotarev, 1986; Nolan, 1997), which are available in package *libstable* that provides good approximation values (del Val et al., 2017). KS distance is one of the most major standards for numerical assessments when discussing stable laws. We set aside any issues related to numerical approximations of stable distributions, so that we can focus on the performance between the methods. The root mean square (RMS) of the KS distance is used for the numerical assessment to make the small differences of the comparison results more apparent.

Figure 2.2 shows the simulation results of the KS distance for several cases of stable distributions; $S(\alpha, 0.1, 1, 0)$, $S(1.7, \beta, 1, 0)$, $S(1.3, 0.2, \gamma, 0)$, and $S(0.7, -0.4, 1, \delta)$. The RMS of the KS distance is calculated for each case with various values of parameters ranging within parameter ranges. We find in Figure 2.2 (c) that the estimation for the scaling parameter $\gamma \neq 1$ poses significant estimation errors. This is caused by the effect of sample errors induced by the scaling parameter γ far from the standardized form, as shown in equation (2.3.1). On the other hand, our proposed method achieves the smallest value of KS distances for all cases of parameter combinations. This proves that we are also successful in improving the estimation of the entire stable distribution.

Table 2.1: Simulation results for the performance of all four stable law parameters. The comparison of the proposed method with other methods based on Bibalan et al., Krutto, and QM are examined for different values of (α,β) with a standardized form of $(\gamma,\delta) = (1,0)$. Absolute values of bias are given below the MSE in parentheses for all cases. The minimum value of MSEs among the methods are shown in bold for each case of parameters.

			α					
			0.5		1.5		1.8	
			β		β		β	
		$(\times 10^{-4})$	0	0.5	0	0.5	0	0.5
$\hat{\alpha}$	proposed	MSE	**0.859**	**0.767**	**3.353**	**2.881**	**2.128**	**2.100**
		bias	(1.047)	(5.376)	(9.776)	(4.193)	(1.567)	(2.140)
	Bibalan et al.		5.252	4.803	4.015	3.757	2.346	2.234
			(8.435)	(4.880)	(2.793)	(16.51)	(2.994)	(1.710)
	Krutto		1.387	1.429	4.958	4.604	2.816	2.728
			(13.48)	(2.535)	(18.95)	(4.333)	(0.231)	(3.642)
	QM		—	—	3.915	5.306	9.282	8.857
			(—)	(—)	(4.732)	(16.75)	(16.63)	(16.97)
$\hat{\beta}$	proposed	MSE	**6.867**	**7.522**	**11.54**	**11.55**	40.68	48.78
		bias	(13.78)	(3.230)	(0.629)	(12.33)	(24.90)	(16.48)
	Bibalan et al.		20.95	20.64	15.09	16.61	47.62	56.67
			(19.32)	(5.274)	(17.51)	(4.882)	(36.72)	(19.40)
	Krutto		11.66	12.64	15.71	15.18	**37.05**	**42.97**
			(0.736)	(3.166)	(9.488)	(3.711)	(7.387)	(29.83)
	QM		—	—	11.59	13.01	61.39	162.3
			(—)	(—)	(6.575)	(64.02)	(3.764)	(373.2)
$\hat{\gamma}$	proposed	MSE	15.95	**13.20**	**1.444**	1.396	**0.842**	0.857
		bias	(14.74)	(20.28)	(5.552)	(3.004)	(0.748)	(9.113)
	Bibalan et al.		**13.66**	13.29	1.450	**1.386**	0.845	**0.854**
			(24.70)	(44.02)	(5.306)	(3.741)	(0.984)	(9.016)
	Krutto		31.33	32.42	1.910	1.841	0.895	0.938
			(48.27)	(25.64)	(13.73)	(4.923)	(1.007)	(9.917)
	QM		—	—	1.613	1.989	1.483	1.518
			(—)	(—)	(11.55)	(27.58)	(9.162)	(20.74)
$\hat{\delta}$	proposed	MSE	**10.80**	**14.25**	**8.401**	**10.27**	**3.147**	3.428
		bias	(11.90)	(33.02)	(10.70)	(1.020)	(0.243)	(2.800)
	Bibalan et al.		30.86	35.41	10.72	13.43	3.497	3.965
			(15.92)	(20.27)	(26.94)	(8.638)	(3.954)	(3.118)
	Krutto		61.87	88.23	9.796	12.00	3.151	**3.275**
			(23.49)	(56.67)	(4.332)	(10.58)	(2.116)	(4.712)
	QM		—	—	9.394	11.68	3.710	3.815
			(—)	(—)	(14.87)	(46.61)	(1.920)	(32.97)

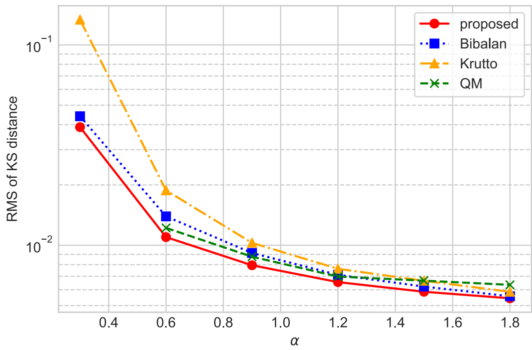

(a) RMS of KS distances for $S(\alpha,0.1,1,0)$

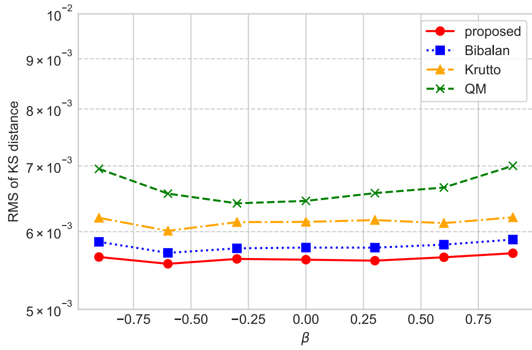

(b) RMS of KS distances for $S(1.7,\beta,1,0)$

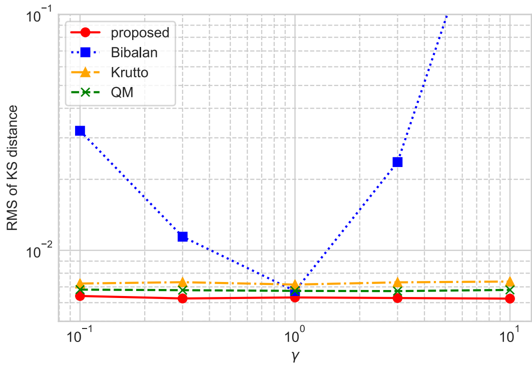

(c) RMS of KS distances for $S(1.3,0.2,\gamma,0)$

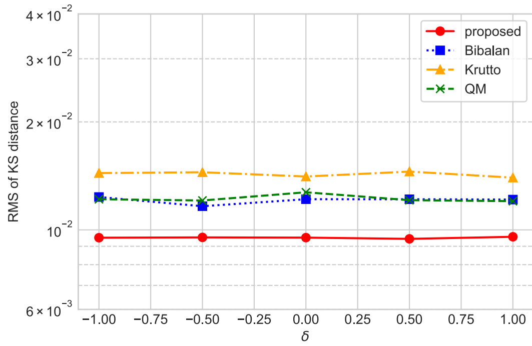

(d) RMS of KS distances for $S(0.7,-0.4,1,\delta)$

Figure 2.2: Comparison of the KS distances for the methods based on the proposed approach, Bibalan et al.'s approach, Krutto's approach, and the QM method. The RMS values of KS distances are studied for several cases of stable distributions with parameters (a) α (b) β (c) γ (d) δ ranging within its parameter range ($N = 10000, L = 500$).

Table 2.2: Basic statistics of USDJPY and WTI return time series with time intervals of 1-hour and one day, respectively. Mean is the average of the return time series, SD is the standard deviation, and N is the number of sample sizes.

	Mean	SD	Skew	Kurt	Min	Max	N
USDJPY	1.027×10^{-5}	0.0062	-0.0531	4.7880	-0.0384	0.0550	4190
WTI	-7.312×10^{-6}	0.0041	0.5900	23.945	-0.0576	0.1068	54356

2.4.3 Effect of sample size

Needless to say, the accuracy of the estimation method strongly depends on the number of samples. Larger sample sizes give more information of the dataset whereas smaller sample sizes have only little information making it challenging to detect the true values. We examine the effect of sample size by comparing the performance among the estimation methods. Figure 2.3 displays the MSE of each parameter of stable distribution as the sample size N changes from 300 to 10000. The study is examined for the case of $S(1.4, 0.2, 1, 0)$. The MSE simulated by means of our method decreases with the order $\mathcal{O}(1/N)$ while the MSE simulated by means of other representative methods also exhibited similar behaviors of order. Our proposed approach offers the best performance except for the location parameter δ, where the QM method sometimes give more accurate estimates for large datasets.

2.5 Application to Financial Empirical Data

This section shows application of the proposed estimation method to real financial data. We provide several empirical studies to present that our proposed approach is appliable for a wide range of empirical analysis in finance.

Asset price returns in various financial markets tend to show interesting properties of stable laws ever since Mandelbrot (1963) first revealed that stable distribution fits cotton price returns better than the classical Gaussian distribution. This argument have attracted attention to identifying price behaviors in many financial fields such as equities (Fama, 1965; Mantegna and Stanley, 1995; Xu et al., 2011), price consumer index inflation (Chronis, 2016), metal markets (Krężolek, 2012), oil markets (Yuan et al., 2014), and Cryptocurrency markets (Kakinaka and Umeno, 2020a). We investigate return distributions of the Japanese Yen currency exchange rate in terms of the US dollar (USDJPY) and the West Texas Intermediate (WTI) crude oil futures market, both of which are potent indices in finance. The data that support the findings of this study are openly available in Hist-

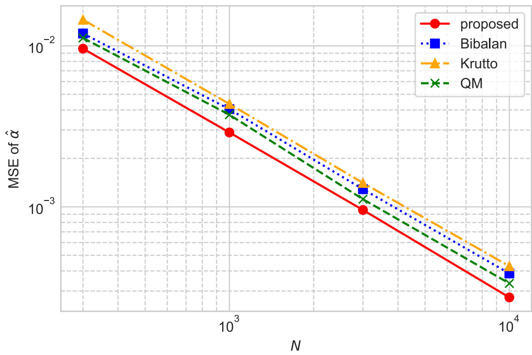

(a) MSE(α) for cases of $S(1.4, 0.2, 1, 0)$

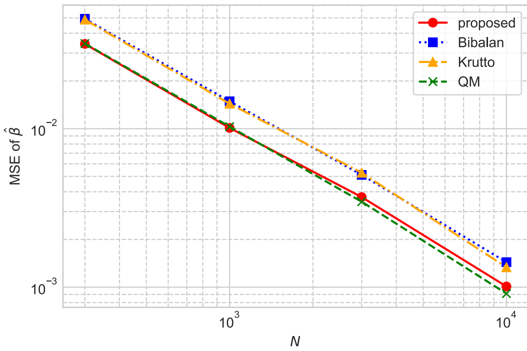

(b) MSE(β) for cases of $S(1.4, 0.2, 1, 0)$

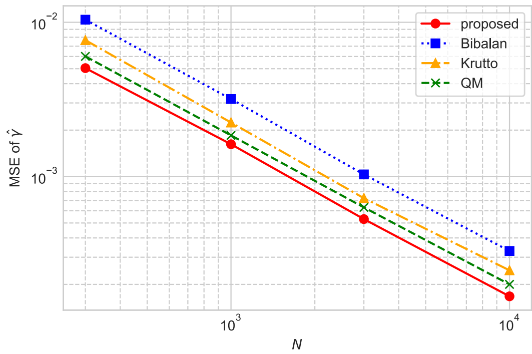

(c) MSE(γ) for cases of $S(1.4, 0.2, 1, 0)$

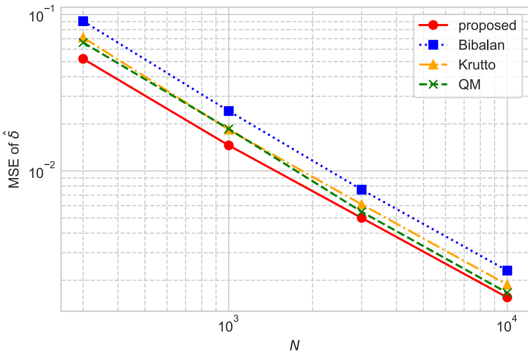

(d) MSE(δ) for cases of $S(1.4, 0.2, 1, 0)$

Figure 2.3: Comparison of the MSE for the methods based on the proposed approach, Bibalan et al.'s approach, Krutto's approach, and the QM method with different values of sample sizes $N = 300, 1000, 3000, 10000$. The MSE values of each stable parameter (a) α (b) β (c) γ (d) δ are studied for cases of $S(1.4, 0.2, 1, 0)$ over $L = 500$ synthetic datasets.

Table 2.3: Parameters of the fitted stable distribution for daily return time series of USDJPY exchange rate (2004/01/05-2019/12/31) and KS-distance calculated based on several estimation methods ($N = 4190$).

method	α	β	γ	δ	KS
proposed	1.708	-0.121	0.0035	-0.00004	**0.0214**
Bibalan et al.	1.884	-0.261	0.0039	-0.00002	0.0396
Krutto	1.767	-0.138	0.0036	-0.00004	0.0279
QM	1.584	-0.064	0.0034	-0.00012	0.0216

Data.com (http://www.histdata.com/download-free-forex-data/). The basic statistics of the indices are provided in Table 2.2. We explore both cases of common daily analysis and high-frequency data analysis. In particular, we use daily and one-hour return time series for the USDJPY and the WTI market, respectively. Since the scale of returns for both cases are too small for the method based on Bibalan et al. (2017) to give plausible estimates, we do a pre-standardization process beforehand. We multiply returns by 100 and after the estimation the parameters γ and δ are adjusted by dividing them by 100. Table 2.3 presents the estimates of the fitted stable distribution associated with the KS-distance between the empirical distribution and the estimated stable distribution for USDJPY, calculated based on four controversial estimation methods. Our primary focus is on the KS-distance value. The results show that the estimated distribution based on our proposed method presents the smallest value among other estimation methods. The smallest KS-distance implies that our method exhibits stable laws that best describes the observed data. Parameter estimates and the distance measure for the WTI market are shown in Table 2.4. The result indicates that the outstanding performance of our method also holds for high-frequency data with the lowest KS-distance. What makes the development of the estimation method a crucial matter is that the parameter estimates can differ so much among the methods when applied to empirically observed data, even for large datasets. We find in Table 2.4 that the estimate of α marks a low 1.260 based on the QM method whereas Bibalan et al.'s method presents 1.846, which the value differs quite a lot between the methods in spite of the large sample size of dataset with $N = 54356$. A method that accomplishes the inference of the closest distribution or set of parameters provides a more reliable model. Hence, our proposed estimation approach play a significant role as a tool for modeling with stable laws.

Table 2.4: Parameters of the fitted stable distribution for 1-hour return time series of WTI crude oil futures market (2010/11/14-2019/12/31) and KS-distance calculated based on several estimation methods ($N = 54356$).

method	α	β	γ	δ	KS
proposed	1.357	-0.045	0.0015	-0.00007	**0.018**
Bibalan et al.	1.846	-0.012	0.0024	-0.00002	0.088
Krutto	1.487	-0.071	0.0017	-0.00007	0.036
QM	1.260	-0.031	0.0015	-0.00009	0.019

2.6 Summary and Discussions

This chapter has proposed a new approach for estimating stable laws and applied this approach to the exploration of price behaviors in financial markets. Our new technique is developed under the method of moments, which is one of the widely known CF-based methods that require the choice of appropriate momental points. The points necessary for the estimation process are flexibly chosen, as the estimation accuracy of stable laws depends heavily on their true parameter values. We have focused on the fact that the index parameter α and the desired momental points exhibit a distinctive relationship, which is a new perspective in the literature. This relation is modelled as $g(\alpha,\eta) = 0$, based on the idea of employing points η at which the weighted absolute values of the CF present the maximum sensitivity. To detect appropriate points, we have suggested a procedure relying on the combination of empirical searches and algorithmic approaches. The advantage of employing these points is that the parameters of stable laws can be estimated in a more precise manner while remaining straightforwardly the implementation of the method. The relative performance of the parameter estimates is benchmarked against other existing methods, specifically the QM and the methods of Bibalan et al. (2017) and Krutto (2018), through simulation studies in terms of the MSE and KS-distance criteria. The results have implied that our method is the *most powerful* with the best performance. Our approach assures that the estimates of all four parameters of stable laws present a closed-form expression without any restrictions on parameter ranges, making the method significantly practical. We have also explored the behaviors of price fluctuations in several financial markets to show that our method is applicable for empirical financial studies. For the USD-JPY exchange rate and the WTI crude oil future price, our method supports stable laws with the highest performance among all the other methods discussed in this chapter. This would motivate us to further develop analytical methods for examining stable laws, as well as to further investigate various features of financial markets.

Chapter 3

Power Laws in Cryptocurrencies

This chapter corresponds to paper 2 in the author's papers list.

3.1 Introduction

Analysis of financial price fluctuations has long been assumed to follow a Gaussian distribution for its simplicity and the background of the Central Limit Theorem (CLT). As an example, the famous Black-Scholes model (Black and Scholes, 1973) was formulated under this assumption. However, it is well known that Gaussianity fails to capture volatile observations and leads to underestimating tail risks. Extreme fluctuations have been observed repeatedly in financial markets: notable examples include the financial crisis of 2007-2008, which caused turbulence of the market. Physical (or econophysics) concepts have been offering useful tools for analyzing such economic phenomena. In the past decades, there have been studies giving an account of asset returns well complied with a Lévy's stable distribution, which has fatter tails with power-functions compared to a Gaussian distribution (Mandelbrot, 1963; Fama, 1965; Hsu et al., 1974; Mantegna and Stanley, 1995). It is one of the most famous parametric fat-tailed distributions and allows us to model not only financial modeling but also a wide range of scientific fields from natural phenomena to computational science (Xu et al., 2011; Menabde and Sivapalan, 2000; Koblents et al., 2016; Chronis, 2016; Scalas and Kim, 2007). A common motivation in these studies is analyzing extreme values observed in social issues and measuring the liquidity conditions in terms of the parameters of stable laws. Moreover, in a theoretical context, Lévy's stable distribution is closely related to an essential theorem— the Generalized Central Limit Theorem (GCLT) (Gnedenko and Kolmogorov, 1954) that thoroughly explains the scaling phenomena in financial markets. This theorem suggests that the sum of i.i.d. random variables with infinite variance converge only to a Lévy's stable distribution. Besides, an extension of the GCLT is studied recently (Shintani and Umeno, 2018) with the application of the form of Lévy's stable distribution. Such arguments enable us to capture the inherent characteristics of asset price fluctuations and help identify the probability distribution of asset returns. Thus, analysis of price fluctuation behaviors using Lévy's stable distribution can be crucial to understand the mechanism of financial markets (Jovanovic and Schinckus, 2016).

A paper by Begušić et al. (2018) studies the fat-tailed nature of price fluctuations for Bitcoin and reveals that α is $2.0 \sim 2.5$, by using the traditional Hill estimator method. The method focuses on finding a local fit for tails, and although the results provide interesting findings of power-law behaviors, it does not account for the entire distribution. On the other hand, the framework of Lévy's stable distribution covers the entire dataset, allowing us to investigate extreme and non-extreme price fluctuations from the same standpoint.

In this chapter, we analyze the price fluctuation behaviors of emerging cryptocurrency markets with the Lévy's stable distribution and examine the validity of the model. We first show that the probability density of price returns are in a good agreement with the Lévy's stable distribution through the parameter estimation in the case of a fixed 1-hour time interval. We next consider different time intervals for extensive analyses and provide empirical evidence that price fluctuations in cryptocurrency markets do not follow a Gaussian distribution and can be better described by a Lévy's stable distribution. To confirm this, we propose a numerical assessment by using a function representing the distance between theoretical and empirical distributions, which is obtained from the Parseval's relation. An advantage of this approach is to evaluate stable distributions *quantitatively*, and at the same time, to avoid the analytical difficulties. In addition, we examine the scaling property of returns to check whether the Lévy stable regime holds. The combination of these approaches helps lead to a practical analysis for detecting stable laws in cryptocurrency markets. We discuss that if we admit some intrinsic noise errors, returns can be assumed to follow a Lévy stable regime within a certain range of time intervals— outside the range, there are either quantitative or theoretical failures. Furthermore, we discuss whether the Lévy's stable distribution can be an appropriate model by examining the model-fitting for returns under the Lévy's stable distribution and under other fat-tailed distributions. Our study compares fitting approaches covering the large portion of the distribution with those covering only the tail parts of the distribution, including the Hill estimator. The idea proposed in this study is helpful not only to value the liquidity conditions of the market but also provide clues towards financial modeling in a more careful manner.

3.2 Methodology of Power Law Analysis

This section explains the methods used for analysis in this study. In first subsection we discuss what method applies to parameter estimation. The second subsection introduces a quantitative valuation by means of characteristic function, which can be expected as a tool to evaluate the fit with Lévy's stable distributions. Finally, the last subsection describes a method used for testing the fit compared to other forms of distributions.

3.2.1 Power law estimations

Numerous approaches are known for parameter estimation. Since the PDF is not always expressed in a closed form, there are some challenges to overcome the analytic difficulties.This has long been a motivation for researchers to construct a variation of estimation methods, and the representatives are for instance; the approximate maximum likelihood estimation (DuMouchel, 1973; Brorsen and Yang, 1990; Mittnik et al., 1999; Nolan, 2001), non-parametric quantile (QM) method (Fama and Roll, 1971; McCulloch, 1986), fractional lower order moment (FLOM) method (Ma and Nikias, 1995), method of log-cumulant (Nicolas and Anfinsen, 2001; Pastor et al., 2016), the characteristic function (CF) based method (Koutrouvelis, 1980; Bibalan et al., 2017; Press, 1972; Kakinaka and Umeno, 2020b) and more.

While these methods aim to get estimators related to the stable distribution, there are some methods that can be applied to the case where the data is expected to follow a power-law. One common approach is the traditional Hill estimator (Hill, 1975), which focuses on estimating the tail index parameter α. The approach pays attention to discover the power law decay of the *tail* portion of the cumulative distribution, $P(X > x) \sim x^{-\alpha}$ (then the PDF decays with $\alpha + 1$). This method is known to be a right choice of tool for identifying and qualifying the tail properties in empirical studies (Plerou and Stanley, 2008; Gopikrishnan et al., 1999; Begušić et al., 2018), and often reveals the *inverse cubic law* in many financial asset returns. Before the estimation, one first needs to set the lower bound $x_{\min}$, which means that the power law is studied only for values larger than the lower bound. The idea of the method is to estimate local slopes of the tail portion of the distribution as,

$$\hat{\alpha} = n \left(\sum_{i=1}^{n} \ln \frac{x_i}{x_{\min}} \right)^{-1},$$

where x_i $(i = 1, 2, \ldots, n)$ is the n largest data out of N observed data, such that $x_i \geq x_{\min}$. Note that the method is based on the technique of *maximum likelihood* *estimator*. Hill estimator is known to be asymptotically normal and consistent for $n, N \to \infty, n/N \to 0$, and the standard error on $\hat{\alpha}$ is $\sigma = \hat{\alpha}/\sqrt{n}$.

The choice of the lower bound $x_{\min}$ is a crucial issue when applying to empirical data. If we choose $x_{\min}$ too small, estimation for local slopes for the tail portion will be more inaccurate (Clauset et al., 2009). Fitting local tails becomes difficult because of including other portions of the distribution, which usually tends to show properties different from the tail. On the other hand, if $x_{\min}$ too large is chosen, we will get a biased estimate due to the lack of sample numbers. Moreover, the estimator gives excellent results when the data follows a power-law form, but also give some estimation for data that is not necessarily drawn from a power-law distribution. In other words, the estimator calculates α accurately that best fits the simple power-law form $x^{-\alpha}$for any data in the range of $x \geq x_{\min}$. Although the far tails of cumulative distribution for stable distribution show the simple power law form as well: $P(X > x) \sim cx^{-\alpha}$, with the constants $c = \Gamma(\alpha)(\sin(\pi\alpha/2))(1+\beta)/\pi$, it tends to have overestimated $\hat{\alpha}$ when choosing the proper $x_{\min}$ is not taken into account(Weron, 2001).

To mitigate this issue, we employ the method of estimating the best choice of $x_{\min}$(Clauset et al., 2009), which helps to see whether the Hill estimator is valid for stable distributions. The idea is the use of the Kolmogorov-Smirnov (KS) statistic, which represents the maximum distance between two distributions in terms of cumulative distribution function (CDF) shown as:

$$D = \max_{x \geq x_{\min}} |P(x) - Q(x)|,$$

where $P(x)$ is the CDF obtained from empirical data, and $Q(x)$ is the CDF that best fits the power law model. With a given lower bound $x_{\min}$, KS statistic can be obtained using data points in the range of $x \geq x_{\min}$. The estimation for the lower bound $\hat{x}_{\min}$ is then the one that minimizes the KS statistic D. This method gives good results and achieves to estimate $\hat{x}_{\min}$ precisely and adequately. However, when the distribution follows a power law only in the limit of very large x, it can be unrealistic assuming to fit with distribution $x^{-\alpha}$ for any specific range of x. Stable distributions have forms to illustrate this case; the far tails are equivalent to the pure power-law form $x^{-\alpha}$ but only in an asymptotic behavior. Finding the actual value of $x_{\min}$ is obscured by the fact that stable distribution does not exactly correspond to the pure form $x^{-\alpha}$ within ranges of observed values. Therefore, the Hill estimator may not be appropriate for detecting the power law under the assumption of stable distributions.

In response to this fact, a method that can take enough data into consideration is preferred when dealing with stable distributions. Many of the representative methods suggested at the beginning of this subsection tend to have several issues, such as a limited range of estimation, a high computational cost, and the requirement of a larger dataset. The CF-based method makes good use of CF's distinctive features and is most frequently applied for its relatively less defect compared to other methods (Kateregga et al., 2017). In particular, the regression-based method (Koutrouvelis, 1980; Kakinaka and Umeno, 2020b) provides a straightforward approach with the application of regressions using the CF form, which is the estimator of our choice. It shows fast and accurate computation well enough to estimate cryptocurrency data.

3.2.2 Appraisal for the Lévy stable regime through the characteristic function

For the goodness-of-fit, statistical tests have analytical difficulties in practice due to the lack of fundamental statistics, especially the lack of a closed-form of PDF. Numerically accurate expressions are known for stable distributions, but often have several constraints (Crisanto-Neto et al., 2018; Arias-Calluari et al., 2018). Therefore, statistical indicators such as KS statistics and KL divergence have fundamental problems to be applied when modeling with stable distributions. As an alternative, we focus on the CF, following the fact that the inversion formula for the CF indicates a one-to-one correspondence between the PDF and the CF. The CF of the stable distribution can be expressed analytically as equation (1.2.2). Our attempt here is to calculate the difference or the distance between the PDF of the estimated stable distribution (theoretical) and the PDF obtained from a large number of real data (empirical). The distance we consider is a simple form shown as,

$$\int_{-\infty}^{\infty} |\hat{p}(x) - p(x)|^2 \, dx.$$

where $\hat{p}(x)$ is the PDF for the estimated stable distribution in a continuous form and $p(x)$ for the empirical distribution as well. When we discuss the empirical PDF $p_N(x)$ from N observed data, we should consider it in a discrete version due to its discontinuous form. In the belief that continuous-time signals of the empirical PDF could be discretized into discrete-time signals, we obtain

$$\sum_{n=-\infty}^{\infty} |\hat{p}[n] - p_N[n]|^2,$$

where $\hat{p}[n]$ and $p_N[n]$ represents the discretized form of $\hat{p}(x)$ and $p_N(x)$, respectively. We do not conduct the process of discretization in practice but instantly use the Parseval's theorem based on Discrete-time Fourier Transform (DTFT), which yields

$$\begin{aligned}\sum_{n=-\infty}^{\infty} |\hat{p}[n] - p_N[n]|^2 &= \frac{1}{2\pi}\int_{-\pi}^{\pi} \left|\hat{\phi}(k) - \phi_N(k)\right|^2 dk \\ &= \lim_{\Delta k \to 0}\left(\frac{1}{2\pi}\sum_{k=-\pi}^{\pi} \left|\hat{\phi}(k) - \phi_N(k)\right|^2 \Delta k\right) \\ &\simeq \frac{\Delta k}{2\pi}\sum_{i=1}^{\frac{2\pi}{\Delta k}} \left|\hat{\phi}(k_i) - \phi_N(k_i)\right|^2. \end{aligned} \tag{3.2.1}$$

where Δk is the width of bin for Riemann sums. Note that the Parseval's theorem holds under the assumption of the sampling theorem, which requires sampling intervals to be refined enough. The process of Riemann sum in equation (3.2.1) approximately holds when both conditions satisfy: a large enough number of data to obtain an unbiased estimate of $\hat{\phi}(k_i)$, and a small enough width of bin Δk. In this study, for all cases, Δk is assumed as small an amount as $2\pi/100$ for computation convenience in the process of summation, which means the distance is calculated as 100 sums of $\frac{1}{100}\left|\hat{\phi}(k_i) - \phi_N(k_i)\right|^2$ for the range of $k_i \in [-\pi, \pi]$ ($k_1 = -\pi, k_2 = -\pi + \Delta k, \ldots, k_{100} = \pi$). This method implies that the distance between the theoretical and the empirical PDF could be calculated with the same idea based on the form of CF.

Similar function forms are introduced as the minimum distance method for parameter estimation (Press, 1972; Paulson et al., 1975); however, they have put a weight function to the distance function. Heathcote extended to develop a more general setting, but the method still has the difficulties of selecting the proper values (Heathcote, 1977). The distance function we propose is advantageous for many application due to its simple form and presents less computational drawbacks.

Next, we remark on the validity of the distance function. We check the applicability of the distance function to make further discussions possible for fitting data to stable laws. Figure 3.1 shows the basic properties and results needed for explaining the concept. Sub-figure (a) shows the simulated distance between theoretical stable distributions and generated stable distributions. The deviation error for distance (variance from finite-size effects) is also shown. Here, the random generator for stable distributions is based on the method proposed by Weron (1996). When $\phi_N(k)$ obtained from i.i.d. distributed data X_n ideally follows some theoretical distribution and becomes the true value $\phi(k)$ as $N \to \infty$, it can be shown that

$$E\left[\left|\phi(k) - \phi_N(k)\right|^2\right] = \frac{1}{N}\left(1 - |\phi(k)|^2\right), \tag{3.2.2}$$

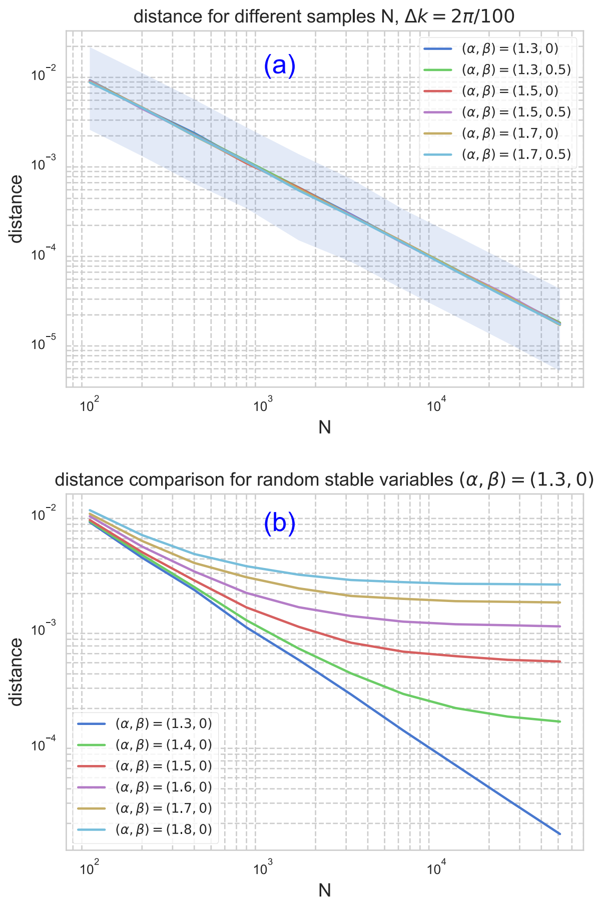

Figure 3.1: (a) represents calculated distance between the theoretical stable distribution and the empirical distribution derived from the original stable distribution. First, a number of N synthetic data is generated by the stable random generator method. Then the distance is calculated as shown in equation (3.2.1). Theoretical values for the theoretical stable distribution are given for different combinations of the parameters (α, β). For the effects of variance, we show the average of 1000 simulated distance associated with the 95% confidence intervals of the synthetic 1000 distances (shadowed in light blue). Simulation results show that distance depends on the number of data N, and the average decreases with the order $\mathcal{O}(1/N)$, as demonstrated in equation (3.2.2), with deviation error that also decreases with the order $\mathcal{O}(1/N)$. (b) shows the behavior of the distance between the average of 1000 generated stable distributions derived from $S(1.3, 0, 1, 0)$ and the theoretical stable distribution with different α, as the number of data N changes. The calculated average distance converges to the actual value for a more significant number of datasets. Most notably, the more α drifts away from 1.3, the larger the distance becomes for any number of data.

where $E[\cdot]$ is the expectation with respect to the data distribution. Then the expectation of the distance function is the average of (3.2.2) for $k \in [-\pi, \pi]$, which decreases with the order $\mathcal{O}(1/N)$. The bias of distance decreases with the same order $\mathcal{O}(1/N)$, which is clarified through simulation. Sub-figure (b) checks if there is no inconsistency between the theoretical distance and the synthetic distance. According to these simulation results, we know that the distance function is independent of the parameters (α, β), as well as showing larger values for a stronger degree of parameter differences. No exceptional or inconsistent results are observed, which indicates that it can potentially be used as an appropriate tool to obtain a numerical expression in order to grasp the relationship between the theoretical and the empirical distribution. When a sufficient amount of data, N, is given or known, the distance is determined and can be obtained as a particular value. This value not only indicates simply the distance between the two distributions but also be a standard measure to discuss error evaluations of the calculated distance.

3.2.3 Comparison with alternative distribution

Although the parameter estimation method and our evaluation method proposed in the previous subsection illustrate how to analyze data with stable distributions, they may still be unsatisfactory for discussing the validity of the model. These methods find and evaluate the best fit under the condition of stable laws, but it does not necessarily mean that the stable distribution exactly describes the data. Thus, we compare the model-fits under the stable distribution with those under other controversial distributions.

Regardless of how well the empirical data fit with a stable distribution, the data may fit more with other distributions. An alternative distribution, for instance, a power-law or exponential distribution, may show a better fit. Even when the data does not follow any typical form of distribution, or when the exact distribution cannot be identified empirically, the comparison approach tells us which model can be reasonable for the fit. Here we employ a *likelihood ratio test*, applied by Clauset et al. (2009) to directly compare two candidate distributions against each other and decide which provides a better fit. The method is based on calculating the likelihood of the data. With given PDFs of $p_1(x)$ and $p_2(x)$, the log-likelihood ratio is obtained as

$$\mathcal{R} = \ln \prod_{i=1}^{n} \frac{p_1(x_i)}{p_2(x_i)} = \sum_{i=1}^{n} \{\ln p_1(x_i) - \ln p_2(x_i)\}, \tag{3.2.3}$$

which is equivalent to the logarithm of the ratio of the two likelihoods. As a higher likelihood indicates a better fit, a positive value of $\mathcal{R}$ implies that the former distribution is better than the latter. Thus, the ratio value of $\mathscr{R}$ can be an indicator for judging which distribution is efficient for the fit.

In practice, making a judgment is difficult when $\mathscr{R}$ is close to zero, almost in the event of a tie, since the results depend on statistical fluctuations of the likelihood values. To avoid misclassification, we calculate the p-value, associated with the normalized log-likelihood ratio $\mathscr{R}/\left(\sigma\sqrt{n}\right)$ (σ is shown in equation (3.2.5)), to confirm whether the obtained ratio shows a statistically significant result (see Clauset et al. (2009) for more). The p-value can be calculated as the probability that the log-likelihood ratio becomes larger than the absolute value of observed $\mathscr{R}$. The sum of i.i.d. observations, $\mathscr{R}$, becomes normally distributed by the CLT. Thus the value is calculated as

$$p = \operatorname{erfc}\left(|\mathscr{R}|/\sqrt{2n}\sigma\right), \tag{3.2.4}$$

where erfc denotes the complementary Gaussian error function,

$$\operatorname{erfc}(z) = \frac{2}{\sqrt{\pi}}\int_z^\infty \mathrm{e}^{-t^2}dt,$$

and σ denotes the estimated standard deviation of a single term on $\mathscr{R}$:

$$\sigma^2 = \frac{1}{n}\sum_{i=1}^{n}\left\{(\ln p_1(x_i) - \ln p_2(x_i)) - \left(\overline{\ln p_1(x)} - \overline{\ln p_2(x)}\right)\right\}^2, \tag{3.2.5}$$

where bar denotes the average of terms. If the value is small enough ($p < 0.1$), the result is statistically significant. In this case, it is sufficient to make a judgment for discriminating which distribution model is proper for fitting the data.

3.3 Empirical Study

In this section, four subsections are beginning with the presentation of 5 types of cryptocurrency datasets for analyzing returns. The second subsection shows the results of the parameter estimation for cryptocurrency returns with a time scale of Δt = 1hour when explained by a stable distribution. Furthermore, returns for different time scales are discussed in the third subsection in terms of the estimated index parameter α and the distance measure. We strengthen the importance of time scaling for the stable model but also address the issues for practical use and applications. The last subsection shows the comparison of the model with other representative fat-tail models to discuss the validity of the stable distribution for cryptocurrency returns.

Table 3.1: Basic data facts of cryptocurrencies (2019/01/15)

Cryptocurrency	Market Cap[$]	Price[$]
Bitcoin (BTC)	64,308,311,082	3,678.28
Ethereum (ETH)	13,391,497,879	128.29
Ripple (XRP)	13,534,746,905	0.33
Litecoin (LTC)	1,938,420,144	32.29
Monero (XMR)	761,083,680	45.58

3.3.1 Data presentation

This subsection explains the basic characteristics of our data on cryptocurrencies. Table 3.1 shows the market capitalization and the price of 5 major cryptocurrencies, Bitcoin (BTC); Ethereum (ETH); Ripple (XRP); Litecoin (LTC) and Monero (XMR). Basic data facts are taken from Cryptocurrency Market Capitalization (https://coinmarketcap.com).

Bitcoin is the most dominant cryptocurrency, whereas the others are considered as minor coins. However, recently, some minor coins (alto-coins) such as Ripple and Litecoin have also emerged rapidly since the arrival of the cryptocurrency boom in mid-2017. Figure 3.2 shows price fluctuations of cryptocurrencies for a time period of 2017/01/01 to 2019/01/01. Cryptocurrency price data are obtained from *poloniex* (https://poloniex.com), with all the price exchange rates against USDT. USDT is an abbreviation of Tether USD, a cryptocurrency asset that maintains the same price and value as the legal US dollar. During the investigated period, Bitcoin appears to be too volitile (Bouoiyour et al., 2016). Studies find that positive shocks increase the volatility more than negative shocks (Baur and Dimpfl, 2018). These volatile behaviors of price fluctuations have attracted considerable attention; market capitalization reached a peek more than a billion dollars momentarily. Since Bitcoin is not under control and disconnected from central banks, it is not affected by monetary policy news but only by its own events (Vidal-Tomás and Ibañez, 2018). Given these impacts of the cryptocurrency market on the economy, the importance of analyzing alto-coins has increased greatly.

3.3.2 Parameter estimation

From the data above, we estimate the parameters of the stable distribution that best describes the empirical returns.

We estimate the parameters of the returns for every five currencies over the period from 01/01/2017 to 01/01/2019. Note that the data set here is every 1-hour data (N=17520). For each currency, log-returns (returns) are firstly calculated

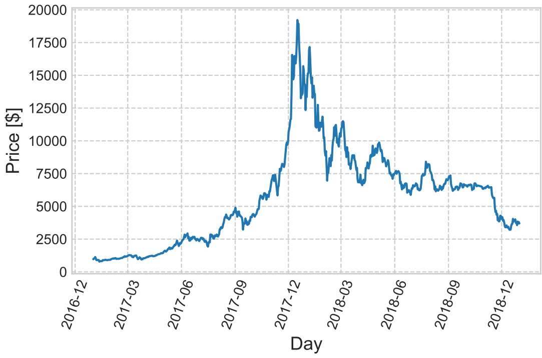

(a) BTC

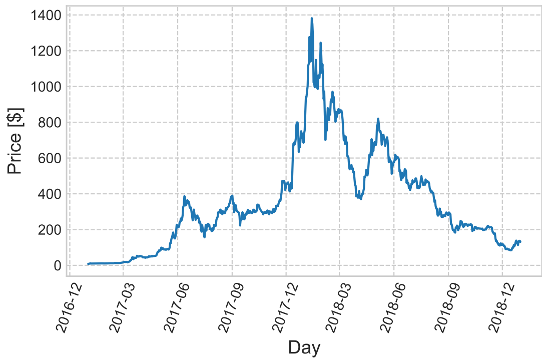

(b) ETH

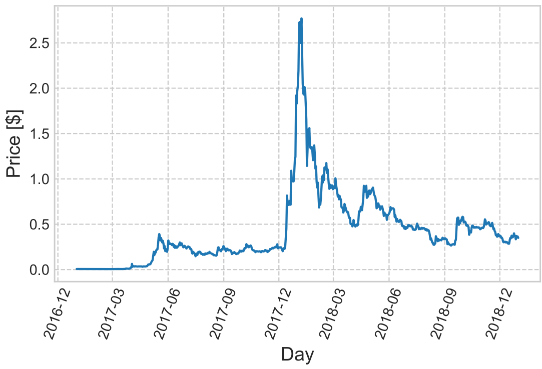

(c) XRP

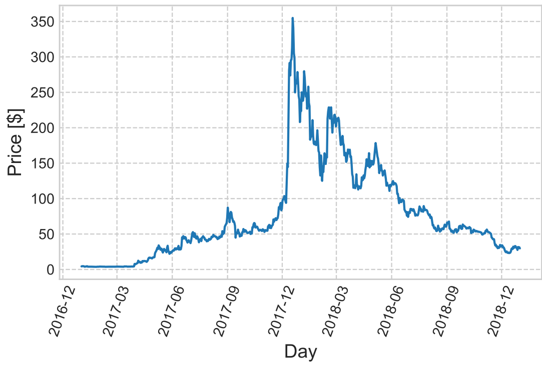

(d) LTC

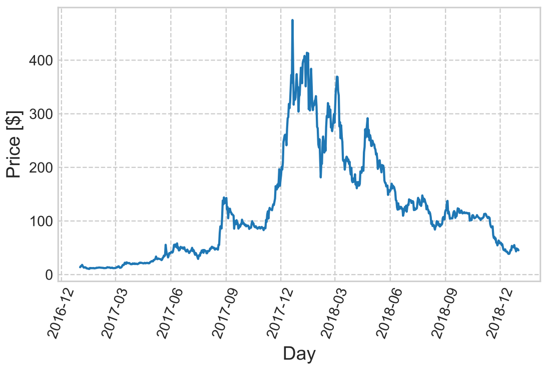

(e) XMR

Figure 3.2: Price fluctuations of Bitcoin (BTC), Ethereum (ETH), Ripple (XRP), Litecoin (LTC), and Monero (XMR) for 2017/01/01 to 2019/01/01. The cryptocurrency boom in the end of year 2017 have attracted many people.

from the price Y_t as

$$X_t = \log Y_{t+\Delta t} - \log Y_t,$$

where Δt is the time interval. Then the four parameters $\alpha, \beta, \gamma, \delta$ are estimated using the proposed method of Kakinaka and Umeno (2020b).

For the index parameter α, the traditional Hill estimator method (Hill, 1975) discovers that local tails of returns fit an exponent of $\alpha \simeq 2.0 \sim 2.5$, especially for the Bitcoin market (Begušić et al., 2018), however, if we consider fitting a stable distribution, we find different results. Table 3.2 shows that the tail index parameter α are estimated roughly in between 1.3 and 1.5. The values are undoubtedly smaller than the α=2 Gaussian distribution, which indicates that cryptocurrency asset returns are universally *non-Gaussian* with fat tails. Figure 3.3 shows the fitted histogram using the stable distribution. The estimated stable distribution well characterizes the fat-tail behaviors and the bulk portion of cryptocurrency asset return distributions, as well as observed in other assets (Mandelbrot, 1963; Mantegna and Stanley, 1995) and financial index (Lera and Sornette, 2018). It is worthy of mentioning that Bitcoin and Ripple appear to have α smaller than the other currencies, which is consistent with its fluctuation with prices skyrocketing and falling heavily at the beginning of 2017.

Table 3.2: Parameter estimation of stable laws for cryptocurrency series with 1-hour time interval data (2017/01/01-2019/01/01).

Cryptocurrency (/USDT)	α	β	γ	δ
Bitcoin (BTC)	1.339	−0.034	0.004	0.80×10^{-4}
Ethereum (ETH)	1.395	0.031	0.006	3.40×10^{-4}
Ripple (XRP)	1.343	0.010	0.007	-0.11×10^{-4}
Litecoin (LTC)	1.413	0.016	0.006	1.11×10^{-4}
Monero (XMR)	1.504	0.020	0.007	1.20×10^{-4}

Both parameters, α and β, can offer clues to explain the properties of returns. However, β is not so robust to large price fluctuations and tends to have significant estimation errors. Still, the estimated β is close to 0, which means that returns are not so skewed. The results provide additional views that price fluctuations for cryptocurrency markets exhibit a *symmetric* behavior, which is also our finding. In this study, we focus on the tail index parameter α, which refers to the measure of the tail behaviors and helps further applications of numerical analysis.

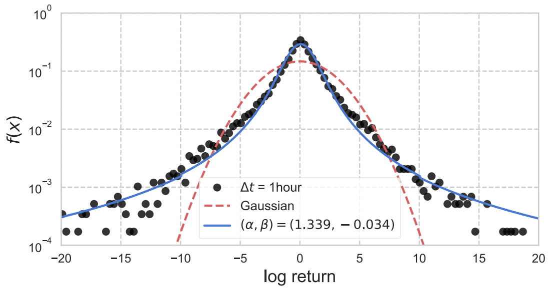

(a) btc

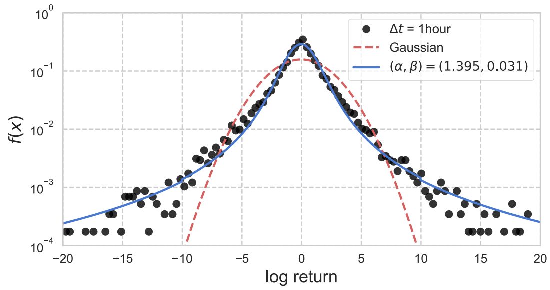

(b) eth

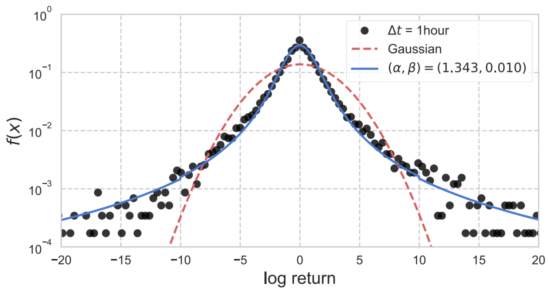

(c) xrp

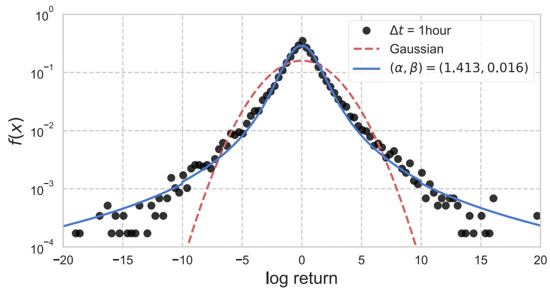

(d) ltc

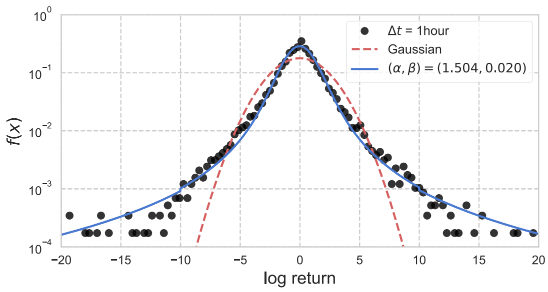

(e) xmr

Figure 3.3: Histogram of standardized empirical data (black plot) and fitted histogram from estimated stable distribution (blue solid line) compared with Gaussian distribution (red dashed line). Note that the standardization process is done according to equation (1.2.1). Although for extreme returns, there is a deficient of data, the estimation well represents the distribution.

3.3.3 Time scaling behavior of cryptocurrency

We have argued that in addition to the cryptocurrency market having non-Gaussian features as observed in other financial markets, stable distributions characterize returns well in terms of α for a fixed 1-hour time interval. This subsection focuses on analyzing cryptocurrency returns with different time scales in order to further understand its behavior. Meanwhile, we discover the *limitations* of the stable distribution for modeling returns in the latter half of this subsection.

Since the analysis of price fluctuations can be done at various time intervals, we go into various time scales. We use the same datasets for five currencies mentioned in the previous subsection. The details for time intervals Δt are given as follows: 5 minutes, 15 minutes, 30 minutes, 1 hour, 2 hours, 4 hours, 8 hours, and intraday. With a fixed length of the observation period, the number of data is inversely proportional to Δt: 210240, 70080, 35040, 17520, 8759, 4379, 2190, and 729, respectively.

We show results in Table 3.3 from the fitting of stable distribution and Gaussian distribution to each of these datasets using the distance measurement. We first estimate the parameters for stable distributions and use them to obtain the distance, as shown in equation (3.2.1). Since the distance is calculated via the CF expression, each Gaussian distribution is not estimated from the mean and standard deviation but by setting the parameter to $\alpha = 2$. The skew parameter β is not taken in consideration, because the CF does not depend on β when α is 2. By doing such numerical assessment, we confirm that stable distribution fit returns *better* than the Gaussian distribution— for *all* cases of currencies and time interval conditions. We also find that both forms of distribution share roughly the same Δt with the smallest calculated distance.

We next check the validity of the calculated distance against the stable model. If observed data entirely agrees with the stable distribution, and if we have unbiased parameter estimates, the distance value should be close to $1/N$ with deviation error with the order $\mathcal{O}(1/N)$, as discussed in section 2.3. However, Figure 3.4 shows that the calculated distances are likely to be quite above the assumed distance. The results indicate that observed data is not ultimately consistent with the stable distribution to a complete degree.

One crucial point of issue is that stable distribution presents infinite variance. This point contradicts the fact that the variance of returns for empirical observations turn out to be finite and supports the presence of a finite second moment (local tails appear to be $\alpha \geq 2.0$) (Grabchak and Samorodnitsky, 2010; Begušić et al., 2018). Moreover, in the classical study of Mantegna and Stanley (1995), stable distributions appear to fit the empirical returns well in the bulk part, but in the very far tails, it seems to overestimate for the sake of its infinite variance (Mantegna and Stanley, 1995). Strictly speaking, far tails are fatter than those of the

Table 3.3: Calculated distances between empirical distributions and estimated stable distributions (top row), in addition to calculated distances between empirical distributions and estimated Gaussian distributions (bottom row). The minimum distance value of each currency is shown in bold for each form of distribution, respectively.

Δt	BTC	ETH	XRP	LTC	XMR
	Estimated stable distribution ($\alpha < 2$) ($\times 10^{-3}$)				
5 min	4.00	10.28	26.66	29.76	36.37
15 min	1.56	1.68	4.51	4.57	10.94
30 min	**1.42**	**1.22**	1.42	1.68	2.46
1 hour	1.52	1.63	**0.84**	**1.30**	**0.86**
2 hours	1.74	1.64	1.22	1.61	1.01
4 hours	6.11	1.98	1.07	3.61	1.03
8 hours	5.88	3.42	2.07	2.35	2.39
1 Day	5.48	6.19	3.39	2.96	4.07
	Estimated Gaussian distribution ($\times 10^{-3}$)				
5 min	10.66	17.78	45.07	47.78	123.2
15 min	**7.72**	6.50	11.69	10.89	16.80
30 min	7.77	**6.06**	7.31	6.81	6.30
1 hour	8.53	7.56	**6.64**	6.58	**4.26**
2 hours	8.80	7.25	7.54	7.46	4.94
4 hours	14.93	8.03	8.49	10.01	4.75
8 hours	12.54	7.76	9.03	7.80	6.52
1 Day	12.29	12.79	14.30	**6.22**	7.16

empirical returns. Those observations are the same for cryptocurrency markets—actual price fluctuations do not show return values *too* large (for instance, the largest fluctuation for Bitcoin is 26.9%), whereas random stable variables include unrealistic extreme values (100% or 200% or even larger fluctuations). This phenomenon may be explained by the causes and effects of the system built in the mechanisms in financial markets, such as the circuit breaker system. Besides such causes, cryptocurrency prices differ between exchanges. These attributes are factors outside the natural fluctuation behaviors but may affect the data we obtain to some extent. Taking this standpoint gives reasonable assumption to consider that observed data is unfortunately somewhat uncertain, and not ideally perfect to be explained by a stable distribution. Still, many empirical studies suggest the stable model as a model to examine non-Gaussian behaviors for asset returns because it has solid theoretical reasons to reveal relationships of large and small terms (Xu et al., 2011; Bibalan et al., 2017; Lera and Sornette, 2018; Chronis, 2016; Scalas and Kim, 2007). As long as stable distributions show the potential to describe cryptocurrency returns, it is essential to understand the possibilities and limitations of stable models, and to what extent the model is applicable.

If we suppose that unexpected impacts are included in observed data as *noise*, one possible stopgap approach to evaluate the distance including bias and noise effects can be given as

$$\begin{aligned}
&\frac{1}{2\pi}\int_{-\pi}^{\pi}\left|\hat{\varphi}(k)-\varphi(k)+\varepsilon_k\right|^2 dk \\
=&\frac{1}{2\pi}\int_{-\pi}^{\pi}\left|\hat{\varphi}(k)-\varphi(k)\right|^2 dk+\frac{1}{2\pi}\int_{-\pi}^{\pi}\left\{2\,\mathrm{Re}\left(\left(\hat{\varphi}(k)-\varphi(k)\right)\overline{\varepsilon_k}\right)\right\}dk \\
&+\frac{1}{2\pi}\int_{-\pi}^{\pi}|\varepsilon_k|^2\,dk,
\end{aligned} \tag{3.3.1}$$

where $\hat{\varphi}(k)$ is the CF based on estimated parameters, $\varphi(k)$ is the true value of the CF, and ε_k represents the error value of the CF with respect to k. Here, we assume that the empirical CF, $\varphi_N(k)$, is considered as the addition of errors and the true CF, $\varphi(k)$. The first term on the right hand of equation (3.3.1) represents distance error caused by parameter estimation errors, the second term is the cross-term between $\hat{\varphi}(k)-\varphi(k)$ and ε_k, and the last term represents the error caused by noise. If data is ideal, noise is only related to the random nature of the sampling process. This case is equivalent to the condition discussed in Section 2.3, and it is evident that the distance decreases with the order $\mathcal{O}(1/N)$. Whereas if noise is large enough to affect the errors ε_k, the cross-term errors (second term) cannot be ignored as well as the errors in the last term. It is known that

$$\sqrt{N}\left(\varphi_N(k)-\varphi(k)\right)$$

is asymptotically normal with mean 0 (Feuerverger and McDunnough, 1981), and hence the cross-term decreases with the order $\mathcal{O}\left(1/\sqrt{N}\right)$. The leading order of the whole distance equation then becomes $\mathcal{O}\left(1/\sqrt{N}\right)$ for large N. Therefore, if we admit some observational noises, it may be reasonable and acceptable that the distances of empirical studies are larger than the natural distance error $1/N$. If we have biased parameter estimates for $\hat{\varphi}(k)$, we will have even more considerable distances. However, it should be noticed in Figure 3.4 that even though we consider unexpected noise in cryptocurrency data, we find numerical evidence of stable distributions fail to capture returns under some conditions of time intervals. Figure 3.4 shows that for high-frequency data (Δt shorter than 30 minutes), the distance values become too large. In other words, although we have more abundant data available, distances tend to increase, which implies that stable models do not perform well with Δt shorter than 30 minutes. Some of the possible

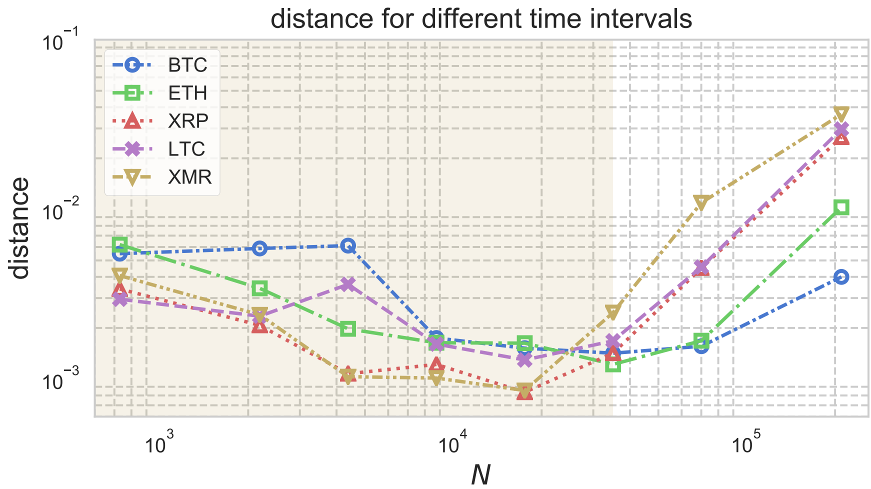

Figure 3.4: The values of distance defined in Section 3.2.2 are shown for different time intervals Δt. The distance decreases with the order $\mathcal{O}\left(1/\sqrt{N}\right)$, but not with the order $\mathcal{O}(1/N)$ due to non-ideal conditions of observed data. For a range of intervals shorter than 30 minutes ($\Delta t < 30$ min; outside the range in yellow), the distance value increases considerably; this contradicts the idea that the value should decrease (deviation error should also decrease) as the interval becomes shorter with a more significant number of data. Therefore, outside the yellow range is not plausible for modeling price fluctuations with stable distribution.

causes of the distance separation could be, for instance, the scarcity of tick-to-tick fluctuation patterns on less active exchanges and the market microstructure noise seen in high-frequency data (Ait-Sahalia et al., 2010). What is more, data may no longer be stationary with overly high-frequent conditions owing to the volatility clustering phenomenon. If data is non-stationary, *ergodicity* does not hold.

In Mandelbrot's pioneering investment of cotton prices (Mandelbrot, 1963), he observed that in addition to being non-Gaussian, returns show another endogenous interest— the invariant property of *time scaling*, which means that the return distribution for every various time interval Δt potentially show a similar class of functions conforming to a stable distribution. This behavior is certainly well connected with the Generalized Central Limit Theorem (GCLT), and hence the idea of exploring the scaling behavior is natural and essential when modeling financial assets with stable distributions. Mandelbrot has discovered that Δt ranging from 1 day up to 1 month shows consistent forms with the stable distribution. Gopikrishnan et al. (1999) also studied another asset of the S&P 500 index, showing that the distribution for Δt smaller than 4 days have consistent forms as well (Gopikrishnan et al., 1999). In a trivial sense, however, not all ranges of Δt

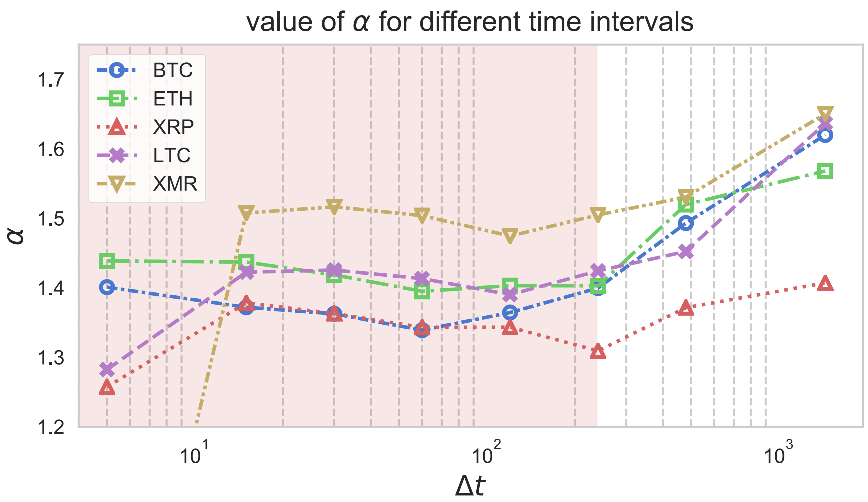

Figure 3.5: The estimate value of α are shown for different time intervals Δt in order to investigate the property of time scaling. While the stable regime holds for intervals smaller than 4 hours ($\Delta t < 4$ hours; range in pink), for longer time scales, α tends to increase towards $\alpha = 2$: the Gaussian regime. Although the crossover between the two regimes seem to take slightly different values depending on the choice of cryptocurrency, $\Delta t = 4$ hours is a general agreement.

show excellent compatibility with stable distributions. In addition, these previous studies show that financial asset returns tend to have less fat tails when analyzed with long timescales. This is because finite empirical observations do not support the GCLT, and the scaling property does not hold for long timescales but converges to a Gaussian distribution by the Central Limit Theorem (CLT).

To overcome these issues, Mantegna and Stanley (1994) were the first to propose the Truncated Lévy Distribution (TLD) (Mantegna and Stanley, 1994). The central part of the TLD is consistent with the stable distribution, but its far tail has a discrete cutoff. Koponen (1995) improved the TLD by introducing a smooth exponential cutoff to make it possible to derive an analytic expression for the CF and easier computation simulations (Koponen, 1995). For both cases, far tails have a faster decay compared to the stable laws. This assures the variance to be finite, and fortunately, more or less preserves the stable properties. This development can be explained when we consider the sums of independent and identically random variables following the TLD, known as the Truncated Lévy Flight (TLF). Since most of the distribution is like a stable distribution but has a finite variance, the TLF process *converges slowly* to the Gaussian distribution (Mantegna and Stanley, 1994; Koponen, 1995). For relatively short timescales, the influence of the truncated tails is too slight to affect the stochastic process for the CLT to be applied. It does not converge to the expected Gaussian distribution, but still under the GCLT. Therefore, as long as the stable regime holds, such a stochastic process can approximately be expressed as a stable distribution. Once the process reaches the crossover, it starts to go towards the Gaussian behavior. Overall, stable processes accounting for TLD provides two forms of distributions in terms of time scaling: *stable regime* and *Gaussian regime*.

Figure 3.5 displays the shift of α for different time scaling in cryptocurrency markets, which enables us to discuss the correspondence between the empirical behavior and the theoretical background of the GCLT. The results imply that the stable model is inappropriate for Δt larger than 4 hours (low-frequency data), where the GCLT is not valid, and the stable regime does not hold. We have reported in Figure 3.4 that in the case of high-frequency data ($\Delta t < 30$min), distance results are undoubtfully too large to support the model. If we consider the presence of observational noises in data, a range of approximately 30min $\leq \Delta t \leq$ 4h seems to be moderate for analyzing cryptocurrency returns when employing stable distributions. In this range, the return distributions satisfy the stable process with reasonable distance values.

3.3.4 Performance of stable law fit and alternative distribution models

The approaches explained in the previous subsection contribute to demonstrating how to apply the stable model properly to cryptocurrency markets. However, the approaches do not necessarily identify the actual model that describes the fluctuation system. An alternative model may be more appropriate even when the conditions, including time scaling, for supporting the stable model are satisfied. As we have mentioned before, the infinite properties of stable distributions make it challenging to build a 'good' modeling for the far tail portions. The power-law model is widely accepted, mainly when focusing on the tails, and often rules out the stable regime in empirical data with finite variance.

To identify the appropriate model for fitting cryptocurrency data, we employ the *likelihood ratio test* explained in subsection 3.2.3. We compare the stable model with each of the two alternative models of one-sided distributions: power-law and exponential distributions. We first focus on the identical range of local tails for the two distributions, since the comparison should be made under the same tail conditions. As explained in subsection 3.2.1, the tail is defined as the one that shows the best fit with the alternative distribution in terms of KS statistics. Tables A.1 and A.2 of Appendix A show the results of fitting the data of returns with each of the two alternative distributions for the positive and the negative tails, respectively. We confirm that the tail portions show plausible fits when using the power-law and exponential model.

Tables 3.4 and 3.5 show the results of the likelihood ratio tests (the likelihood ratio $\mathscr{R}$ and the corresponding p-value) under several tail portions for the positive and the negative tails of the standardized empirical returns, respectively. Time intervals $\Delta t = 1$ hour and $\Delta t = 2$ hours are examined, where the time scaling conditions are well satisfied for the stable model, as presented in subsection 3.3.3. It should be noted that the standard density and distribution functions of the stable distribution are numerically derived approximately by implementing the Fourier integral formulas (Zolotarev, 1986; Nolan, 1997), which are available in package *libstable* (del Val et al., 2017). We set aside any issues related to numerical approximations of the stable distributions since we aim to directly compare the fitting between models rather than the assessments of a specific model. Under the estimated tails (columns $\hat{x}_{\min}$ in the Tables 3.4 and 3.5), the values of $\mathscr{R}$ are negative for most cases, meaning that alternative distributions achieve a better fit than the stable distribution. Moreover, the results in Appendix A imply that empirical returns in the estimated tails are plausible with power laws. These are consistent with the arguments in many empirical studies that *local* tails of financial returns often exhibit the inverse cubic law.

However, our primary objective is to evaluate the entire or a wider range of returns. Since the estimated tail portions sometimes leave too many observations out of consideration, analyzing the data covering more observations, including the estimated tail portions, is needed to capture the characteristics of the data in a more comprehensive manner. In addition, we can explain the advantages of stable distribution only when the entire distribution is considered, according to the GCLT. We select the largest and lowest 5%, 15%, 30%, and 45% portions of the data as the lower and upper bound of tails, respectively, in order to reveal which distribution shows a better fit for larger portions of tails. The likelihood ratios for the 5% tail portion show negative values for most cases, like those with the estimated tails. However, as the tail portions become large, the likelihood ratios generally turn to positive values, particularly for the tail portions larger than 15%. Although some results are statistically insignificant, we confirm that the stable model tends to present a better fitting of returns for large portions of tails. Our results indicate that when we focus on the tails, for example, investigating the tail risks, the power-law or exponential model is suggested. But when we examine the characteristics of cryptocurrency price fluctuations from the entire data, the stable distribution is suggested to be an appropriate model for the analysis of behavior issues. A perfect model to explain the behaviors remains to be a challenging issue, but our strategies of coping with stable models are helpful for any extension of the model.

Table 3.4: The *likelihood ratio tests* for the *positive* tail of standardized cryptocurrency returns. The tests compare the stable model with each of the two alternative models of one-sided distributions: power-law and exponential distributions, for the tail behavior. In addition to the estimated local tails with lower bound $\hat{x}_{\min}$, we select the largest 5%, 15%, 30%, and 45% portions of the data as the lower bound of tails, respectively. For each tail portion, the stable distribution is compared with the alternative distribution that shows the best fit in terms of KS statistics. The likelihood ratios $\mathscr{R}$ in equation (3.2.3) and the corresponding p-values are given for each case. Positive values of $\mathscr{R}$ indicate that the stable model-fitting is better than the estimated alternative model-fitting. If the values are smaller than 0.1, we say that the calculated $\mathscr{R}$ are statistically significant (shown in bold).

Power law		$\hat{x}_{\min}$		5%		15%		30%		45%	
dataset	Δt	$\mathscr{R}$	p	$\mathscr{R}$	p	$\mathscr{R}$	p	$\mathscr{R}$	p	$\mathscr{R}$	p
BTC	1h	-62.25	**0.000**	-92.49	**0.000**	-10.27	**0.009**	392.4	**0.000**	2057	**0.000**
	2h	-48.86	**0.000**	-42.52	**0.000**	-3.458	**0.073**	166.6	**0.000**	959.7	**0.000**
ETH	1h	-43.98	**0.000**	-83.91	**0.000**	18.28	**0.000**	440.5	**0.000**	3038	**0.000**
	2h	-38.92	**0.000**	-38.23	**0.000**	-0.122	0.967	208.5	**0.000**	1347	**0.000**
XRP	1h	-43.78	**0.000**	-43.60	**0.000**	1.410	0.651	337.2	**0.000**	2946	**0.000**
	2h	-26.02	**0.000**	-21.53	**0.000**	0.714	0.741	163.7	**0.000**	1170	**0.000**
LTC	1h	-50.77	**0.000**	-64.00	**0.000**	19.39	**0.000**	394.2	**0.000**	2906	**0.000**
	2h	-31.59	**0.000**	-33.88	**0.000**	1.620	0.559	227.1	**0.000**	1457	**0.000**
XMR	1h	-17.42	**0.000**	-46.46	**0.000**	13.79	**0.003**	484.6	**0.000**	3464	**0.000**
	2h	-28.78	**0.000**	-25.53	**0.000**	4.613	**0.100**	216.7	**0.000**	1272	**0.000**
Exponential		$\hat{x}_{\min}$		5%		15%		30%		45%	
dataset	Δt	$\mathscr{R}$	p	$\mathscr{R}$	p	$\mathscr{R}$	p	$\mathscr{R}$	p	$\mathscr{R}$	p
BTC	1h	-106.2	**0.000**	-107.9	**0.000**	-80.86	**0.000**	-50.67	0.102	2.191	0.947
	2h	-46.25	**0.000**	-47.12	**0.000**	-44.97	**0.005**	-31.32	0.157	-12.63	0.587
ETH	1h	-48.84	**0.000**	-74.09	**0.000**	-62.2	**0.006**	-14.57	0.639	12.72	0.700
	2h	10.72	0.646	-33.58	**0.000**	-12.14	0.458	0.947	0.965	13.92	0.547
XRP	1h	-47.55	**0.000**	-38.22	**0.002**	82.49	**0.004**	245	**0.000**	313.9	**0.000**
	2h	-17.40	**0.089**	-10.62	0.424	47.02	**0.071**	122	**0.001**	176.2	**0.000**
LTC	1h	-55.50	**0.000**	-52.75	**0.001**	-31.41	0.247	48.93	0.178	78.8	**0.041**
	2h	-33.13	**0.000**	-37.33	**0.000**	-9.039	0.558	8.683	0.688	40.67	**0.079**
XMR	1h	32.71	0.251	-46.88	**0.000**	-4.252	0.853	12.17	0.664	26.29	0.356
	2h	3.875	0.848	-28.61	**0.001**	-10.63	0.495	3.713	0.850	3.746	0.853

Table 3.5: The *likelihood ratio tests* for the *negative* tail of standardized cryptocurrency returns.

Power law		$\hat{x}_{\min}$		5%		15%		30%		45%	
dataset	Δt	$\mathscr{R}$	p	$\mathscr{R}$	p	$\mathscr{R}$	p	$\mathscr{R}$	p	$\mathscr{R}$	p
BTC	1h	-66.40	**0.000**	-80.60	**0.000**	12.24	**0.000**	388.2	**0.000**	2908	**0.000**
	2h	-52.20	**0.000**	-51.59	**0.000**	11.88	**0.000**	218.6	**0.000**	1883	**0.000**
ETH	1h	-53.69	**0.000**	-71.70	**0.000**	0.585	0.838	340	**0.000**	2228	**0.000**
	2h	-36.67	**0.000**	-36.12	**0.000**	6.657	**0.005**	188.2	**0.000**	1288	**0.000**
XRP	1h	-54.26	**0.000**	-67.15	**0.000**	-4.634	0.283	346.1	**0.000**	2633	**0.000**
	2h	-34.36	**0.000**	-36.12	**0.000**	1.342	0.656	181.1	**0.000**	1340	**0.000**
LTC	1h	-46.22	**0.000**	-65.94	**0.000**	9.777	**0.004**	371.9	**0.000**	2496	**0.000**
	2h	-36.41	**0.000**	-36.18	**0.000**	-0.345	0.893	180.5	**0.000**	1127	**0.000**
XMR	1h	37.94	**0.000**	-49.90	**0.000**	10.24	**0.021**	390.1	**0.000**	2978	**0.000**
	2h	-21.93	**0.000**	-27.74	**0.000**	7.060	**0.020**	206.6	**0.000**	1535	**0.000**
Exponential		$\hat{x}_{\min}$		5%		15%		30%		45%	
dataset	Δt	$\mathscr{R}$	p	$\mathscr{R}$	p	$\mathscr{R}$	p	$\mathscr{R}$	p	$\mathscr{R}$	p
BTC	1h	-90.91	**0.000**	-91.94	**0.000**	-62.70	**0.012**	46.68	0.199	140.7	**0.000**
	2h	-46.31	**0.000**	-48.01	**0.000**	-42.72	**0.006**	5.091	0.823	39.74	0.106
ETH	1h	-72.61	**0.000**	-76.96	**0.000**	-48.97	**0.037**	24.59	0.444	64.02	**0.059**
	2h	-47.50	**0.000**	-41.22	**0.000**	-35.36	**0.020**	3.836	0.854	26.47	0.226
XRP	1h	-16.63	**0.000**	-41.53	**0.014**	37.64	0.226	140.8	**0.001**	183.7	**0.000**
	2h	63.29	**0.034**	-29.82	**0.006**	-0.554	0.978	40.43	0.137	63.84	**0.031**
LTC	1h	-75.08	**0.000**	-74.09	**0.000**	-51.94	**0.023**	15.08	0.621	38.18	0.233
	2h	-47.56	**0.000**	-47.78	**0.000**	-32.85	**0.016**	-9.873	0.603	5.591	0.778
XMR	1h	-11.35	0.720	-44.36	**0.003**	-12.18	0.625	29.73	0.328	35.56	0.247
	2h	4.018	0.829	-32.15	**0.000**	-16.89	0.231	4.705	0.794	7.220	0.696

3.4 Summary and Discussions

This chapter has explored the behaviors of price fluctuations in cryptocurrency markets by applying the Lévy's stable distribution and discussed its validity for the empirical analysis. We provide numerical, theoretical, and justifications for supporting the stable distribution as a practical model to understand the fluctuation phenomena in financial systems.

We focus on characterizing the entire dataset of returns, including the tail behaviors. The stable distribution takes into account the entire observations. With the use of the proper estimation method, we find that returns exhibit stable laws with tail index $\alpha \simeq 1.4$ and $\beta \simeq 0$ (symmetric). We introduce a numerical approach based on the CF and a theoretical approach based on the GCLT to find evidence for stable laws, by focusing on the time scaling behavior with different time intervals. Similar to other financial asset returns, our results of the numerical approach suggest that cryptocurrency price returns follow a fat-tailed stable distribution better than the Gaussian distribution for *all* time scales. However, we find that even if we admit some observational noise terms, the numerical distance shows implausible results for high-frequency data. On the other hand, the theoretical approach based on the GCLT represents implausible results for low-frequency data, where the stable regime breaks down to a Gaussian regime. From both points of view, our assessment implies that the stable model is not necessarily acceptable for any analysis condition. We propose that the combination of these approaches helps understand the intriguing properties of asset fluctuations, and gives us insight into appropriate ranges of time scaling for modeling with stable distribution in a more careful sense. In particular, a time scaling condition of ranging roughly 30 minutes to 4 hours is concluded to be a suitable range of intervals for cryptocurrency markets, where both quantitative and theoretic properties are consistent with the stable model.

Moreover, we confirm the potency of modeling returns with stable distributions under some time scaling conditions by clarifying which distribution shows a better fit among controversial fat-tailed distributions. We find statistical evidence that when a wider range of tail portion of data is considered, the stable distribution dominates other alternative distributions. The results imply that the stable model is comparatively appropriate for characterizing the entire or a broad range of the data. At the same time, we find that the far tails generally follow a power law, which coincides with the results in many empirical studies on tail behaviors of returns. Therefore, these ideas can be developed to create some benchmarks for portfolio theories and risk management. To reach a more rigorous conclusion on whether stable models may work in practical applications, however, a more elaborate discussion would be necessary.

Chapter 4

Fractal Correlation Dynamics of Cryptocurrencies

This chapter is corresponds to paper 3 in the author's papers list.

4.1 Introduction

The spread of coronavirus (COVID-19) was officially declared as a pandemic in March 2020 and has become a threat to people's daily lives on a global scale. The on-going prevalence has triggered many channels relevant to the global economy such as stock markets (Topcu and Gulal, 2020; Zhang et al., 2020; Zaremba et al., 2020; Baker et al., 2020) and labor markets (Groshen, 2020), making investors and financial researchers increasingly concerned and nervous.

Since cryptocurrencies often show different features from conventional assets due to their unique block-chain technology, there is growing interest in the impact of COVID-19 on cryptocurrency markets. Conlon et al. (2020) and Ji et al. (2020) examine the performance of cryptocurrencies as a safe haven during the COVID-19 pandemic. Drożdż et al. (2020) show the impact of the outbreak on the internal structure of the market. More importantly, a number of studies focus on the major research subject of the efficient market hypothesis (EMH) for understanding cryptocurrency market characteristics. The EMH suggests that market prices of assets immediately reflect all available information including past data and its relevant data, so that price fluctuations can be best described as a random walk movement and thus it is impracticable to predict market prices or earn profits from returns. It has been recognized in the finance literature that financial markets often exhibit anomalies, and hence informational efficiency is not always achieved. Although Bitcoin returns show the efficiency for certain periods, they do not follow a random walk behavior in general (Urquhart, 2016; Tiwari et al., 2018). The (in)efficiency of financial markets can also be time-varying (Jiang et al., 2018; Frezza et al., 2021). Wang and Wang (2021) finds that during the COVID-19 pandemic, the Bitcoin market became less inefficient than stock markets using an entropy-based analysis.

Extreme conditions of crisis and epidemic diseases often formulate behavioral biases of herding (Chang et al., 2000; Chiang and Zheng, 2010; Economou et al., 2011), and the presence of multifractality is a consequence of the presence of herding behavior (Cajueiro and Tabak, 2009). The concept of multifractality regards complexity and provides an explanation of market patterns and correlations in terms of self-similarity, long-memory, and scaling patterns, all of which the EMH fails to capture (Fernández-Martínez et al., 2019). According to the alternative fractal markets hypothesis (FMH) initiated by Peters (1994), short- and long-term investors have different investment horizons and different valuations for information flows. Market stability is achieved when the numbers of long-term investors balance those of short-term ones. However, once they start focusing on the current interim market fluctuations, the market equilibrium breaks down (Weron and Weron, 2000). The predominance of short-term investors leads to crashes in reaction to bad news. Moreover, herding behavior exhibits asymmetric characteristics between upward and downward trends (Tan et al., 2008; Chiang and Zheng, 2010), so the asymmetric herding behavior of cryptocurrency markets have also attracted attention (Stavroyiannis and Babalos, 2019; Mensi et al., 2019b; Kristjanpoller et al., 2020).

Several studies have examined cryptocurrency markets during the COVID-19 pandemic in a framework of fractal analysis, but the results seem rather mixed. Mnif et al. (2020) and Yarovaya et al. (2020) investigate the long-term properties of cryptocurrencies and find that the market became more efficient after the outbreak, thus concluding that COVID-19 does not significantly increase herding. Naeem et al. (2021), on the other hand, finds traces of temporarily increased inefficiency during the COVID-19 pandemic by using a time-varying approach to detect self-similarity and its asymmetric properties. One missing point is that past studies discuss the efficiency without explicitly incorporating possible differences between short and long investment horizons. To fill the gap, this study extends our limited understandings of short- and long-term behaviors of cryptocurrency markets during the COVID-19 pandemic.

For this purpose, we analyze market efficiency of cryptocurrency markets during the pre- and post-COVID-19 periods, accounting for short and long investment horizons with different scaling regimes, by applying the asymmetric multifractal detrended fluctuation analysis (A-MFDFA) proposed by Cao et al. (2013). This method allows us to detect the asymmetric efficiency level of cryptocurrency markets. For a given range of scales, the A-MFDFA method well quantifies the generalized Hurst exponents for uptrend and downtrend price movements under different magnitudes of price fluctuations. The main finding suggests that after the outbreak, major cryptocurrency markets became more efficient in the long-run, but in the short-run, the markets exhibit an increase in the degree of inefficiency, which implies the presence of herding. We also confirm that the outbreak has changed asymmetric patterns in cryptocurrency markets. Our results are crucial for financial regulators and investment managers to mitigate cryptocurrency market distortion and conduct effective risk controls during extreme conditions, like the COVID-19 pandemic.

4.2 Data presentation: COVID19 and surrounding periods

Several studies suggest using such high-frequency data because inefficiency and asymmetric behaviors are more likely to be highlighted than intra-day data (Zargar and Kumar, 2019; Stavroyiannis et al., 2019; Naeem et al., 2021). We use hourly-based Bitcoin (BTC) and Ethereum (ETH) prices traded on https://poloniex.com/ against the cryptocurrency Tether (USDT), which is designed to maintain the same value as the US dollar, during the period from 2019/01/01 to 2020/12/31. Given that the first case of COVID-19 cluster was reported to the WHO China Country Office on December 31, 2019, we split the whole sample into two subperiods: the year 2019 (before outbreak) and the year 2020 (after outbreak).[1]

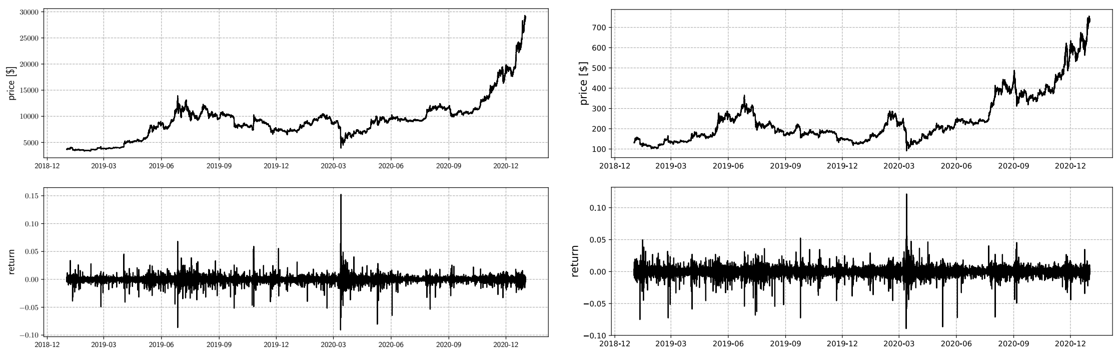

Figure 4.1: Price and 1-hour return series of Bitcoin (left) and Ethereum (right) for the investigated period (2019/01/01 to 2020/12/31).

[1]Other relevant studies such as Mnif et al. (2020) and Aslam et al. (2020) also employ this date to divide the period for analyzing financial markets before and after the COVID-19 outbreak.

Table 4.1: Descriptive statistics for 1-hour Bitcoin and Ethereum return series for the periods before and after the COVID-19 outbreak. For the Jarque-Bera test, *** denotes statistical significance at 1% level.

	BTC		ETH	
	before outbreak	after outbreak	before outbreak	after outbreak
Mean(%)	0.0076	0.0159	-0.0003	0.0198
Median(%)	0.0083	0.0133	-0.0003	0.0153
Std. Dev.(%)	0.7043	0.7935	0.8528	0.9702
Max.(%)	9.0774	16.122	9.7788	13.892
Min.(%)	-9.1708	-19.200	-14.191	-23.273
Skewness	0.0800	-2.5899	-1.0883	-1.9389
Kurtosis	26.754	119.30	27.807	62.920
Jarque-Bera	261243^{***}	5218673^{***}	283917^{***}	1454321^{***}
ADF	-93.436^{***}	-19.080^{***}	-95.628^{***}	-98.403^{***}
KPSS	0.096	0.073	0.059	0.056

The return series are calculated as $r_t = \ln p_t - \ln p_{t-1}$ where p_t denotes the price at time t. We show in Figure 4.1 the price and return series of BTC and ETH for the investigated period and we report in Table 4.1 the descriptive statistics of returns for each sample period. Both major cryptocurrencies have a more significant level of deviation, kurtosis and non-gaussianity after the outbreak. Significant statistics of Augmented Dickey-Fuller (ADF) tests and insignificant statistics of Kwiatkowski–Phillips–Schmidt–Shin (KPSS) tests show that the return series are stationary for all cases.

4.3 A-MFDFA analysis

4.3.1 Asymmetric multifractality in short- and long-terms

Figures 4.2 and 4.3 depict the log-log plots of the fluctuation functions ($F_q(s)$, $F_q^+(s)$, and $F_q^-(s)$) versus the time scale s during the periods before and after the COVID-19 outbreak for Bitcoin and Ethereum. As mentioned in Thompson and Wilson (2016), we consider the scale ranges from 20 to $N/10$ to avoid biases and assure the validity of the scaling exponent estimates. We find a crossover point s^* of each fit at $\ln(s^*) \simeq 5.5$ ($s^* \simeq 10$ days) for both markets, where short- and long-term component dynamics are described by different scaling regimes.[2] Moreover, the location of this point seems to be consistent over different market trends and

[2] See Wang et al. (2009) and Tiwari et al. (2017) for detailed discussions about crossover points.

periods. The presence of the crossover uncovers that investors' behaviors differ depending on horizons, and their strategies have distinctive features in terms of herding and multifractal behavior. The generalized Hurst exponents for the short-term components are calculated by using the log-log regression within the scale ranges $20 \le s \le s^*$, and those for the long-term components are calculated within the scale ranges $s^* < s \le N/10$.

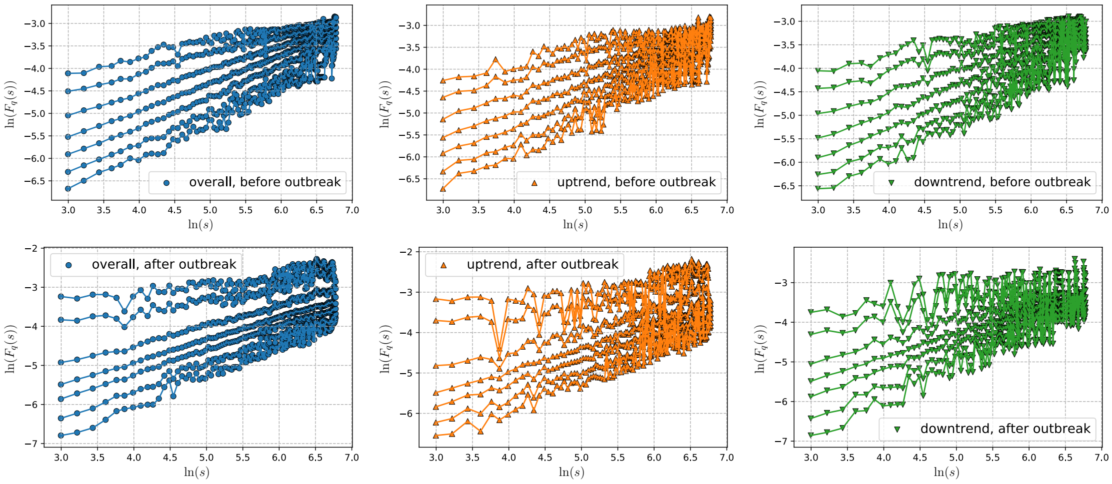

Figure 4.2: The case of Bitcoin. Log-log plot of $F_q(s)$ versus time scale s for different market trends and before and after the outbreak where q take the values of -10, -5, -2, 0, 2, 5, and 10.

Figures 4.4 and 4.5 show the results of $h(q)$, $h^+(q)$, and $h^-(q)$ for Bitcoin and Ethereum, respectively. Both short- and long-term components show signs of multifractality since the values of the generalized Hurst exponents decrease as q becomes large. When focused on the Hurst exponent $H = h(q = 2)$, the values are nearby 0.5, meaning that the series may show signs of weak persistence or anti-persistence. For smaller fluctuations ($q < 0$), the markets are more persistent in the short-term after the outbreak (left-side panels in Figures 4.4 and 4.5), but the opposite is observed in the long-term (right-side panels in Figures 4.4 and 4.5). Asymmetric properties of persistence are also detected. Throughout our investigated period, we find the tendency of less asymmetry in the short-term where uptrend and downtrend markets show similar scaling properties (left-side panels), but the markets are more likely to exhibit asymmetry in the long-term (right-side panels). This is consistent with the findings of Naeem et al. (2021) which suggests that asymmetry results from the tendency of investors paying more attention to persistence in the longer term. Moreover, to some extent, both multifractality and asymmetry vary after the outbreak.

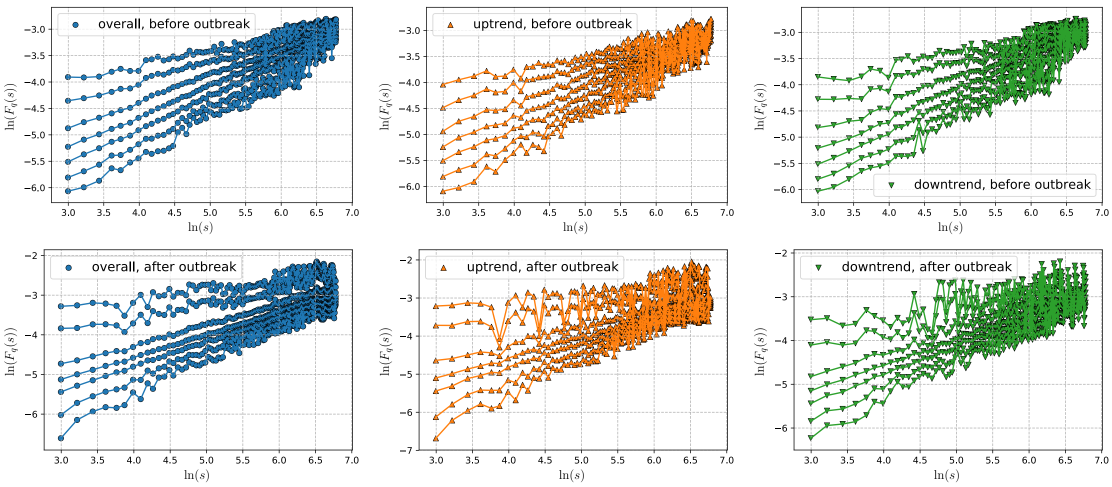

Figure 4.3: The case of Ethereum. Log-log plot of $F_q(s)$ versus time scale s for different market trends and before and after the outbreak.

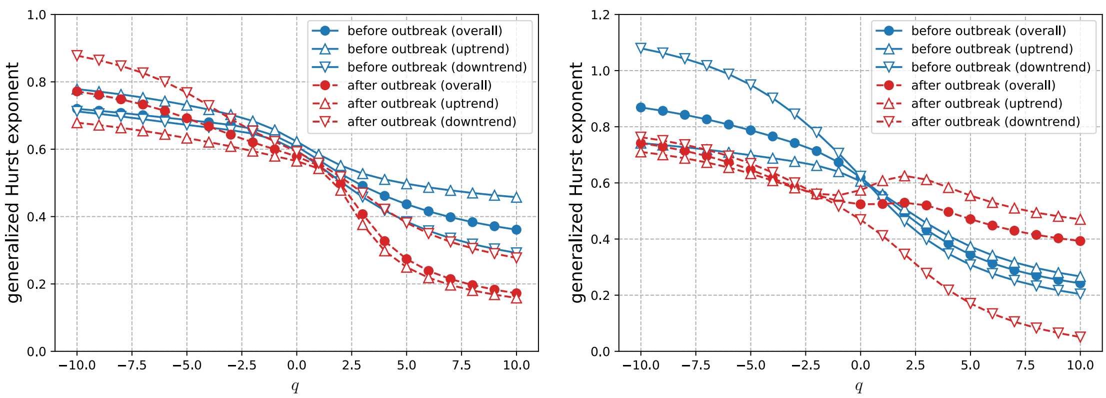

Figure 4.4: The case of Bitcoin. q dependencies of generalized Hurst exponents with different trends in the short-term $s < s^*$ (left) and in the long-term $s > s^*$ (right), where $\ln(s^*) = 5.5$. The blue solid lines present the results for the period of before the outbreak, and the red lines after the outbreak.

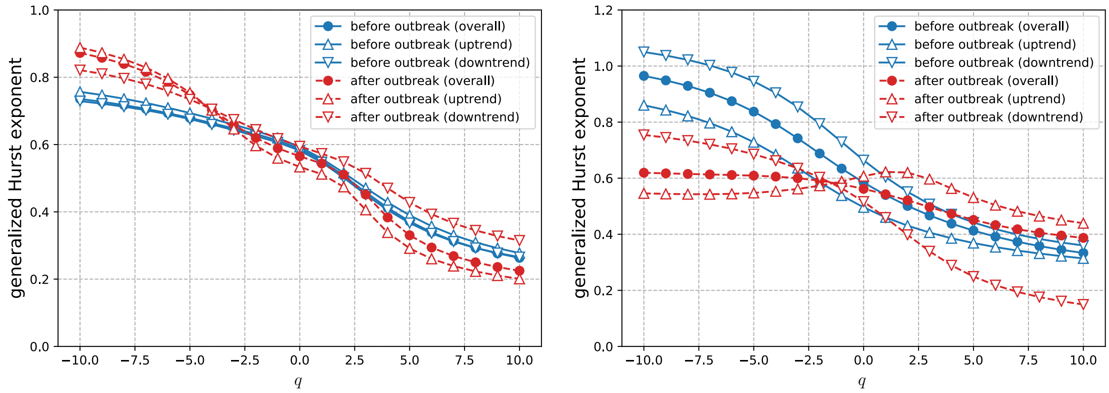

Figure 4.5: The case of Ethereum. q dependences of generalized Hurst exponents with different trends in the short-term $s < s^*$ (left) and in the long-term $s > s^*$ (right), where $\ln(s^*) = 5.5$.

4.3.2 Market inefficiency degree

To quantify the degree of multifractality and inefficiency, we use the market deficiency measure (MDM) defined in Wang et al. (2009):

$$D = \frac{1}{2}(|h(-10) - 0.5| + |h(10) - 0.5|). \tag{4.3.1}$$

This measure illustrates the discrepancy from an efficient market by evaluating the deviation from a random walk process in terms of both large ($q = 10$) and small ($q = -10$) fluctuations. Zero value of the MDM implies market efficiency with monofractal structure satisfying $h(q) = 0.5$ for any q. Large values of the MDM indicate strong inefficiency. We find that regardless of market trends, the values decrease after the outbreak in the long-term ($s > s^*$) (Table 4.2). This result is consistent with Mnif et al. (2020) and Naeem et al. (2021) which find that in the long-term, multifractality is reduced and thus the pandemic has a positive impact on cryptocurrency market efficiency. However, when focusing on short-term horizon ($s < s^*$), we find the opposite result where the MDM values significantly increase after the outbreak, and thus the markets become inefficient. These results imply that after the outbreak, cryptocurrency investors shift their strategy towards shorter horizons, which means that strong herding behavior is present in the short-term.

We further examine the asymmetric herding behaviors between upward and downward market trends for each of the different periods and horizons. Figures 4.6 and 4.7 show the degree of asymmetry for the two investigated cryp-

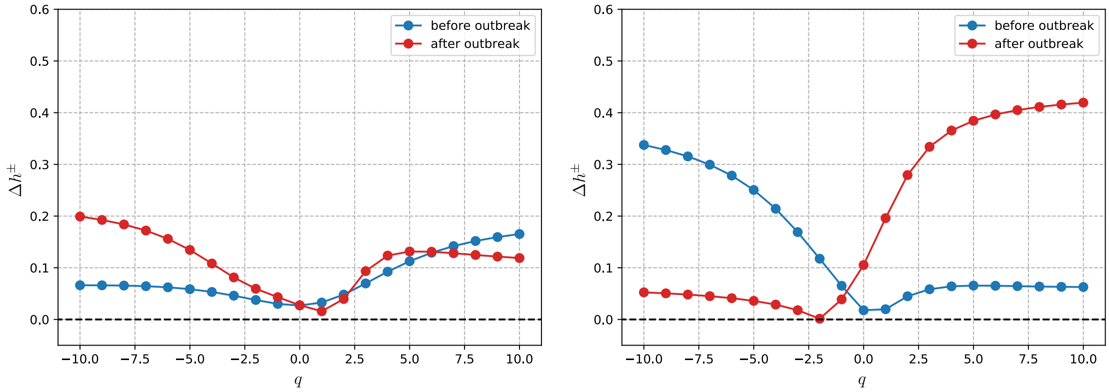

Figure 4.6: The case of Bitcoin. Asymmetric degree of multifractality between uptrend and downtrend for the short-term horizon (left) and long-term horizon (right), respectively. We represent the results for the period before the outbreak in blue and after the outbreak in red.

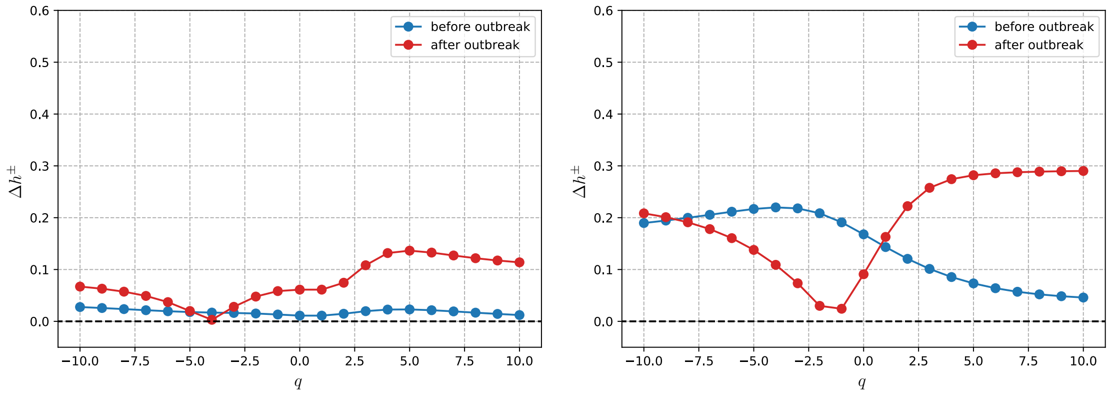

Figure 4.7: The case of Ethereum. Asymmetric degree of multifractality between upward trends and downward trends for the short-term horizon (left) and long-term horizon (right), respectively.

Table 4.2: Values of the MDM for short-term and long-term under different market trends. The larger values between before and after the outbreak are shown in bold.

		short-term ($s < s^*$)		long-term ($s > s^*$)	
		before outbreak	after outbreak	before outbreak	after outbreak
BTC	overall	0.179	**0.300**	**0.313**	0.174
	uptrend	0.160	**0.260**	**0.238**	0.120
	downtrend	0.210	**0.300**	**0.438**	0.356
ETH	overall	0.236	**0.324**	**0.316**	0.116
	uptrend	0.240	**0.344**	**0.273**	0.053
	downtrend	0.232	**0.253**	**0.345**	0.302

tocurrencies:

$$\Delta h^{\pm}(q) = |h^{+}(q) - h^{-}(q)|, \tag{4.3.2}$$

which corresponds to various fluctuation magnitudes. Larger values of $\Delta h^{\pm}(q)$ indicate higher asymmetry of multifractality between upward trends and downward trends. It is evident that asymmetric features are not constant over time. The results show that the degree of asymmetry increases only slightly in the short-term (left-side panels in Figures 4.6 and 4.7).

4.3.3 Source of inefficiency

However, asymmetric properties in the long-term horizon (left-side panels) is different from those observed in the short-term horizon. For relatively smaller fluctuations ($q < 0$), the degree of asymmetry, particularly for Bitcoin, greatly decreases during the pandemic so that the market persistence becomes close to symmetry. On the contrary, for relatively larger fluctuations ($q \geq 0$), the degree significantly increases and the persistence is no longer symmetric. In line with the long-term study of Bitcoin, Ethereum also shows evidence of weaker degree of asymmetry for small fluctuations but stronger degree of asymmetry for large fluctuations. Our results imply that the pandemic urged long-term cryptocurrency investors to switch their attention from smaller toward larger fluctuations, which results in the presence of asymmetric multifractality for larger q under different signs of market returns (Chiang and Zheng, 2010). The pandemic did not inspire short-term investors to focus on certain fluctuation magnitudes, because the asymmetry level was not raised significantly for any q.

Although the empirical findings uncover properties of asymmetric multifractality and how they have changed during the pandemic, further implications of multifractality need to be addressed to advance the discussions of EMH. Therefore, we explore the sources of multifractality. It is well known that the multifractality of financial time series is mainly a consequence of the two major phenomenon: the broad probability density function and long-range correlations between elements of time series. To understand the contribution of long-range correlations, we compare the level of multifractality between the original series and random shuffled series. The shuffling procedure can destroy all correlations of returns, while the distribution remains unchanged. To understand the contribution of broad probability density function, we surrogate the returns with Gaussian distribution, while maintaining the same rank ordering by sorting the generated returns, and compare its multifractality with the original one. This procedure eliminates the fat-tails but the linear correlations are preserved (Cao et al., 2013). To quantify the level of multifractality, we employ the following measure (Cao et al., 2013):

$$\Delta h = \max_q (h(q)) - \min_q (h(q)). \tag{4.3.3}$$

Greater values indicate stronger multifractality.

Table 4.3: The level of multifractality Δh for the shuffled and surrogated series with respect to short-term horizons. The smaller values between shuffled and surrogated series are shown in bold.

		before outbreak			after outbreak		
short-term ($s < s^*$)		original	shuffled	surrogated	original	shuffled	surrogated
BTC	overall	0.359	0.459	**0.086**	0.599	0.568	**0.255**
	uptrend	0.321	0.464	**0.161**	0.520	0.565	**0.244**
	downtrend	0.420	0.450	**0.037**	0.600	0.578	**0.206**
ETH	overall	0.473	0.446	**0.154**	0.647	0.528	**0.251**
	uptrend	0.479	0.423	**0.193**	0.687	0.502	**0.273**
	downtrend	0.464	0.440	**0.151**	0.506	0.520	**0.213**

We show in Tables 4.3 and 4.4 the level of multifractality for the shuffled and surrogated series of Bitcoin and Ethereum returns before and after the outbreak with respect to different investment horizons.[3] When focused on the short-term horizon (Table 4.3), the multifractality levels of the shuffled series are hardly weaker than those of the original series, but the surrogated ones are obviously weaker during both periods. This indicates that fat-tailed distribution is the main

[3]For the level of multifractailty, we employ the average of 100 synthetic Δh calculated from the shuffled/surrogated series to avoid strong biases due to sample size.

Table 4.4: The level of multifractality Δh for the shuffled and surrogated series with respect to the long-term horizon. The smaller values between shuffled and surrogated series are shown in bold.

		before outbreak			after outbreak		
long-term ($s > s^*$)		original	shuffled	surrogated	original	shuffled	surrogated
BTC	overall	0.627	0.174	**0.093**	0.349	0.274	**0.162**
	uptrend	0.475	0.194	**0.018**	0.240	0.271	**0.122**
	downtrend	0.875	**0.199**	0.275	0.712	**0.308**	0.332
ETH	overall	0.632	**0.174**	0.278	0.232	**0.207**	0.242
	uptrend	0.546	0.187	**0.162**	0.183	0.226	**0.157**
	downtrend	0.690	**0.193**	0.346	0.605	**0.220**	0.415

cause of multifractality and correlations of large and small fluctuations is not an essential factor. We note that this nature does not change before and after the outbreak. In the long-term horizon (Table 4.4), we can see that both sources have significant impacts on multifractality, especially before the outbreak. The impact of both sources become smaller after the outbreak, which highlights the positive effect on EMH in the long-run. Nevertheless, the surrogated results suggest that fat-tailed distribution contributes to multifractality in the long-run as well, meaning that local behaviors caused by fat-tails are likely to be reflected in the global behaviors. Interestingly, the levels of multifractality are weaker for the surrogated series in uptrend markets, while they are weaker for the shuffled series in downtrend markets. This implies that fat-tails contribute more to multifractality than autocorrelations when the market value goes up, while autocorrelations contribute more than fat-tails when the market value goes down. Therefore, substantial asymmetric properties of Bitcoin and Ethereum in the long-term horizon, shown in the right panels of Figs. 4.6 and 4.7, can be due to the presence of different predominant sources of multifractality between bull and bear markets.

4.4 Summary and Discussions

This study evaluated market efficiency and asymmetric multifractality of the two major cryptocurrencies (Bitcoin and Ethereum) during the periods before and after the COVID-19 outbreak, accounting for the different scaling regimes on fast and slow time scales. By using the A-MFDFA method, we found that the markets have asymmetric multifractality with crossovers of approximately 10 days, indicating that scaling behaviors are dependent of investment horizons. Our results provided empirical evidence of increasing inefficiency for the short-term, while the markets show traces of efficiency for the long-term. In other words, COVID-19 significantly increased herding in the short-run but not in the long-run. This study also discussed the features of asymmetric properties between upward and downward trends. For the short-term, there was only a subtle change of asymmetry after the outbreak, but for the long-term, there was a substantial shift in the degree of asymmetry where investors have focused more on larger fluctuations. Although fat-tailed distribution of returns generally causes the multifractal behavior, the contribution of autocorrelations to multifractality becomes substantial in the long-term when the market is in a downtrend (bear market). The presence of different predominant sources of multifractality between bull and bear markets could be a driver to the substantial asymmetric properties of Bitcoin and Ethereum observed in the long-term. Our findings argue that analyzing different scales of horizons can be a key to reveal complex behaviors during crisis periods, although the relationship between multifractality and asymmetric efficiency of the on-going COVID-19 pandemic is still debatable. Similar study of Zitis et al. (2023) also reports interesting results during the pandemic period using the asymmetric multifractal analysis in addition to other complex measure analysis. These results offer opportunities for investors and portfolio managers to understand cryptocurrency market efficiency that plays a crucial role in their decision-making.

Chapter 5

Fractal Cross-correlation Dynamics of Cryptocurrencies

This chapter corresponds to paper 4 in the author's papers list.

5.1 Introduction

One of the fundamental issues in financial markets is the behavior of the relationship between price and volatility. The cross-correlations between international stock returns of highly developed economies fluctuate strongly with time, and increase in periods of high market volatility Solnik et al. (1996). In addition, it is known that the conditional variance of equity returns are more affected by negative news compared to positive news Black (1976). In this sense, negative returns increase the volatility by more than positive returns due to the leverage effect, also known as the asymmetric volatility effect Baur and Dimpfl (2018). This is related to the trading of informed and uninformed investors posing different impacts on the return process. Specifically, uninformed traders lead to higher serial correlations in returns that make the volatility increase, whereas informed traders suggest no autocorrelation Avramov et al. (2006). Many studies have traditionally applied the asymmetric Generalized Autoregressive Conditional Heteroscedasticity (GARCH) models to analyze the asymmetric reactions of volatility to returns. Baur and Dimpfl (2018) use the TGRACH model and find an intriguing aspect of cryptocurrency price behavior differently from other traditional assets— the presence of inverse-asymmetric volatility effect. In other words, positive shocks increase the volatility by more than negative shocks, where speculative investments made by uninformed noise traders are dominant after positive shocks. Cheikh et al. (2020) employ a flexible model of ST-GARCH and also report similar results of a positive return-volatility relationship.

Although the anomalies in volatility dynamics justify the application of GARCH class models (Katsiampa, 2017), they focus more on the linear correlations of returns and volatility fluctuations without the scaling properties (Ghazani and Khosravi, 2020). Applying the DFA based analysis could be advantageous to accomplish a more essential understanding of the dynamics of price and volatility because it accounts for the widely acknowledged nonlinearity and scaling properties. In addition, the method does not require the specification of a statistical model, so it is easy to implement and can directly calculate the scaling exponents.

This study employs the MF-ADCCA approach to investigate the asymmetric multifractal properties of cross-correlations between price fluctuations and realized volatility fluctuations in cryptocurrency markets, which is the first contribution to the literature. Our empirical findings reveal traces of asymmetric multifractality and its dependence on the directions of price movements. Next, we address the financial issue of asymmetric volatility effect, crucial for financial investors and regulators. We propose to use a framework of fractal analysis, which differs from the conventional GARCH-class models where how one-time price shock influences volatility is analyzed. This is the second contribution to the literature. We show that the asymmetric volatility effect can be examined by the assessment of asymmetric cross-correlations between bull and bear markets over various time scales from short to long time periods. The levels of cross-correlations are quantitatively investigated for each time scale relying on the asymmetric DCCA coefficient (Cao et al., 2018) based on the idea of the DCCA coefficient (Zebende, 2011; Podobnik et al., 2011). We find the presence of different reactions of volatility to price in major cryptocurrencies, where price-volatility is more strongly cross-correlated under negative market trends compared to positive market trends. However, for the relatively minor ones, cross-correlations are stronger under positive market trends, implying that the inverse-asymmetric volatility effect is present. Our findings not only provide new insights into the nature of the price-volatility dynamics, but also contribute to other relevant issues such as volatility spillovers, speculative trading, and the maturity of cryptocurrency markets.

The rest of this chapter is organized as follows. Section 5.2 describes the data used in the analysis. Section 5.3 explains the two nonlinear dynamical methods used in the analysis, the MF-ADCCA approach and the asymmetric DCCA coefficient, to further investigate volatility dynamics. Section 5.4 present the results and discussions of the empirical analysis. Section 5.5 provides discussions and summarizes the chapter.

5.2 Data presentation

In this study, we use cryptocurrency price data traded on https://poloniex.com/ [1] for four major coins of BTC, ETH, XRP, and LTC all against Tether (USDT), which is a cryptocurrency designed to maintain the same value as the US dollar. We analyze the period starting from June 1st, 2016, and ending on December 28th, 2020. This period includes the cryptocurrency boom at the end of 2018 and the crash at the beginning of 2019. Recently the prices of many cryptocurrencies are increasing, for instance, the Bitcoin price marked a record-breaker of over $27,200 on December 28, 2020.

As a proxy of the volatility series, we employ the realized bipower variation (Barndorff-Nielsen, 2004). Realized bipower variation is determined using high frequency price data:

$$\mathrm{BPV}_t = \sum_j |r_{t,t_j}||r_{t,t_{j+1}}|, \tag{5.2.1}$$

where r_{t,t_j} is the return or the log-difference of price calculated from δt-minute sampling intervals, and $t_j = j\delta t$ denotes the time on day t. Although it is well-known that realized volatility (realized variance), the sum of squared intraday returns, is expected to converge to the integrated volatility σ_t^2 in the limit $\delta t \to 0$, its pure form is not an appropriate measure when frequent jumps and microstructure noise are observed in the series. The realized bipower variation is somewhat robust to jumps providing a model-free and consistent alternative to realized variance (Barndorff-Nielsen, 2004). In this study, we use the 5-minute sampling interval because it avoids strong bias derived from extremely high frequencies and maintains an accurate measure of volatility (Bandi and Russell, 2006; Liu et al., 2015). The price increments (returns) and volatility increments (volatility changes) are respectively calculated as

$$r_t = \ln p_t - \ln p_{t-1}, \tag{5.2.2}$$

$$v_t = \ln \hat{\sigma}_t - \ln \hat{\sigma}_{t-1}, \tag{5.2.3}$$

where $\hat{\sigma}_t = \sqrt{\mathrm{BPV}_t}$, and p_t denotes daily closing price. To check whether the log-volatility series ($\ln \hat{\sigma}_t$) are non-stationary or not, we implemented two statistical tests; the Augmented Dickey-Fuller (ADF) test (Dickey and Fuller, 1979) and Kwiatkowski-Philips-Schmidt-Shin (KPSS) test (Kwiatkowski et al., 1992).

[1] We take advantage of Poloniex that the exchange provides high frequency data without missing data throughout the investigated period. Although Poloniex certainly may not be one of the most known exchanges, it provides transactions over 100 active cryptocurrencies. In the exchange, the markets such as BTC, ETH, XRP, and LTC have enough liquidity so that market analysis can be conducted without encountering zero values of intraday returns.

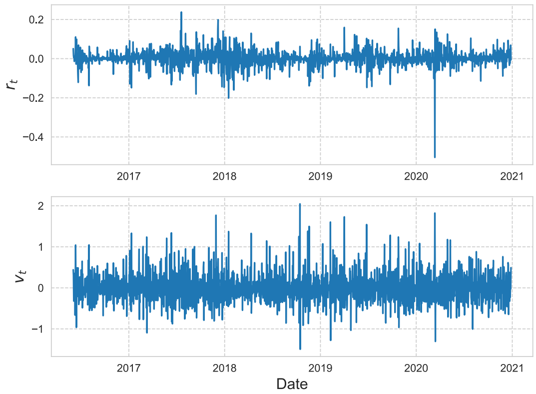

(a) BTC

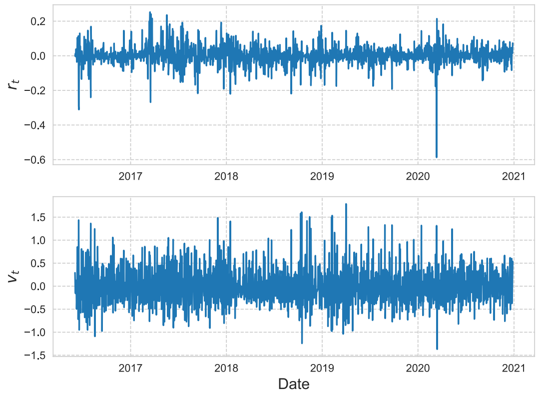

(b) ETH

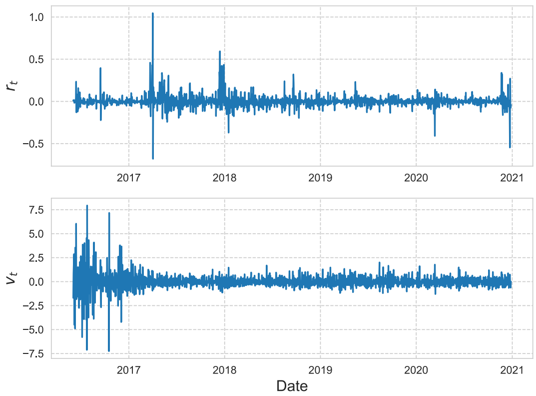

(c) XRP

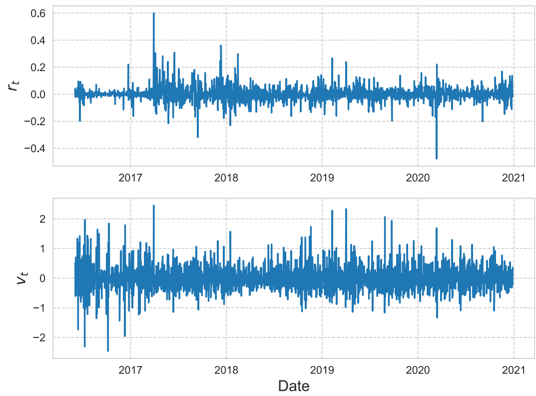

(d) LTC

Figure 5.1: The series of daily returns r_t and the series of volatility changes v_t calculated from 5 minute intervals for (a) BTC, (b) ETH, (c) XRP, and (d) LTC.

We confirm that for all cases, the series are non-stationary and thus the log-differences should be considered. In particular, the ADF tests show that the null hypothesis of the existence of unit root cannot be rejected at 1% significance level, and the KPSS tests show that the null hypothesis of sationarity is rejected at 1% significance level (see Appendix). The data length of r_t and v_t equally consists of $N = 1669$ for all the series we use in the analysis. The series are shown in Fig. 5.1.

In Table 5.1, we report the descriptive statistics for the returns of the investigated cryptocurrencies. As we can see from the results of the Jarque-Bera test, all of them are remarkably far from the Gaussian distribution with high values of kurtosis and a certain degree of skewness (*** denotes statistical significance at 1% level). Similarly, descriptive statistics for the volatility changes in Table 5.2

Table 5.1: Descriptive statistics for cryptocurrency market time series (returns)

	BTC	ETH	XRP	LTC
Mean(%)	0.233	0.234	0.233	0.198
Median(%)	0.243	0.042	-0.152	-0.067
Std. Dev.(%)	4.174	5.701	7.397	5.934
Max.(%)	23.814	25.274	104.605	60.051
Min.(%)	-50.435	-58.697	-68.039	-47.796
Skewness	-1.107	-0.704	2.182	0.877
Kurtosis	15.557	9.800	37.335	12.740
Jarque-Bera[1]	17172***	6816.1***	98255***	11501***

Table 5.2: Descriptive statistics for cryptocurrency market time series (bipower volatility change)

	BTC	ETH	XRP	LTC
Mean(%)	0.044	0.050	0.054	0.137
Median(%)	-2.702	-3.017	-4.498	-3.454
Std. Dev.(%)	37.672	39.560	80.847	47.053
Max.(%)	204.646	178.746	794.343	245.149
Min.(%)	-149.576	-136.984	-725.121	-246.325
Skewness	0.747	0.600	0.264	0.506
Kurtosis	2.446	1.360	25.454	2.993
Jarque-Bera[1]	571.44***	228.82***	44588***	693.64***

tell us that the series also have non-gaussian behavior, but tend to have higher variance and lower kurtosis in comparison with the return series.

5.3 Methodology of fractal cross-correlation analysis

5.3.1 MF-ADCCA analysis

This subsection presents a slightly modified version of the MF-ADCCA method of Cao et al. (2014), where the asymmetric proxy is not directly the return series but the price index, similar to the index-based MFDFA proposed by Lee et al. (2017). This method describes the asymmetric cross-correlations between two time series $\{x_t : t = 1,\dots,N\}$ and $\{y_t : t = 1,\dots,N\}$ in terms of whether the aggregated index shows a positive increment or a negative increment.

First, we start by constructing the profiles from the series

$$X(k) = \sum_{t=1}^{k} (x_t - \bar{x}), \ t = 1, \ldots, N,$$
$$Y(k) = \sum_{t=1}^{k} (y_t - \bar{y}), \ t = 1, \ldots, N$$

where $\bar{x}$ and $\bar{y}$ is the average over the entire return series, respectively. We also calculate the index proxy series $I(k) = I(k-1)\exp(x_k)$ for $k = 1, \ldots, N$ with $I(0) = 1$, used for judging the positive and negative directions of the index series afterwards. Next, the profiles $X(k)$, $Y(k)$, and the index proxy $I(k)$ are divided into $N_s = \lfloor N/s \rfloor$ non-overlapping segments of length s. The division is repeated starting from the other end of the series to consider the entire profile, since N is unlikely to be a multiple of s and there may be remains in the profile. Thus, we have $2N_s$ segments in total for each series.

We next move on to the procedure of detrending the series. For each segment $v = 1, \ldots, 2N_s$ of length s, the local trend of the profiles are calculated by fitting a least-square degree-2 polynomial $\tilde{X}_v$ and $\tilde{Y}_v$, which is used to detrend $X(k)$ and $Y(k)$, respectively. At the same time we determine the local asymmetric direction of the index series by estimating the least-square linear fit $\tilde{I}_v(i) = a_{I_v} + b_{I_v} i$ ($i = 1, \ldots, s$) for each segment. Positive (upward) or negative (downward) trends depend on the sign of the slope b_{I_v}.

Then the detrended covariance for each of the $2N_s$ segments is calculated as:

$$f^2(s,v) = \frac{1}{s} \sum_{i=1}^{s} \left| X((v-1)s+i) - \tilde{X}_v(i) \right| \cdot \left| Y((v-1)s+i) - \tilde{Y}_v(i) \right|$$

for $v = 1, \ldots, N_s$ and

$$f^2(s,v) = \frac{1}{s} \sum_{i=1}^{s} \left| X(N-(v-N_s)s+i) - \tilde{X}_v(i) \right| \cdot \left| Y(N-(v-N_s)s+i) - \tilde{Y}_v(i) \right|$$

for $v = N_s + 1, \ldots, 2N_s$.

The upward and downward q-th order fluctuation functions are calculated by taking the average over all segments as:

$$F_q^+(s) = \left\{ \frac{1}{M^+} \sum_{v=1}^{2N_s} \frac{1+\mathrm{sgn}(b_{I_v})}{2} \left[f^2(s,v) \right]^{q/2} \right\}^{1/q},$$
$$F_q^-(s) = \left\{ \frac{1}{M^-} \sum_{v=1}^{2N_s} \frac{1-\mathrm{sgn}(b_{I_v})}{2} \left[f^2(s,v) \right]^{q/2} \right\}^{1/q}, \tag{5.3.1}$$

for any real value $q \neq 0$, and

$$F_0^+(s) = \exp\left\{\frac{1}{2M^+}\sum_{v=1}^{2N_s}\frac{1+\mathrm{sgn}(b_{I_v})}{2}\ln\left[f^2(s,v)\right]\right\},$$
$$F_0^-(s) = \exp\left\{\frac{1}{2M^-}\sum_{v=1}^{2N_s}\frac{1-\mathrm{sgn}(b_{I_v})}{2}\ln\left[f^2(s,v)\right]\right\}, \tag{5.3.2}$$

for $q = 0$. $M^+ = \sum_{v=1}^{2N_s}\frac{1+\mathrm{sgn}(b_{I_v})}{2}$ and $M^- = \sum_{v=1}^{2N_s}\frac{1-\mathrm{sgn}(b_{I_v})}{2}$ respectively represent the numbers of segments with positive and negative trends under the assumption of $b_{I_v} \neq 0$ for all $v = 1,\ldots,2N_s$, such that $M^+ + M^- = 2N_s$. The q-th order fluctuation functions for the overall trend corresponds to the MF-DCCA method shown as:

$$F_q(s) = \left\{\frac{1}{2N_s}\sum_{v=1}^{2N_s}\left[f^2(s,v)\right]^{q/2}\right\}^{1/q}, \tag{5.3.3}$$

for $q \neq 0$ and when $q = 0$,

$$F_0(s) = \exp\left\{\frac{1}{4N_s}\sum_{v=1}^{2N_s}\ln\left[f^2(s,v)\right]\right\}. \tag{5.3.4}$$

If the series x_k and y_k are long-range power-law cross-correlated, then the q-th order fluctuation functions follow a power-law of the forms $F_q^+(s) \sim s^{h_{xy}^+(q)}$, $F_q^-(s) \sim s^{h_{xy}^-(q)}$, and $F_q(s) \sim s^{h_{xy}(q)}$. The long-range power-law correlation properties are represented in terms of the scaling exponent also known as the generalized Hurst exponent.

The scaling exponent can easily be calculated by performing a log-log linear regression. However, the performance of the regression more or less depends on the choice of which range of scales to be implemented. As recommended in Thompson and Wilson (2016), we employ the scale ranging from $s_{\min} = \max(20, N/100)$ to $s_{\max} = \min(20s_{\min}, N/10)$ and using 100 points in the regression, in order to avoid biases and maintain the validity of the estimation.

In cases of no cross-correlations, $h_{xy}(q) = 0.5$ satisfies. If $h_{xy}(q) > 0.5$, the cross-correlations between the series are persistent with long-memory. On the contrary, $h_{xy}(q) < 0.5$ indicates that the cross-correlations between the series are anti-persistent with short-memory. The same explanation certainly holds for $h_{xy}^+(q)$ and $h_{xy}^-(q)$, but the scaling exponents of cross-correlations are individually measured for positive and negative increments.

The order q implies to what degree the various magnitudes of fluctuations are to be evaluated. Scaling exponents for $q > 0$, where the fluctuation function $F_q(s)$ is dominated by large fluctuations, reflect the behavior of larger fluctuations. Scaling exponents for $q < 0$ reflect the behavior of smaller fluctuations since small fluctuations dominate the fluctuation function. If $h_{xy}(q)$ is independent of q, then the cross-correlation of the series is monofractal since the scaling behavior of the detrended covariance $F^2(s,v)$ is identical for all segments. On the other hand, if the value differs depending on q, small and large behaviors have different scaling properties and the cross-correlations of the series are multifractal. It should be mentioned that when $q = 2$, $h_{xy}(q)$ corresponds to the Hurst exponent.

The features of the multifractality can be further explored by the Rényi's exponent given as

$$\tau_{xy}(q) = qh_{xy}(q) - 1. \tag{5.3.5}$$

If $\tau_{xy}(q)$ is a linear function of q, the cross-correlation of the series is monofractal but otherwise, it is multifractal. From the Legendre transform, the singularity spectrum is obtained as follows:

$$\begin{aligned} \alpha &= h_{xy}(q) + qh'_{xy}(q) \\ f_{xy}(\alpha) &= q(\alpha - h_{xy}(q)) + 1, \end{aligned} \tag{5.3.6}$$

where α is the singularity of the bivariate series. The singularity spectrum width $\Delta\alpha = \alpha_{\max} - \alpha_{\min}$ represents the degree of multifractality of the bivariate series, where $\alpha_{\max}$ and $\alpha_{\min}$ are respectively the α values at the maximum and minimum of $f_{xy}(\alpha)$ support. In the case of monofractality, $\Delta\alpha$ heads to zero, and thus the singularity spectra is theoretically just a point. The discussions above can also be expanded to examine the multifractal properties for asymmetric cases of generalized Hurst exponents $h^+_{xy}(q)$ and $h^-_{xy}(q)$. Thus the asymmetric cases of the Rényi's exponent, $\tau^+_{xy}(q)$ and $\tau^-_{xy}(q)$, and the singularity spectra, $f^+_{xy}(\alpha)$ and $f^-_{xy}(\alpha)$, can be calculated as well.

It must be noticed that when the series x_j and y_j are identical, the method aims to study the properties of autocorrelations and the method is consistent with the A-MFDFA.

5.3.2 Asymmetric DCCA coefficient analysis

The cross-correlation between two series with a high degree of non-stationarity and self-similarity can be quantified via the DCCA coefficient, which utilizes the analysis based on the DCCA. An asymmetric extension of the cross-correlation coefficient is proposed by Cao et al. (2018), where the coefficient of the bivariate series for the cases of when prices increase and decrease can be examined separately.

The cross-correlation coefficient of Zebende (2011) and Podobnik et al. (2011) between the series $\{x_t : t = 1,\ldots,N\}$ and $\{x_t : t = 1,\ldots,N\}$ is derived relying on the fluctuation functions calculated from overlapping $N-s$ segments of length $s+1$ as

$$F^2_{\mathrm{DCCA}}(s) = \frac{1}{N-s}\sum_{i=1}^{N-s} f^2_{\mathrm{DCCA}}(s,i), \tag{5.3.7}$$

where $f^2_{\mathrm{DCCA}}(s,i)$ is the detrended covariance of the residuals for each segment defined as

$$f^2_{\mathrm{DCCA}}(s,i) = \frac{1}{s+1}\sum_{k=i}^{1+s}(R_x(k)-\tilde{R}_x(k))(R_y(k)-\tilde{R}_y(k)), \tag{5.3.8}$$

where $R_x(k) = \sum_{t=1}^{k} x_t$, $R_y(k) = \sum_{t=1}^{k} y_t$, and the degree-2 polynomial fits $\tilde{R}_x(k)$ and $\tilde{R}_y(k)$ are used to detrend $R_x(k)$ and $R_y(k)$. When we are considering the correlations between two identical series, the fluctuation function $F^2_{\mathrm{DCCA}}(s)$ is reduced to $F^2_{\mathrm{DFA}}(s)$ defined in terms of the DFA method.

Based on the fluctuation functions above, the cross-correlation coefficient is defined as follows:

$$\rho_{\mathrm{DCCA}}(s) = \frac{F^2_{\mathrm{DCCA}}(s)}{F_{\mathrm{DFA}x}(s)F_{\mathrm{DFA}y}(s)}, \tag{5.3.9}$$

where $F^2_{\mathrm{DFA}x}(s)$ and $F^2_{\mathrm{DFA}y}(s)$ is the DFA fluctuation function for each of the series x and y, respectively. Note that with a given scale of s, $F^2_{\mathrm{DCCA}}(s)$ represents cross-correlation features at that scale, and $F^2_{\mathrm{DFA}}(s)$ represents autocorrelation features of each series at scale s. This coefficient, therefore, reveals the degree of cross-correlations for various scales.

In the asymmetric DCCA coefficient, the cross-correlation coefficients for the upward and downward trends are taken in consideration as follows:

$$\begin{aligned}
\rho_{\mathrm{DCCA}+}(s) &= \frac{F^2_{\mathrm{DCCA}+}(s)}{F_{\mathrm{DFA}x+}(s)F_{\mathrm{DFA}y+}(s)},\\
\rho_{\mathrm{DCCA}-}(s) &= \frac{F^2_{\mathrm{DCCA}-}(s)}{F_{\mathrm{DFA}x-}(s)F_{\mathrm{DFA}y-}(s)},
\end{aligned} \tag{5.3.10}$$

where $F^2_{\mathrm{DCCA}+}(s)$ and $F^2_{\mathrm{DCCA}-}(s)$ are obtained from the calculation process in line with equation (5.3.1), using the detrended covariance of the residuals for each segment shown in equation (5.3.8). The coefficients ρ_{DCCA}, $\rho_{\mathrm{DCCA}+}$, and $\rho_{\mathrm{DCCA}-}$ range from -1 to 1, and the value equal to 1 indicates the existence of a perfect cross-correlation, and -1 indicates perfect anti-cross-correlation.

5.4 Fractal cross-correlations of price–volatility

This section explores asymmetric multifractal features of price-volatility cross-correlations and quantifies their coupling levels to clarify the presence of asymmetric volatility effects in cryptocurrency markets.

5.4.1 Multifractality and their asymmetric properties

Before we conduct the MF-ADCCA method, we first test the presence of cross-correlations between price changes and volatility changes to confirm that application of DFA-based methods is appropriate for the analyses. We apply the statistic test proposed by Podobnik et al. (2009) to check the presence of cross-correlations between the bivariate series. The cross-correlation statistic for the series $\{x_i\}$ and $\{y_i\}$ of equal length N is defined as:

$$Q_{cc}(m) = N^2 \sum_{i=1}^{m} \frac{X_i^2}{N-i}, \tag{5.4.1}$$

where X_i is the cross-correlation function defined as:

$$X_i = \frac{\sum_{k=i+1}^{N} x_k y_{k-i}}{\sqrt{\sum_{k=1}^{N} x_k^2 \sum_{k=1}^{N} y_k^2}}. \tag{5.4.2}$$

Since the statistic $Q_{cc}(m)$ is approximately $\chi^2(m)$ distributed with m degrees of freedom, it can be used to test the null hypothesis that the first m cross-correlation coefficients are nonzero. If the value of $Q_{cc}(m)$ is larger than the critical value of $\chi^2(m)$, the null hypothesis is rejected and thus the series have a significant cross-correlation.

The cross-correlation test statistics in eqs.(5.4.1) and (5.4.2) for price changes and volatility changes of the four cryptocurrencies are calculated with various degrees of freedom m, ranging from 1 to 700. The results are shown in Fig. 5.2 together with the critical values of the $\chi^2(m)$ distribution at the 5% level of significance. We find that for all the investigated cryptocurrencies, the statistic $Q_{cc}(m)$ deviates from the corresponding critical value, indicating that there are nonlinear cross-correlations between price changes and volatility changes. For XRP and LTC, the test statistic deviates from the critical value more than those of BTC and ETH. This implies the presence of stronger nonlinear cross-correlations in the minor cryptocurrencies compared to the major ones.

Now that we have verified the existence of nonlinear cross-correlations in the bivariate series, we next analyze the multifractal properties of asymmetric cross-correlations for each cryptocurrency via the MF-ADCCA method. Figure 5.3

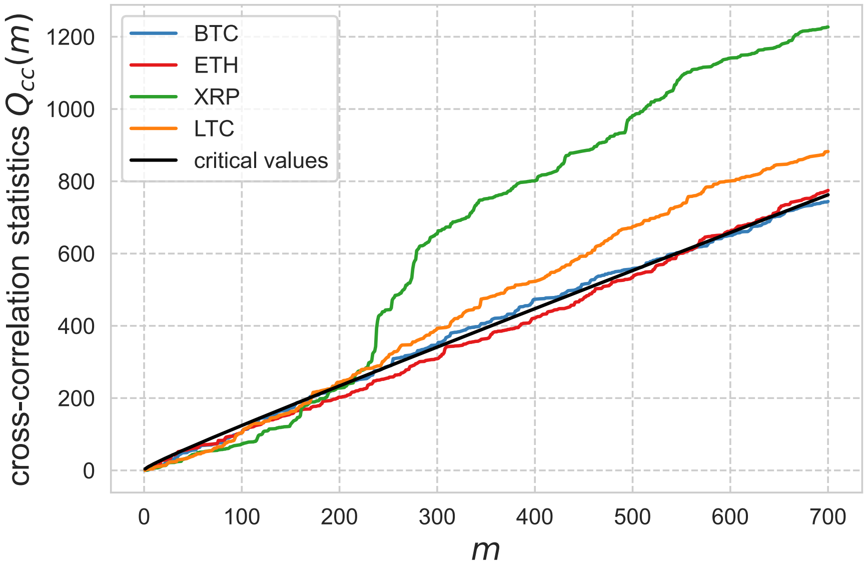

Figure 5.2: Cross-correlation statistics between the return series and volatility change series of the four major cryptocurrencies. The black line represents the critical values at the 5% level of significance.

shows the q-th order fluctuation functions calculated from the returns and volatility changes with various q ranging from -10 to 10. The fluctuation functions under different situations of bull and bear markets (uptrend and downtrend) are also depicted with the overall trend. For all cases, we observe that the fluctuation functions generally follow a power-law against the scale, which means that the cross-correlations between the bivariate series have a long-range power-law property. Therefore the MF-ADCCA is expected to be an effective method for analyzing cross-correlations, along with the asymmetry between uptrend and downtrend cross-correlations.

Figure 5.3 shows that the behavior of power-law cross-correlations varies among market situations of different trends. To measure the degree of asymmetry of the cross-correlations, we calculate the metric defined as

$$\Delta h_{xy}(q) = h^{+}_{xy}(q) - h^{-}_{xy}(q), \tag{5.4.3}$$

for given q. The greater the value, the greater the asymmetric behavior in terms of different trends. If $\Delta h_{xy}(q) > 0$ ($\Delta h_{xy}(q) < 0$), the cross-correlation for uptrend situations has a larger (smaller) exponent compared to those of downtrend situations. When the bivariate series are essentially identified by the same scaling exponent, $\Delta h_{xy}(q)$ is theoretically zero and the two series have symmetric cross-

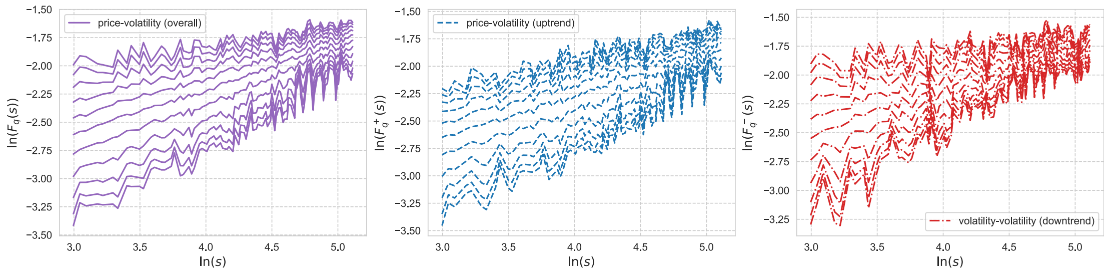

(a) BTC

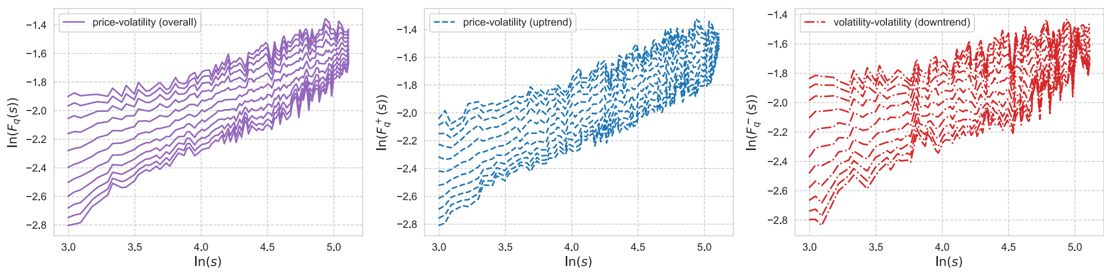

(b) ETH

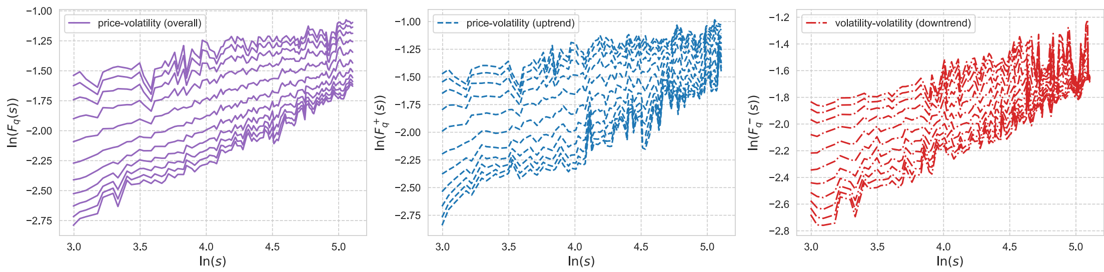

(c) XRP

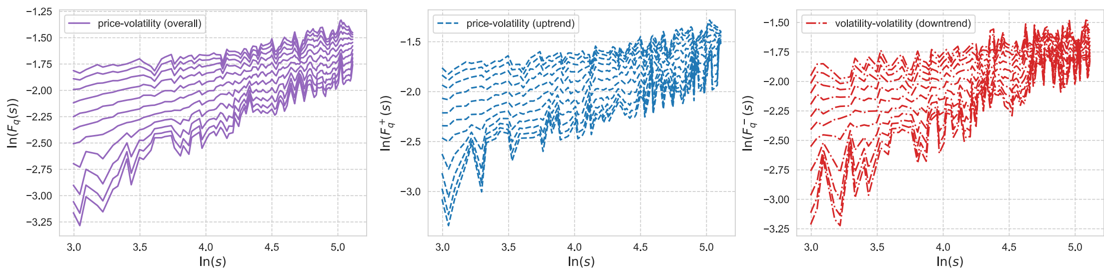

(d) LTC

Figure 5.3: Log-log plots of $F_q(s)$,$F_q^+(s)$ and $F_q^-(s)$ versus time scale s for the four cryptocurrency series of (a) BTC, (b) ETH, (c) XRP, and (d) LTC. We show the cases of $q = -10, -8, -6, \ldots, 10$. The power-law relations indicate that the bivariate series have long-range power-law cross-correlations.

correlations. We calculate the cases of $q = -10$ (small fluctuations), $q = 2$ (corresponding to the Hurst exponent), and $q = 10$ (large fluctuations). We clearly find in Table 5.3 that regardless of small and large fluctuations, $\Delta h_{xy}(q)$ is positive for all the investigated cryptocurrencies (except for the case of $q = -10$ in LTC). Fig. 5.4 also supports these findings where $h^{+}_{xy}(q)$ is larger than $h^{-}_{xy}(q)$. Cross-correlations of price-volatility in the uptrend markets generally have slightly higher persistency at all levels of fluctuations compared to those in the downtrend markets. To investigate the statistical validity of the asymmetric multifractal degree, we implement Monte Carlo simulations and obtain confidence intervals of $\Delta h_{xy}(q)$ calculated from 1000 generated series of returns and realized bipower volatility changes. The daily returns and realized bipower volatility changes are constructed based on the shuffled series of the original 5-minute high frequency returns. We find that BTC, ETH, and XRP exhibit asymmetry at the 1% or 5% significance level, while LTC have rather insignificant asymmetry. We also find that the major currencies of BTC and ETH present significant asymmetry especially in large fluctuations, but the minor currencies tend to present more asymmetry in smaller fluctuations.

Table 5.3: Asymmetric degree of price-volatility cross-correlations in terms of uptrend and downtrend price movements shown together with the multifractal degree for each of the four cryptocurrencies. Note that ***, **, and * denote 1%, 5%, and 10% significance levels, respectively.

	$\Delta h_{xy}(-10)$	$\Delta h_{xy}(2)$	$\Delta h_{xy}(10)$	D_{xy}
BTC	0.044	0.075^{**}	0.123^{***}	0.233
ETH	0.021	0.111^{***}	0.158^{***}	0.127
XRP	0.074^{**}	0.079^{**}	0.020	0.151
LTC	−0.050	0.045	0.029	0.178

The presence of multifractality can be examined by looking into whether or not the generalized Hurst exponents are dependent on its order q. Given that $h_{xy}(q)$ decreases as q increases in Fig. 5.4, $h_{xy}(q)$ is not constant for q and hence multifractal behaviors exsist in the cross-correlations between the bivariate series. To numerically explain the deviation from monofractality and efficiency, we use the market efficiency measure (MDM) of Wang et al. (2009) defined as

$$D_{xy} = \frac{1}{2}(|h_{xy}(-10) - 0.5| + |h_{xy}(10) - 0.5|). \tag{5.4.4}$$

If D_{xy} is zero or close to zero, then the relationship between the series are efficient. Larger values of D_{xy} indicate higher inefficiency, and smaller values indicate lower inefficiency. This metric is useful to determine the ranking of the

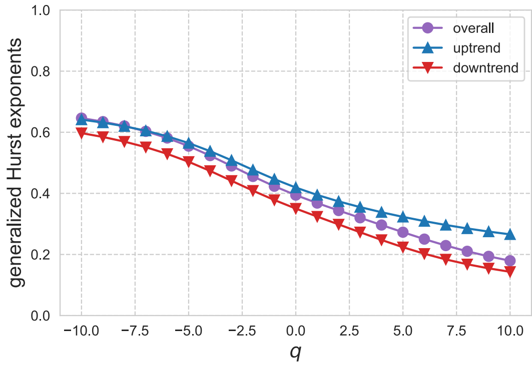

(a) BTC

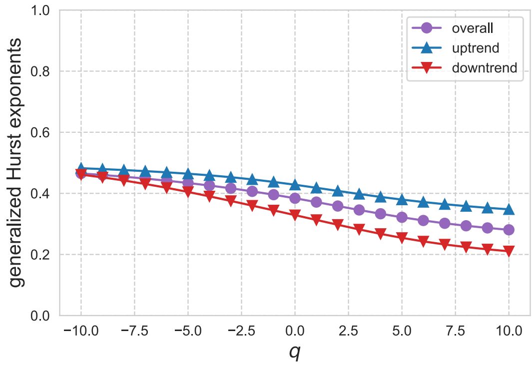

(b) ETH

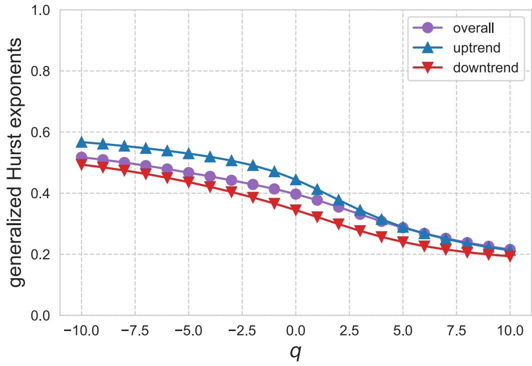

(c) XRP

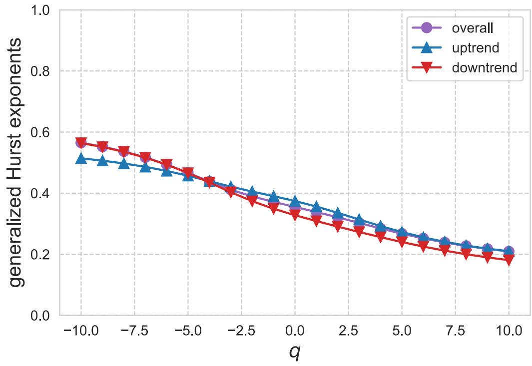

(d) LTC

Figure 5.4: Relationship between the generalized Hurst exponents and the order q for the cases of (a) BTC, (b) ETH, (c) XRP, and (d) LTC.

(in)efficiency degree (Mensi et al., 2017). From the results shown in Table 5.3, we suggest that BTC is the most inefficient with $D_{xy} = 0.233$, and ETH is the most closest to efficiency with $D_{xy} = 0.127$.

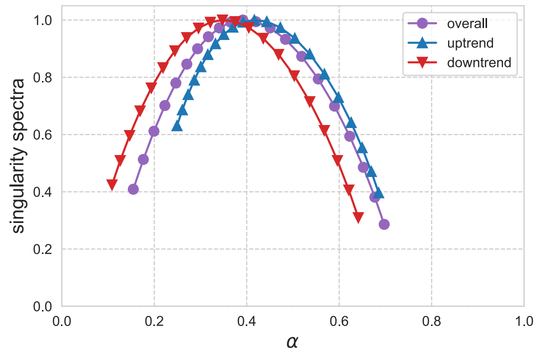

(a) BTC

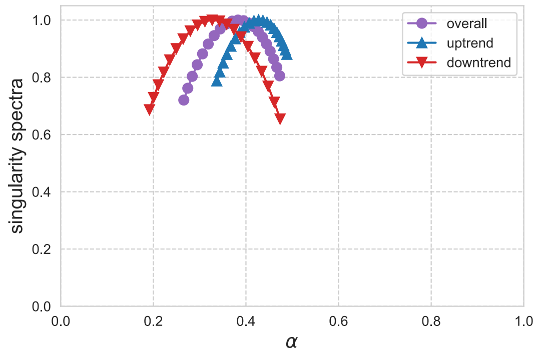

(b) ETH

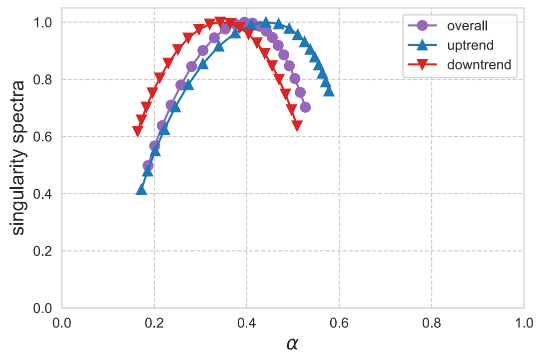

(c) XRP

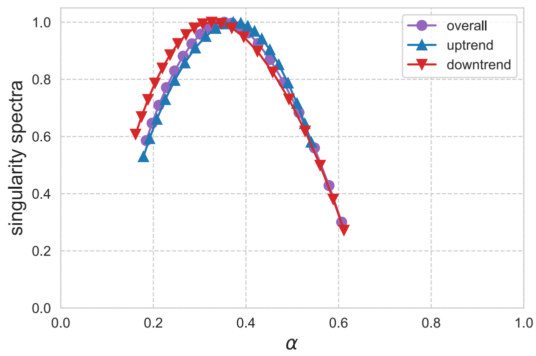

(d) LTC

Figure 5.5: Singularity spectra $f_{xy}(\alpha)$, $f^{+}_{xy}(\alpha)$, and $f^{-}_{xy}(\alpha)$ for the cases of (a) BTC, (b) ETH, (c) XRP, and (d) LTC.

To further study the multifractal properties, we display the singularity spectra $f_{xy}(\alpha)$, $f^{+}_{xy}(\alpha)$, and $f^{-}_{xy}(\alpha)$ in Fig. 5.5 where the asymmetric market trends are considered. The spectra are quite broad as expected, and the width differs with respect to cryptocurrencies and market trends. In particular, among the investigated markets, spectrum width in BTC for the overall trends present the largest degree of multifractality of $\Delta\alpha = 0.5427$. On the contrary, spectrum width in ETH for uptrends present the smallest degree of $\Delta\alpha = 0.1513$. In addition, we discuss the multifractal features from another metric of the asymmetric spectrum parameter, $A_\alpha = \frac{\Delta\alpha_L - \Delta\alpha_R}{\Delta\alpha_L + \Delta\alpha_R}$, where $\Delta\alpha_L = \alpha_0 - \alpha_{\min}$, $\Delta\alpha_R = \alpha_{\max} - \alpha_0$, and α_0 is the value of α at the maximum of the singular spectrum (Drożdż and Oświęcimka, 2015).

Note that the asymmetry here is not in terms of different market trends but the distortion of the singularity spectrum $f_{xy}(\alpha)$. The metric A_α provides information to identifying the compositions of the bivariate series. If $A_\alpha > 0$ ($A_\alpha < 0$), the singular spectrum has a left-sided (right-sided) asymmetry, which indicates that the scaling properties are determined by $q > 0$ ($q < 0$) and hence larger fluctuations (smaller fluctuations) dominate the multifractal behavior (Drożdż and Oświęcimka, 2015). Therefore, it can be interpreted that multifractality owes to larger fluctuations for the left-sided case, and the opposite for the right-sided case. If $A_\alpha = 0$, the left and right sides of spectrum width are equivalent, and thus the small and large fluctuations operate equally on multifractality.

Table 5.4: The asymmetric degree of singularity spectra A_α and α_0, $\alpha_{\max}$, and $\alpha_{\min}$ with respect to price-volatility coupling. We show also the asymmetric spectrum parameter and the values α for asymmetric market trends (uptrend and downtrend).

	Overall				Uptrend				Downtrend			
	A_α	α_0	$\alpha_{\max}$	$\alpha_{\min}$	A_α^+	α_0^+	$\alpha_{\max}^+$	$\alpha_{\min}^+$	A_α^-	α_0^-	$\alpha_{\max}^-$	$\alpha_{\min}^-$
BTC	-0.127	0.392	0.697	0.155	-0.233	0.416	0.685	0.249	-0.103	0.348	0.641	0.109
ETH	0.129	0.383	0.473	0.266	0.193	0.427	0.488	0.337	-0.039	0.327	0.474	0.192
XRP	0.226	0.395	0.527	0.187	0.328	0.441	0.578	0.172	0.036	0.343	0.509	0.164
LTC	-0.200	0.352	0.607	0.185	0.071	0.373	0.541	0.179	-0.270	0.326	0.612	0.162

We report in Table 5.4 the asymmetric spectrum parameter A_α and values of α for the three different market trends: overall, uptrend, and downtrend. In real-world finance data, left-sided spectrum is more common and in such case, it is reasonable to have peculiar features in the larger fluctuations and a noise-like behavior in the smaller fluctuations Drożdż and Oświęcimka (2015). However, we find uncommon features in some cases. The asymmetric spectrum parameters A_α, A_α^+, and A_α^- take negative values in BTC and LTC markets (except for A_α^+ in LTC taking a positive value), and the right-skewed spectra explain that smaller events play a more important role in the underlying multifractality. In contrast, larger events contribute more to the multifractal behavior in the XRP market because the asymmetric spectrum parameters take positive values. It is interesting to mention that regardless of the market trends, multifractality of the price-volatility coupling for BTC and XRP exhibit the same behavior of asymmetry $f_{xy}(\alpha)$ either with the right- or left-sided spectrum, i.e., the same distortion. On the other hand, ETH and LTC show different multifractal properties depending on market trends, where large fluctuations are dominant in bull markets but small fluctuations are dominant in bear markets. We find that LTC tends to show relatively stronger right-skewed $f_{xy}(\alpha)$ with smaller values of A_α, whereas XRP shows the strongest left-skewed $f_{xy}(\alpha)$ with the largest values of A_α for all market trends. In addition to the right-skewed property of BTC and LTC, they tend to have wider spectrum width $\Delta\alpha$, demonstrating that these markets exhibit a highly complex price-volatility behavior.

Although the bivariate extension of scaling exponents and singularity spectra captures power-law cross-correlations and helps characterize complex behaviors between the two series, the discussion without each of its univariate exponents and spectra may not provide a satisfactory interpretation. Focusing on the bivariate Hurst exponent ($H_{xy} = h_{xy}(2)$), many empirical studies have reported that $H_{xy} > \frac{1}{2}(H_x + H_y)$ or $H_{xy} = \frac{1}{2}(H_x + H_y)$ (He and Chen, 2011; Oświeçimka et al., 2014), whereas numerical and theoretical studies have found that $H_{xy} < \frac{1}{2}(H_x + H_y)$ or $H_{xy} = \frac{1}{2}(H_x + H_y)$ (Sela and Hurvich, 2012). Kristoufek (2013) (Kristoufek, 2013) defines a mixed-correlated ARFIMA (MC-ARFIMA) process, which allows for generating power-law cross-correlations and controlling the H_{xy} parameter, and shows that there is no combination of parameters leading to $H_{xy} > \frac{1}{2}(H_x + H_y)$. A theoretical basis in terms of the frequency domain using the squared spectrum coherency also supports the finding that $H_{xy} > \frac{1}{2}(H_x + H_y)$ is impossible (Kristoufek, 2015a). However, the empirical estimation of H_{xy} or specifically its comparison with $\frac{1}{2}(H_x + H_y)$ can lead to unreliable and controversial results due to the underlying bias such as short-term dependence bias, bias in the presence of heavy tails, and finite sample bias, which is often observed in the econophysic work of empirical studies (Kristoufek, 2020). We find that among the investigated cryptocurrencies, BTC, ETH, and LTC satisfy $H_{xy} < \frac{1}{2}(H_x + H_y)$. On the other hand, XRP shows higher bivariate Hurst exponent than the average of two separate ones, with $H_{xy} = 0.355$ and $\frac{1}{2}(H_x + H_y) = 0.342$, implying the biased results. Towards an intuitive interpretation of cross-correlations without relying solely on H_{xy}, Kristoufek (2020) suggests two ways to overcome the issue: utilizing the DCCA-based cross-correlation coefficient and focusing on the case of $H_{xy} < \frac{1}{2}(H_x + H_y)$. We focus on the former method, since it is straightforward to implement and the DCCA measure can lead to find novel relationships between price and volatility in cryptocurrency markets. Since our discussion so far has been based on the multifractal analysis, not only the issue of Hurst exponent but also the issue of generalized Hurst exponent should be addressed. The estimation of $h_{xy}(q)$ and its comparison with $\frac{1}{2}(h_x(q) + h_y(q))$, as well as in the framework of the singular spectra $f_{xy}(\alpha)$, would play a crucial role in giving interpretation when multifractal properties are present in cross-correlations. A further work that explains the theoretical aspect of these connections is left for future work.

5.4.2 Asymmetric volatility assessment

We next apply the DCCA coefficient analysis to quantify the asymmetric cross-correlations between price and volatility and to examine the asymmetry volatility effects in cryptocurrency markets. Fig. 5.6 depicts the coefficients for the overall trend, $\rho_{\mathrm{DCCA}}(s)$, and the upward (bull) and downward (bear) market trends, $\rho_{\mathrm{DCCA+}}(s)$ and $\rho_{\mathrm{DCCA-}}(s)$, for various time scales s ranging from 10 to 334 days. For the entire period (overall trend), the coefficients are not so far from zero at all time scales. Analyzing the case of the overall trend appears to suggest that price and volatility are less interrelated. However, once we consider uptrend and downtrend, we can realize different pictures of the markets. The asymmetric DCCA coefficient approach enables us to separately figure out the interrelationship between price and volatility under bull and bear regimes.

As shown in Fig. 5.6, the coefficients are positive for uptrend markets but negative for downtrend markets. This reconfirms that both positive and negative price changes have a certain degree of the impact on volatility. When $|\rho_{\mathrm{DCCA-}}(s)| > |\rho_{\mathrm{DCCA+}}(s)|$ is satisfied, i.e., price and volatility are more strongly cross-correlated in downtrend markets than in uptrend markets, we can say that asymmetric volatility is present at a certain time scale. On the contrary, when $|\rho_{\mathrm{DCCA-}}(s)| < |\rho_{\mathrm{DCCA+}}(s)|$ holds, we can say that inverse-asymmetric volatility is present where uptrend markets have stronger price-volatility cross-correlations.

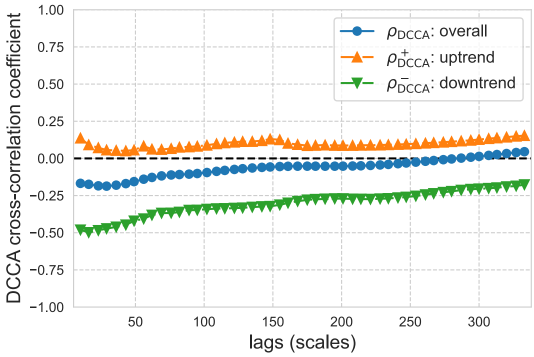

(a) BTC

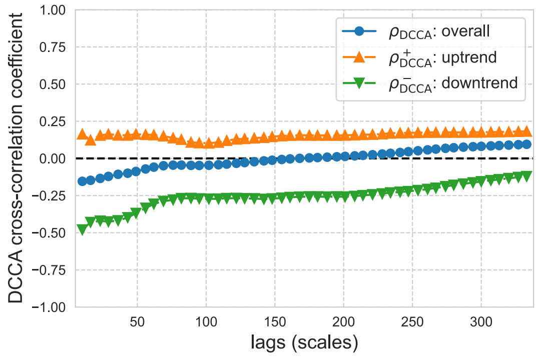

(b) ETH

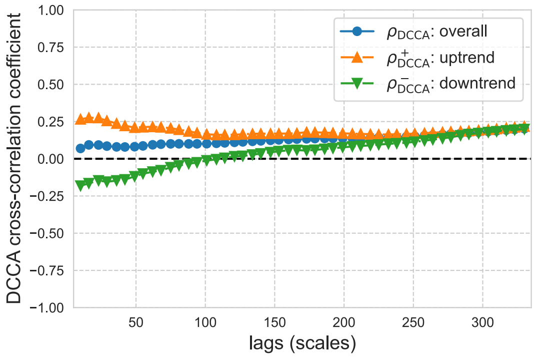

(c) XRP

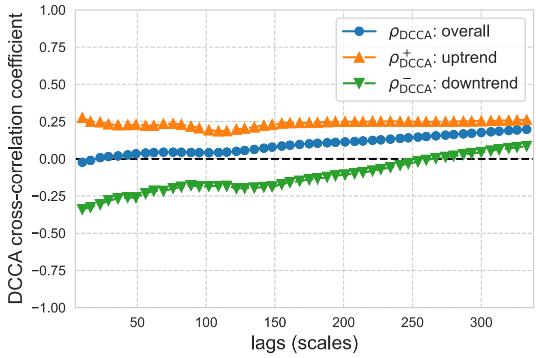

(d) LTC

Figure 5.6: DCCA cross-correlation coefficients $\rho_{\mathrm{DCCA}}(s)$, $\rho_{\mathrm{DCCA+}}(s)$, and $\rho_{\mathrm{DCCA-}}(s)$ between the price-volatility relationships under various scales s for the cases of (a) BTC, (b) ETH, (c) XRP, and (d) LTC. The scales represent the lag of days.

Table 5.5: Estimate results of conditional variance for cryptocurrencies. The EGARCH model and GJR-GARCH model are estimated over the period from June 3, 2016 to December 28, 2020. Standard errors of estimates are reported in parentheses. Note that ***, **, and * denote 1%, 5%, and 10% significance levels, respectively. $Q^2(10)$ is the square Q-statistic and the p-values are presented in brackets.

	EGARCH				GJR-GARCH			
	BTC	ETH	XRP	LTC	BTC	ETH	XRP	LTC
ω	-0.6827^{***}	-0.7089^{***}	-1.0252^{***}	-0.3762^{***}	0.0001^{***}	0.0003^{***}	0.0004^{***}	0.0001^{***}
	(0.0661)	(0.0712)	(0.0422)	(0.0303)	(0.0000)	(0.0000)	(0.0000)	(0.0000)
α_1	0.2609^{***}	0.2893^{***}	0.4441^{***}	0.1758^{***}	0.1217^{***}	0.1585^{***}	0.4089^{***}	0.0775^{***}
	(0.0208)	(0.0185)	(0.0182)	(0.0129)	(0.0160)	(0.0172)	(0.0269)	(0.0101)
α_2	**-0.0586*****	**-0.0071**	**0.0828*****	**0.0193*****	**0.1162*****	**0.0176**	**-0.1161*****	**-0.0256*****
	(0.0080)	(0.0097)	(0.0097)	(0.0060)	(0.0165)	(0.0171)	(0.0257)	(0.0082)
β	0.9217^{***}	0.9135^{***}	0.8706^{***}	0.9549^{***}	0.7769^{***}	0.7649^{***}	0.6297^{***}	0.8997^{***}
	(0.0083)	(0.0106)	(0.0060)	(0.0040)	(0.0176)	(0.0195)	(0.0141)	(0.0096)
Log likelihood	3079.33	2553.73	2412.35	2419.25	3083.58	2556.66	2428.99	2466.02
AIC	-3.6818	-3.0524	-2.8831	-2.9775	-3.6869	-3.0559	-2.9030	-2.9473
$Q^2(10)$	2.4476	8.4555	4.7584	1.7640	4.2086	10.143	3.2243	1.2243
	[0.992]	[0.584]	[0.907]	[0.998]	[0.937]	[0.428]	[0.976]	[1.000]

The results provide clear evidence that for BTC and ETH, price and volatility are more strongly cross-correlated in downtrend markets than in uptrend markets. In particular, we find $\rho_{\text{DCCA}-}(s) \approx -0.5$ and $\rho_{\text{DCCA}+}(s) \approx 0$ for BTC, and $\rho_{\text{DCCA}-}(s) \approx -0.5$ and $\rho_{\text{DCCA}+}(s) \approx 0.15$ for ETH under approximately one-month time scales ($s \approx 30$). This implies the absence of uninformed noise traders during bull markets, but they are active during bear markets. Similar results are observed when studied at longer time scales of half a year ($s \approx 180$), with the DCCA coefficients $\rho_{\text{DCCA}-}(s) \approx -0.25$ and $\rho_{\text{DCCA}+}(s) \approx 0.1$ for both markets. Higher levels of cross-correlations in downtrends are found across all time scales for BTC and ETH, suggesting the presence of asymmetric volatility dynamics.

In the case of XRP, however, we find inverse-asymmetry in volatility dynamics because $|\rho_{\text{DCCA}+}(s)|$ is always larger than $|\rho_{\text{DCCA}-}(s)|$ for all time scales. Uninformed noise traders are more dominant when the price increases than when the price decreases. More interestingly, LTC exhibits different volatility-asymmetry depending on which time scale the cross-correlation analysis was implemented at. At relatively longer time scales ($s > 150$), $|\rho_{\text{DCCA}+}(s)|$ is larger than $|\rho_{\text{DCCA}-}(s)|$, but at relatively shorter time scales, $|\rho_{\text{DCCA}-}(s)|$ surpasses the value of $|\rho_{\text{DCCA}+}(s)|$. In other words, inverse-asymmetric volatility is present at scales of $s > 150$, but not at scales shorter than $s = 150$. Such explanations cannot be confirmed by the conventional GARCH-class models, which generally focus on the effects of one-time price shock on volatility. The approach in this study challenges to a dynamical effects of price on volatility while accounting for the directions of price trends with various time scales. Focusing on the time scales, we find that cross-correlations for uptrend markets are generally constant; however, the loss of cross-correlations is observed for downtrend markets at longer time scales.

The asymmetric DCCA coefficient is derived from the fractal analysis and therefore reflects the scaling properties of the price-volatility nexus in a nonlinear way. However, the asymmetric behavior of the price-volatility is often assessed using the GARCH-class models which focus more on linear correlations. To make sure that our empirical findings based on the fractal framework show the same direction of asymmetric volatility with the conventional methods, we also implement two types of GARCH models that can explain the asymmetric effects on volatility. The first model is the exponential GARCH (EGARCH) written as follows (Nelson, 1991):

$$\ln \sigma_t^2 = \omega + \alpha_1 \frac{|r_{t-1}|}{\sigma_{t-1}} + \alpha_2 \frac{r_{t-1}}{\sigma_{t-1}} + \beta \ln \sigma_{t-1}^2, \tag{5.4.5}$$

with $r_t = \varepsilon_t \sigma_t$, where σ_t^2 is the conditional variance at time t, and ε_t denotes an error term with i.i.d. standard Gaussian noise $\mathcal{N}(0,1)$. The second model is the threshold GJR-GARCH written as follows (Glosten et al., 1993):

$$\sigma_t^2 = \begin{cases} \omega + \alpha_1 r_{t-1}^2 + \beta\sigma_{t-1}^2, & r_{t-1} \geq 0 \\ \omega + (\alpha_1 + \alpha_2) r_{t-1}^2 + \beta\sigma_{t-1}^2, & r_{t-1} < 0 \end{cases} \tag{5.4.6}$$

where the term $\alpha_2 r_{t-1}^2$ is operated only when the market goes downwards. For convenience, both models are with one lag of the innovation ($p = 1$) and one lag of volatility ($q = 1$), since the selection of optimized lags often produces similar estimation results. The GARCH models above are represented by the parameters ω, α_1, α_2, and β. Among these parameters, α_2 is the responsible one that determines the asymmetric responses of volatility to market shocks. Significantly positive values of α_2 for the EGARCH model imply that positive shocks increase volatility more than negative shocks. Note that the positive/negative direction is reversed for the GJR-GARCH model, where negative shocks increase the volatility more when α_2 is positive. As shown in Table 5.5, the values of α_2 are negative in EGARCH and positive in GJR-GARCH for BTC and ETH, and hence the volatility is increased more by negative shocks. We find opposite results for the XRP and ETH because α_2 are positive in EGARCH and negative in GJR-GARCH. In such cases, volatility is increased more by positive shocks. Note that for the ETH, the asymmetric parameter is insignificant and thus the asymmetric effect cannot be statistically confirmed by the implemented GARCH models.

The results of GARCH models appear to highlight that our empirical findings of the DCCA coefficient analysis on asymmetric cross-correlations are relevant to the asymmetric volatility dynamics. Both asymmetric-GARCH models and detrended cross-correlation analysis reveal consistent results of the underlying asymmetric/inverse-asymmetric volatility in cryptocurrency markets. Past studies have shown inverse-asymmetric volatility dynamics of cryptocurrency markets (Baur and Dimpfl, 2018; Cheikh et al., 2020). Our findings conclude that unlike in the earlier periods, the volatility for the two major coins of BTC and ETH, are no longer inverse-asymmetric. One possible reason may be the less presence of uninformed noise traders and increasing participants of informed traders in the market, and the major coins head to maturity in recent years. Minor coins are immature with inverse-asymmetric volatility where speculated noise traders still dominate the market and play a significant role in raising the volatility especially during the uptrend periods. The appearance of stronger negative cross-correlation of price-volatility at shorter scales for LTC could be a key clue to explain the process that minor coins are expected to head for mature markets. As asymmetric cross-correlations are available at different scales, our findings can be applied to form models for optimal portfolio diversification under different investment horizons, which helps address the nonlinear interactions and asymmetric responses prevalent in the cryptocurrency market. In particular, investors can introduce a correlation matrix based on the asymmetric DCCA coefficient as an alternative to the conventional one, allowing investment allocations to depend on time scales. The performance of such portfolios and whether the diversification strategy is effective for making profit are left for future works.

5.5 Summary and Discussions

This chapter examined the nexus between daily price and realized volatility in cryptocurrency markets. The MF-ADCCA approach revealed that the price-volatility relationship exhibits power-law cross-correlations as well as multifractal properties. We discussed the multifractal characteristics of the asymmetric cross-correlations when the market is rising and falling, together with the overall market trend, and found that the bivariate series have different properties between positive and negative market trends. We investigated the multifractal features in detail by using the generalized Hurst exponents and the singular spectrum. The results pointed out that generally for the investigated cryptocurrencies, cross-correlations of price and volatility in the uptrend markets have slightly higher persistency compared to those in the downtrend markets, irrespective of small and large fluctuations. Distinctive features of how small and large fluctuations operate on multifractality were also discovered and reported by investigating the spectrum distortion for each cryptocurrency and its market trends.

More importantly, the level of the asymmetric cross-correlations for each cryptocurrency was quantitatively evaluated by employing the asymmetric DCCA coefficient. Our empirical findings showed that depending on market directions or trends, the level of cross-correlations differs. We found the presence of stronger cross-correlations in bear markets than in bull markets for the maturing major coins (BTC and ETH), whereas the opposite results were observed for the still-developing minor coins (XRP and LTC). As long as price-volatility is our subject, we provided evidence that such an approach enables us to discuss whether asymmetric/inverse-asymmetric volatility dynamics are present with various time scales, which is an intriguing financial phenomenon for investors and financial regulators. The detection of asymmetric volatility works well since the results of our fractal analysis were in line with those of the conventional asymmetric GARCH-class models. Taking the advantage of the multifractal features, power-law cross-correlations, and scaling behaviors of price-volatility within various time scales, our approach can be an alternative approach for discussing dynamical volatility behaviors in cryptocurrency markets.

Chapter 6

Asymmetric Volatility Dynamics in Cryptocurrency Markets on Multi-time Scales

This chapter corresponds to paper 5 in the author's papers list.

6.1 Introduction

One of the economic behaviors well-established in the finance literature is that volatility of financial series responds asymmetrically to return shocks (Black, 1976; Bollerslev et al., 2009; Bentes, 2018). The so-called "leverage effect", also known as the "asymmetric volatility effect", is described in stock markets that bad news (negative return shocks) increase the volatility by more than good news (positive return shocks) (Schwert, 1989; Cheung and Ng, 1992). The concept of this asymmetric effect has been theoretically studied and modeled utilizing various statistical volatility models (e.g., GARCH-type models), and how asymmetric responses are produced is generally demonstrated by factors built on the traditional framework of EMH (Black, 1976; Christie, 1982). However, the asymmetric volatility effect has not been well-studied in terms of the fractal framework. Financial time series as well as cryptocurrencies are rather inefficient and are likely to represent remarkable properties of fractality associated with multi-time scales. Motivated by evidence of significant scale-dependent consequences in cryptocurrencies and limited empirical evidence of asymmetric volatility effect due to the markets' short history, the objective of this study is to examine whether and why volatility responds asymmetrically in cryptocurrency markets, in a more precise manner accounting for scaling dependence of the market behavior given the high complexity. We take advantage of the bivariate fractal regression analysis of Wang et al. (2018) to detect whether the volatility of price change is positively or negatively related to its return shocks at different time scales. The approach allows us to consider FMH-based features of asymmetric volatility that cannot be captured by the conventional models.

Following several works that discover a reversed leverage among early emergence periods of cryptocurrency markets (Bouri et al., 2017a; Baur and Dimpfl, 2018; Cheikh et al., 2020; Kakinaka and Umeno, 2021), this study also finds evidence of the presence of an "inverse" asymmetric volatility effect in cryptocurrency markets— contrary to conventional markets, the return volatility is higher when a positive shock occurs. The consequences are discussed in the context of who is trading in the market and heterogeneity of the investors. According to Glosten and Milgrom (1985) and Easley et al. (1996), the trading of informed and uninformed investors leads to different traces in the return process due to the inefficiency of market information. In particular, informed traders do not generate auto-correlation, while uninformed traders drive serial correlation in the return process, thereby increasing the volatility (Avramov et al., 2006). Utilizing this idea, we will examine under what market conditions uninformed investors dominate the market and discuss the asymmetric factors of our empirical findings.

We reconfirm that except for the prominent markets of Bitcoin and Ethereum, the minor markets substantially exhibit a positive relation between return shocks and volatility. More interestingly, our dynamical fractal approach reveals further the multi-time scale components of the asymmetric volatility phenomenon under different time scales. Since asymmetric response may be time-varying (Takaishi, 2021), we also attempt to examine inverse/non-inverse effects under different data periods. Our approach can be an alternative to existing models, providing a new view based on investors' speculative trading and how they are the source of asymmetry, which could play a crucial role in investment decisions, pricing, risk management, and monetary policy.

The rest of this chapter is organized as follows. Section 6.2 describes the methodology associated with analyzing asymmetric volatility. Section 6.3 introduces the dataset used in this study, and presents the results and empirical findings we have reached. Finally, Section 6.4 draws the main summary and discussions.

6.2 Detection Methodology

6.2.1 DFA-based bivariate regression estimator

By translating the standard regression analysis into the DFA and DCCA-based language, Kristoufek (2015b) proposed the fractal regression analysis that enables quantifying scale-dependent interactions between time series. The method provides richer information than the standard regression framework in that it deals with complexity and nonlinearity in dynamical systems, as well as the actual response of the series at multi-time scales. The fractal regression analysis was then extended to the case of two impulse series, namely the DFA-based bivariate regression analysis (Wang et al., 2018). A further development was made recently by Tilfani et al. (2022), where multivariate regression model in the fractal framework is illustrated for financial applications. In effect, these multi-time scale approaches are practical for modeling heterogeneity in economic and financial systems and their underlying scale structure (Tilfani et al., 2022).

By combining DFA with the standard bivariate linear regression method, we estimate the scale-dependent regression coefficients between return and volatility series in cryptocurrency markets, which are considered to exhibit non-stationary and complex behaviors (Telli and Chen, 2020; Wątorek et al., 2021). The advantage of this method is that we can investigate a multi-time scale procedure and check the nonlinear dependence between a response series and an impulse series at different levels of scales.

We slightly modify the DFA process of the above DFA-based bivariate regression analysis of Wang et al. (2018). We follow the initial approach of Podobnik and Stanley (2008), where they derive the fluctuation functions relying on *overlapping* segments of the dataset instead of *non-overlapping* segments. Although the process requires more segments to be averaged over the fluctuation functions, it avoids the significant variance of the estimates due to the small number of sample segments to be averaged.

The key point of fractal regression methods is to use the scale-dependent variance and covariance derived from the "detrended function", instead of the standard variance form. For a given time series $\{x_t\}$ with length N, we split its cumulative sum, or in other words the profile series, $X(t) = \sum_{i=1}^{t} x_i$, for $t = 1, 2, \ldots, N$, into $N - s$ overlapping segments of length $s + 1$. The degree-2 polynomial fits $\tilde{X}(t)$ are used to detrend $X(t)$ for each segment, and then calculate the detrended variance function for each segment defined as

$$f_{XX}^2(s, v) = \frac{1}{s+1} \sum_{t=v}^{v+s} \left[X(t) - \tilde{X}(t) \right]^2. \tag{6.2.1}$$

By averaging $f_{XX}^2(s, v)$ over all the segments, we get the fluctuation function, or the scale-dependent variance

$$F_{XX}^2(s) = \frac{1}{N-s} \sum_{v=1}^{N-s} f_{XX}^2(s, v). \tag{6.2.2}$$

The scale-dependent covariance can be derived in a similar way by the detrended covariance function of bivariate series $\{x_t\}$ and $\{y_t\}$ with the same length determined as

$$F_{XY}^2(s) = \frac{1}{N-s}\sum_{v=1}^{N-s} f_{XY}^2(s,v), \tag{6.2.3}$$

where

$$f_{XY}^2(s,v) = \frac{1}{s+1}\sum_{t=v}^{v+s}\left[X(t)-\tilde{X}(t)\right]\left[Y(t)-\tilde{Y}(t)\right]. \tag{6.2.4}$$

Note that Eq. (6.2.3) and Eq. (6.2.4) can take positive as well as negative values.

To illustrate the dependences of bivariate series, we consider a bivariate linear regression model

$$Z_t = \beta_0 + \beta_1 X_t + \beta_2 Y_t + \varepsilon_t \ (t = 1,\ldots,N), \tag{6.2.5}$$

where Z_t is a response variable, X_t and Y_t are impulse variables, and ε_t is a Gaussian error term with zero mean. Partial regression coefficients β_1 and β_2 characterize the dependence of response variables on impulse variables. In accordance with the standard OLS method and replacing variance (covariance) with scale-dependent variance (covariance), we get the scale-dependent coefficient estimators as follows:

$$\hat{\beta}_1^{\mathrm{DFA}}(s) = \frac{F_{XZ}^2(s)F_{YY}^2(s) - F_{YZ}^2(s)F_{XY}^2(s)}{F_{XX}^2(s)F_{YY}^2(s) - \left[F_{XY}^2(s)\right]^2}, \tag{6.2.6}$$

$$\hat{\beta}_2^{\mathrm{DFA}}(s) = \frac{F_{YZ}^2(s)F_{XX}^2(s) - F_{XZ}^2(s)F_{XY}^2(s)}{F_{XX}^2(s)F_{YY}^2(s) - \left[F_{XY}^2(s)\right]^2}. \tag{6.2.7}$$

By using the scale-dependent residual

$$\hat{e}_t(s) = Z_t - \hat{\beta}_1^{\mathrm{DFA}}(s)X_t - \hat{\beta}_2^{\mathrm{DFA}}(s)Y_t - \left\langle Z_t - \hat{\beta}_1^{\mathrm{DFA}}(s)X_t - \hat{\beta}_2^{\mathrm{DFA}}(s)Y_t \right\rangle,$$

we can calculate the fluctuation function $F_{\varepsilon\varepsilon}^2(s)$ in the same manner as Eq. (6.2.2), and the variance of the above coefficients can be estimated as below:

$$\mathrm{var}\left[\hat{\beta}_1^{\mathrm{DFA}}(s)\right] = \frac{1}{N-3}\frac{F_{YY}^2(s)F_{\varepsilon\varepsilon}^2(s)}{F_{XX}^2(s)F_{YY}^2(s) - \left[F_{XY}^2(s)\right]^2}, \tag{6.2.8}$$

$$\mathrm{var}\left[\hat{\beta}_2^{\mathrm{DFA}}(s)\right] = \frac{1}{N-3}\frac{F_{XX}^2(s)F_{\varepsilon\varepsilon}^2(s)}{F_{XX}^2(s)F_{YY}^2(s) - \left[F_{XY}^2(s)\right]^2}. \tag{6.2.9}$$

Now that the coefficients are estimated for some specific scale s, we can do the same procedure under other scales by changing s. It is worth noting that Fan and

Wang (2020) introduces a similar approach of DMA-based bivariate regression estimator, which uses the centered moving average technique when detrending the profile series, i.e., $X(t)$ in Eq. (6.2.1). Since the centered DMA analysis requires some reference to future data, we focus on the DFA that can be carried on with the data at hand.[1]

In this study, we use the DFA and DCCA fluctuation functions to implement the fractal regression analysis. Discussions based on the fractal regression analysis provide a more transparent view of multi-time scale connections between the variables because the regression model intends to design the actual dependence rather than just looking at the strength of its correlation.[2] Moreover, it plays a role in meeting the need to regard asymmetric effects of asymmetric volatility by devising the fractal regression model presented in the following subsection.

6.2.2 Modelling asymmetric volatility behavior

We provide an alternative approach to model asymmetric effects of return shocks on volatility. To clarify the dependence at different time scales, we develop the DFA-based bivariate fractal regression and construct the following regression model:

$$Z_t = \beta_0 + \beta_1 X_t + \beta_2 Y_t + \varepsilon_t \ (t = 2, \ldots, N), \tag{6.2.10}$$

$$\begin{cases} X_t = \frac{|r_{t-1}|}{\sqrt{\mathrm{RV}_{t-1}}} \\ Y_t = \frac{r_{t-1}}{\sqrt{\mathrm{RV}_{t-1}}} \\ Z_t = \ln \mathrm{RV}_t \end{cases}$$

where RV_t is the realized volatility series in Eq. (6.3.1), r_t is the return series in Eq. (6.3.2), and $|r_t|$ is the absolute value of return series. The independent variable $\frac{r_{t-1}}{\sqrt{\mathrm{RV}_{t-1}}}$ represents the positive and negative return shocks relative to volatility, in the previous time step. The independent variable $\frac{|r_{t-1}|}{\sqrt{\mathrm{RV}_{t-1}}}$ represents its magnitude—the larger the value, the greater the impact, i.e., impact of shocks relative to volatility. In other words, these variables are filtered by volatility. This filtering procedure removes short range dependencies and reduces possible volatility bias among different time windows (Tilfani et al., 2019). The information on market sign enables to model potential asymmetry of the impact on

[1] In general, the DFA-based methods are powerful and robust tools for determining remarkable stylized facts of long-range correlations and scale dependencies in one's series and across other series.

[2] Zebende (2011) uses the DFA and DCCA fluctuation functions to calculate the cross-correlation coefficient at multi-time scales defined as $\rho_{\mathrm{DCCA}}(s) = \frac{F^2_{XY}(s)}{F_{XX}(s) F_{YY}(s)}$.

volatility. Asymmetric response of positive and negative shocks can be quantified through the regression coefficients β_1 and β_2; a positive shock in the market is responsible for the increase in volatility as much as $(\beta_1+\beta_2)\frac{|r_{t-1}|}{\sqrt{\mathrm{RV}_{t-1}}}$, whereas a negative shock in the market is responsible for the increase in volatility as much as $(\beta_1-\beta_2)\frac{|r_{t-1}|}{\sqrt{\mathrm{RV}_{t-1}}}$. Therefore, among the coefficients, β_2 determines the asymmetric volatility behavior. Significantly positive (negative) values of β_2 in the model imply that positive (negative) shocks increase volatility by more than shocks whose sign is opposite.

Rewriting Eq. (6.2.10) as

$$\ln \mathrm{RV}_t = \beta_0 + \beta_1 \frac{|r_{t-1}| + \gamma r_{t-1}}{\sqrt{\mathrm{RV}_{t-1}}} + \varepsilon_t, \tag{6.2.11}$$

where $\gamma = \frac{\beta_2}{\beta_1}$, appears to resemble the structure of the conventional EGARCH model, which is one of the most common GARCH model capable of investigating asymmetric effects. The EGARCH model and our fractal regression model are similar to some extent. For both the impulse variable of our regression model and the process of return innovations in the EGARCH model, the sign of past return shocks yields separate effects on volatility, and for the response variable, the logarithm of the volatility relaxes the positiveness constraint of model coefficients and allows values to be negative. While the EGARCH model describes the volatility and variance of the current error term or innovation conditioned to previous error terms and innovations, the DFA-based regression model aims to demonstrate the nonlinear dependence of volatility with lagged return series across different time scales. The conditional volatility term is not included in our model because the DFA-based method accounts for the nonlinear elements of volatility, such as long-range dependence. Since the whole history of returns are already incorporated into the fractal regression model in terms of long-range correlations, taking additional lagged return innovations may be inappropriate in fractal regressions. The fractal regression framework addresses the dynamic behavior, even in simple regression models. Under a specific time scale of s, the model of Eq. (6.2.10) can be expressed as

$$\ln \mathrm{RV}_t = \beta_0(s) + \beta_1(s)\frac{|r_{t-1}|}{\sqrt{\mathrm{RV}_{t-1}}} + \beta_2(s)\frac{r_{t-1}}{\sqrt{\mathrm{RV}_{t-1}}} + \varepsilon_t(s)\ (t=2,\ldots,N), \tag{6.2.12}$$

where the scales can be interpreted as investment horizons. For each specific scale, we can estimate the model coefficients separately. Our model provides a new view of how good and bad news affect the volatility on multi-time scales and how they differ across investment horizons when detecting asymmetric volatility.

6.3 Empirical Analysis

6.3.1 Data presentation

We collect price data from https://poloniex.com/, one of the largest cryptocurrency exchanges with various cryptocurrencies available. By using the public API, we obtain high-frequency 5-minute interval closing price of Bitcoin (BTC), Ethereum (ETH), Ripple (XRP), Litecoin (LTC), Monero (XMR), and Dash (DASH) for the period from 2016/06/02 to 2021/09/25.[3] are against Tether (USDT), a currency designed to maintain the same value as the US dollar. The data include the period of the boom in 2017 when cryptocurrency prices experienced a substantial increase. The choice of cryptocurrencies is the large ones with a market capitalization of \$50 million or more as of June 2016, when they began to show growth in more active online trading (except for XMR, which had a market capitalization of only \$10 million but has grown rapidly to over \$200 million within a year, so we also select this cryptocurrency). Since cryptocurrencies do not belong to a particular country or an institution, the closing price data we use is based on the Coordinated Universal Time (UTC). Note that the "closing" price here does not indicate that the market itself closes (cryptocurrency markets are open 24-7).

Barndorff-Nielsen and Shephard (2002) propose to use the realized volatility (RV), i.e., intraday square returns, as a proxy of the daily volatility series:

$$\mathrm{RV}_t = \sum_j r_{t,t_j}^2, \tag{6.3.1}$$

where r_{t,t_j} denotes intraday returns, i.e., the log-difference of price calculated from high frequent sample intervals, and t_j denotes the j-th value on day t. It is widely known that when sample intervals are set closer to zero and infinite numbers of intraday returns are summed up, the realized volatility estimator converges to the integrated volatility σ_t^2, which is a former standard measure used in various sets of studies. We use 5-minute intervals since such a sampling base is a reasonable choice for avoiding strong bias driven by extremely high frequencies and thus maintaining an accurate measure of volatility (Bandi and Russell, 2006; Liu et al., 2015). The daily return series are calculated as the log difference in prices shown as

$$r_t = \ln p_t - \ln p_{t-1}, \tag{6.3.2}$$

where p_t denotes the price at day t. We equally have 1941 return and volatility observations for each cryptocurrency.

We show in Figure 6.1 the return series r_t and the volatility measure of $\sqrt{\mathrm{RV}_t}$ for each cryptocurrency, along with their descriptive statistics (see Table 6.1 and

[3]Due to data availability, all cryptocurrencies in our analyses

Table 6.2). Note that for $\sqrt{\mathrm{RV}_t}$ we do not show the mean, standard deviation, and the Jarque-Bera test since the data is far from stationary and normality. All cryptocurrency returns present similar positive mean values to some extent; however, higher moments tend to differ among the major and relatively minor coins. Negative skewness is observed for BTC and ETH, whereas positive skewness and larger standard deviation are found for the others. This is a consequence of BTC and ETH being more exposed to negative returns, while other coins are more exposed to volitile positive returns. Kurtosis values of the investigated cryptocurrencies are all well above 3, suggesting that the distribution of returns is highly leptokurtic, having a broader or flatter shape with fatter tails. The Jarque-Bera test reconfirms its significant deviation from normality. In Table 6.2, we see how the extreme events of XRP led to very high skewness and kurtosis of the volatility indicator.

Table 6.1: Descriptive statistics and moments of the return series r_t. For the Jarque-Bera test statistic, *** indicates significance at the 1% level.

	BTC	ETH	XRP	LTC	XMR	DASH
Mean (%)	0.2254	0.2758	0.2624	0.179	0.2854	0.1545
Median (%)	0.236	0.1126	-0.1312	-0.0411	0.2024	0.0356
Std. Dev. (%)	4.2175	5.7697	7.5973	6.0541	6.4134	6.2678
Max. (%)	23.814	25.274	104.61	60.051	59.249	45.668
Min. (%)	-50.435	-58.697	-68.039	-47.796	-54.466	-47.595
Skewness	-0.9362	-0.6665	1.8394	0.4671	0.2289	0.3336
Kurtosis	13.086	8.756	30.195	12.043	12.126	8.7689
J.B.	14132***	6344.2***	74829***	11800***	11909***	6254.7***

Table 6.2: Descriptive statistics and moments of the realized volatility measure $\sqrt{\mathrm{RV}_t}$.

	BTC	ETH	XRP	LTC	XMR	DASH
Median	0.0354	0.0496	0.0592	0.0573	0.0621	0.0642
Max.	0.3192	0.4320	1.7104	0.4100	0.4160	0.4183
Min.	0.0070	0.0112	0.0094	0.0131	0.0141	0.0075
Skewness	2.8323	3.1065	8.2063	2.7228	2.5840	2.3125
Kurtosis	13.943	16.779	150.56	12.697	10.354	9.8965

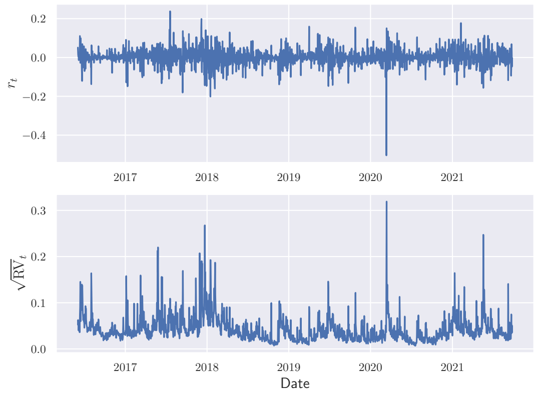

(a) BTC

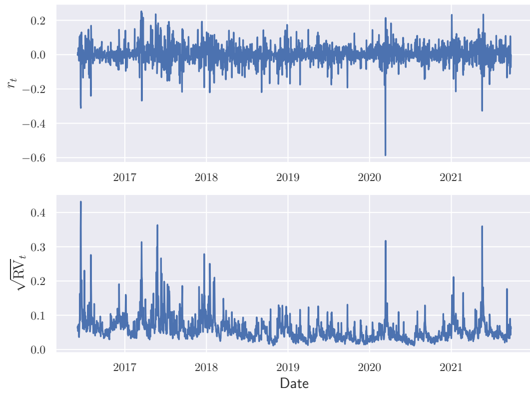

(b) ETH

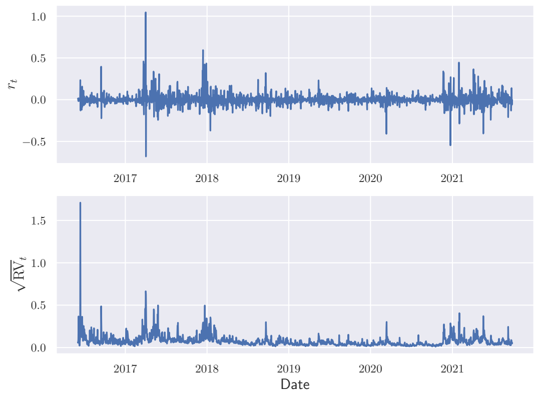

(c) XRP

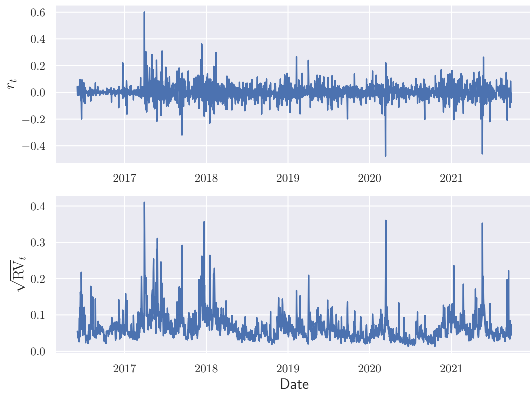

(d) LTC

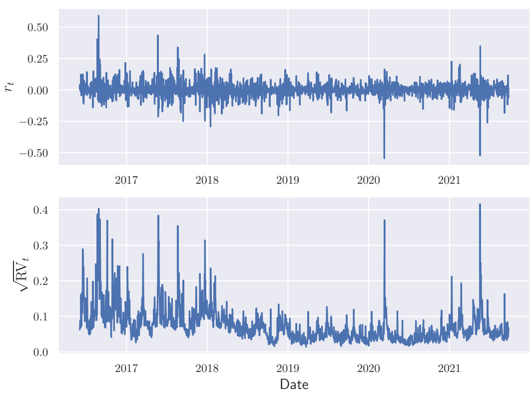

(e) XMR

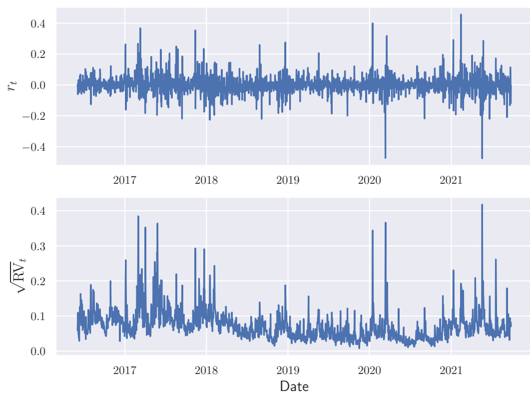

(f) DASH

Figure 6.1: Daily return and volatility series of (a) Bitcoin, (b) Ethereum, (c) Ripple, (d) Litecoin, (e) Monero, and (f) Dash, for the investigated period (2016/06/02 to 2021/09/25).

6.3.2 Scaling dependencies of asymmetric volatility effect

After we calculate return and realized volatility series from 5-minute interval cryptocurrency data as presented in Subsection 6.3.1, we analyze the multi-time scale property of the return-volatility structure regarding its asymmetry following the procedures in Section 6.2. We show in Fig. 6.2 the estimated values of the scale-dependent coefficients $\hat{\beta}_1^{\mathrm{DFA}}(s)$ and $\hat{\beta}_2^{\mathrm{DFA}}(s)$ of model Eq. (6.2.10) for each cryptocurrency. We also depict together with colored ranges the 95% confidence intervals of the estimates. Clearly, the coefficients are not monotonous— the dependence of the series oscillates at different time scales. The coefficients $\hat{\beta}_1^{\mathrm{DFA}}(s)$ are always significantly above zero in all cases, as expected, since the standardized absolute return (corresponding impulse variable) and the volatility index (response variable) are both a representation of volatility. The coefficient value increases as scales become larger. We find that the impact of good and bad news to volatility, $\hat{\beta}_1^{\mathrm{DFA}}(s)+\hat{\beta}_2^{\mathrm{DFA}}(s)$ and $\hat{\beta}_1^{\mathrm{DFA}}(s)-\hat{\beta}_2^{\mathrm{DFA}}(s)$, always stay positive (Fig. 6.3). In our model, as long as $\hat{\beta}_1^{\mathrm{DFA}}(s)+\hat{\beta}_2^{\mathrm{DFA}}(s)>0$ and $\hat{\beta}_1^{\mathrm{DFA}}(s)-\hat{\beta}_2^{\mathrm{DFA}}(s)>0$ satisfy, only the sign of coefficient $\hat{\beta}_2^{\mathrm{DFA}}(s)$ sufficiently determines the asymmetric reaction. Therefore, we focus on $\hat{\beta}_2^{\mathrm{DFA}}(s)$ to discuss whether negative or positive price movements have more impact on volatility. We find different asymmetric features among the investigated cryptocurrencies and that they can be broadly classified into three categories; positive, negative, and both positive and negative effects. [4]

First of all, we find that $\hat{\beta}_2^{\mathrm{DFA}}(s)$ are always negative for the two major currencies of BTC and ETH, indicating the presence of an asymmetric volatility effect regardless of time scale— negative news has a greater impact on volatility increment than positive news at all scales. This leverage effect is consistent with what is commonly observed in stock markets (Jeribi et al., 2015; Fakhfekh et al., 2016; Bentes, 2018), however, its origin should not be associated with financial leverage (Hens and Steude, 2009; Hasanhodzic and Lo, 2019). More generally, such an asymmetric phenomenon has its explanation on the background of who trades and how they transact in practice (Black, 1976; Antoniou et al., 1998). This is especially true in cryptocurrency markets (Baur and Dimpfl, 2018), since a "financial" explanation of the effect may be challenging. Traces of market price fluctuations are a consequence of informed traders correcting market asymmetries caused by irrational transactions and herding behavior of uninformed traders. In this regard, uninformed traders are responsible for the striking rises in volatility, so

[4] To check the stability of the results we have also performed an analysis using volume-weighted averaged daily prices (VWAP) in case the asymmetric volatility effect is a consequence of market illiquidity. By taking the ratio of the value of cryptocurrency traded to the total volume of daily transactions, the trading prices are averaged out, thus reducing market illiquidity. We report no notable changes compared to the results for the closing price case, indicating that illiquidity does not greatly contribute to asymmetric volatility effect (see Fig. B.2 and Fig. B.3 in Appendix B.3).

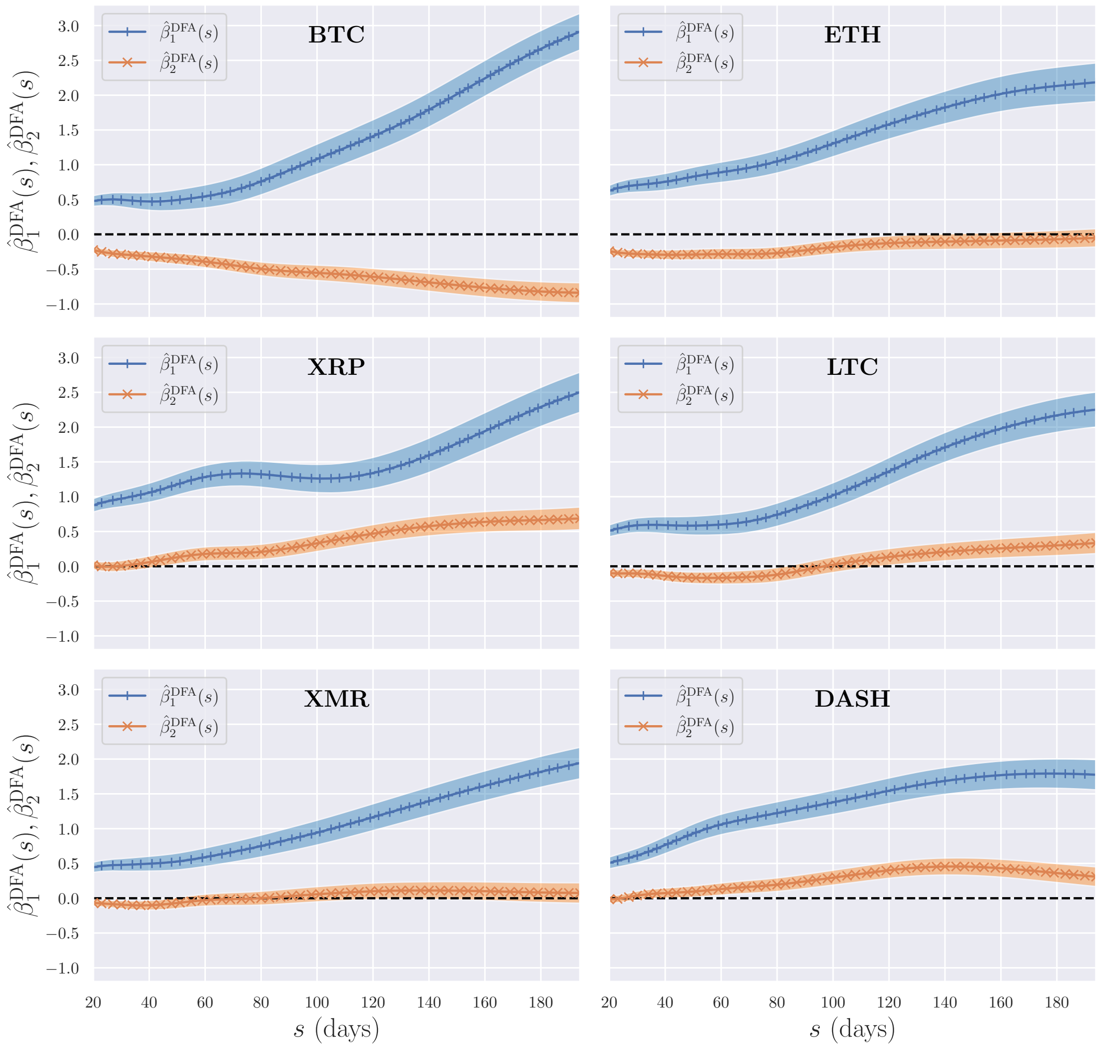

Figure 6.2: DFA-based bivariate regression estimates of cryptocurrency series. The coefficients $\hat{\beta}_1^{\mathrm{DFA}}(s)$ and $\hat{\beta}_2^{\mathrm{DFA}}(s)$ are shown for each cryptocurrency; BTC, ETH, XRP, LTC, XMR, and DASH. The colored ranges denote 95% confidence intervals calculated as $\hat{\beta}_i^{\mathrm{DFA}}(s) \pm 2\sqrt{\mathrm{var}(\hat{\beta}_i^{\mathrm{DFA}}(s))}$, for $i = 1, 2$.

Figure 6.3: The impact of good and bad news to volatility, $\hat{\beta}_1^{\mathrm{DFA}}(s) + \hat{\beta}_2^{\mathrm{DFA}}(s)$ and $\hat{\beta}_1^{\mathrm{DFA}}(s) - \hat{\beta}_2^{\mathrm{DFA}}(s)$, respectively. We show the results for each cryptocurrency; BTC, ETH, XRP, LTC, XMR, and DASH.

speculative investments of uninformed traders' in BTC and ETH are more active when the markets experience negative return shocks. We find that the effect is remarkable, especially in BTC.

However, a completely opposite effect can be observed for the relatively minor cryptocurrencies of XRP and DASH. As shown in the figure, the coefficients $\hat{\beta}_2^{\mathrm{DFA}}(s)$ turn out positive. This outcome indicates the presence of an "inversed" asymmetric volatility effect in these markets, meaning that positive returns affect volatility more than negative returns. The rise in volatility can be interpreted as being due to uninformed traders, this time reacting to positive news. We can confirm this effect across scales. According to Baur and Dimpfl (2018), the pump-and-dump scheme, telling people to buy a particular currency, and the fear of missing out, not feeling that they are taking full advantage of information towards future prices, are in the background of this reaction. These attributes can remarkably drive to raise cryptocurrency prices, and as a result, volatility will increase more than in rising markets compared to falling markets. In addition, the relatively small market size of XRP and DASH may attribute to increasing volatility especially when the market is in its rising trend with soaring prices. Such markets tend to be susceptible to attracting more uninformed traders to speculative investment where informed traders become less capable of exerting pressure on reducing market volatility.

Interestingly, the remaining LTC and XMR currencies exhibit a composite structure with different signs of asymmetric volatility. As shown in Fig. 6.2, the coefficients $\hat{\beta}_2^{\mathrm{DFA}}(s)$ oscillate around zero and do not constantly take the same sign— they can be either positive or negative depending on which time scale we focus. LTC and XMR have in common that $\hat{\beta}_2^{\mathrm{DFA}}(s)$ take negative values for $s < 80$ and positive values for $s > 100$. Although the values are close to zero and the volatility effect seems to be almost absent, either positive or negative return news can lead to larger volatility increments. Asymmetric volatility effect may be present on scales smaller than approximately three months, but on larger scales, the effect is slightly reversed or, in the worst case, disappear. The findings imply that uninformed investors who seek short-term horizons play a prominent role in downside markets to amplify the asymmetry of volatility effect.

Although the scale-dependent regression coefficients seem to be mostly well above or below zero value, including their confidence intervals (orange ranges in Fig. 6.2), they may be an outcome where asymmetric behavior is absent. The theoretical value of $\hat{\beta}_2^{\mathrm{DFA}}(s) = 0$ can be calculated only for an infinitely long time series. As long as datasets are finite, empirical estimations can vary due to sample size effects, and even if there is no dependence between the variables, the coefficient estimates can be far from zero to some extent. To assure whether the regression relationship under different scales is genuine or not, we employ the statistical test of Wang et al. (2018) that tests the absence of dependencies between Z and X or Y of the regression model $Z_t = \beta_0 + \beta_1 X_t + \beta_2 Y_t + \varepsilon_t$, i.e., the null hypothesis of $\beta_i(s) = 0$ for $i = 1, 2$. They introduce the scale-dependent t-statistics defined as $t_i(s) = \frac{\hat{\beta}_i^{\mathrm{DFA}}(s) - \beta_i}{\sqrt{\mathrm{var}(\hat{\beta}_i^{\mathrm{DFA}}(s))}}$, similar to the t-statistics used in the standard regression analysis. The subject series are firstly shuffled in practice, and then the scale-dependent t-statistics of the regression coefficients are calculated. This procedure is repeated many times to carry out the computation of scale-dependent critical values $t^{\mathrm{c}}(s)$ based on Podobnik et al. (2011), defined such that the integral of the probability distribution function of $t_i(s)$, $[-t^{\mathrm{c}}(s), t^{\mathrm{c}}(s)]$, is equal to $1-\alpha$, where α denotes confidence level. Thereby, we can determine the range of $t_i(s)$ that can be considered statistically significant under some specific time scale. We shuffle $Z_t = \ln \mathrm{RV}_t$ (the volatility series) and $Y_t = r_{t-1}/\sqrt{\mathrm{RV}_{t-1}}$ (return shocks series) while setting $X_t = |Y_t|$ in order to correspond to our model in Eq. (6.2.10). In this way, positive and negative return shocks are always associated with their magnitude (impulse variables) while their correlation with volatility (response variable) is destroyed, thus $\beta_2 = 0$. We calculate the empirical values of $t_2(s)$ and perform the hypothesis test of $\beta_2(s) = 0$ by repeating 1000 times the procedure of calculating the scale-dependent t-statistics from the shuffled series. For robustness check, we also use the bootstrap method to test whether the $\beta_2(s)$ coefficients are significantly different from 0. For each scale we compute the quantile of the coefficient and its confidence interval is obtained. Details of the procedure and the estimation results can be found in Appendix B.2.

We depict in Fig. 6.4 the values of $t_2(s)$ with the scale-dependent critical values at the 5% and 10% levels of significance ($\alpha = 0.1, 0.05$). If the value is not within the critical band, the hypothesis can be rejected. We find that in BTC, the values of $t_2(s)$ are always lower than the critical band, so the absence of an asymmetric response is rejected and hence asymmetric volatility effect exists for all scales. However, in other cryptocurrencies, it is not always assured whether asymmetric reaction exists across scales. For instance, we find in ETH that $t_2(s)$ stay way below the band only for $s < 90$ (three months). In other words, asymmetric volatility effect is significant on scales shorter than three months but not for scales larger than that. In XRP and DASH, which appeared to show an inverse asymmetric volatility effect, we find that $t_2(s)$ stay mainly within the critical band for small scales. An inverse effect can be confirmed on mid-scales around $s = 120$ (four months) or more, where the scale-dependent t-statistics go over the upper critical bound of 95% confidence level. For other scales (small and large scales) the corresponding t-statistics are not rigorously statistically significant, however, they are rather close to the upper critical values suggesting that good news in XRP and DASH tends to help increase volatility slightly more than bad news on average. The results tell us the possibility of an interesting story in which the uninformed traders' herding is dominant in rising markets but not in falling markets, and that its effect is strongest at mid-term horizons. Investors seem to have speculative expectations of mid- to long-term growth in these markets. In LTC and XMR, which may present both signs of asymmetric volatility, $t_2(s)$ fall out of the lower 95% critical band for scales smaller than approximately $s = 30$ (one month). Therefore, the null hypothesis is rejected and assures the presence of an asymmetric volatility effect only at small scales. The result implies that herding of uninformed traders on shorter time horizons has significantly increased the volatility in falling markets. On the other hand, for large scales of $s > 30$ (one month), we find no statistical evidence of asymmetric volatility, neither positive nor negative. This indicates that the inverse asymmetric volatility phenomenon (positive effect) at large scales is likely to be simply within the statistical accident of size effects.

In addition, we present in Table 6.3 the asymmetry results estimated by the EGARCH(1,1) model to check the differences and similarities with the results estimated by our model. Since the scaling properties are not considered in the EGARCH model, the sign of γ_2 alone represents the overall asymmetric response of volatility to good and bad news. As expected, a significant negative effect ($\gamma_2 < 0$) is found for BTC. We also find negative in ETH, but the effect is insignificant. All the other cryptocurrencies show an inverse asymmetric volatilty effect ($\gamma_2 > 0$), and their coefficients are found to be statistically significant. These results tell us that the traditional model provides us a plausible overall picture of asymmetry, but fails to address the heterogeneous effect among scales— for example, the negative effect we have confirmed in LTC for small scales cannot be detected by the EGARCH model. Our model thus helps us find some interesting results throughout the various investment horizons.

6.3.3 Time-varying property

As the cryptocurrency market heads to maturity with more active online trades, the asymmetric volatility response to return shocks may vary due to the change in informed and uninformed traders' behavior. In effect, using the asymmetric GARCH models, Takaishi (2021) reports that Bitcoin exhibits different signs of asymmetric volatility for other historical periods and infers that such an underlying time-varying property may be one of the reasons why a constant picture is not observed in the Bitcoin market. Therefore, we examine how the asymmetry and scaling factors changed through the evolution of cryptocurrency history, including other representative cryptocurrencies.

We focus on analyzing two periods, from 2016/6/2 to 2019/4/30 and 2018/11/1

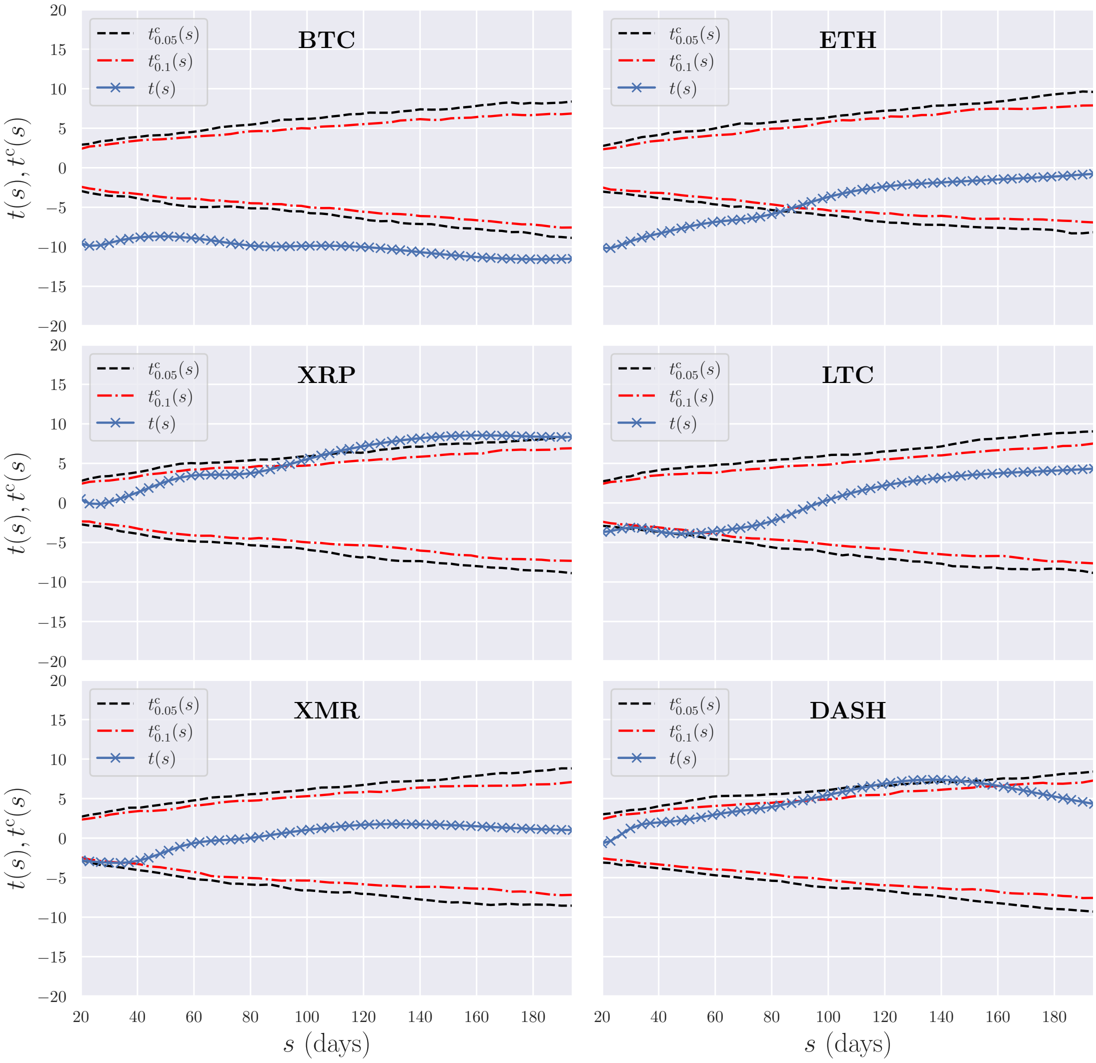

Figure 6.4: Statistic significance tests of the DFA-based bivariate regression estimates. Among the synthetic distribution of the scale-dependent t-statistics of the coefficient $\hat{\beta}_2^{\mathrm{DFA}}(s)$, the black dashed line indicates the critical values of the 95% band, and the red dash-dotted line indicates the critical values of the 90% band.

Table 6.3: Estimation results of the EGARCH model; $\ln\sigma_t^2 = \omega + \gamma_1 \frac{|r_{t-1}|}{\sigma_{t-1}} + \gamma_2 \frac{r_{t-1}}{\sigma_{t-1}} + \alpha \ln\sigma_{t-1}^2$ and $r_t = \varepsilon_t \sigma_t$, where σ_t^2 is the conditional variance at time t, and ε_t denotes an error term with i.i.d. standard Gaussian noise. Standard errors of estimates are reported in parentheses. The asymmetric parameter γ_2 is shown in bold. Note that ***, **, and * denote 1%, 5%, and 10% significance levels, respectively.

	BTC	ETH	XRP	LTC	XMR	DASH
ω	-0.5935^{***}	-0.6653^{***}	-1.1289^{***}	-0.3691^{***}	-0.4701^{***}	-0.6078^{***}
	(0.0582)	(0.0646)	(0.0410)	(0.0276)	(0.0419)	(0.0500)
γ_1	0.2256^{***}	0.2724^{***}	0.4895^{***}	0.1772^{***}	0.2574^{***}	0.3224^{***}
	(0.0184)	(0.0170)	(0.0179)	(0.0123)	(0.0146)	(0.0184)
γ_2	**-0.0514*****	**-0.0068**	**0.0924*****	**0.0196*****	**0.0292*****	**0.0333*****
	(0.0066)	(0.0087)	(0.0103)	(0.0060)	(0.0054)	(0.0075)
α	0.9317^{***}	0.9187^{***}	0.8554^{***}	0.9562^{***}	0.9487^{***}	0.9330^{***}
	(0.0074)	(0.0097)	(0.0060)	(0.0036)	(0.0063)	(0.0073)

to 2021/9/25, with data long enough to run our fractal regression analysis.[5] They include typical cryptocurrency bubbles and crashes, the first occurring in late 2017 to early 2018 and the second in 2021. Cryptocurrencies during these periods have experienced remarkable rises and intense falls in prices. In such situations, the existence of noise traders cannot be ignored, and it is clear that they, in part, play an essential role in influencing the asymmetric behavior of market volatility in the short- and long-term. In Table 6.4 and Table 6.5, we show the DFA-based bivariate regression coefficient estimates associated with the t-statistics for each period. We consider the following investment horizon settings; short-term ($s = 30$), mid-term ($s = 60$), and long-term scales ($s = 120$). During the first period (Table 6.4), the scale-dependent coefficients $\hat{\beta}_2^{\mathrm{DFA}}(s)$ of BTC stay negative for all investment horizons, indicating that BTC volatility is higher following negative return shocks on whatever scale. A similar outcome is found in ETH, although the coefficient is insignificant for long-term scales. For the minor coins of XRP and DASH, the coefficients turn out to be slightly positive for all scales. This indicates that volatility may rather be higher following positive return shocks, however, the coefficients are generally not statistically significant. The remaining minor coins of LTC and XMR show no remarkable evidence of asymmetry; on the one hand, we

[5]The first sub-period corresponds to one year before and after the bubble and crash periods of 2017 to 2018, in order to also consider the periods when prices are in a stable state. Remarkable rises and falls in prices in 2021 are ongoing, and the second sub-period is set to have roughly the same data length as the first sub-period.

find negative coefficients for short- and mid-term scales but a positive coefficient for long-term scales. This trend is in line with the findings mentioned earlier in Fig. 6.2, Fig. 6.3 and Fig. 6.4.

Table 6.4: DFA-based bivariate regression estimates of cryptocurrency series for the period of 2016/6/2 to 2019/4/30, corresponding to the first cryptocurrency boom and crash. The scale-dependent coefficients $\hat{\beta}_1^{\mathrm{DFA}}(s)$ and $\hat{\beta}_2^{\mathrm{DFA}}(s)$ associated with their variance ($\times 10^{-3}$; shown in parenthesis) are shown with the scale-dependent t-statistics $t_2(s)$. We show the results for the cases of short-term scales ($s = 30$ days), mid-term scales ($s = 60$ days), and long-term scales ($s = 120$ days). Note that *,**, and *** denotes 90%, 95%, and 99% confidence level, respectively.

	BTC			ETH			XRP		
	$s = 30$	$s = 60$	$s = 120$	$s = 30$	$s = 60$	$s = 120$	$s = 30$	$s = 60$	$s = 120$
$\hat{\beta}_1^{\mathrm{DFA}}(s)$	0.517	1.061	2.313	0.920	1.462	2.428	1.055	1.519	1.051
	(5.542)	(11.50)	(22.05)	(5.296)	(9.439)	(18.59)	(7.113)	(12.60)	(25.33)
$\hat{\beta}_2^{\mathrm{DFA}}(s)$	−0.391	−0.792	−0.884	−0.300	−0.501	−0.174	0.048	0.024	0.595
	(1.829)	(3.226)	(6.126)	(1.954)	(3.096)	(4.783)	(3.082)	(4.712)	(9.316)
$t_2(s)$	-9.148^{***}	-13.94^{***}	-11.30^{***}	-6.776^{***}	-9.001^{***}	−2.521	0.865	0.344	6.163^{*}
	LTC			XMR			DASH		
	$s = 30$	$s = 60$	$s = 120$	$s = 30$	$s = 60$	$s = 120$	$s = 30$	$s = 60$	$s = 120$
$\hat{\beta}_1^{\mathrm{DFA}}(s)$	0.677	0.970	1.655	0.804	1.101	1.795	0.636	1.101	1.869
	(6.315)	(11.97)	(18.54)	(4.386)	(9.503)	(22.31)	(5.082)	(9.105)	(19.35)
$\hat{\beta}_2^{\mathrm{DFA}}(s)$	−0.089	−0.289	0.241	−0.041	−0.045	0.558	0.013	0.038	0.456
	(2.420)	(4.296)	(7.311)	(1.771)	(4.160)	(8.627)	(1.916)	(3.202)	(7.451)
$t_2(s)$	−1.803	-4.408^{*}	2.816	−0.963	−0.699	6.011^{*}	0.302	0.671	5.277^{*}

Table 6.5: DFA-based bivariate regression estimates of cryptocurrency series for the period of 2018/11/01 to 2021/9/25, corresponding to the second cryptocurrency boom and crash.

	BTC			ETH			XRP		
	$s=30$	$s=60$	$s=120$	$s=30$	$s=60$	$s=120$	$s=30$	$s=60$	$s=120$
$\hat{\beta}_1^{\mathrm{DFA}}(s)$	0.584	0.876	0.876	0.603	0.791	0.836	0.539	0.624	0.775
	(1.057)	(1.515)	(1.956)	(1.191)	(1.486)	(2.028)	(0.598)	(0.727)	(1.051)
$\hat{\beta}_2^{\mathrm{DFA}}(s)$	−0.122	−0.123	−0.405	−0.214	−0.193	−0.324	−0.008	0.059	0.005
	(0.588)	(1.151)	(2.707)	(0.760)	(1.372)	(2.310)	(0.595)	(1.086)	(1.376)
$t_2(s)$	-5.016^{***}	−3.632	-7.787^{**}	-7.775^{***}	-5.208^{**}	-6.741^{*}	−0.317	1.784	−0.138
	LTC			XMR			DASH		
	$s=30$	$s=60$	$s=120$	$s=30$	$s=60$	$s=120$	$s=30$	$s=60$	$s=120$
$\hat{\beta}_1^{\mathrm{DFA}}(s)$	0.701	0.889	1.046	0.686	1.138	1.187	0.764	1.127	1.164
	(1.224)	(1.384)	(1.792)	(1.758)	(2.051)	(2.278)	(1.240)	(1.339)	(1.812)
$\hat{\beta}_2^{\mathrm{DFA}}(s)$	−0.093	−0.150	−0.158	−0.078	−0.042	−0.262	−0.004	−0.015	0.051
	(0.708)	(1.157)	(2.272)	(1.013)	(1.906)	(2.919)	(0.761)	(1.177)	(1.889)
$t_2(s)$	-3.498^{**}	-4.421^{*}	−3.318	−2.459	−0.953	−4.842	−0.163	−0.430	1.165

The results so far provide not so much a different picture from that of using the entire period. However, we find different asymmetric effects and scaling dependencies in the second period (Table 6.5). All scale-dependent coefficients $\hat{\beta}_2^{\mathrm{DFA}}(s)$ and their scale-dependent t-statistics $t_2(s)$ of BTC are closer to zero, meaning that compared to the first period, the degree of asymmetry became weaker.[6] Noteworthy, the BTC market still holds a significant asymmetric volatility effect, and also, the ETH does. More importantly, in the relatively minor cryptocurrencies, traces of the inverse asymmetric volatility effect is no longer present on most scales because these markets are prone to show negative coefficients more often than in the first period. The shift from positive to negative asymmetric effect, in addition to the reduction of asymmetry in major cryptocurrencies, is in good agreement with the argument that cryptocurrency markets are steadily heading toward maturity (Drożdż et al., 2018). As the market matures, informed investors will be more dominant, helping to reduce market asymmetry.

The asymmetric results among different time periods may be attributed to the safe-haven property of cryptocurrencies and their change in recent times. Bouri et al. (2017a) demonstrate that any evidence of an inverse asymmetric volatility in cryptocurrency markets may point toward a safe-haven property. When cryptocurrency prices rise in periods of financial turmoil in which traditional market prices (e.g., stock prices) fall, investors interpret this as an increase in macroeconomic environment and uncertainty. In this situation, investors (in particular the uninformed) buy cyptocurrencies and transmit the increased volatility of the stock market to cryptocurrency markets. On the contrary, when cryptocurrency prices fall in periods of rising stock prices, uninformed investors consider that the uncertainty of macroeconomic environment is low. They thereby transmit the decreased volatility of stock markets to cryptocurrency markets, which operates to mitigate downside market risks in cryptocurrencies and prevents volatility from rising. Accordingly, the existence of an inverse leverage during the first sub-period justifies the possibility that they are a consequence of cryptocurrencies acting as a safe-haven against leveraged traditional assets.[7] However, the potential is lost in the second period, and thereby the market can no longer be associated with the safe-haven property. The market has grown to show asymmetric outcomes similar to those generally seen in mature markets. In this context, the results warn financial risk managers that using cryptocurrencies on the route to maturity for hedging requires careful investigation of their dynamic interdependence between return and volatility. It is expected that the discussion will be further developed by investigating the connection of cryptocurrencies to global traditional markets.

[6] Urquhart (2016) provides empirical evidence that Bitcoin is an inefficient market but may be in the process of moving towards an efficient market.

[7] In fact, the cryptocurrency crash of 2017 and 2018 is said to be detached from the global financial system and thus the market is uncorrelated with traditional markets.

Moreover, one can extend the DFA-based fractal regression model to address another critical component of financial time series— multifractal characteristics— by extending the DFA to the MFDFA. A deeper investigation of multifractal dynamics in the return-volatility nexus may further develop the understanding of complex behaviors of volatility in cryptocurrency markets and how return shocks play an essential role in producing asymmetric responses in the market. These are left for future work.

6.4 Summary and Discussions

This study develops a fractal regression framework to evaluate how return volatility responds asymmetrically to return shocks in six representative cryptocurrency markets of Bitcoin, Ethereum, Ripple, Litecoin, Monero, and Dash. We make two major contributions in this chapter. First, we reveal the presence of a scaling-dependent structure in the asymmetric relationship between return shocks and return volatility— volatility of cryptocurrencies can negatively or positively be influenced by return shocks dependent on time scales, i.e., investment horizons. We focus on discussing the asymmetric volatility effect and its inverse effect using the fractal regression analysis, which allows us to quantify the scaling factors of dependencies between the series. The proposed fractal regression model has its advantage in modeling heterogeneity between asymmetric shocks and between large and small scales. In this sense, our approach is more general than the traditional models that do not account for multi-time scales. The findings illustrate that the asymmetry of volatility effect is determined not only by proximate return shocks but also by shocks across scales. The empirical results present a more precise insight that regardless of scales, the major BTC and ETH show a strong asymmetric volatility effect (negative effect), where negative shocks tend to have a greater impact on volatility. On the contrary, for some specific ranges of mid-term scales, minor cryptocurrencies (especially XRP and DASH) show an inverse asymmetric volatility effect (positive effect), where positive shocks tend to have a greater impact on volatility. The reason is discussed in the context of uninformed traders dominating the market in different situations. The impact of informed short sellers trading during the downside market is worth future discussion, since it is another possibility that could affect volatility.

Second, we study how the scale-dependent asymmetric volatility effect in cryptocurrencies changed by experiencing two prominent bubbles and crashes. Under the proposed fractal regression model, we highlight the asymmetric outcomes for the two periods. Volatility in major cryptocurrencies is higher following a negative return shock for both periods. In minor cryptocurrencies, the features tend to be time-varying, where the effect shifted from positive to negative for a wide range of scales. This negative effect is consistent with that reported in recent major cryptocurrencies and other traditional financial assets. The reduction of such an asymmetric effect reveals traces of the markets' increasing maturity with a larger predominance of informed traders mitigating the effect of uninformed traders' herding.

To sum up, our approach has the ability to explain the asymmetric return-volatility relationship in addition to their scaling-dependencies. Since understanding the features of volatility plays a crucial role in various determinants in real-world finance, our findings should be of interest to academic researchers, market investors, and policymakers.

Chapter 7

Scale-dependent Fractal Portfolio Optimization

This chapter corresponds to paper 6 in the author's papers list.

7.1 Introduction

Modern portfolio theory, which determines the allocation of investments in financial assets, requires controlling and minimizing risk to achieve diversification. In the traditional mean-variance analysis, the investor's decision-making is characterized by expected returns and variances, and the optimal combination of assets should be identical among investors (Markowitz, 1952). However, since there are different types of investors with different trading strategies and investment horizons, it is unlikely that they are homogeneous in their expectations with an agreement on specific risk measures as called for the Efficient Market Hypothesis (EMH) (Fama, 1991; Kristoufek, 2018). Markets are rather inefficient, complex, and likely to exhibit heterogeneous behaviors (Battiston et al., 2016; Tilfani et al., 2020), and portfolio selection based on traditional approaches may not be appropriate (Kristoufek, 2018; Tilfani et al., 2019; Zhang et al., 2022). According to the alternative framework of the Fractal Market Hypothesis (FMH) proposed by Peters (1994), financial series exhibit fractal properties due to the different valuations for information flows among investment horizons, thereby justifying sudden spikes in market volatility and lack of market liquidity during crashes. Zhang et al. (2022) developed the mean-DCCA analysis by incorporating the fractal correlation characteristics of multiple assets into the mean-variance portfolio strategy, where the detrended cross-correlation analysis (DCCA) function (Podobnik and Stanley, 2008) was used in place of the covariance function to substitute the risk definition. At different scales, in other words, at different investment time horizons, the portfolio risk can be defined nonlinearly and allows investment allocations from various decision-making standards.

The mean-DCCA portfolio performs well, assuming that investors' scale preference stays constant (Zhang et al., 2022). However, their preference may shift to a different level since they change positions in response to changes in economic states. Ferson and Schadt (1996) and Evans (1994) show that time-varying risk prices play an important role in the expected returns of the stock market by using conditional factor models. In addition, although the mean-DCCA analysis incorporates the monofractal aspect of asset fluctuations, it does not consider the multifractal aspect. Incorporating the different scaling properties between small and large market price fluctuations may help improve portfolio performance. Motivated by the fact that investors' preference for time horizons may vary over time and that their emphasis on short scales triggers market crashes (Peters, 1994), we examine whether incorporating changes in scale preference improves portfolio performance. In particular, we construct a strategy that switches preference between short and long scales in response to maximum drawdown. Given the fact that multifractality is found prevalent in asset fluctuations, we adopt the multifractal cross-correlation function (MFCCA) (Oświęçimka et al., 2014) as an alternative risk function and propose a new approach, the mean-MFCCA analysis, which is an extension of the mean-DCCA analysis. Our results confirm that incorporating multifractality aspects into the portfolio analysis improves the performance and reduces portfolio risks. Moreover, our results indicate that short-scale preference strategy of the mean-MFDCCA gains risk control during volatile market conditions, which supports the background hypothesis of the FMH.

7.2 Mean-MFCCA portfolio

In the mean-variance (MV) analysis, the portfolio is selected to minimize variance under some required expected return. The mean-DCCA (MD) analysis utilizes the DCCA (covariance) function instead of variance to consider fractal correlations and multiscale properties of assets. We generalize the MD portfolio into a multifractal form based on the MFCCA, namely, the mean-MFCCA (MMF) portfolio. The MFCCA function is calculated as follows (Oświęçimka et al., 2014):

For a given time series $\{x_t\}_{t=1}^N$ and $\{y_t\}_{t=1}^N$, we first split its cumulative sum, $X(t)=\sum_{i=1}^t x_i$ and $Y(t)=\sum_{i=1}^t y_i$, into $N_s=\lfloor N/s \rfloor$ non-overlapping segments of length s. The division is repeated from the other end, so we have $2N_s$ segments in total. Then, for each segment we eliminate the local trend and calculate

$$f_{XY}^2(s,v)=\frac{1}{s}\sum_{t=1}^{s}\left\{X_v(t)-\tilde{X}_v(t)\right\}\left\{Y_v(t)-\tilde{Y}_v(t)\right\}, \tag{7.2.1}$$

where $\tilde{X}_v(t)$ and $\tilde{Y}_v(t)$ denotes the degree-2 polynomial fits used to detrend the vth segment of $X(t)$ and $Y(t)$, respectively. Note that $f^2_{XY}(s,v)$ can take negative values. Note that $f^2_{XY}(s,v)$ can take negative values. The qth-order covariance function is calculated by averaging $f^2_{XY}(s,v)$ over all segments,

$$F^q_{XY}(s) = \frac{1}{2N_s}\sum_{v=1}^{2N_s} \operatorname{sgn}\left[f^2_{XY}(s,v)\right]\left|f^2_{XY}(s,v)\right|^{q/2}. \tag{7.2.2}$$

The MFCCA function (Eq. (7.2.2)) is scale-dependent and often characterized by long-range power-law correlations $F^q(s) \sim s^{h(q)}$, which provides valuable supplemental information on the key outcomes of financial time series. [1] When $q = 2$, the function degenerates to the DCCA function. These functions uncover different correlation levels of heterogeneous investment horizons.

On the basis of the MV portfolio, the MMF portfolio of n assets is constructed using the MFCCA function and the expected portfolio return calculated from the expected return of each asset, $\bar{r}_i$. With the constraint that risk minimization is achieved under some given return greater than r_e, the investment weight $w_i(q,s)$ can be obtained by solving the following optimization problem:

$$\begin{aligned} \underset{w}{\text{minimize}} \quad & \sum_{i,j=1}^{n} w_i(q,s)w_j(q,s)F^q_{ij}(s) \\ \text{subject to} \quad & \sum_{i=1}^{n} \bar{r}_i w_i(q,s) \geq r_e, \; \sum_{i=1}^{n} w_i(q,s) = 1, \\ & w_i(q,s) \geq 0, \; i = 1,\ldots,n. \end{aligned} \tag{7.2.3}$$

Each weight is determined to meet the optimal values under each different scale s and fluctuation q-order. Since the FMH explains that the market is composed of investors trading from all kinds of investment horizons, the impact from multiple time scales must be reflected in the optimal weights. The weight under a single time horizon $w_i(q,s)$ is only one component of the complex multiscale market behavior, and therefore not appropriate to conclude as the optimal investment weight. Additional steps are required to ensure the effectiveness of the MD as well as the MMF portfolio. Following Zhang et al. (2022), we consider a set of multiple time scales $S = \{s_1 = s_{\min}, s_2, \ldots, s_{n-1}, s_n = s_{\max}\}$, where $s_{\min}$ and $s_{\max}$ are the minimum and maximum elements of set S, so that we obtain investment weights $w_i(q,s)$ under scales that satisfy $s \in S$. In the same vein, we consider a set of multiple fluctuation q-orders $Q = \{q_{\min}, \ldots, q_{\max}\}$ to regard multifractal effects of assets.

[1] For instance, the scaling exponent $h(q)$ helps find traces of long- and short-memory in addition to the prevailing multifractal behaviors.

The optimal investment weight w_i^{opt} is then defined as the weighted average of the scale-dependent weight $w_i(s)$ expressed as

$$w_i^{\text{opt}} = \sum_{s\in S}\sum_{q\in Q} \alpha_i(s)\beta_i(q)w_i(q,s), \tag{7.2.4}$$

where $\sum_{s\in S}\alpha_i(s) = 1$ holds and $\alpha_i(s) \in [0,1]$ represents the investor's relative preference degree for time scale s, and $\sum_{q\in Q}\beta_i(q) = 1$ holds for $\beta_i(q) \in [0,1]$. The preference degree can be adjusted depending on how we associate $\alpha_i(s)$ with s. Given the heterogeneity of investors, we consider three types of investment strategies according to their scale preference— equal preference among time scales, more preference for shorter time scales, and more preference for longer time scales. If, for example, investors have no specific preference among different investment horizons, we set $\alpha_i(s) = \frac{1}{\#S}$, where $\#S$ denotes the total number of elements in set S. For the fluctuation preference $\beta_i(q)$, we set $\beta_i(q) = \frac{1}{\#Q}$, which means that investors have no specific preference between large and small fluctuations.

7.3 Numerical Experiments

7.3.1 Multiscale diversification

To confirm the availability of the proposed MMF analysis towards an effective risk diversification, we check the performance of the portfolio using two types of simulated time series. In order to investigate the effect of multiscale properties, we first utilize the *two-component autoregressive fractionally integrated moving average (ARFIMA) stochastic process model* to generate series that exhibit power-law auto-correlations and power-law cross-correlations. In this case each variable depends not only on its own past, but also on the past values of the other variable (Podobnik et al., 2009; Zebende, 2011),

$$\begin{aligned} y_t &= W\sum_{j=1}^{\infty} a_j(d_1)y_{t-j} + (1-W)\sum_{j=1}^{\infty} a_j(d_2)y'_{t-j} + \varepsilon_t \\ y'_t &= (1-W)\sum_{j=1}^{\infty} a_j(d_1)y_{t-j} + W\sum_{j=1}^{\infty} a_j(d_2)y'_{t-j} + \varepsilon'_t, \end{aligned} \tag{7.3.1}$$

where $a_j(d)$ represents statistical weights using the Gamma function Γ and the exponent parameter d ranging from -0.5 to 0.5, defined as

$$a_j(d) = \frac{\Gamma(j-d)}{\Gamma(-d)\Gamma(1+j)}.$$

Note that d is closely related to the Hurst exponent in terms of the DFA analysis, where $H = d + 0.5$ holds (Podobnik et al., 2009; Zebende, 2011). The residuals ε_t and ε'_t denote two independent and identically distributed (i.i.d.) Gaussian variables with zero mean and unit variance. The parameter W is called a "free parameter" ranging from 0.5 to 1.0 and controls the strength of power-law cross-correlations between the variables y_t and y'_t. By using the two-component AFRIMA process of Eq. 7.3.1, we generate two new series y_t and y'_t characterized by different values of parameters d_1, d_2, W, ε_t, and ε'_t. In the case of $W = 1$, the series will have minimum strength of power-law cross-correlations in the long-term , while $W = 0$ the series will have maximum strength of power-law cross-correlations in the long-term. In the case of $\varepsilon_t = \varepsilon'_t$, in the short-term, there is a perfect cross-correlation in the short-term, and if $\varepsilon_t = -\varepsilon'_t$, there is a perfect anti cross-correlation. When $\varepsilon_t \neq \varepsilon'_t$, cross-correlation is absent in the short-term.

For the purpose of testing the potential of MMF reflecting different diversification effects on different scales, we generate series with the parameters $d_1 = 0.4$, $d_2 = -0.4$, $W = 0.7$, and $\varepsilon_t = -\varepsilon'_t$ of length 2^{12}. For the two generated series, we calculate the cross-correlation levels at different scales defined by the DCCA coefficient of Zebende (2011) defined as

$$\rho_{\mathrm{DCCA}}(s) = \frac{F^2_{XY}(s)}{F_{XX}(s)F_{YY}(s)}. \tag{7.3.2}$$

The cross-correlations appear to be scale-dependent, with strong anti cross-correlations in the short-term and no correlation in the long-term (Fig. 7.1).

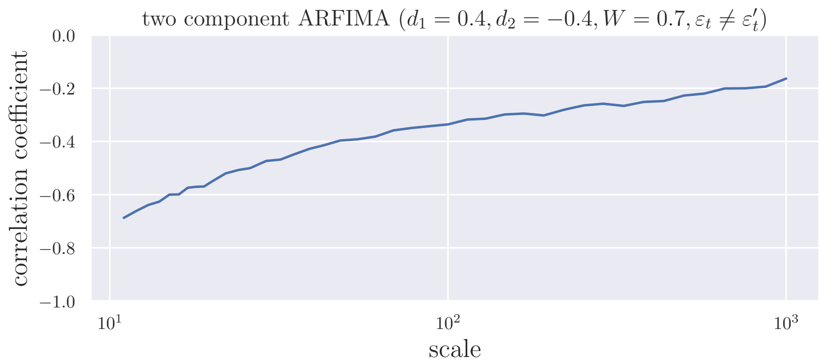

Figure 7.1: Cross-correlations between scale-dependent simulated series generated by the two-component ARFIMA model. Coefficients are significantly negative due to strong anti cross-correlations in the short-term ($\varepsilon_t = -\varepsilon'_t$), but the values gradually increase as scale become larger due to the existence of power-law cross-correlations in the long-term ($W = 0.7$).

Comparing the efficient frontiers of the these series based on the MV analysis and the MMF analysis with scales $s = 10, 100, 1000$ and fluctuation order $q = 2$, we confirm that the shape differs among scales (Fig. 7.2). This result indicates that the scale dependence of the serial correlations and cross-correlations can be captured in the portfolio in a more precise manner.[2] The efficient frontier approaches to a straight line as the scale increase, which is consistent with the fact that the simulated series y_t and y'_t become more and more uncorrelated for large scales. Therefore, portfolio selection based on the MMF analysis can accurately reflect scale dependence among assets.

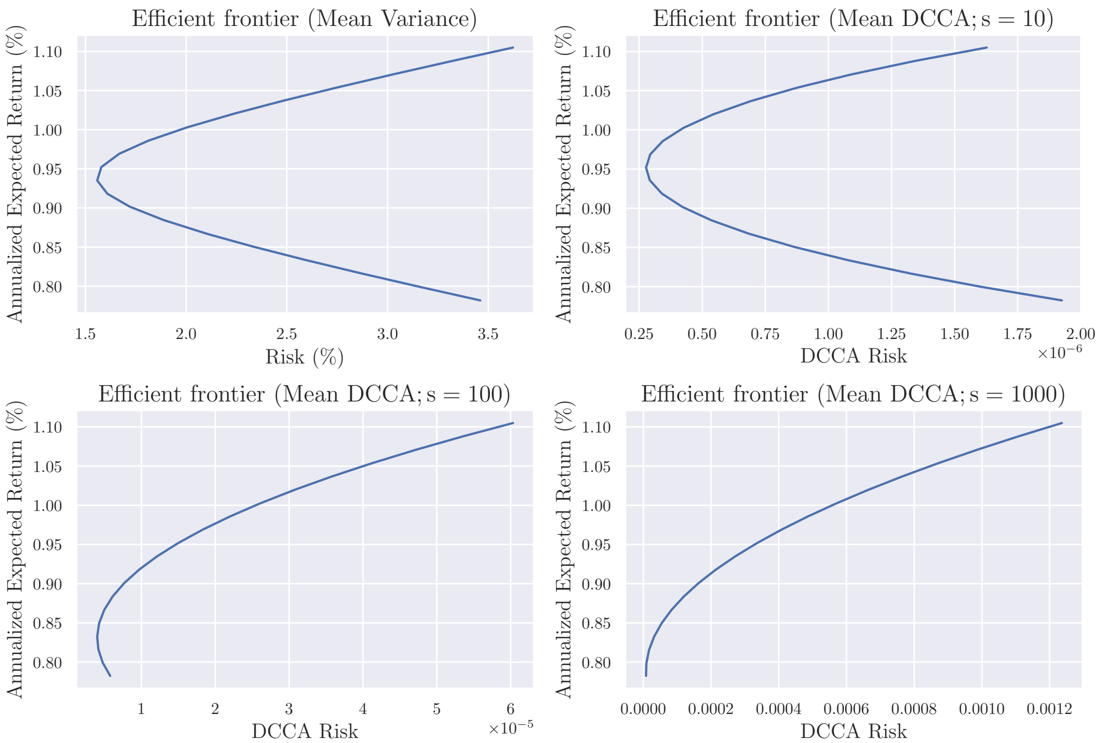

Figure 7.2: Efficient frontiers of the fractal portfolio ($q = 2$) under different scales ($s = 10, 100, 1000$). We confirm that the shape of the frontier varies by scale, successfully providing different levels of diversification effects.

[2]The risk value itself is not essential here, as the definition of the risk function changes with scale. The shape of the efficient frontier matters when discussing portfolio diversification effects.

7.3.2 Multifractal diversification

In order to examine whether the MMF analysis can yield diversification effects that reflect the multifractal characteristics of the series, we next utilize the *multifractal binomial measure* and generate series that exhibit multifractal characteristics. The series can be differently correlated with each other for different multifractal order q (Jiang and Zhou, 2011). In an iterative way each multifractal signal $\{x(i) : i = 1, 2, \ldots, 2k\}$ and $\{y(i) : i = 1, 2, \ldots, 2k\}$ is obtained based on the multifractal cascade p-model (Meneveau and Sreenivasan, 1987). Starting with $k = 0$ with data $z^{(0)}(1) = 1$ consisting of one value, the dataset $\{z^{(k)}(i) : i = 1, 2, \ldots, 2k\}$ in the kth iteration is obtained from

$$\begin{aligned} z^{(k)}(2i-1) &= p_z z^{(k-1)}(i), \\ z^{(k)}(2i) &= (1-p_z) z^{(k-1)}(i), \end{aligned} \tag{7.3.3}$$

for $i = 1, 2, ..., 2^{k-1}$. Especially for $k \to \infty, z^{(k)}(i)$ approaches a binomial measure with an analytical scaling exponent function.

In our simulation, we have set $p_1 = 0.25$ for $x(i)$ and $p_2 = 0.45$ for $y(i)$ and performed $k = 13$ iterations. For the two generated series, we calculate the cross-correlation levels at different fluctuation order q defined by the qDCCA coefficient of Kwapień et al. (2015) defined as

$$\rho_{q\mathrm{DCCA}}(s) = \frac{F^q_{XY}(s)}{\sqrt{F^q_{XX}(s) F^q_{YY}(s)}}. \tag{7.3.4}$$

Note that when $q = 2$, the qDCCA coefficient degenerates to the DCCA coefficient. For simplicity, the scale is set at $s = 100$. The strength of cross-correlations change for different q-order values (Fig. 7.3).

Comparing the efficient frontiers based on the MV analysis and the MMF analysis with q-orders $q = 0.5, 3, 6$ and scale $s = 100$, we confirm that the shape differs, as expected, among fluctuation orders (Fig. 7.4). This result indicates that multifractal characteristics in the serial and cross-correlations of the series can be reflected in the portfolio. The efficient frontier approaches to a straight line as the q increase, which is consistent with the fact that the simulate series $x(2k)$ and $y(2k)$ become more and more uncorrelated for large q. Therefore, portfolio selection based on the MMF analysis can accurately reflect not only scale dependence but also q-order dependence among assets.

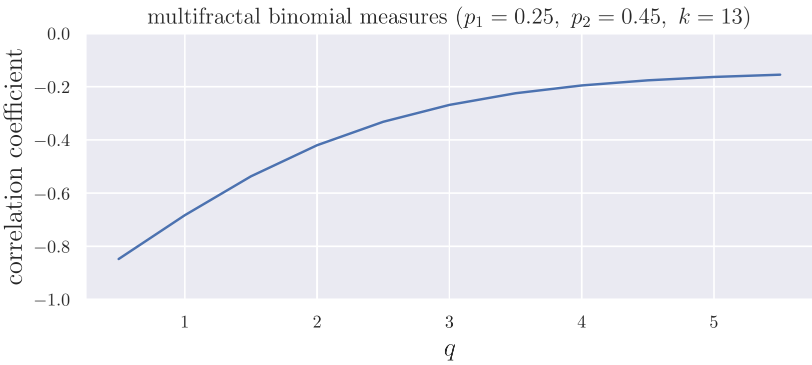

Figure 7.3: Cross-correlations between multifractal simulated series generated by the multifractal binomial measure model. The qDCCA coefficients are calculated at a fixed scale $s = 100$. There are strong anti-correlations for small fluctuations, but not for large fluctuations.

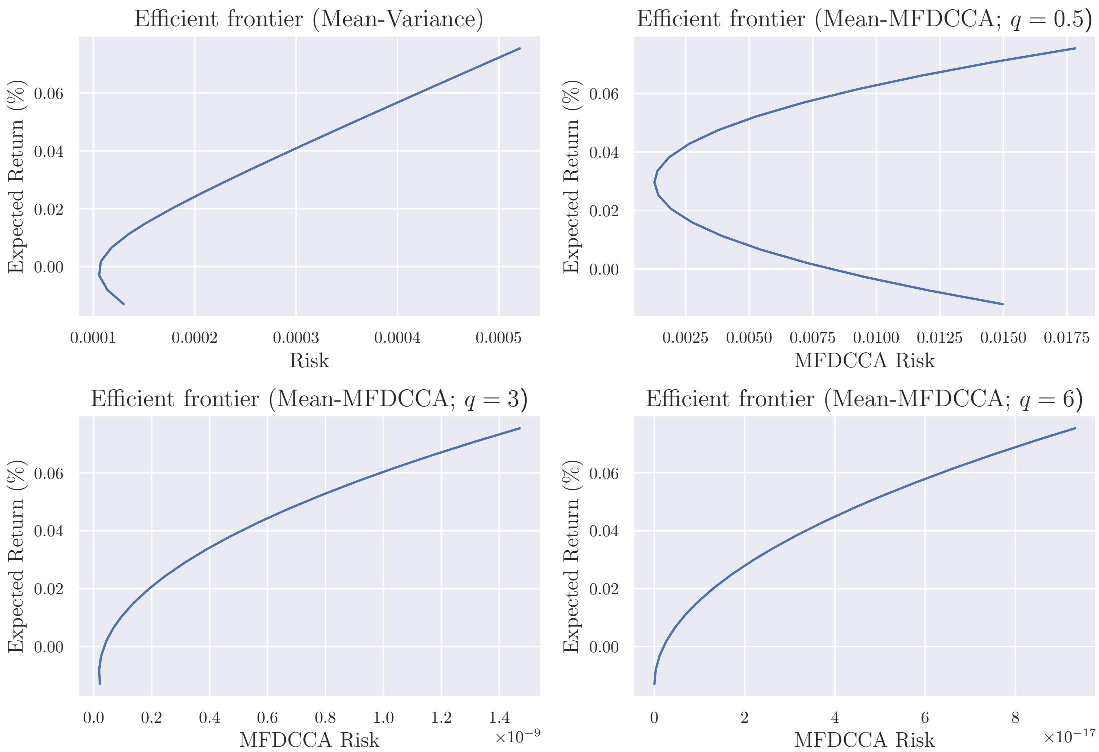

Figure 7.4: Efficient frontiers of the multifractal portfolio ($s = 100$) under different q-order ($q = 0.5, 3, 6$). We confirm that the shape of the frontier varies by the multifractal order q, successfully providing different levels of diversification effects.

7.4 Portfolio Construction and Applications

7.4.1 Dataset and their multiscale property

The fractal MMF portfolio is applied to Four assets including Bitcoin price in USD (BTC), S&P500 stock price , West Text Intermediate price in USD (WTI), and gold spot price versus USD (XAU), from January 2016 to December 2020. Daily price data are obtained from http://www.histdata.com/. The daily return series are shown in Fig. 7.5.

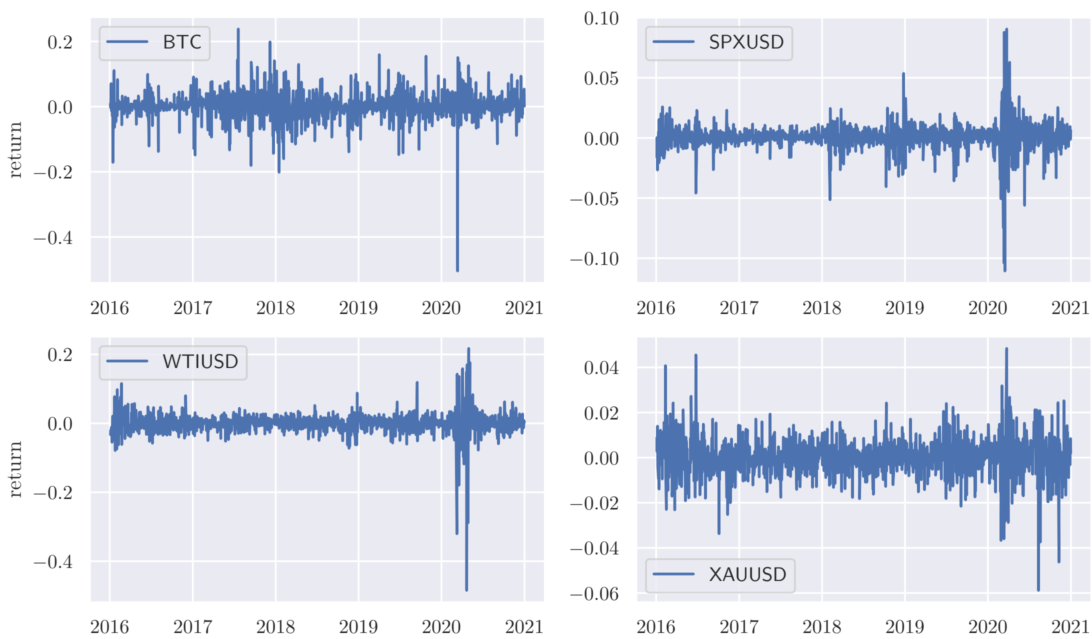

Figure 7.5: Daily return series of the data for the investigated period (2016/01/06 to 2020/12/31).

In Appendix C, we also implement a MD portfolio using major financial assets other than cryptocurrencies. 8 empirical daily indexes of S&P500 stock, US Treasury bond (1-3 Year, 10 year), US High-yield corporate bond, and US Investment-grade corporate bond (Aaa, Aa, A, Baa) are applied for the period of 5 January 2004 to 31 December 2021. High-yield bond provides higher yields than Investment-grades, and they are riskier with lower credit ratings.

7.4.2 Performance under different scaling preference

Before implementing the MMF analysis, we investigate whether the fractal portfolio reflects the diversification effect, if any, among the datasets at study. For each pair of daily returns, we calculate the DCCA cross-correlation of Zebende (2011) at different scales (Fig. 7.6). We confirm that coefficients tend to vary depending on scales. This means that there exist different diversification effects at heterogeneous scales. As reported in Zhang et al. (2022), the fractal portfolio improves the performance of the MV portfolio by incorporating such scaling effects.

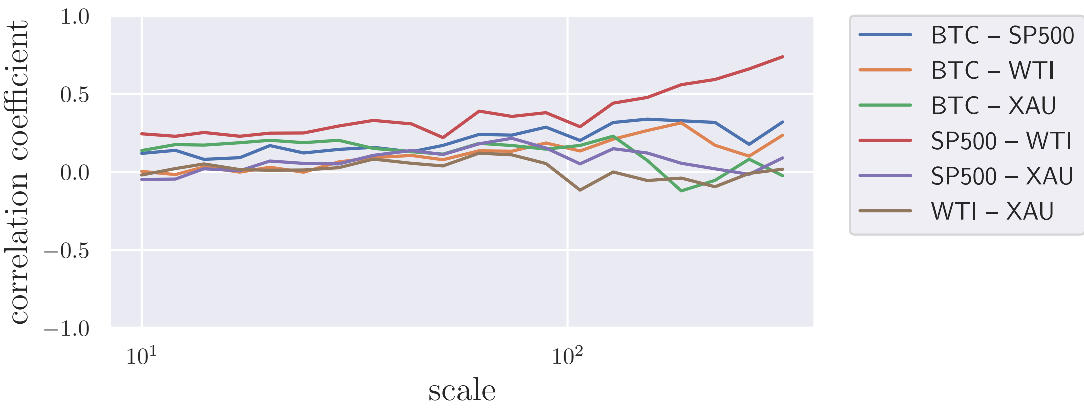

Figure 7.6: Multiscale cross-correlation coefficients of the investigated assets.

In addition, we go further to investigate whether the MMF approach reflects the multifractal properties, if any, within and between the series. For each pair of daily returns, we calculate the qDCCA coefficient of Kwapień et al. (2015) to examine the cross-correlation levels at different fluctuation order q. We confirm that scale-dependent coefficients are dependent on q-th order of fluctuations (Fig. 7.7). This means that the constructed portfolio exhibits different diversification effects not only at heterogeneous scales but also at hierarchical levels of fractality. Thus, the MMF approach can shed light on the scale-dependent multifractality property and has potential for portfolio improvement.

Given that the market exhibits multifractal correlations in addition to different diversification effects by scale, we construct a multifractal portfolio that takes into account the investors' scale preferences classified into three types; long-, short-, and balanced-scales. In particular, referring to Eq. (7.2.4), we set $\alpha_i(s_j) = s_j / \sum_{s\in S} s$ for long-scale preference, and $\alpha_i(s_j) = s_{\#S+1-j} / \sum_{s\in S} s$ for short-scale preference, where s_j denotes the jth element of subset $S = \{s_1, \ldots, s_j, \ldots, s_{\#S}\}$. For the balanced-scale type, the optimal weight is calculated by averaging all the scale-dependent weights. In our analysis, we use a window of 1 year and employ

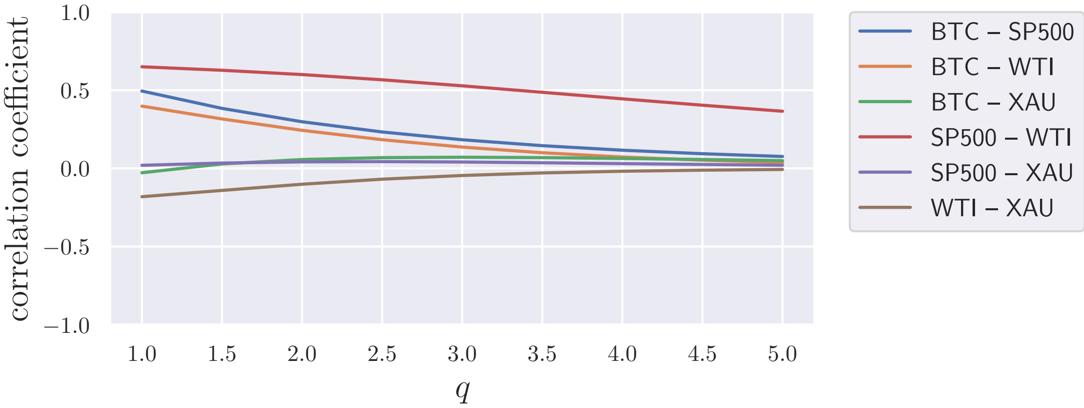

Figure 7.7: Multifractal cross-correlation coefficients of the investigated assets.

$S = \{5, 10, 15, \ldots, 65\}$ as the scale preference subset. For the fluctuation preference subset, we set $Q = \{2, 3, 4\}$ to avoid bias from extremely large levels of price fluctuations.

Table 7.1 presents the maximum drawdown performance of MV and MMF portfolios based on the three strategy types, with the minimum risk measure. All three types of MMF portfolio generally outperform the traditional MV. More interestingly, the higher performance among the MMF strategies appears to vary by market period. The results imply that understanding the heterogeneity of investors and their scale inclination plays an essential role in increasing portfolio risk control. According to the FMH concept, investors tend to focus more on the short-term in downside situations. Thus, in a relatively unstable market condition, short-scale MMF is expected to minimize portfolio risk the most.

Table 7.1: Maximum drawdown performance (%) of the portfolios with the minimum risk measure

	MV	MMF-balanced	MMF-short	MMF-long
2016	-5.221	-4.782	-5.307	**-4.459**
2017	-2.451	**-1.907**	-1.978	-1.958
2018	**-11.27**	-13.15	-13.09	-13.20
2019	-3.077	-2.939	**-2.922**	-2.955
2020	-16.23	-14.99	-15.23	**-14.75**

7.4.3 Outsample performance of the switching strategy

The out-sample performance of the MMF portfolio is also discussed by backtesting. We use a 1-year rolling window (260 daily returns) estimation with quarterly rebalancing. To regard the effect of the heterogeneity of investors under different market conditions, we introduce a new strategy, that is, when rebalancing the portfolio, we switch the scale preference types among the three MMF strategies. If the maximum drawdown of the balanced-scale MMF over the past two years is worse than -10%, we consider the market to be in an unfavorable state and select the short-scale strategy. Otherwise, we assume the market to be out of recession or not in its downtrend and expectations for longer investment horizons have increased; thus, we select the long-scale strategy. Figure 7.8(a) shows the switch and maximum drawdown throughout the entire period. In Figure 7.8(b), we confirm that the MMF-switching strategy outperforms portfolio risk and achieves to gain profit compared to MV and other types of MMF. Table 7.2 shows that the portfolio reduces maximum drawdown, Value-at-Risk (VaR), and expected shortfall (ES) and increases portfolio returns. Therefore, changing the scale preference of the MMF portfolio in response to market conditions is effective in gaining more portfolio risk control.

Table 7.2: Backtest performance (annual average) of portfolios.

	MV	MMF			
		balanced	short	long	switching
max. drawdown (%)	-10.25	-10.02	-10.07	-9.989	**-9.970**
10-day 99%VaR (%)	-6.452	-6.163	-6.194	-6.126	**-6.117**
10-day 97.5%ES (%)	-6.324	-6.075	-6.121	-6.034	**-6.027**
annual return (%)	9.530	9.532	9.565	9.499	**9.701**

7.5 Summary and Discussions

The application of the fractal MD as well as the MMF portfolio provides insight into the scale dependence of the optimal allocation, especially when assets have multiscale relationships with each other. Since investors' scale preference and scale dependence shift to a different level according to changing economic conditions, further development is achieved by incorporating time-varying features in the MMF portfolio. The short-scale preference strategy increases the diversification effect when the market outlook is uncertain, while the long-scale preference strategy is more effective when the market is less turbulent. Such a strategy works well for both in-sample and out-sample data and improves maximum

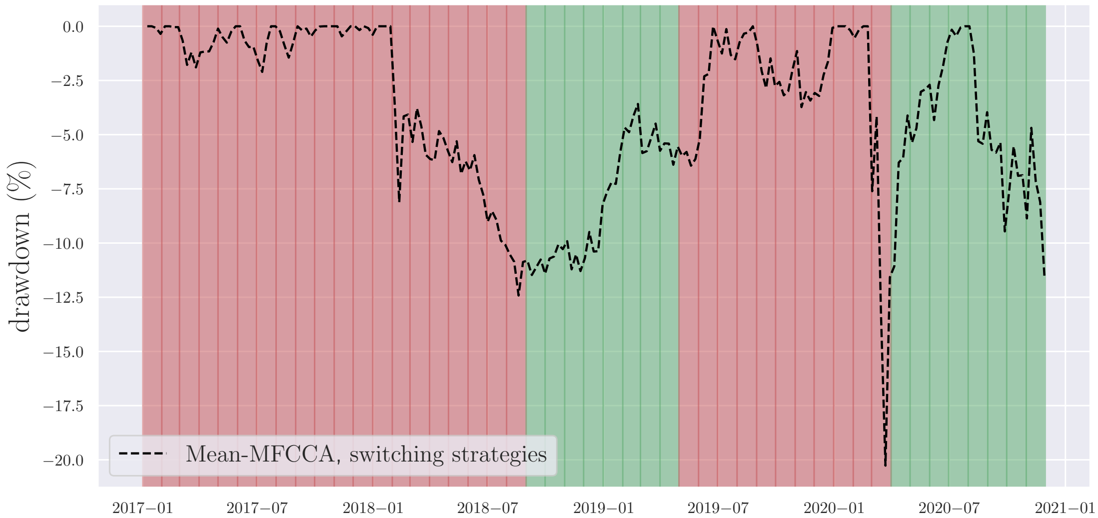

(a) Strategy switching and maximum drawdown throughout the period. The red (green) ranges represent long (short) scale preference.

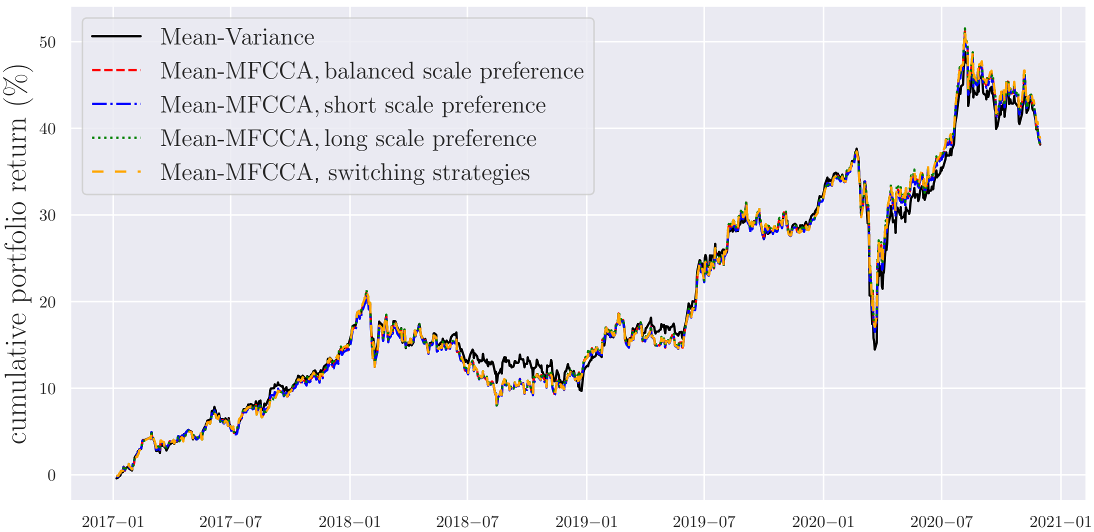

(b) Cumulative portfolio returns

Figure 7.8: Backtest results of the MV and MMF portfolio with different types of scale preference strategies.

drawdown, VaR, and ES, and hence should be of interest not only to academic researchers but also to portfolio managers and policy makers. An extension of our study would be to consider asymmetry in the multifractality of the assets by employing the MF-ADCCA function instead of DCCA or MFCCA when calculating the risk function. This may allow for a more sophisticated portfolio diversification taking consideration of the differences between downside and upside market risks.

More importantly, our results emphasise the importance of revealing the multiscale behaviors and heterogeneous properties of price fluctuation and correlation, supporting that the FMH hypothesis framework illuminates additional views to systematic and mathematical approaches to portfolio construction. Although the emphasis tends to be on optimization methods that reduce portfolio risk and increase returns, the results of these fractal methods remind us that attention should be paid to defining and assessing risk measures that play a crucial role in quantifying portfolio risk. This framework not only addresses the shortcomings of the MPT, but also those of the EMH, which deviates significantly from reality, such as the assumption that markets are efficient and that investors have equal access to the same information. Investors have other objectives, such as socially positive/negative impact and market events, showing evidence of heterogeneity— which appears mathematically as the fractal principle.

Chapter 8

Conclusion

In this thesis, we have focused on alternative approaches toward analyzing cryptocurrency series from a nonlinear physical approach. In particular, we have applied the stable distribution, a class of power-law distibution, to further develop investigation of intense fluctuation behaviors of cryptocurrency markets. In addition, we have attempted to clarify some of the notable behaviors based on the Fractal Market Hypothesis, and to shed light on the background mechanism through an interpretation based on the behavioral finance theory. The concept of fractal correlations helps analyzing dynamical complex systems of financial markets including cryptocurrencies.

In Chapter 2, we have proposed a new approach for estimating stable law parameters and have applied to the exploration of price behaviors in financial markets. We tackle the issue of a primary defect in the CF-based estimation process that the lack of stable densities and cumulative distribution functions face challenges when modelling empirical distributions with stable laws. By proposing a technique that allows us to benefit from the interrelations between the scaling exponent parameter and the characteristic parameter, the points necessary for the estimation process are flexibly chosen, making the process more practical without any inconvenient restrictions on parameter ranges. The proper points at which the characteristic function should be evaluated are chosen through an iteration procedure relying on the combination of empirical searches and algorithmic approaches. Benchmarked against other existing methods, we have compared the estimation performance through Monte Carlo simulation in terms of the MSE and KS-distance. The proposed method not only improved the performance of each parameter, but also reduced distributional estimation errors. We also applied our method to several financial markets to show that our method is practical.

In Chapter 3, we have explored the behavior of cryptocurrency price fluctuations by applying the stable distribution and discussed its validity for empirical analysis. We provided numerical and theoretical justifications for supporting the stable distribution as a practical model when analyzing financial time series. We find that returns exhibit stable laws with tail index $\alpha \simeq 1.4$ and $\beta \simeq 0$. To find evidence of stable laws, a numerical approach based on the CF and a theoretical approach based on the GCLT was introduced by focusing on the time scaling behavior with different time intervals. However, we find evidence that the stable model is not acceptable under certain time frequencies, where the stable regime breaks down to a Gaussian regime. A time scaling ranging roughly 30 minutes to 4 hours is concluded to be a suitable range of intervals for cryptocurrency markets. Moreover, we confirm the potency of stable distributions by investigating which distribution shows a better fit among controversial fat-tailed distributions. We find statistical evidence that when a wider range of tail portion of data is considered, the stable distribution dominates other alternative distributions. On the other hand, the far tail generally follows a power law, which coincides with the results in many empirical studies on tail behaviors of returns. To reach a more rigorous conclusion on whether stable models may work in practical applications, however, a more elaborate discussion would be necessary.

In Chapter 4, we have evaluated market efficiency and asymmetric multifractality of the two major cryptocurrencies (Bitcoin and Ethereum) during the periods before and after the COVID-19 outbreak, accounting for the different scaling regimes on long and short time scales. By using the A-MFDFA method, we found that the markets have asymmetric multifractality with crossovers of approximately 10 days, indicating that scaling behaviors are dependent of investment horizons. Our results provided empirical evidence of increasing inefficiency for the short-term, while the markets show traces of efficiency for the long-term. In other words, COVID-19 significantly increased herding in the short-run but not in the long-run. This study also discussed the features of asymmetric properties between upward and downward trends. Although fat-tailed distribution of returns generally causes the multifractal behavior, the contribution of autocorrelations to multifractality becomes substantial in the long-term especially when the market is in a downtrend. The presence of different predominant sources of multifractality between bull and bear markets could be a driver to the substantial asymmetric properties observed in the long-term. Our findings argue that analyzing different scales can be a key to reveal complex behaviors during crisis periods, although the relationship between multifractality and asymmetric efficiency of the on-going COVID-19 pandemic is still debatable.

In Chapter 5, we have examined the nexus between daily price and realized volatility in cryptocurrency markets using the MF-ADCCA approach. The approach revealed that the price-volatility relationship exhibits power-law cross-correlations as well as multifractal properties. More interestingly, the multifractal characteristics of the cross-correlation present different properties between positive and negative market trends. The details of these features are confirmed through the generalized Hurst exponents and the singular spectrum. Our results pointed out that generally for the investigated cryptocurrencies, cross-correlations of price and volatility in the uptrend markets have slightly higher persistency compared to those in the downtrend markets. Distinctive features of how small and large fluctuations operate on multifractality were also discovered and reported by looking at the spectrum distortion for each cryptocurrency and for each market trend. Moreover, the level of the asymmetric cross-correlations for each cryptocurrency was quantitatively evaluated by employing the asymmetric DCCA coefficient. Our empirical findings showed that depending on market directions or trends, the level of cross-correlations differs. We found the presence of stronger cross-correlations in bear markets than in bull markets for the maturing major coins (BTC and ETH), whereas the opposite results were observed for the still-developing minor coins (XRP and LTC).

In Chapter 6, we have developed a fractal regression framework to evaluate how return volatility responds asymmetrically to return shocks in six representative cryptocurrency markets of Bitcoin, Ethereum, Ripple, Litecoin, Monero, and Dash. We reveal the presence of a scaling-dependent structure in the asymmetric relationship between return shocks and return volatility, that is, volatility of cryptocurrencies can negatively or positively be influenced by return shocks dependent on time scales. The findings illustrate that the asymmetry of volatility effect is determined not only by proximate return shocks but also by shocks across scales. The empirical results indicates that regardless of scales, the major BTC and ETH show a strong asymmetric volatility effect (negative effect), where negative shocks tend to have a greater impact on volatility. On the contrary, for some specific ranges of mid-term scales, minor cryptocurrencies (especially XRP and DASH) show an inverse asymmetric volatility effect (positive effect), where positive shocks tend to have a greater impact on volatility. The reason is discussed in the context of uninformed traders dominating the market in different situations. In addition, we confirmed that the scale-dependent asymmetric volatility effect in cryptocurrencies changes by experiencing two prominent bubbles and crashes. Therefore, our approach has the ability to explain the asymmetric return-volatility relationship in addition to their scaling-dependencies.

In Chapter 7, we have developed the portfolio selection approach in terms of the FMH framework. The application of the fractal MD as well as the MMF portfolio provides insight into the scale dependence of the optimal allocation, especially when assets have multiscale relationships with each other. Since investors' scale preference and scale dependence shift to a different level according to changing economic conditions, further development is achieved by incorporating time-varying features in the MMF portfolio. The short-scale preference strategy increases the diversification effect when the market outlook is uncertain, while the long-scale preference strategy is more effective when the market is less turbulent. Such a strategy works well for both in-sample and out-sample data and improves maximum drawdown, VaR, and ES.

To sum up, understanding the features of price fluctuation, the interrelationships of volatility and their asymmetric behavior, and multiscale definition of portfolio risk play a crucial role in various determinants in real-world finance. Our findings underscore the significance of understanding the multiscale characteristics and varied properties of financial fluctuation and correlation, and demonstrate that the FMH hypothesis framework provides new perspectives for systematic and mathematical approaches to risk hedging and portfolio building. Therefore, our findings should be of interest to academic researchers, market investors, portfolio managers, and policymakers, who wish to enhance their decision-making with cryptocurrencies.

Acknowledgement

I, the author, Shinji Kakinaka, would like to express my deepest gratitude to supervisor Professor Ken Umeno, for his unwavering support, guidance and encouragement throughout my Ph.D. journey. His expertise and insights have been invaluable in shaping the direction and development of my research. I also like to thank Professor Nobuo Yamashita and Associate Professor Kenji Kashima for their kind comments.

Special thanks goes to Mr. Kazuyuki Takeda of Mizuho–DL Financial Technology Co., Ltd., Mr. Tadaaki Hayakawa of Mizuho Bank, Ltd., and Mr. Daisuke Kato of Mizuho Research & Technologies, Ltd., for valuable suggestions and comments on my research.

The author would like to express his appreciation to Professor Stelios M. Potirakis and Mr. Pavlos I. Zitis of Department of Electrical and Electronics Engineering, University of West Attica, for their constructive suggestions and collaboration on the project.

I am also greatful to my co-members, Ryosuke Yoneda, Hikaru Shindo, and Shonosuke Harada, and my family for their love and support during this challenging yet rewarding journey.

Last but not least, I gratefully acknowledge my wife, Tomoko, for her constant encouragement and motivation. Her unwavering support and understanding have greatly been a source of energy and strength for me.

Appendix A

Power Law Properties

A.1 Fitting Local Tails with One-sided Distributions

This Appendix shows the results of the best local fit with two types of one-sided distribution models, the power-law and exponential distributions, for cryptocurrency data. Before showing the results, we provide a technical description of the goodness-of-fit test.

Concerning the case of the power-law distributions, as mentioned in subsection 2.2, the method of fitting data with power-laws relies on the combination of KS statistics and the maximum likelihood estimators (Hill estimator) suggested by Clauset et al. (Clauset et al., 2009). They also propose how to test the goodness-of-fit to see whether the hypothetical model is plausible for fitting the data. The idea is based on the resampling method with the procedures given as follows. After fitting the data with the power-law model, we generate synthetic datasets that follow a power law with the parameter estimate $\hat{\alpha}$ and the lower bound $\hat{x}_{\min}$. The same method of fitting with power laws is applied again to these datasets to obtain synthetic distances between the generated CDF and the newly estimated CDF associated with the minimum KS statistic. A sufficiently large number ($L = 1000$) of synthetic datasets are generated, and each synthetic distance D_i ($i = 1,\ldots,L$) is then compared with the empirical distance D. Finally, the p-value for the null hypothesis that the data follows the estimated model is calculated by using the number of times that satisfy $D_i \geq D$ ($i = 1,\ldots,L$). The confidence level is set at 90%, in other words, if $p \geq 0.1$, we can say that the model shows a plausible fit. Regarding the case of the exponential distributions, we conduct similar procedures as the case of the power-law distributions.

Table A.1 shows the results of fitting the data of standardized returns, presented in subsection 3.2, with power-law and exponential models for the positive

Table A.1: Estimation results of the power-law and exponential fit with standardized cryptocurrency returns for the *positive* tail and its goodness-of-fit test with the p-value. Δt is the time interval, $\hat{x}_{\min}$ is the lower bound of the estimated tail, and n_{tail} represents the number of data used for the estimation (data number of the tail portion). $\hat{\alpha}$ and $\hat{\lambda}$ is the estimated power-law parameter and the estimated exponential parameter, respectively. Statistically significant fit ($p \geq 0.1$) are shown in bold.

Power law	Δt	n_{tail}	$\hat{x}_{\min}$	$\hat{\alpha}$	p
BTC	1h	344	5.632	3.098	**0.598**
	2h	226	4.839	2.997	**0.637**
ETH	1h	145	7.527	3.368	**0.907**
	2h	286	4.277	2.631	**0.225**
XRP	1h	169	9.176	2.876	**0.204**
	2h	133	7.403	2.662	**0.989**
LTC	1h	194	6.939	3.221	**0.999**
	2h	103	7.272	3.371	**0.654**
XMR	1h	53	8.978	3.618	**0.980**
	2h	148	5.269	3.139	**0.805**
Exponential	Δt	n_{tail}	$\hat{x}_{\min}$	$\hat{\lambda}$	p
BTC	1h	1121	3.106	0.442	0.000
	2h	539	3.046	0.472	0.012
ETH	1h	245	5.916	0.328	**0.376**
	2h	4342	0.003	0.673	0.000
XRP	1h	346	6.220	0.234	0.016
	2h	266	4.985	0.260	0.000
LTC	1h	497	4.553	0.365	0.004
	2h	163	5.758	0.334	**0.756**
XMR	1h	8459	0.0002	0.696	0.000
	2h	4350	0.0001	0.707	0.000

Table A.2: Estimation results of the power-law and exponential fit with standardized cryptocurrency returns for the *negative* tail (in absolute values) and its goodness-of-fit test with the p-value. Statistically significant fit ($p \geq 0.1$) are shown in bold.

Power law	Δt	n_{tail}	$\hat{x}_{\min}$	$\hat{\alpha}$	p
BTC	1h	229	7.279	3.156	**0.943**
	2h	341	4.258	2.567	**0.301**
ETH	1h	345	5.535	2.950	0.044
	2h	414	3.612	2.353	0.001
XRP	1h	329	5.833	2.571	**0.827**
	2h	221	5.043	2.547	**0.234**
LTC	1h	128	7.882	3.778	**0.914**
	2h	149	5.743	3.168	**0.420**
XMR	1h	379	4.620	2.983	**0.135**
	2h	61	7.557	3.993	**0.902**
Exponential	Δt	n_{tail}	$\hat{x}_{\min}$	$\hat{\lambda}$	p
BTC	1h	1178	3.140	0.380	0.000
	2h	891	2.203	0.444	0.002
ETH	1h	1753	2.202	0.471	0.000
	2h	256	4.525	0.383	**0.755**
XRP	1h	71	10.46	0.174	**0.807**
	2h	80	7.560	0.245	**0.597**
LTC	1h	700	3.806	0.420	0.005
	2h	459	3.331	0.449	0.031
XMR	1h	8827	0.009	0.731	0.000
	2h	4278	0.018	0.702	0.000

tail, and Table A.2 shows the results for the negative tail. The analysis generally confirms that the tail portion of cryptocurrency returns plausibly fit with a power law exponent with α approximately ranging from 2.5 to 3.5, which is slightly higher than the finding in the previous study for the Bitcoin (BTC) (Begušić et al., 2018). On the other hand, the exponential model is not appropriate for many cases. However, since the exponential model sometimes shows a plausible fit with empirical data, we consider it as an critical model. Thus, we discuss the model-fit for the tail portion of returns by comparing the stable distribution with the exponential distribution in subsection 3.4.

Appendix B

Scale-dependent Regressions

B.1 Literature Review of the Asymmetric Volatility Effect

The negative response of volatility to return shocks was originally referred to the financial leverage, because the decrease of stock prices naturally brings in the rise in firm's leverage, making the stock become riskier and increasing its volatility (Black, 1976; Christie, 1982; Schwert, 1989; Cheung and Ng, 1992). However, many papers warn us that such an effect should not be associated with financial leverage. Hens and Steude (2009) explain the effect in an experimental stock market under a controlled setting where students are given instructions to trade artificial securities with each other using an electronic trading system with no financial leverage. They find that the effect can be observed even in the absence of financial leverage. Similar results are presented by Hasanhodzic and Lo (2019), where they confirm the existence of leverage effect in all-equity-financed firms having no debt. The volatility feedback is another possible factor that explains the negative correlation between volatility and expected rate of return (Campbell and Hentschel, 1992). In response to favorable information (good news), the increase in return is mitigated by the effect of price decline due to increased risk. In response to unfavorable information (bad news), the price decline due to increased risk is added, magnifying the decrease in the rate of return. Nevertheless, since both factors of financial leverage and volatility feedback are built on the EMH, they do not fully explain the leverage effect. Namely, the inefficiency of market information can also give rise to asymmetric volatility, so it has arisen as an important factor.[1] The informational inefficiency imposes different impacts on the return process, i.e., asymmetric volatility occurs when investors trade based on

[1] In the study of Antoniou et al. (1998), they reject the traditional leverage effect and conclude that information inefficiency in markets is the cause of asymmetry in volatility.

noise rather than information. Black (1976) calls them "noise traders" because they overreact to information and trade irrationally. These uninformed investors affect liquidity to the market (Easley et al., 1996) and generate asymmetric fluctuations in market prices (Avramov et al., 2006; Baur and Dimpfl, 2018). In this context, noise traders happen to be dominant after negative shocks in many of the conventional markets, where higher volatility follows.

On the other hand, some markets show an inverse asymmetric volatility phenomenon where higher volatility follows after positive shocks. Chen and Mu (2021) reveal the presence of an inverse leverage in a wide range of commodity markets, including agricultural products, energy, industrial metals, and precious metals, except for crude oil. Kliber (2016) finds evidence of inverse leverage in the sovereign credit default swap spreads (sCDS) for the countries of Portugal, Poland, Greece, and Slovenia. The author refers it to the Prospect Theory of Tversky and Kahneman (1992), where the decision making of investors is explained under different risk conditions. Under several assumptions, the author justifies that inverse-leveraged sCDS in the above cases are due to market participants feeling that the probability of default is higher than the one implied by the spread.

In respect of cryptocurrencies, a number of studies have attempted to model the behavior of volatility. Whether volatility of price changes is positively or negatively related to return shocks has traditionally been modeled by making explicit the conditional variance of returns. Katsiampa (2017) compares several competing GARCH-type models and concludes that the Component GARCH (CGARCH), a model that allows a short-run and a long-run component of conditional variance, provides the optimal fit level of Bitcoin data for the period between July 2010 and October 2016. It is worth noting that during the period, the log-likelihood value under the CGARCH model is higher than that of under its asymmetric model, the asymmetric component GARCH (ACGARCH) model. This result implies that asymmetric models are not always the most appropriate to explain Bitcoin volatility, and thus symmetric models can sometimes provide a better explanation. The information criteria for diagnosing model selection discussed in the literature also support the findings that the (symmetric) CGARCH model presents a plausible fit.

However, asymmetric models under other GARCH-type models generally outperform symmetric models in many cases, and they have the potential to address significant asymmetry in volatility. On implementing the well-known GJR-GARCH model of Glosten et al. (1993) and the EGARCH model of Nelson (1991), Bouri et al. (2017a) investigate the relation between price returns and volatility changes in the Bitcoin market against various world currencies and test if there is a difference in the asymmetric structure before and after the price crash of 2013. They report that before the crash, positive returns helped increase the conditional variance more than negative returns but not after the crash, suggesting that positive (inverse) asymmetric volatility effect is relevant to a safe-haven property of Bitcoin rather than the financial leverage or volatility feedback. Cheikh et al. (2020) attempt to capture different impacts of positive versus negative shocks regarding a flexible intermediate state between variance regimes. They employ the smooth transition GARCH (ST-GARCH) model and investigate four representative cryptocurrencies of Bitcoin, Ethereum, Ripple, and Litecoin using data from April 28, 2013, to December 1, 2018. They find a positive relationship between return shocks and volatility for the majority of currencies except for the case of Ethereum, where no asymmetry can be detected under the ST-GARCH, EGARCH, threshold GJR-GARCH, and threshold GARCH (ZGARCH) models. Using a wide range of data periods available through August 2018, Baur and Dimpfl (2018) test the existence of an asymmetric volatility effect in as many as 20 major and minor cryptocurrencies by employing the TGARCH model in addition to the quantile autoregressive model (QAR). They find that positive shocks increase volatility more than negative shocks for most cases, with the most notable exceptions being the two largest currencies, Bitcoin and Ethereum. They attempt to explain the phenomenon in terms of informed and uninformed (noise) traders' trading activities—asymmetry is due to uninformed traders' herding and buying activity boosted by the fear of missing out (FOMO) on rising cryptocurrency prices, as well as the pump-and-dump schemes. In this context, the authors argue that the two largest Bitcoin and Ethereum play a special and different role because, in the most mature peer-to-peer currencies, the market is dominated by informed traders who have the ability to reduce some of the prominent asymmetry generated by uninformed traders.

Fakhfekh and Jeribi (2020) refer to the importance of focusing on long-memory properties of time series in finding the most optimum model or sets for depicting volatility. By introducing fractionally integrated models of FIGARCH and FIEGARCH, they take into account long-memory factors in the conditional heteroskedasticity variance towards modeling sixteen of the most popular cryptocurrencies' volatility. Under the period from August 7, 2017, to December 12, 2018, they apply fourteen GARCH specifications, including typical asymmetric GARCH-type models, with different error distributions. They conclude that, in general, the TGARCH and EGARCH models provide the best model explanation, although the best model fit varies across cryptocurrencies. They also report the presence of an inverse asymmetric volatility effect, more or less in line with other relevant studies. Mensi et al. (2019a) examine structural break impacts on the dual long memory of Bitcoin and Ethereum using four different ARFIMA-GARCH family models, specifically GARCH, FIGARCH, FIAPARCH, and HYGARCH models. By considering long-memory and structural breaks, they find that dual long memory exists in Bitcoin and Ethereum returns and volatility. Their results indicate that market returns and volatility do not follow a random pattern, and thus EMH does not hold for cryptocurrencies. They also point out that FIGARCH with structural breaks is comparatively superior to other models for volatility forecasting.

Al-Yahyaee et al. (2018) show evidence of long-memory feature as well as multifractality in the Bitcoin market and compare the level of market efficiency to gold, stock, and foreign exchange markets by applying the dynamical approach of multifractal detrended fluctuation analysis (MFDFA) proposed by Kantelhardt et al. (2002), which is a method that generalizes the DFA to multifractality. They find evidence of the market being more inefficient with stronger multifractality than other assets. With the use of A-MFDFA, which extends the MFDFA to capture asymmetric structures, Liu and Chen (2018) examine the asymmetric volatility of the dry bulk shipping market brought by the financial crisis. They also demonstrated the fractal method's usefulness in illustrating asymmetric characteristics of long-range correlation, multifractality, and many other data properties in financial time series. In the same framework, with high-frequency Bitcoin and Ethereum data, Mensi et al. (2019b) examine long-memory, asymmetric multifractality, and time-varying efficiency to reveal different market patterns between downside and upside trends. They clarify that both Bitcoin and Ethereum are highly inefficient because different scaling laws and asymmetric fractal patterns exist in the price dynamics, supporting the FMH. Both markets are more inefficient when moving downwards relative to when they are moving upward. Other studies use the MF-ADCCA, an extension of A-MFDFA, in estimating the scaling factor of asymmetric long-range cross-correlations between time series. In the literature of Cao and Xie (2021), the authors highlight the long-memory and asymmetric multifractal characteristics of cross-correlations between cryptocurrencies and Chinese financial markets. These stylized facts are also evident between leading cryptocurrencies, leading conventional currencies (Kristjanpoller and Bouri, 2019), and equity ETFs (Kristjanpoller et al., 2020). The above studies suggest that cryptocurrency markets represent a complex system that can generate asymmetry in its inter-relationship with other financial markets.

Kakinaka and Umeno (2021) utilize the fractal method of MF-ADCCA to investigate asymmetric cross-correlation between price return and return volatility in cryptocurrency markets from June 1, 2016, to December 28, 2020. The literature further quantifies the multi-time scale strength of asymmetric cross-correlation by employing the asymmetric DCCA coefficient at various scales. They report that stronger cross-correlation appears in the downtrend market for the major coins of Bitcoin and Ethereum. In contrast, stronger cross-correlation appears in the uptrend market for the more minor coins of Ripple and Litecoin. One of the main contributions of the work to the field is that they established an approach to investigate dynamical properties of long-range dependent processes of return and volatility at a specific scale, which extends the discussion to the economic phenomenon of asymmetric volatility effect on multi-time scales.

Although the idea of using fractal analysis towards detecting the asymmetric volatility effect under different time scales is demonstrated in Kakinaka and Umeno (2021), its interpretation is limited in terms of correlation coefficients defined between -1 and 1. In our study we will also utilize fractal analysis, but unlike earlier studies, the asymmetric effect is associated with the actual effect of an economic variable (return shocks) on another (volatility) rather than simply the strength of correlation between variables. Our study is also different from other volatility models, i.e., GARCH models, in that we take into account the multi-time scale structure between the variables, while the scaling property is ignored in these conventional models. The multi-time scale fractal regression analysis we implement is complementary to other existing methods built on long-memory, fractality, and scale-dependent processes and works excellent with modeling heterogeneity in economic and financial variables (Tilfani et al., 2022). As the detection of asymmetric volatility effect is crucial towards deciding portfolio positions, modeling its heterogeneity expectations in terms of multi-time scales may provide additional views from past studies. Our study deepens the interdisciplinary understanding of the connection between economic behavior and stylized facts that emerged from the field of physics.

B.2 Bootstrap Confidence Interval

After obtaining $\hat{\beta}_i^{\mathrm{DFA}}(s)$ and the error $\varepsilon_t(s)$ from the model of Eq. (6.2.10) (Eq. (6.2.12)), we resample the error $\varepsilon_t^*(s)$ and construct a new data Z_t^* using $\hat{\beta}_i^{\mathrm{DFA}}(s)$ and $\varepsilon_t^*(s)$. We apply once again the fractal regression and run the procedure 1000 times. Then we obtain a collection of estimated coefficients, so the quantile of $\beta_2^{\mathrm{DFA}}(s)$ can be calculated. Below in Figure B.1, the 95% confidence intervals across scales for each cryptocurrency are depicted. If $\hat{\beta}_2^{\mathrm{DFA}}(s) = 0$ is out of the range in orange, the coefficient is significantly different from 0. We confirm that the results are very similar to those obtained using the scale-dependent t-statistics presented in Figure 6.4.

B.3 Estimation Results Using Volume-Weighted Average Daily Prices

In this section we show the estimates of the DFA-based bivariate regression based on the volume-weighted average daily prices (VWAP) of each cryptocurrency, to check the robustness of our results presented in 6.3.2.

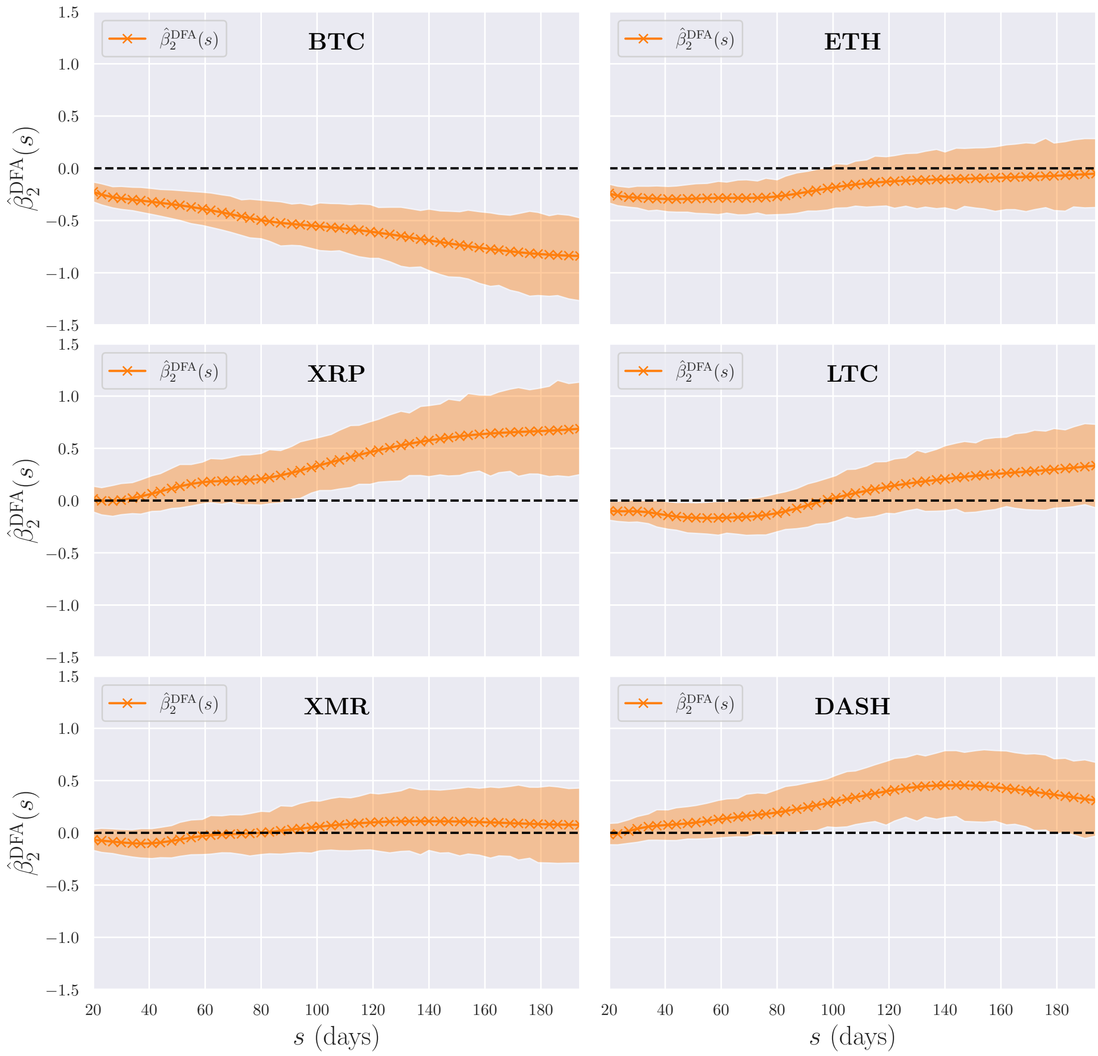

Figure B.1: Bootstrapped 95% confidence interval of DFA-based bivariate regression.

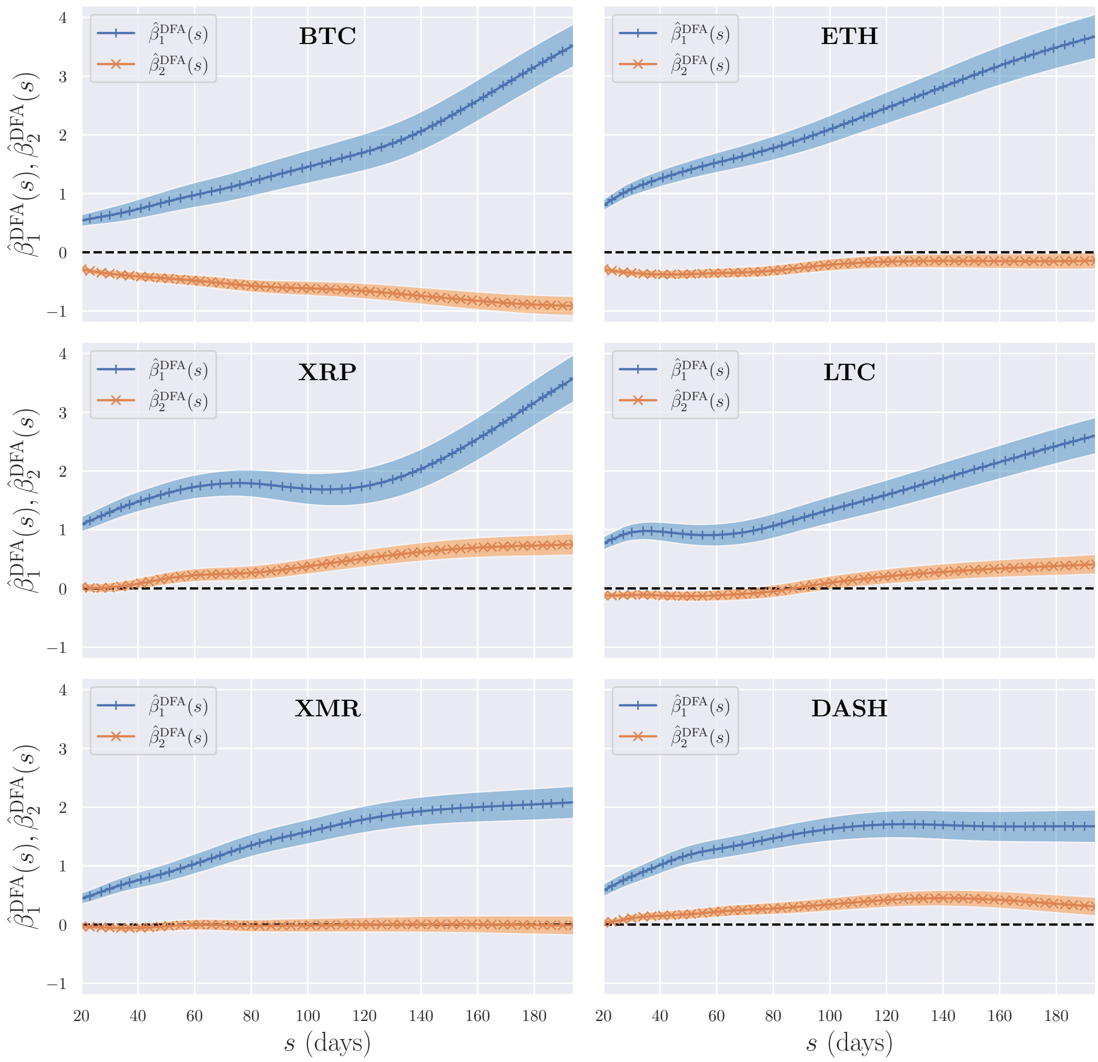

Figure B.2: DFA-based bivariate regression estimates of cryptocurrency series based on VWAP. The coefficients $\hat{\beta}_1^{\mathrm{DFA}}(s)$ and $\hat{\beta}_2^{\mathrm{DFA}}(s)$ are shown for each cryptocurrency; BTC, ETH, XRP, LTC, XMR, and DASH. The colored ranges denote 95% confidence intervals calculated as $\hat{\beta}_i^{\mathrm{DFA}}(s) \pm 2\sqrt{\mathrm{var}(\hat{\beta}_i^{\mathrm{DFA}}(s))}$, for $i = 1, 2$.

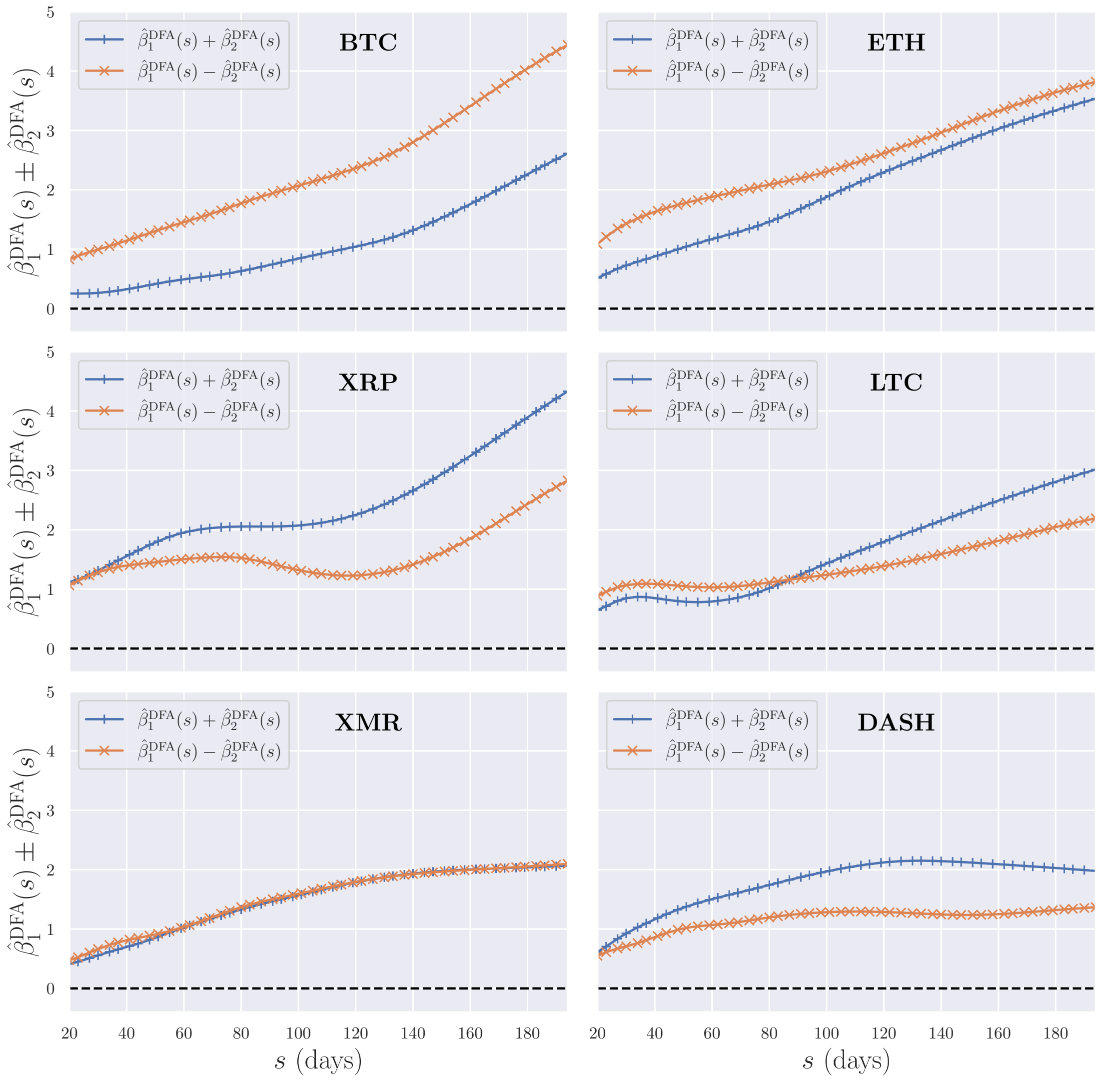

Figure B.3: The impact of good and bad news to volatility, $\hat{\beta}_1^{\mathrm{DFA}}(s)+\hat{\beta}_2^{\mathrm{DFA}}(s)$ and $\hat{\beta}_1^{\mathrm{DFA}}(s)-\hat{\beta}_2^{\mathrm{DFA}}(s)$, respectively. We show the results based on VWAP for each cryptocurrency; BTC, ETH, XRP, LTC, XMR, and DASH.

Appendix C

Mean-DCCA portfolio

C.1 Mean-DCCA portfolio with major financial assets

We investigate whether the fractal approach of MD analysis reflects the diversification effect among the major financial assets. For each pair of daily return series we calculate the cross-correlation levels at different scales defined by the DCCA coefficient (Fig. C.1). We confirm that coefficients tend to vary depending on scales. This means that the constructed portfolio shows different diversification effect under different time scales.

For the scale preference strategy in Eq. (7.2.4), we set $\alpha_i(s_j) = s_j / \sum_{s \in S} s$ for long-scale preference, and $\alpha_i(s_j) = s_{\#S+1-j} / \sum_{s \in S} s$ for short-scale preference associated with the subset $S = \{5, 10, 15, \ldots, 130\}$. For the balanced-scale type, the optimal weight is calculated by averaging all the scale-dependent weights. In our analysis, we use $\boldsymbol{Q} = \{2\}$ and past data length of 2 years to calculate optimal allocations.

Table C.1 presents the maximum drawdown performance of MV and MD portfolios based on the three strategy types, with a given annual return level of 2.5%. All three types of MD generally outperform the traditional MV, and better strategy of MD seems to vary by market period. For example, during the global financial crisis (2008-2009), the MD with short-term preference reduces drawdown the most, whereas after market recovery (2012-2013), the MD with long-term preference reduces the most. In a relatively unstable market condition, short-scale MD minimizes portfolio risk, where investors tend to focus more on the short-term in downside situations.

We also discuss the out-sample performance of the MD portfolio by backtesting. The optimal investment weighting (Eq. (7.2.4)) is calculated using the past 520 data (2 years) and managed for the next quarterly period. Allocations are

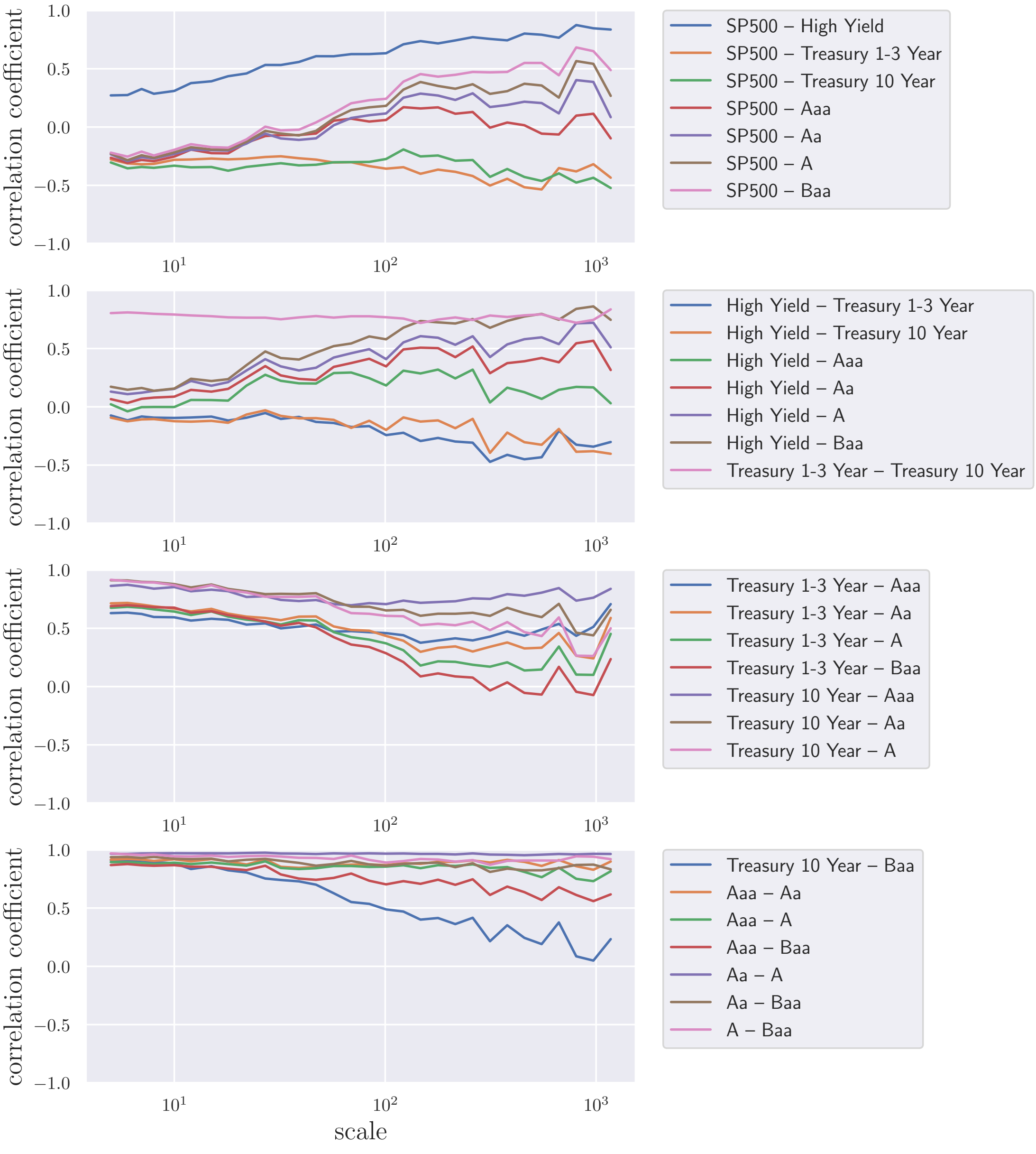

Figure C.1: Multi-scale cross-correlation coefficients of assets.

Table C.1: Maximum drawdown performance (%) of the portfolios under a required annual return level of 2.5%.

sample period	MV	MD-balanced	MD-short	MD-long
2004-2005	-2.227	-2.222	-2.229	**-2.215**
2006-2007	-0.584	-0.533	-0.542	**-0.524**
2008-2009	-1.919	-1.610	**-1.515**	-1.706
2010-2011	-0.662	-0.674	**-0.665**	-0.683
2012-2013	-1.417	-1.206	-1.238	**-1.174**
2014-2015	-1.913	-1.684	**-1.657**	-1.710
2016-2017	-0.606	**-0.518**	-0.540	-0.540
2018-2019	-0.508	-0.480	**-0.469**	-0.492
2020-2021	-2.557	-1.888	-1.990	**-1.786**

recalculated and rebalanced every quarter. We also implement a switching-MD portfolio by switching the scale preference types among the three MD strategies, relying on the level of past maximum drawdown. If the maximum drawdown of the balanced-scale MD over the past two years is worse than -1.5%, we select the short-scale strategy. Otherwise, we select the long-scale strategy. Figure C.2 shows the switch and maximum drawdown throughout the entire period. We confirm that the MD-switching strategy outperforms portfolio risk compared to MV and other types of MD (Figure C.3). The strategy reduces maximum drawdown, Value-at-Risk (VaR), and expected shortfall (ES) of the constructed portfolio and increases portfolio returns under the same level of required returns (Table C.2). Therefore, changing the scale preference of the MD portfolio in response to market conditions is effective for gaining more portfolio risk control not only in cryptocurrency markets but also in major financial assets.

Table C.2: Backtest performance (annual average) of portfolios.

	MV	MD			
		balanced	short	long	switching
max. drawdown (%)	-1.537	-1.303	-1.361	-1.255	**-1.240**
10-day 99%VaR (%)	-0.832	-0.725	-0.760	-0.696	**-0.694**
10-day 97.5%ES (%)	-0.809	-0.706	-0.737	-0.678	**-0.675**
120-day 99%VaR (%)	-0.864	-0.591	-0.678	-0.510	**-0.474**
120-day 97.5%ES (%)	-0.832	-0.570	-0.654	-0.490	**-0.455**
annual return (%)	2.440	2.441	2.416	2.466	**2.550**

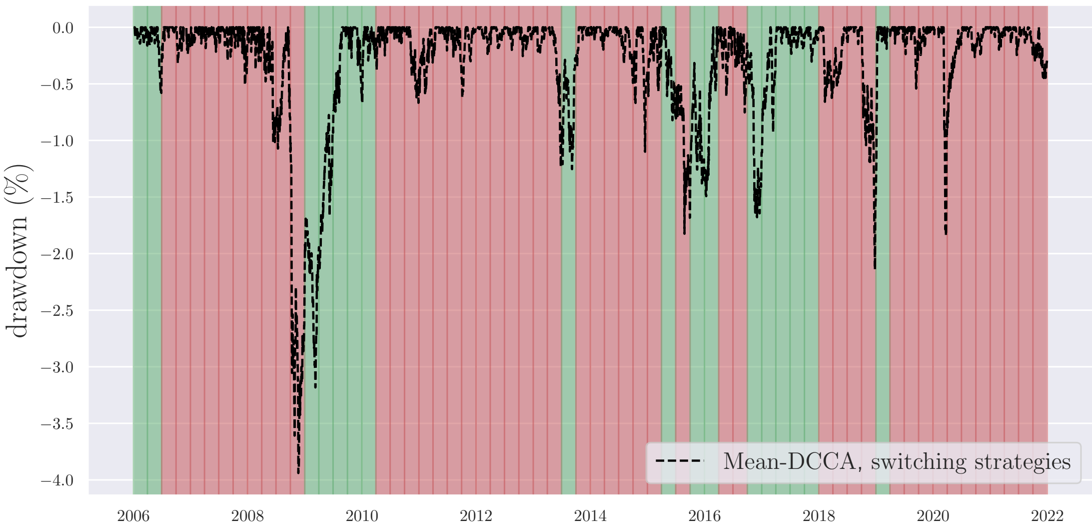

Figure C.2: Strategy switching and maximum drawdown throughout the period. The red (green) ranges represent long (short) scale preference.

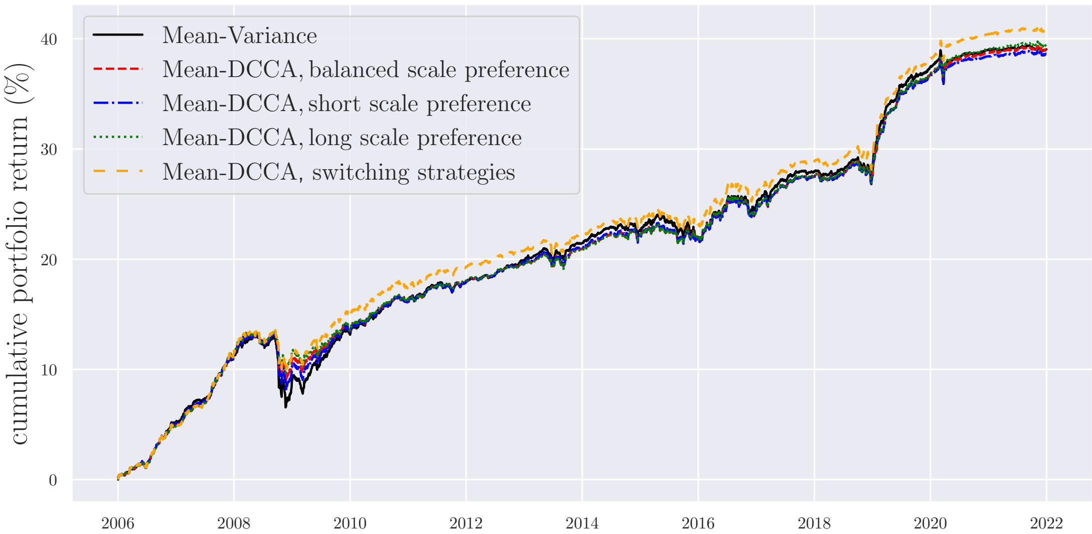

(a) Cumulative portfolio returns

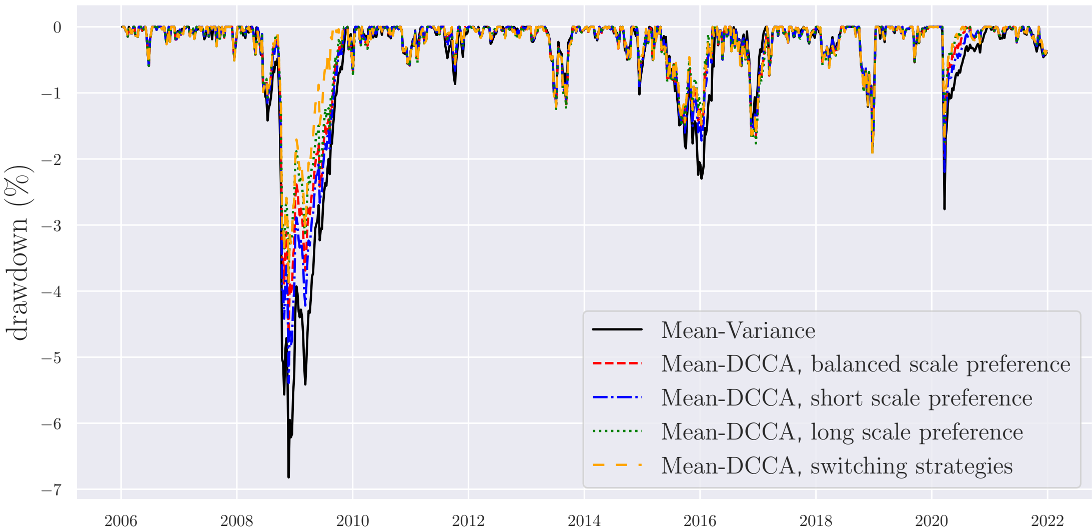

(b) Maximum drawdown

Figure C.3: Backtest results of the MV and MD portfolio with different types of scale preference strategies.

Bibliography

Ait-Sahalia, Y., Fan, J., Xiu, D., 2010. High-Frequency Covariance Estimates With Noisy and Asynchronous Financial Data. Journal of the American Statistical Association 105, 1504–1517. URL: https://doi.org/10.1198/jasa.2010.tm10163, doi:10.1198/jasa.2010.tm10163.

Akgiray, V., Lamoureux, C.G., 1989. Estimation of Stable-Law Parameters: A Comparative Study. Journal of Business & Economic Statistics 7, 85–93. URL: https://doi.org/10.1080/07350015.1989.10509716, doi:10.1080/07350015.1989.10509716.

Al-Yahyaee, K.H., Mensi, W., Yoon, S.M., 2018. Efficiency, multifractality, and the long-memory property of the Bitcoin market: A comparative analysis with stock, currency, and gold markets. Finance Research Letters 27, 228–234. URL: https://doi.org/10.1016/j.frl.2018.03.017, doi:10.1016/j.frl.2018.03.017.

Alaoui, M.E., Bouri, E., Roubaud, D., 2019. Bitcoin price–volume: A multifractal cross-correlation approach. Finance Research Letters 31. URL: https://doi.org/10.1016/j.frl.2018.12.011, doi:10.1016/j.frl.2018.12.011.

Alvarez-Ramirez, J., Rodriguez, E., Echeverria, J.C., 2009. A DFA approach for assessing asymmetric correlations. Physica A: Statistical Mechanics and its Applications 388, 2263–2270. URL: https://doi.org/10.1016/j.physa.2009.03.007, doi:10.1016/j.physa.2009.03.007.

Alvarez-Ramirez, J., Rodriguez, E., Ibarra-Valdez, C., 2018. Long-range correlations and asymmetry in the Bitcoin market. Physica A: Statistical Mechanics and its Applications 492, 948–955. URL: https://doi.org/10.1016/j.physa.2017.11.025, doi:10.1016/j.physa.2017.11.025.

Antoniou, A., Holmes, P., Priestley, R., 1998. The effects of stock index futures trading on stock index volatility: An analysis of the asymmetric response of volatility to news. The Journal of Futures Markets (1986-1998) 18, 151.

Arias-Calluari, K., Alonso-Marroquin, F., Harré, M.S., 2018. Closed-form solutions for the Lévy-stable distribution. Physical Review E 98. URL: https://doi.org/10.1103/physreve.98.012103, doi:10.1103/physreve.98.012103.

Arnol'd, V.I., Avez, A., 1968. Ergodic Problems of Classical Mechanics. New York: Benjamin .

Aslam, F., Aziz, S., Nguyen, D.K., Mughal, K.S., Khan, M., 2020. On the efficiency of foreign exchange markets in times of the COVID-19 pandemic. Technological Forecasting and Social Change 161, 120261. URL: https://doi.org/10.1016/j.techfore.2020.120261, doi:10.1016/j.techfore.2020.120261.

Avramov, D., Chordia, T., Goyal, A., 2006. The Impact of Trades on Daily Volatility. Review of Financial Studies 19, 1241–1277. URL: https://doi.org/10.1093/rfs/hhj027, doi:10.1093/rfs/hhj027.

Baker, S.R., Bloom, N., Davis, S.J., Kost, K., Sammon, M., Viratyosin, T., 2020. The Unprecedented Stock Market Reaction to COVID-19. The Review of Asset Pricing Studies 10, 742–758. URL: https://doi.org/10.1093/rapstu/raaa008, doi:10.1093/rapstu/raaa008.

Bandi, F.M., Russell, J.R., 2006. Separating microstructure noise from volatility. Journal of Financial Economics 79, 655–692. URL: https://doi.org/10.1016/j.jfineco.2005.01.005, doi:10.1016/j.jfineco.2005.01.005.

Bariviera, A.F., 2017. The inefficiency of Bitcoin revisited: A dynamic approach. Economics Letters 161, 1–4. URL: https://doi.org/10.1016/j.econlet.2017.09.013, doi:10.1016/j.econlet.2017.09.013.

Bariviera, A.F., Basgall, M.J., Hasperué, W., Naiouf, M., 2017. Some stylized facts of the Bitcoin market. Physica A: Statistical Mechanics and its Applications 484, 82–90. URL: https://doi.org/10.1016/j.physa.2017.04.159, doi:10.1016/j.physa.2017.04.159.

Barndorff-Nielsen, O.E., 2004. Power and Bipower Variation with Stochastic Volatility and Jumps. Journal of Financial Econometrics 2, 1–37. URL: https://doi.org/10.1093/jjfinec/nbh001, doi:10.1093/jjfinec/nbh001.

Barndorff-Nielsen, O.E., Shephard, N., 2002. Estimating quadratic variation using realized variance. Journal of Applied Econometrics 17, 457–477. URL: https://doi.org/10.1002/jae.691, doi:10.1002/jae.691.

Battiston, S., Farmer, J.D., Flache, A., Garlaschelli, D., Haldane, A.G., Heesterbeek, H., Hommes, C., Jaeger, C., May, R., Scheffer, M., 2016. Complexity theory and financial regulation. Science 351, 818–819. URL: https://doi.org/10.1126/science.aad0299, doi:10.1126/science.aad0299.

Baur, D.G., Dimpfl, T., 2018. Asymmetric volatility in cryptocurrencies. Economics Letters 173, 148–151. URL: https://doi.org/10.1016/j.econlet.2018.10.008, doi:10.1016/j.econlet.2018.10.008.

Begušić, S., Kostanjčar, Z., Stanley, H.E., Podobnik, B., 2018. Scaling properties of extreme price fluctuations in Bitcoin markets. Physica A: Statistical Mechanics and its Applications 510, 400–406. URL: https://doi.org/10.1016/j.physa.2018.06.131, doi:10.1016/j.physa.2018.06.131.

Bentes, S.R., 2018. Is stock market volatility asymmetric? A multi-period analysis for five countries. Physica A: Statistical Mechanics and its Applications 499, 258–265. URL: https://doi.org/10.1016/j.physa.2018.02.031, doi:10.1016/j.physa.2018.02.031.

Bibalan, M.H., Amindavar, H., Amirmazlaghani, M., 2017. Characteristic function based parameter estimation of skewed alpha-stable distribution: An analytical approach. Signal Processing 130, 323–336. URL: https://doi.org/10.1016/j.sigpro.2016.07.020, doi:10.1016/j.sigpro.2016.07.020.

Black, F., 1976. Studies of stock market volatility changes. 1976 Proceedings of the American Statistical Association Business and Economic Statistics Section .

Black, F., Scholes, M., 1973. The Pricing of Options and Corporate Liabilities. Journal of Political Economy 81, 637–654. URL: https://doi.org/10.1086/260062, doi:10.1086/260062.

Blau, B.M., 2017. Price dynamics and speculative trading in bitcoin. Research in International Business and Finance 41, 493–499. URL: https://doi.org/10.1016/j.ribaf.2017.05.010, doi:10.1016/j.ribaf.2017.05.010.

Böhme, R., Christin, N., Edelman, B., Moore, T., 2015. Bitcoin: Economics, Technology, and Governance. Journal of Economic Perspectives 29, 213–238. URL: https://doi.org/10.1257/.29.2.213, doi:10.1257/jep.29.2.213.

Bollerslev, T., Kretschmer, U., Pigorsch, C., Tauchen, G., 2009. A discrete-time model for daily S&P500 returns and realized variations: Jumps and leverage effects. Journal of Econometrics 150, 151–166. URL: https://doi.org/10.1016/j.jeconom.2008.12.001, doi:10.1016/j.jeconom.2008.12.001.

Bouoiyour, J., Selmi, R., et al., 2016. Bitcoin: A beginning of a new phase. Economics Bulletin 36, 1430–1440.

Bouri, E., Azzi, G., Dyhrberg, A.H., 2017a. On the return-volatility relationship in the Bitcoin market around the price crash of 2013. Economics 11. URL: https://doi.org/10.5018/economics-ejournal.ja.2017-2, doi:10.5018/economics-ejournal.ja.2017-2.

Bouri, E., Gil-Alana, L.A., Gupta, R., Roubaud, D., 2018. Modelling long memory volatility in the Bitcoin market: Evidence of persistence and structural breaks. International Journal of Finance & Economics 24, 412–426. URL: https://doi.org/10.1002/ijfe.1670, doi:10.1002/ijfe.1670.

Bouri, E., Molnár, P., Azzi, G., Roubaud, D., Hagfors, L.I., 2017b. On the hedge and safe haven properties of Bitcoin: Is it really more than a diversifier? Finance Research Letters 20, 192–198. URL: https://doi.org/10.1016/j.frl.2016.09.025, doi:10.1016/j.frl.2016.09.025.

Brent, R.P., 2013. Algorithms for Minimization without Derivatives. Courier Corporation .

Brorsen, B.W., Yang, S.R., 1990. Maximum Likelihood Estimates of Symmetric Stable Distribution Parameters. Communications in Statistics - Simulation and Computation 19, 1459–1464. URL: https://doi.org/10.1080/03610919008812928, doi:10.1080/03610919008812928.

Cajueiro, D.O., Tabak, B.M., 2009. Multifractality and herding behavior in the Japanese stock market. Chaos, Solitons & Fractals 40, 497–504. URL: https://doi.org/10.1016/j.chaos.2007.07.091, doi:10.1016/j.chaos.2007.07.091.

Campbell, J.Y., Hentschel, L., 1992. No news is good news: An asymmetric model of changing volatility in stock returns. Journal of Financial Economics 31, 281–318. URL: https://doi.org/10.1016/0304-405x(92)90037-x, doi:10.1016/0304-405x(92)90037-x.

Cao, G., Cao, J., Xu, L., 2013. Asymmetric multifractal scaling behavior in the Chinese stock market: Based on asymmetric MF-DFA. Physica A: Statistical Mechanics and its Applications 392, 797–807. URL: https://doi.org/10.1016/j.physa.2012.10.042, doi:10.1016/j.physa.2012.10.042.

Cao, G., Cao, J., Xu, L., He, L., 2014. Detrended cross-correlation analysis approach for assessing asymmetric multifractal detrended cross-correlations and their application to the Chinese financial market. Physica A: Statistical Mechanics and its Applications 393, 460–469. URL: https://doi.org/10.1016/j.physa.2013.08.074, doi:10.1016/j.physa.2013.08.074.

Cao, G., He, L.Y., Cao, J., et al., 2018. Multifractal detrended analysis method and its application in financial markets. Springer.

Cao, G., Xie, W., 2021. The impact of the shutdown policy on the asymmetric interdependence structure and risk transmission of cryptocurrency and China's financial market. The North American Journal of Economics and Finance 58, 101514. URL: https://doi.org/10.1016/j.najef.2021.101514, doi:10.1016/j.najef.2021.101514.

Chambers, J.M., Mallows, C.L., Stuck, B.W., 1976. A Method for Simulating Stable Random Variables. Journal of the American Statistical Association 71, 340–344. URL: https://doi.org/10.1080/01621459.1976.10480344, doi:10.1080/01621459.1976.10480344.

Chang, E.C., Cheng, J.W., Khorana, A., 2000. An examination of herd behavior in equity markets: An international perspective. Journal of Banking & Finance 24, 1651–1679. URL: https://doi.org/10.1016/s0378-4266(99)00096-5, doi:10.1016/s0378-4266(99)00096-5.

Cheah, E.T., Mishra, T., Parhi, M., Zhang, Z., 2018. Long Memory Interdependency and Inefficiency in Bitcoin Markets. Economics Letters 167, 18–25. URL: https://doi.org/10.1016/j.econlet.2018.02.010, doi:10.1016/j.econlet.2018.02.010.

Cheikh, N.B., Zaied, Y.B., Chevallier, J., 2020. Asymmetric volatility in cryptocurrency markets: New evidence from smooth transition GARCH models. Finance Research Letters 35, 101293. URL: https://doi.org/10.1016/j.frl.2019.09.008, doi:10.1016/j.frl.2019.09.008.

Chen, Y.F., Mu, X., 2021. Asymmetric volatility in commodity markets. Journal of Commodity Markets 22, 100139. URL: https://doi.org/10.1016/j.jcomm.2020.100139, doi:10.1016/j.jcomm.2020.100139.

Cheung, Y.W., Ng, L.K., 1992. Stock Price Dynamics and Firm Size: An Empirical investigation. The Journal of Finance 47, 1985–1997. URL: https://doi.org/10.1111/j.1540-6261.1992.tb04693.x, doi:10.1111/j.1540-6261.1992.tb04693.x.

Chiang, T.C., Zheng, D., 2010. An empirical analysis of herd behavior in global stock markets. Journal of Banking & Finance 34, 1911–1921.

URL: https://doi.org/10.1016/j.jbankfin.2009.12.014, doi:10.1016/j.jbankfin.2009.12.014.

Christie, A., 1982. The stochastic behavior of common stock variances value, leverage and interest rate effects. Journal of Financial Economics 10, 407–432. URL: https://doi.org/10.1016/0304-405x(82)90018-6, doi:10.1016/0304-405x(82)90018-6.

Chronis, G.A., 2016. Modelling the extreme variability of the US Consumer Price Index inflation with a stable non-symmetric distribution. Economic Modelling 59, 271–277. URL: https://doi.org/10.1016/j.econmod.2016.07.012, doi:10.1016/j.econmod.2016.07.012.

Chun, W., Li, H., Wu, X., 2020. PORTFOLIO MODEL UNDER FRACTAL MARKET BASED ON MEAN-DCCA. Fractals 28, 2050142. URL: https://doi.org/10.1142/s0218348x2050142x, doi:10.1142/s0218348x2050142x.

Clauset, A., Shalizi, C.R., Newman, M.E.J., 2009. Power-Law Distributions in Empirical Data. SIAM Review 51, 661–703. URL: https://doi.org/10.1137%2F070710111, doi:10.1137/070710111.

Conlon, T., Corbet, S., McGee, R.J., 2020. Are cryptocurrencies a safe haven for equity markets? An international perspective from the COVID-19 pandemic. Research in International Business and Finance 54, 101248. URL: https://doi.org/10.1016/j.ribaf.2020.101248, doi:10.1016/j.ribaf.2020.101248.

Crisanto-Neto, J.C., da Luz, M.G.E., Raposo, E.P., Viswanathan, G.M., 2018. An efficient series approximation for the Lévy α-stable symmetric distribution. Physics Letters A 382, 2408–2413. URL: https://doi.org/10.1016/j.physleta.2018.07.013, doi:10.1016/j.physleta.2018.07.013.

Dickey, D.A., Fuller, W.A., 1979. Distribution of the Estimators for Autoregressive Time Series with a Unit Root. Journal of the American Statistical Association 74, 427–431.

Diniz-Maganini, N., Diniz, E.H., Rasheed, A.A., 2021. Bitcoin's price efficiency and safe haven properties during the COVID-19 pandemic: A comparison. Research in International Business and Finance 58, 101472. URL: https://doi.org/10.1016/j.ribaf.2021.101472, doi:10.1016/j.ribaf.2021.101472.

Drożdż, S., Gębarowski, R., Minati, L., Oświęcimka, P., Watorek, M., 2018. Bitcoin market route to maturity? Evidence from return fluctuations, temporal correlations and multiscaling effects. Chaos: An Interdisciplinary Journal of

Nonlinear Science 28, 071101. URL: https://doi.org/10.1063/1.5036517, doi:10.1063/1.5036517.

Drożdż, S., Kwapień, J., Oświęcimka, P., Stanisz, T., Wątorek, M., 2020. Complexity in Economic and Social Systems: Cryptocurrency Market at around COVID-19. Entropy 22, 1043. URL: https://doi.org/10.3390/e22091043, doi:10.3390/e22091043.

Drożdż, S., Oświęcimka, P., 2015. Detecting and interpreting distortions in hierarchical organization of complex time series. Physical Review E 91. URL: https://doi.org/10.1103/physreve.91.030902, doi:10.1103/physreve.91.030902.

DuMouchel, W.H., 1973. On the Asymptotic Normality of the Maximum-Likelihood Estimate when Sampling from a Stable Distribution. The Annals of Statistics 1. URL: https://doi.org/10.1214/aos/1176342516, doi:10.1214/aos/1176342516.

Dyhrberg, A.H., 2016a. Bitcoin, gold and the dollar – A GARCH volatility analysis. Finance Research Letters 16, 85–92. URL: https://doi.org/10.1016/j.frl.2015.10.008, doi:10.1016/j.frl.2015.10.008.

Dyhrberg, A.H., 2016b. Hedging capabilities of bitcoin. Is it the virtual gold? Finance Research Letters 16, 139–144. URL: https://doi.org/10.1016/j.frl.2015.10.025, doi:10.1016/j.frl.2015.10.025.

Easley, D., Kiefer, N.M., O'hara, M., Paperman, J.B., 1996. Liquidity, information, and infrequently traded stocks. The Journal of Finance 51, 1405–1436. URL: https://doi.org/10.1111/j.1540-6261.1996.tb04074.x, doi:10.1111/j.1540-6261.1996.tb04074.x.

Economou, F., Kostakis, A., Philippas, N., 2011. Cross-country effects in herding behaviour: Evidence from four south European markets. Journal of International Financial Markets, Institutions and Money 21, 443–460. URL: https://doi.org/10.1016/j.intfin.2011.01.005, doi:10.1016/j.intfin.2011.01.005.

Evans, M.D.D., 1994. Expected Returns, Time-varying Risk, and Risk Premia. The Journal of Finance 49, 655–679. URL: https://doi.org/10.1111/j.1540-6261.1994.tb05156.x, doi:10.1111/j.1540-6261.1994.tb05156.x.

Fakhfekh, M., Hachicha, N., Jawadi, F., Selmi, N., Cheffou, A.I., 2016. Measuring volatility persistence for conventional and islamic banks: An FI-EGARCH approach. Emerging Markets Review 27, 84–99. URL: https://doi.org/10.1016/j.ememar.2016.03.004, doi:10.1016/j.ememar.2016.03.004.

Fakhfekh, M., Jeribi, A., 2020. Volatility dynamics of crypto-currencies' returns: Evidence from asymmetric and long memory GARCH models. Research in International Business and Finance 51, 101075. URL: https://doi.org/10.1016/j.ribaf.2019.101075, doi:10.1016/j.ribaf.2019.101075.

Fama, E.F., 1965. The behavior of stock-market prices. The Journal of Business 38, 34–105.

Fama, E.F., 1970. Efficient Capital Markets: A Review of Theory and Empirical Work. The Journal of Finance 25, 383. URL: https://doi.org/10.2307/2325486, doi:10.2307/2325486.

Fama, E.F., 1991. Efficient Capital Markets: II. The Journal of Finance 46, 1575–1617. URL: https://doi.org/10.1111/j.1540-6261.1991.tb04636.x, doi:10.1111/j.1540-6261.1991.tb04636.x.

Fama, E.F., Roll, R., 1971. Parameter estimates for symmetric stable distributions. Journal of the American Statistical Association 66(334), 331–338.

Fan, Q., Wang, F., 2020. Detrending-moving-average-based bivariate regression estimator. Physical Review E 102. URL: https://doi.org/10.1103/physreve.102.012218, doi:10.1103/physreve.102.012218.

Fernández-Martínez, M., Guirao, J.L.G., Sánchez-Granero, M.Á., Segovia, J.E.T., 2019. Fractal Dimension for Fractal Structures. Springer International Publishing. URL: https://doi.org/10.1007/978-3-030-16645-8, doi:10.1007/978-3-030-16645-8.

Ferson, W.E., Schadt, R.W., 1996. Measuring Fund Strategy and Performance in Changing Economic Conditions. The Journal of Finance 51, 425–461. URL: https://doi.org/10.1111/j.1540-6261.1996.tb02690.x, doi:10.1111/j.1540-6261.1996.tb02690.x.

Feuerverger, A., McDunnough, P., 1981. On some Fourier methods for inference. Journal of the American Statistical Association 76, 379–387.

Frezza, M., Bianchi, S., Pianese, A., 2021. Fractal analysis of market (in)efficiency during the COVID-19. Finance Research Letters 38, 101851. URL: https://doi.org/10.1016/j.frl.2020.101851, doi:10.1016/j.frl.2020.101851.

Gajardo, G., Kristjanpoller, W.D., Minutolo, M., 2018. Does Bitcoin exhibit the same asymmetric multifractal cross-correlations with crude oil, gold and DJIA as the Euro, Great British Pound and Yen? Chaos, Solitons & Fractals 109, 195–205. URL: https://doi.org/10.1016/j.chaos.2018.02.029, doi:10.1016/j.chaos.2018.02.029.

Garcia, R., Renault, E., Veredas, D., 2011. Estimation of stable distributions by indirect inference. Journal of Econometrics 161, 325–337. URL: https://doi.org/10.1016/j.jeconom.2010.12.007, doi:10.1016/j.jeconom.2010.12.007.

Ghazani, M.M., Khosravi, R., 2020. Multifractal detrended cross-correlation analysis on benchmark cryptocurrencies and crude oil prices. Physica A: Statistical Mechanics and its Applications 560, 125172. URL: https://doi.org/10.1016/j.physa.2020.125172, doi:10.1016/j.physa.2020.125172.

Glosten, L.R., Jagannathan, R., Runkle, D.E., 1993. On the Relation between the Expected Value and the Volatility of the Nominal Excess Return on Stocks. The Journal of Finance 48, 1779–1801. URL: https://doi.org/10.1111/j.1540-6261.1993.tb05128.x, doi:10.1111/j.1540-6261.1993.tb05128.x.

Glosten, L.R., Milgrom, P.R., 1985. Bid, ask and transaction prices in a specialist market with heterogeneously informed traders. Journal of Financial Economics 14, 71–100. URL: https://doi.org/10.1016/0304-405x(85)90044-3, doi:10.1016/0304-405x(85)90044-3.

Gnedenko, B.V., Kolmogorov, A.N., 1954. Limit distributions for sums of independent random variables. Addison-Wesley Mathematics Series .

Gopikrishnan, P., Plerou, V., Amaral, L.A.N., Meyer, M., Stanley, H.E., 1999. Scaling of the distribution of fluctuations of financial market indices. Physical Review E 60, 5305–5316. URL: https://doi.org/10.1103/physreve.60.5305, doi:10.1103/physreve.60.5305.

Grabchak, M., Samorodnitsky, G., 2010. Do financial returns have finite or infinite variance? A paradox and an explanation. Quantitative Finance 10, 883–893. URL: https://doi.org/10.1080/14697680903540381, doi:10.1080/14697680903540381.

Groshen, E.L., 2020. COVID-19's impact on the u.s. labor market as of September 2020. Business Economics 55, 213–228. URL: https://doi.org/10.1057/s11369-020-00193-1, doi:10.1057/s11369-020-00193-1.

Hasanhodzic, J., Lo, A.W., 2019. On black's leverage effect in firms with no leverage. The Journal of Portfolio Management 46, 106–122. URL: https://doi.org/10.3905/jpm.2019.46.1.106, doi:10.3905/jpm.2019.46.1.106.

He, L.Y., Chen, S.P., 2011. A new approach to quantify power-law cross-correlation and its application to commodity markets. Physica A: Statistical Mechanics and its Applications 390, 3806–3814. URL: https://doi.org/10.1016/j.physa.2011.06.013, doi:10.1016/j.physa.2011.06.013.

Heathcote, C.R., 1977. The integrated squared error estimation of parameters. Biometrika 64, 255–264. URL: https://doi.org/10.1093/biomet/64.2.255, doi:10.1093/biomet/64.2.255.

Hens, T., Steude, S.C., 2009. The leverage effect without leverage. Finance Research Letters 6, 83–94. URL: https://doi.org/10.1016/j.frl.2009.01.002, doi:10.1016/j.frl.2009.01.002.

Hill, B.M., 1975. A simple general approach to inference about the tail of a distribution. The annals of statistics , 1163–1174.

Hsu, D.A., Miller, R.B., Wichern, D.W., 1974. On the Stable Paretian Behavior of Stock-Market Prices. Journal of the American Statistical Association 69, 108–113. URL: https://doi.org/10.1080/01621459.1974.10480135, doi:10.1080/01621459.1974.10480135.

Hurst, H.E., 1957. A Suggested Statistical Model of some Time Series which occur in Nature. Nature 180, 494–494. URL: https://doi.org/10.1038/180494a0, doi:10.1038/180494a0.

Jeribi, A., Fakhfekh, M., Jarboui, A., 2015. Tunisian revolution and stock market volatility: evidence from FIEGARCH model. Managerial Finance 41, 1112–1135. URL: https://doi.org/10.1108/mf-12-2014-0310, doi:10.1108/mf-12-2014-0310.

Ji, Q., Zhang, D., Zhao, Y., 2020. Searching for safe-haven assets during the COVID-19 pandemic. International Review of Financial Analysis 71, 101526. URL: https://doi.org/10.1016/j.irfa.2020.101526, doi:10.1016/j.irfa.2020.101526.

Jiang, Y., Nie, H., Ruan, W., 2018. Time-varying long-term memory in Bitcoin market. Finance Research Letters 25, 280–284. URL: https://doi.org/10.1016/j.frl.2017.12.009, doi:10.1016/j.frl.2017.12.009.

Jiang, Z.Q., Zhou, W.X., 2011. Multifractal detrending moving-average cross-correlation analysis. Physical Review E 84. URL: https://doi.org/10.1103/physreve.84.016106, doi:10.1103/physreve.84.016106.

Jovanovic, F., Schinckus, C., 2016. Breaking down the barriers between econophysics and financial economics. International Review of Financial Analysis 47, 256–266. URL: https://doi.org/10.1016/j.irfa.2016.03.001, doi:10.1016/j.irfa.2016.03.001.

Kakinaka, S., Umeno, K., 2020a. Characterizing Cryptocurrency Market with Lévy's Stable Distributions. Journal of the Physical Society of Japan 89, 024802. URL: https://doi.org/10.7566/jpsj.89.024802, doi:10.7566/jpsj.89.024802.

Kakinaka, S., Umeno, K., 2020b. Flexible two-point selection approach for characteristic function-based parameter estimation of stable laws. Chaos: An Interdisciplinary Journal of Nonlinear Science 30, 073128. URL: https://doi.org/10.1063/5.0013148, doi:10.1063/5.0013148.

Kakinaka, S., Umeno, K., 2021. Exploring asymmetric multifractal cross-correlations of price–volatility and asymmetric volatility dynamics in cryptocurrency markets. Physica A: Statistical Mechanics and its Applications 581, 126237. URL: https://doi.org/10.1016/j.physa.2021.126237, doi:10.1016/j.physa.2021.126237.

Kantelhardt, J.W., Zschiegner, S.A., Koscielny-Bunde, E., Havlin, S., Bunde, A., Stanley, H., 2002. Multifractal detrended fluctuation analysis of nonstationary time series. Physica A: Statistical Mechanics and its Applications 316, 87–114. URL: https://doi.org/10.1016/s0378-4371(02)01383-3, doi:10.1016/s0378-4371(02)01383-3.

Kateregga, M., Mataramvura, S., Taylor, D., 2017. Parameter estimation for stable distributions with application to commodity futures log-returns. Cogent Economics & Finance 5, 1318813. URL: https://doi.org/10.1080/23322039.2017.1318813, doi:10.1080/23322039.2017.1318813.

Katsiampa, P., 2017. Volatility estimation for Bitcoin: A comparison of GARCH models. Economics Letters 158, 3–6. URL: https://doi.org/10.1016/j.econlet.2017.06.023, doi:10.1016/j.econlet.2017.06.023.

Kliber, A., 2016. The leverage effect puzzle: the case of european sovereign credit default swap market. Review of Derivatives Research 19, 217–235. URL: https://doi.org/10.1007/s11147-016-9121-3, doi:10.1007/s11147-016-9121-3.

Koblents, E., Míguez, J., Rodríguez, M.A., Schmidt, A.M., 2016. A nonlinear population Monte Carlo scheme for the Bayesian estimation of parameters of α-stable distributions. Computational Statistics & Data Analysis 95, 57–74. URL: https://doi.org/10.1016/j.csda.2015.09.007, doi:10.1016/j.csda.2015.09.007.

Kogon, S.M., Williams, D.B., 1998. Characteristic function based estimation of stable distribution parameters. A practical guide to heavy tails: statistical techniques and applications , 311–338.

Koponen, I., 1995. Analytic approach to the problem of convergence of truncated Lévy flights towards the Gaussian stochastic process. Physical Review E 52, 1197–1199. URL: https://doi.org/10.1103/physreve.52.1197, doi:10.1103/physreve.52.1197.

Koutrouvelis, I.A., 1980. Regression-type estimation of the parameters of stable laws. Journal of the American Statistical Association 75(372), 918–928.

Krężolek, D., 2012. Non-Classical Measures of Investment Risk on the Market of Precious Non-Ferrous Metals Using the Methodology of Stable Distributions. Dynamic Econometric Models 12. URL: https://doi.org/10.12775/dem.2012.006, doi:10.12775/dem.2012.006.

Kristjanpoller, W., Bouri, E., 2019. Asymmetric multifractal cross-correlations between the main world currencies and the main cryptocurrencies. Physica A: Statistical Mechanics and its Applications 523, 1057–1071. URL: https://doi.org/10.1016/j.physa.2019.04.115, doi:10.1016/j.physa.2019.04.115.

Kristjanpoller, W., Bouri, E., Takaishi, T., 2020. Cryptocurrencies and equity funds: Evidence from an asymmetric multifractal analysis. Physica A: Statistical Mechanics and its Applications 545, 123711. URL: https://doi.org/10.1016/j.physa.2019.123711, doi:10.1016/j.physa.2019.123711.

Kristoufek, L., 2013. Mixed-correlated ARFIMA processes for power-law cross-correlations. Physica A: Statistical Mechanics and its Applications 392, 6484–6493. URL: https://doi.org/10.1016/j.physa.2013.08.041, doi:10.1016/j.physa.2013.08.041.

Kristoufek, L., 2015a. Can the bivariate hurst exponent be higher than an average of the separate Hurst exponents? Physica A: Statistical Mechanics and its Applications 431, 124–127. URL: https://doi.org/10.1016/j.physa.2015.02.086, doi:10.1016/j.physa.2015.02.086.

Kristoufek, L., 2015b. Detrended fluctuation analysis as a regression framework: Estimating dependence at different scales. Physical Review E 91. URL: https://doi.org/10.1103/physreve.91.022802, doi:10.1103/physreve.91.022802.

Kristoufek, L., 2018. Fractality in market risk structure: Dow Jones Industrial components case. Chaos, Solitons & Fractals 110, 69–75. URL: https://doi.org/10.1016/j.chaos.2018.02.028, doi:10.1016/j.chaos.2018.02.028.

Kristoufek, L., 2020. Power-Law Cross-Correlations: Issues, Solutions and Future Challenges, in: Simplicity of Complexity in Economic and Social Systems. Springer International Publishing, pp. 43–54. URL: https://doi.org/10.1007/978-3-030-56160-4_3, doi:10.1007/978-3-030-56160-4_3.

Kristoufek, L., Ferreira, P., 2018. Capital asset pricing model in Portugal: Evidence from fractal regressions. Portuguese Economic Journal 17, 173–183. URL: https://doi.org/10.1007/s10258-018-0145-5, doi:10.1007/s10258-018-0145-5.

Krutto, A., 2016. Parameter Estimation in Stable law. Risks 4, 43. URL: https://doi.org/10.3390/risks4040043, doi:10.3390/risks4040043.

Krutto, A., 2019. Empirical cumulant function based parameter estimation in stable laws. Acta et Commentationes Universitatis Tartuensis de Mathematica 22, 311–338. URL: https://doi.org/10.12697/acutm.2018.22.26, doi:10.12697/acutm.2018.22.26.

Kuruoglu, E.E., 2001. Density parameter estimation of skewed α-stable distributions. IEEE Transactions on Signal Processing 49, 2192–2201. URL: https://doi.org/10.1109/78.950775, doi:10.1109/78.950775.

Kwapień, J., Oświecimka, P., Drożdż, S., 2015. Detrended fluctuation analysis made flexible to detect range of cross-correlated fluctuations. Physical Review E 92. URL: https://doi.org/10.1103/physreve.92.052815, doi:10.1103/physreve.92.052815.

Kwiatkowski, D., Phillips, P.C., Schmidt, P., Shin, Y., 1992. Testing the null hypothesis of stationarity against the alternative of a unit root. Journal of Econometrics 54, 159–178. URL: https://doi.org/10.1016/0304-4076(92)90104-y, doi:10.1016/0304-4076(92)90104-y.

Lee, M., Song, J.W., Park, J.H., Chang, W., 2017. Asymmetric multi-fractality in the U.S. stock indices using index-based model of A-MFDFA. Chaos, Solitons &

Fractals 97, 28–38. URL: https://doi.org/10.1016/j.chaos.2017.02.001, doi:10.1016/j.chaos.2017.02.001.

Lera, S.C., Sornette, D., 2018. Gross domestic product growth rates as confined Lévy flights: Towards a unifying theory of economic growth rate fluctuations. Physical Review E 97. URL: https://doi.org/10.1103/physreve.97.012150, doi:10.1103/physreve.97.012150.

Lévy, P., 1937. Theéorie de l'addition des variables aléatoires. Paris: Gauthier-Villars .

Liu, J., Chen, F., 2018. Asymmetric volatility varies in different dry bulk freight rate markets under structure breaks. Physica A: Statistical Mechanics and its Applications 505, 316–327. URL: https://doi.org/10.1016/j.physa.2018.02.165, doi:10.1016/j.physa.2018.02.165.

Liu, L.Y., Patton, A.J., Sheppard, K., 2015. Does anything beat 5-minute RV? A comparison of realized measures across multiple asset classes. Journal of Econometrics 187, 293–311. URL: https://doi.org/10.1016/j.jeconom.2015.02.008, doi:10.1016/j.jeconom.2015.02.008.

Liu, Y., Ye, Y., Wang, Q., Liu, X., 2018. Stability Prediction Model of Roadway Surrounding Rock Based on Concept Lattice Reduction and a Symmetric Alpha Stable Distribution Probability Neural Network. Applied Sciences 8, 2164. URL: https://doi.org/10.3390/app8112164, doi:10.3390/app8112164.

Lo, S., Wang, J.C., 2014. Bitcoin as money? Current policy perspectives. Federal Reserve Bank of Boston .

Ma, X., Nikias, C.L., 1995. Parameter estimation and blind channel identification in impulsive signal environments. IEEE Transactions on Signal Processing 43, 2884–2897. URL: https://doi.org/10.1109/78.476432, doi:10.1109/78.476432.

Mandelbrot, B.B., 1963. The variation of certain speculative prices. The Journal of Business , 394–419.

Mandelbrot, B.B., 1997. Three fractal models in finance: Discontinuity, concentration, risk. ECONOMIC NOTES-SIENA- , 171–212.

Mandelbrot, B.B., Hudson, R.L., 2005. The (mis) behavior of markets: a fractal view of risk, ruin, and reward. Basic Books New York.

Mantegna, R.N., Stanley, H.E., 1994. Stochastic Process with Ultraslow Convergence to a Gaussian: The Truncated Lévy Flight. Physical Review Letters 73, 2946–2949. URL: https://doi.org/10.1103/physrevlett.73.2946, doi:10.1103/physrevlett.73.2946.

Mantegna, R.N., Stanley, H.E., 1995. Scaling behaviour in the dynamics of an economic index. Nature 376, 46–49. URL: https://doi.org/10.1038/376046a0, doi:10.1038/376046a0.

Markowitz, H., 1952. Portfolio Selection. The Journal of Finance 7, 77. URL: https://doi.org/10.2307/2975974, doi:10.2307/2975974.

Matsui, M., Takemura, A., 2007. Goodness-of-fit tests for symmetric stable distributions—empirical characteristic function approach. TEST 17, 546–566. URL: https://doi.org/10.1007/s11749-007-0045-y, doi:10.1007/s11749-007-0045-y.

McCulloch, J.H., 1986. Simple consistent estimators of stable distribution parameters. Communications in Statistics-Simulation and Computation 15(4), 1109–1136.

Menabde, M., Sivapalan, M., 2000. Modeling of rainfall time series and extremes using bounded random cascades and levy-stable distributions. Water Resources Research 36, 3293–3300. URL: https://doi.org/10.1029/2000WR900197, doi:10.1029/2000WR900197.

Meneveau, C., Sreenivasan, K.R., 1987. Simple multifractal cascade model for fully developed turbulence. Physical Review Letters 59, 1424–1427. URL: https://doi.org/10.1103/physrevlett.59.1424, doi:10.1103/physrevlett.59.1424.

Mensi, W., Al-Yahyaee, K.H., Kang, S.H., 2019a. Structural breaks and double long memory of cryptocurrency prices: A comparative analysis from Bitcoin and Ethereum. Finance Research Letters 29, 222–230. URL: https://doi.org/10.1016/j.frl.2018.07.011, doi:10.1016/j.frl.2018.07.011.

Mensi, W., Lee, Y.J., Al-Yahyaee, K.H., Sensoy, A., Yoon, S.M., 2019b. Intraday downward/upward multifractality and long memory in Bitcoin and Ethereum markets: An asymmetric multifractal detrended fluctuation analysis. Finance Research Letters 31, 19–25. URL: https://doi.org/10.1016/j.frl.2019.03.029, doi:10.1016/j.frl.2019.03.029.

Mensi, W., Tiwari, A.K., Yoon, S.M., 2017. Global financial crisis and weak-form efficiency of Islamic sectoral stock markets: An MF-DFA analysis. Physica A:

Statistical Mechanics and its Applications 471, 135–146. URL: https://doi.org/10.1016/j.physa.2016.12.034, doi:10.1016/j.physa.2016.12.034.

Mittnik, S., Rachev, S.T., Doganoglu, T., Chenyao, D., 1999. Maximum likelihood estimation of stable Paretian models. Mathematical and Computer Modelling 29, 275–293. URL: https://doi.org/10.1016/s0895-7177(99)00110-7, doi:10.1016/s0895-7177(99)00110-7.

Mnif, E., Jarboui, A., Mouakhar, K., 2020. How the cryptocurrency market has performed during COVID 19? A multifractal analysis. Finance Research Letters 36, 101647. URL: https://doi.org/10.1016/j.frl.2020.101647, doi:10.1016/j.frl.2020.101647.

Naeem, M.A., Bouri, E., Peng, Z., Shahzad, S.J.H., Vo, X.V., 2021. Asymmetric efficiency of cryptocurrencies during COVID19. Physica A: Statistical Mechanics and its Applications 565, 125562. URL: https://doi.org/10.1016/j.physa.2020.125562, doi:10.1016/j.physa.2020.125562.

Nakamoto, S., 2008. Bitcoin: A peer-to-peer electronic cash system. Decentralized Business Review , 21260.

Nelson, D.B., 1991. Conditional Heteroskedasticity in Asset Returns: A New Approach. Econometrica 59, 347. URL: https://doi.org/10.2307/2938260, doi:10.2307/2938260.

Nicolas, J.M., Anfinsen, S.N., 2001. Introduction to second kind statistics: Application of log-moments and log-cumulants to the analysis of radar image distributions. Traitement du Signal 19, 139–167.

Nikias, C.L., Shao, M., 1995. Signal processing with alpha-stable distributions and applications. Wiley-Interscience .

Nolan, J.P., 1997. Numerical calculation of stable densities and distribution functions. Communications in Statistics. Stochastic Models 13, 759–774. URL: https://doi.org/10.1080/15326349708807450, doi:10.1080/15326349708807450.

Nolan, J.P., 2001. Maximum Likelihood Estimation and Diagnostics for Stable Distributions, in: Lévy Processes. Birkhäuser Boston, pp. 379–400. URL: https://doi.org/10.1007/978-1-4612-0197-7_17, doi:10.1007/978-1-4612-0197-7_17.

Nolan, J.P., 2003. Stable distributions - models for heavy-tailed data. New York: Birkhauser .

Oświeçimka, P., Drożdż, S., Forczek, M., Jadach, S., Kwapień, J., 2014. Detrended cross-correlation analysis consistently extended to multifractality. Physical Review E 89. URL: https://doi.org/10.1103/physreve.89.023305, doi:10.1103/physreve.89.023305.

Pastor, G., Mora-Jimenez, I., Caamano, A., Jantti, R., 2016. Asymptotic Expansions for Heavy-tailed Data. IEEE Signal Processing Letters 23(4), 444–448. URL: https://doi.org/10.1109/lsp.2016.2526625, doi:10.1109/lsp.2016.2526625.

Paulson, A.S., Holcomb, E.W., Leitch, R.A., 1975. The estimation of the parameters of the stable laws. Biometrika 62, 163–170.

Peng, C.K., Buldyrev, S.V., Havlin, S., Simons, M., Stanley, H.E., Goldberger, A.L., 1994. Mosaic organization of DNA nucleotides. Physical Review E 49, 1685–1689. URL: https://doi.org/10.1103/physreve.49.1685, doi:10.1103/physreve.49.1685.

Peters, E.E., 1994. Fractal market analysis: applying chaos theory to investment and economics. volume 24. John Wiley & Sons.

Plerou, V., Stanley, H.E., 2008. Stock return distributions: Tests of scaling and universality from three distinct stock markets. Physical Review E 77. URL: https://doi.org/10.1103/physreve.77.037101, doi:10.1103/physreve.77.037101.

Podobnik, B., Grosse, I., Horvatić, D., Ilic, S., Ivanov, P.C., Stanley, H.E., 2009. Quantifying cross-correlations using local and global detrending approaches. The European Physical Journal B 71, 243–250.

Podobnik, B., Jiang, Z.Q., Zhou, W.X., Stanley, H.E., 2011. Statistical tests for power-law cross-correlated processes. Physical Review E 84. URL: https://doi.org/10.1103/physreve.84.066118, doi:10.1103/physreve.84.066118.

Podobnik, B., Stanley, H.E., 2008. Detrended Cross-Correlation Analysis: A New Method for Analyzing Two Nonstationary Time Series. Physical Review Letters 100. URL: https://doi.org/10.1103/physrevlett.100.084102, doi:10.1103/physrevlett.100.084102.

Polasik, M., Piotrowska, A.I., Wisniewski, T.P., Kotkowski, R., Lightfoot, G., 2015. Price Fluctuations and the Use of Bitcoin: An Empirical Inquiry. International Journal of Electronic Commerce 20, 9–49. URL: https://doi.org/10.1080/10864415.2016.1061413, doi:10.1080/10864415.2016.1061413.

Press, S.J., 1972. Estimation in univariate and multivariate stable distributions. Journal of the American Statistical Association 67(340), 842–846.

Rocha, É.C., da Luz, M.G.E., Raposo, E.P., Viswanathan, G.M., 2019. Why Lévy α-stable distributions lack general closed-form expressions for arbitrary α. Physical Review E 100. URL: https://doi.org/10.1103/physreve.100.010103, doi:10.1103/physreve.100.010103.

S. Borak, W. Härdle, R.W., 2005. Stable distributions. Statistical Tools for Finance and Insurance , 21–44.

Samorodnitsky, G., Taqqu, M., 1994a. Non-Gaussian Stable Processes: Stochastic Models with Infinite Variance. Chapman ft Hall, London .

Samorodnitsky, G., Taqqu, M.S., 1994b. Stable Non-Gaussian Random Processes: Stochastic Models with Infinite Variance. Chapman ft Hall, New York .

Scalas, E., Kim, K., 2007. The art of fitting financial time series with Levy stable distributions. Journal of the Korean Physical Society 50, 105–111.

Schwert, G.W., 1989. Why Does Stock Market Volatility Change Over Time? The Journal of Finance 44, 1115–1153. URL: https://doi.org/10.1111/j.1540-6261.1989.tb02647.x, doi:10.1111/j.1540-6261.1989.tb02647.x.

Sela, R.J., Hurvich, C.M., 2012. The averaged periodogram estimator for a power law in coherency. Journal of Time Series Analysis 33, 340–363. URL: https://doi.org/10.1111/j.1467-9892.2011.00770.x, doi:10.1111/j.1467-9892.2011.00770.x.

Shintani, M., Umeno, K., 2018. Super Generalized Central Limit Theorem —Limit Distributions for Sums of Non-identical Random Variables with Power Laws—. Journal of the Physical Society of Japan 87, 043003. URL: https://doi.org/10.7566/jpsj.87.043003, doi:10.7566/jpsj.87.043003.

Shrestha, K., 2019. Multifractal Detrended Fluctuation Analysis of Return on Bitcoin. International Review of Finance 21, 312–323. URL: https://doi.org/10.1111/irfi.12256, doi:10.1111/irfi.12256.

da Silva Filho, A.C., Maganini, N.D., de Almeida, E.F., 2018. Multifractal analysis of Bitcoin market. Physica A: Statistical Mechanics and its Applications 512, 954–967. URL: https://doi.org/10.1016/j.physa.2018.08.076, doi:10.1016/j.physa.2018.08.076.

Solnik, B., Boucrelle, C., Fur, Y.L., 1996. International Market Correlation and Volatility. Financial Analysts Journal 52, 17–34. URL: https://doi.org/10.2469/faj.v52.n5.2021, doi:10.2469/faj.v52.n5.2021.

Soros, G., 2015. The alchemy of finance. John Wiley & Sons.

Stavroyiannis, S., Babalos, V., 2019. Herding behavior in cryptocurrencies revisited: Novel evidence from a TVP model. Journal of Behavioral and Experimental Finance 22, 57–63. URL: https://doi.org/10.1016/j.jbef.2019.02.007, doi:10.1016/j.jbef.2019.02.007.

Stavroyiannis, S., Babalos, V., Bekiros, S., Lahmiri, S., Uddin, G.S., 2019. The high frequency multifractal properties of Bitcoin. Physica A: Statistical Mechanics and its Applications 520, 62–71. URL: https://doi.org/10.1016/j.physa.2018.12.037, doi:10.1016/j.physa.2018.12.037.

Takaishi, T., 2018. Statistical properties and multifractality of Bitcoin. Physica A: Statistical Mechanics and its Applications 506, 507–519. URL: https://doi.org/10.1016/j.physa.2018.04.046, doi:10.1016/j.physa.2018.04.046.

Takaishi, T., 2021. Time-varying properties of asymmetric volatility and multifractality in Bitcoin. PlOS ONE 16, e0246209. URL: https://doi.org/10.1371/journal.pone.0246209, doi:10.1371/journal.pone.0246209.

Tan, L., Chiang, T.C., Mason, J.R., Nelling, E., 2008. Herding behavior in Chinese stock markets: An examination of A and B shares. Pacific-Basin Finance Journal 16, 61–77. URL: https://doi.org/10.1016/j.pacfin.2007.04.004, doi:10.1016/j.pacfin.2007.04.004.

Telli, Ş., Chen, H., 2020. Multifractal behavior in return and volatility series of Bitcoin and gold in comparison. Chaos, Solitons & Fractals 139, 109994. URL: https://doi.org/10.1016/j.chaos.2020.109994, doi:10.1016/j.chaos.2020.109994.

Thompson, J.R., Wilson, J.R., 2016. Multifractal detrended fluctuation analysis: Practical applications to financial time series. Mathematics and Computers in Simulation 126, 63–88. URL: https://doi.org/10.1016/j.matcom.2016.03.003, doi:10.1016/j.matcom.2016.03.003.

Tilfani, O., Ferreira, P., Boukfaoui, M.Y.E., 2019. Building multi-scale portfolios and efficient market frontiers using fractal regressions. Physica A: Statistical Mechanics and its Applications 532, 121758. URL: https://doi.org/10.1016/j.physa.2019.121758, doi:10.1016/j.physa.2019.121758.

Tilfani, O., Ferreira, P., Boukfaoui, M.Y.E., 2020. Multiscale optimal portfolios using CAPM fractal regression: estimation for emerging stock markets. Post-Communist Economies 32, 77–112. URL: https://doi.org/10.1080/14631377.2019.1640983, doi:10.1080/14631377.2019.1640983.

Tilfani, O., Kristoufek, L., Ferreira, P., Boukfaoui, M.Y.E., 2022. Heterogeneity in economic relationships: Scale dependence through the multivariate fractal regression. Physica A: Statistical Mechanics and its Applications 588, 126530. URL: https://doi.org/10.1016/j.physa.2021.126530, doi:10.1016/j.physa.2021.126530.

Tiwari, A.K., Albulescu, C.T., Yoon, S.M., 2017. A multifractal detrended fluctuation analysis of financial market efficiency: Comparison using Dow Jones sector ETF indices. Physica A 483, 182–192.

Tiwari, A.K., Jana, R., Das, D., Roubaud, D., 2018. Informational efficiency of Bitcoin— An extension. Economics Letters 163, 106–109. URL: https://doi.org/10.1016/j.econlet.2017.12.006, doi:10.1016/j.econlet.2017.12.006.

Topcu, M., Gulal, O.S., 2020. The impact of COVID-19 on emerging stock markets. Finance Research Letters 36, 101691. URL: https://doi.org/10.1016/j.frl.2020.101691, doi:10.1016/j.frl.2020.101691.

Tversky, A., Kahneman, D., 1992. Advances in prospect theory: Cumulative representation of uncertainty. Journal of Risk and Uncertainty 5, 297–323. URL: https://doi.org/10.1007/bf00122574, doi:10.1007/bf00122574.

Umeno, K., 1998. Superposition of chaotic processes with convergence to Lévy's stable law. Physical Review E 58, 2644–2647. URL: https://doi.org/10.1103/physreve.58.2644, doi:10.1103/physreve.58.2644.

Urquhart, A., 2016. The inefficiency of Bitcoin. Economics Letters 148, 80–82. URL: https://doi.org/10.1016/j.econlet.2016.09.019, doi:10.1016/j.econlet.2016.09.019.

del Val, J.R., Simmross-Wattenberg, F., Alberola-López, C., 2017. Libstable: Fast, Parallel and High-Precision Computation of α-Stable Distributions in C/C++ and MATLAB. Journal of Statistical Software 78. URL: https://doi.org/10.18637/jss.v078.i01, doi:10.18637/jss.v078.i01.

Vidal-Tomás, D., Ibañez, A., 2018. Semi-strong efficiency of Bitcoin. Finance Research Letters 27, 259–265. URL: https://doi.org/10.1016/j.frl.2018.03.013, doi:10.1016/j.frl.2018.03.013.

Wang, F., Wang, L., Chen, Y., 2018. A DFA-based bivariate regression model for estimating the dependence of PM2.5 among neighbouring cities. Scientific Reports 8. URL: https://doi.org/10.1038/s41598-018-25822-w, doi:10.1038/s41598-018-25822-w.

Wang, J., Wang, X., 2021. COVID-19 and financial market efficiency: Evidence from an entropy-based analysis. Finance Research Letters , 101888URL: https://doi.org/10.1016/j.frl.2020.101888, doi:10.1016/j.frl.2020.101888.

Wang, X., Li, K., Gao, P., Meng, S., 2015. Research on Parameter Estimation Methods for Alpha Stable Noise in a Laser Gyroscope's Random Error. Sensors 15, 18550–18564. URL: https://doi.org/10.3390/s150818550, doi:10.3390/s150818550.

Wang, Y., Liu, L., Gu, R., 2009. Analysis of efficiency for Shenzhen stock market based on multifractal detrended fluctuation analysis. International Review of Financial Analysis 18, 271–276. URL: https://doi.org/10.1016/j.irfa.2009.09.005, doi:10.1016/j.irfa.2009.09.005.

Wątorek, M., Drożdż, S., Kwapień, J., Minati, L., Oświęcimka, P., Stanuszek, M., 2021. Multiscale characteristics of the emerging global cryptocurrency market. Physics Reports 901, 1–82. URL: https://doi.org/10.1016/j.physrep.2020.10.005, doi:10.1016/j.physrep.2020.10.005.

Weron, A., Weron, R., 2000. Fractal market hypothesis and two power-laws. Chaos, Solitons & Fractals 11, 289–296. URL: https://doi.org/10.1016/s0960-0779(98)00295-1, doi:10.1016/s0960-0779(98)00295-1.

Weron, R., 1996. On the Chambers-Mallows-Stuck method for simulating skewed stable random variables. Statistics & Probability Letters 28, 165–171. URL: https://doi.org/10.1016/0167-7152(95)00113-1, doi:10.1016/0167-7152(95)00113-1.

Weron, R., 2001. Levy-Stable Distributions Revisited: Tail Index > 2 Does Not Exclude The Levy-Stable Regime. International Journal of Modern Physics C 12, 209–223. URL: https://doi.org/10.1142%2Fs0129183101001614, doi:10.1142/s0129183101001614.

White, R., Marinakis, Y., Islam, N., Walsh, S., 2020. Is Bitcoin a currency, a technology-based product, or something else? Technological Forecasting and Social Change 151, 119877. URL: https://doi.org/10.1016/j.techfore.2019.119877, doi:10.1016/j.techfore.2019.119877.

Xu, W., Wu, C., Dong, Y., Xiao, W., 2011. Modeling Chinese stock returns with stable distribution. Mathematical and Computer Modelling 54, 610–617. URL: https://doi.org/10.1016/j.mcm.2011.03.004, doi:10.1016/j.mcm.2011.03.004.

Yarovaya, L., Matkovskyy, R., Jalan, A., 2020. The Effects of a 'Black Swan' Event (COVID-19) on Herding Behavior in Cryptocurrency Markets: Evidence from Cryptocurrency USD, EUR, JPY and KRW Markets. SSRN Electronic Journal URL: https://doi.org/10.2139/ssrn.3586511, doi:10.2139/ssrn.3586511.

Yermack, D., 2015. Is Bitcoin a Real Currency? An Economic Appraisal, in: Handbook of Digital Currency. Elsevier, pp. 31–43. URL: https://doi.org/10.1016/b978-0-12-802117-0.00002-3, doi:10.1016/b978-0-12-802117-0.00002-3.

Yuan, Y., tian Zhuang, X., Jin, X., qiang Huang, W., 2014. Stable distribution and long-range correlation of Brent crude oil market. Physica A: Statistical Mechanics and its Applications 413, 173–179. URL: https://doi.org/10.1016/j.physa.2014.06.064, doi:10.1016/j.physa.2014.06.064.

Zaremba, A., Kizys, R., Aharon, D.Y., Demir, E., 2020. Infected Markets: Novel Coronavirus, Government Interventions, and Stock Return Volatility around the Globe. Finance Research Letters 35, 101597. URL: https://doi.org/10.1016/j.frl.2020.101597, doi:10.1016/j.frl.2020.101597.

Zargar, F.N., Kumar, D., 2019. Informational inefficiency of Bitcoin: A study based on high-frequency data. Research in International Business and Finance 47, 344–353. URL: https://doi.org/10.1016/j.ribaf.2018.08.008, doi:10.1016/j.ribaf.2018.08.008.

Zebende, G., 2011. DCCA cross-correlation coefficient: Quantifying level of cross-correlation. Physica A: Statistical Mechanics and its Applications 390, 614–618. URL: https://doi.org/10.1016/j.physa.2010.10.022, doi:10.1016/j.physa.2010.10.022.

Zhang, D., Hu, M., Ji, Q., 2020. Financial markets under the global pandemic of COVID-19. Finance Research Letters 36, 101528. URL: https://doi.org/10.1016/j.frl.2020.101528, doi:10.1016/j.frl.2020.101528.

Zhang, W., Wang, P., Li, X., Shen, D., 2018a. The inefficiency of cryptocurrency and its cross-correlation with Dow Jones Industrial Average. Physica A: Statistical Mechanics and its Applications 510, 658–670. URL: https://doi.org/10.1016/j.physa.2018.07.032, doi:10.1016/j.physa.2018.07.032.

Zhang, W., Wang, P., Li, X., Shen, D., 2018b. Multifractal Detrended Cross-Correlation Analysis of the Return-Volume Relationship of Bitcoin Market. Complexity 2018, 1–20. URL: https://doi.org/10.1155/2018/8691420, doi:10.1155/2018/8691420.

Zhang, X., Wu, X., Zhang, L., Chen, Z., 2022. The Evaluation of Mean-Detrended Cross-Correlation Analysis Portfolio Strategy for Multiple risk Assets. Evaluation Review 46, 138–164. URL: https://doi.org/10.1177/0193841x221078642, doi:10.1177/0193841x221078642.

Zhang, X., Yang, L., Zhu, Y., 2019. Analysis of multifractal characterization of Bitcoin market based on multifractal detrended fluctuation analysis. Physica A: Statistical Mechanics and its Applications 523, 973–983. URL: https://doi.org/10.1016/j.physa.2019.04.149, doi:10.1016/j.physa.2019.04.149.

Zhou, W.X., 2008. Multifractal detrended cross-correlation analysis for two non-stationary signals. Physical Review E 77. URL: https://doi.org/10.1103/physreve.77.066211, doi:10.1103/physreve.77.066211.

Zitis, P., Kakinaka, S., Umeno, K., Hanias, M., Stavrinides, S., Potirakis, S., 2023. Investigating Dynamical Complexity and Fractal Characteristics of Bitcoin/US dollar and Euro/US dollar Exchange Rates Around the COVID-19 Outbreak. Entropy 25.

Zolotarev, V.M., 1986. One-dimensional stable distributions. American Mathematical Soc. 65.

List of author's papers related to this thesis

1. Shinji Kakinaka and Ken Umeno, Flexible Two-point Selection Approach for Characteristic Function-based Parameter Estimation of Stable Laws, *Chaos* 30, 073128 (2020).

2. Shinji Kakinaka and Ken Umeno, Characterizing Cryptocurrency Market with Lévy's Stable Distributions, *Journal of the Physical Society of Japan* 89(2):024802 (2020).

3. Shinji Kakinaka and Ken Umeno, Cryptocurrency market efficiency in short- and long-term horizons during COVID-19: An asymmetric multifractal analysis approach, *Finance Research Letters* 46, 102319 (2022).

4. Shinji Kakinaka and Ken Umeno, Exploring asymmetric multifractal cross-correlations of price-volatility and asymmetric volatility dynamics in cryptocurrency markets. *Physica A* 581, 126237 (2021).

5. Shinji Kakinaka and Ken Umeno, Asymmetric volatility dynamics in cryptocurrency markets on multi-time scales. *Research in International Business and Finance* 62, 101754 (2022).

6. Shinji Kakinaka, Tadaaki Hayakawa, Daisuke Kato, and Ken Umeno, Fractal portfolio strategies: Does scale preference of investors matter? *submitted to Applied Economics Letters*.

- Chapter 2 is based on paper 1.
- Chapter 3 and Appendix A are based on paper 2.
- Chapter 4 is based on paper 3.
- Chapter 5 is based on paper 4.
- Chapter 6 and Appendix B are based on paper 5.
- Chapter 7 and Appendix C are based on paper 6.